Flame Turbulence Interaction In Premixed Turbulent Combustion

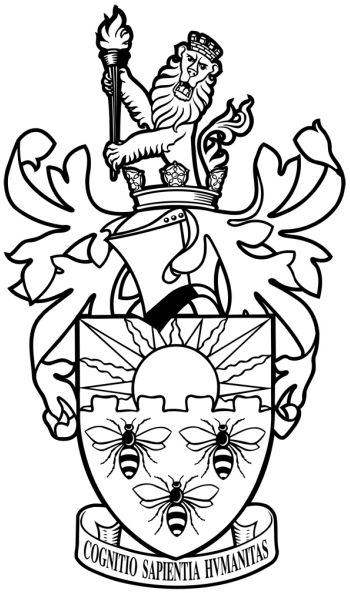

A thesis submitted to The University of Manchester

for the degree of Doctor of Philosophy

in the faculty of Engineering and Physical Sciences

By

Umair Ahmed

2013

School of Mechanical Aerospace and Civil Engineering

Contents

List of Tables

List of Figures

Abstract

University of Manchester

Umair Ahmed

Doctor of Philosophy

Flame Turbulence Interaction in Premixed Turbulent Combustion

December 2013

It is well known that the behaviour of the mean reaction rate $\left(\overline{\dot{\omega}}_c\right)$ is predicated on the scalar dissipation $(\widetilde{\epsilon}_c)$, through which are also felt the effects of mean mixing rates and other turbulent phenomenon [21, 149]. In the first part of the thesis the sensitivity of $\overline{\dot{\omega}}_c$ to alternative closures for $\widetilde{\epsilon}_c$ has been examined in the context of the Bray Moss Libby (BML) model. A rod stabilised turbulent premixed V-flame has been chosen as a representative configuration. Algebraic closures proposed by Swaminathan and Bray [149], Kolla et al [85, 86] and Vervisch et al [157] have been examined. The location of the flame, and the mean velocities in the axial and transverse directions have been compared with the Particle Image Velocimetry (PIV) data from the experiment of Bell et al [9]. It is observed that the flame behaviour changes when different models for $\widetilde{\epsilon}_c$ are used. It has also been found that the mean velocities and flame locations predicted by all of the models used for $\widetilde{\epsilon}_c$ tend to deviate from the experimental results in the far wake region of the stabilising rod. It is argued here that the disagreement between the experimental data and the predicted values from the $\widetilde{\epsilon}_c$ models is due to the approximation of the flame turbulence interaction $\left(\widetilde{\Delta}_c\right)$ term in the $\widetilde{\epsilon}_c$ models.

In the second part of the thesis a transport equation for the $\widetilde{\Delta}_c$ is proposed. This equation gives a detailed insight into flame turbulence interaction phenomenon and provides an alternative approach to model the important physics represented by $\widetilde{\Delta}_c$. The $\widetilde{\Delta}_c$ evolution equation is derived in detail and an order of magnitude analysis is carried out to determine the leading order terms in the $\widetilde{\Delta}_c$ evolution equation. The leading order terms are then studied by using a Direct Numerical Simulation (DNS) of a turbulent premixed V-flame. It is found that the behaviour of $\widetilde{\Delta}_c$ is determined by the competition between diffusion processes, turbulent strain rate and the dilatation rate. Closures for the leading order terms in $\widetilde{\Delta}_c$ evolution equation have been proposed and compared with the DNS data. It is found that the comparison of modelled predictions and the DNS values are in good agreement for the combustion conditions considered in this thesis. A time scale for flame turbulence interaction, based on the closures of the leading order terms, is proposed. This time scale gives a measure of the characteristic time required by the flame gradient to change alignment with respect to the strain rate eigenvector.

Declaration

No portion of the work referred to in this thesis has been submitted in support of an application for another degree or qualification of this or any other university or other institute of learning.

Copyright

Acknowledgements

I would to thank my supervisor Dr Robert Prosser for his constant support and patience (it was much needed) during the course of this project. He has not only taught me turbulent combustion, but has also taught me some important lessons in life. I would also like to thank my co-supervisor Dr Alistair Revell for his constant encouragement and support during my time as a PhD student. I would like to thank Dr Tom Dunstan from Cambridge University for his help in providing the important DNS data for this work. Without his support and help this work would not have been possible. Acknowledgements are also due to Dr Robert Cheng from Lawrence Berkeley National Laboratory for making the experimental data available.

The PhD has been more than just research, I have met a lot of nice and helpful people on the way. I want to say a special thanks to Dean Wilson, Arno Mayrhofer, Ioannis Asproulias and James McNaughton for discussing my technical and non technical problems and contributing to the solutions to the best of their ability. I would also like to take this opportunity to thank Dr Juan Uribe, Dr Flavian Billard and Dr Stefano Rolfo who have always been there to help me when I needed them. I would like to thank the rest of the George Begg office mates who have been a great company, in particular Maryam, Pablo, Fernando, Adam, Tom, Huw, Craig, Khalil, Alan and Andrew. I am grateful to them for their support, and help in what ever way possible. I would also like to thank all my friends in particular William, Richard, Adnan, Johannes, Hitesh and the lovely people at the local Oxfam shop who have provided me with much needed support during the PhD.

Last but not the least I would like to thank my Mum for supporting me for every thing I have achieved so far.

Nomenclature

Roman Symbols

$\dot{m}_F$	mass flow rate of fuel
$\dot{m}_O$	mass flow rate of oxidiser
$\hat{C}$	constant for the turbulent burning velocity correlation
$\hat{L}_y$	integral length scale of wrinkling
$\|\|S\|\|$	strain invariant
$\Re^0$	universal gas constant
A	cross sectional area of a control volume
A_0	model constant in the modelled flame surface density transport equation
A_T	surface area of the wrinkled laminar flame
B_0	model constant in the modelled flame surface density transport equation
C	molar concentration
c	progress variable
$C_{\epsilon 1}$	constant in the turbulent dissipation transport equation
$C_{\epsilon 2}$	constant in the turbulent dissipation transport equation
C_μ	predetermined coefficient for turbulent viscosity
C_a	scaling factor in the modelled $\widetilde{\Delta}_c$ evolution equation

C_b scaling factor in the modelled $\widetilde{\Delta}_c$ evolution equation

C_c scaling factor in the modelled $\widetilde{\Delta}_c$ evolution equation

C_D ratio of turbulence time scale to the scalar time scale

C_{EBU} constant in the EBU model

C_k molar concentration

C_l constant in the one equation model

C_M mean reaction rate constant in the BML approach

C_p the specific heat capacity at constant pressure

D mass diffusivity

D_{fi} diffusion terms in the $\widetilde{\Delta}_c$ evolution equation

D_{kl} diffusion from species k to l

Da Damköhler number

Da_L local Damköhler number

e efficiency factor

e_α extensive eigenvector

e_β intermediate eigenvector

e_γ compressive eigenvector

E_a activation energy

e_k energy of species k

e_{sk} sensible energy for species k

F_{1i} source terms in the $\widetilde{\Delta}_c$ evolution equation

F_2	terms due to turbulent transport in the $\widetilde{\Delta}_c$ evolution equation
F_{3i}	dilatation terms in the $\widetilde{\Delta}_c$ evolution equation
F_{4i}	turbulent straining terms in the $\widetilde{\Delta}_c$ evolution equation
F_5	dilatation due to turbulent transport in the $\widetilde{\Delta}_c$ evolution equation
F_D	leading order dilatation terms in the $\widetilde{\Delta}_c$ evolution equation
F_{TS}	leading order turbulent straining terms in the $\widetilde{\Delta}_c$ evolution equation
h_k	enthalpy of species k
h_{sk}	sensible enthalpy for species k
I_0	factor for strain rate and curvature
K	constant related to the flame location
k	turbulent kinetic energy
Ka	Karlovitz number
Ka_L	local Karlovitz number
l_{mix}	mixing length
l_t	integral length scale
Le	Lewis number
m	mass of the gas in this volume
m_i	mass of species i per unit volume of a solution
M_k	symbol for species k
N	total number of species
N_B	Bray number
N_c	instantaneous scalar dissipation rate of the progress variable

N_t	total number of snapshots
N_z	total number of nodes in the z direction
p	pressure
Pr	Prandtl number
Q	heat release due to complete combustion
Re	Reynolds number
Re_{l_t}	turbulent Reynolds number
s	mass stoichiometric ratio
s_c	consumption speed
S_{ij}	strain rate tensor
Sc	Schmidt number
T	temperature
t	time
T_{11}	turbulent transport of $\widetilde{\epsilon}_c$ in evolution equation
T_{12}	influence of curvature of the mean scalar field in $\widetilde{\epsilon}_c$ evolution equation
T_2	dilatation in the $\widetilde{\epsilon}_c$ evolution equation
T_{31}	effects of mean scalar gradient on flame turbulence interaction in $\widetilde{\epsilon}_c$ evolution equation
T_{32}	flame turbulence interaction in $\widetilde{\epsilon}_c$ evolution equation
T_{33}	effects of mean strain on flame turbulence interaction in $\widetilde{\epsilon}_c$ evolution equation
T_4	effects of chemical reaction in $\widetilde{\epsilon}_c$ evolution equation
$u^{'}$	root mean square velocity

u_η	Kolmogorov velocity scale
u_i	instantaneous velocity
u_L^0	laminar burning velocity
u_P	slip velocity on the product side
u_{ref}	reference velocity
u_R	slip velocity on the reactant side
u_T	turbulent burning velocity
V_F	diffusion velocity of fuel
V_k	diffusion velocity of species k
W	mean molecular weight
W_k	atomic weight of species k
x^+	length normalised by δ_L^0 in the x direction
x_i	position
X_k	mole fraction
Y	reduced mass fraction
y^*	non-dimensional distance away from the wall
y^+	length normalised by δ_L^0 in the y direction
Y_F	mass fraction of fuel
Y_F^R	fuel mass fraction in the reactants
Y_k	mass fraction
Y_{PP}	mass fraction of products in fully burned product gases
Y_P	mass fraction of products

Greek Symbols

α	probability of finding reactants
α_T	heat diffusivity coefficient
β	probability of finding products
$\delta(c)$	Dirac delta function
δ_B	turbulent flame brush thickness
Δ_c	flame turbulence interaction
δ_{ij}	Kronecker delta
δ_L	laminar diffusive thickness of the flame
δ_L^0	laminar thermal thickness of the flame
$\dot{\omega}_k$	rate of reaction of species k
$\dot{\omega}_c$	reaction rate of the progress variable
$\dot{\omega}_F$	local reaction rate of fuel
ϵ	turbulent dissipation
η	Kolmogorov length scale
Γ	specific reaction-rate constant
γ	probability of finding reacting gas
κ_c	strain rate due flame propagarion and curvature
κ_m	strain rate due to mean flow
κ_t	strain rate due to turbulent motion
λ	thermal conductivity
λ_T	Taylor microscale

μ	dynamic viscosity
$\mu^{'}$	bulk viscosity
$\nu_k^{''}$	stoichiometric coefficients of species k appearing as product
$\nu_k^{'}$	stoichiometric coefficients of species k appearing as reactant
ν_R	kinematic viscosity of the reactants
ν_t	turbulent viscosity
Ω_F	total fuel consumption in the flame
ϕ	equivalence ratio
ϕ_g	global equivalence ratio
ρ	density
ρ_p	density of the products
ρ_R	density of the reactants
Σ	flame surface density
σ_ϵ	turbulent schmidt number for turbulent dissipation transport equation
σ_c	turbulent Schmidt number for the progress variable
σ_{ij}	stress tensor
σ_k	turbulent Schmidt number for turbulent kinetic energy equation
τ	heat release parameter
τ_η	Kolmogorov time scale
τ_c	chemical time scale
τ_{EBU}	time scale used in the EBU model

τ_{ij} viscous tensor

τ_t turbulent time scale

θ_α angle between the scalar gradient and e_α

θ_β angle between the scalar gradient and e_β

θ_γ angle between the scalar gradient and e_γ

Ξ flame wrinkling factor

ξ mixture fraction

C_{Mi} concentration

ϵ_c scalar dissipation for the variance of the progress variable

Mathematical Symbols

$<>$ surface averaging

$\tilde{}$ Favre average quantity

$''$ fluctuation quantity in Favre averaging

$'$ fluctuation quantity in Reynolds averaging

$\bar{}$ time-averaged quantity

Abbreviations

BML Bray Moss Libby Model

CFD Computational Fluid Dynamics

CGD Counter Gradient Diffusion

DNS Direct Numerical Simulation

EBU Eddy Break Up

EVM Eddy Viscosity Model

FTI Flame Turbulence Interaction

GD Gradient Diffusion

NSCBC Navier Stokes Characteristic Boundary Conditions

OMA Order of Magnitude Analysis

PDF Probability Density Function

PIV Particle Image Velocimetry

RANS Reynolds Averaged Navier Stokes

1 Introduction

Combustion is a means of converting primary (chemical) energy into secondary (heat) energy. It is one of the most important sources of generating mechanical energy [10]. Most of the mechanical power obtained from combustion is used for the generation of electricity, for transport and also for industrial processes which include materials processing, casting iron and steel [10].

Coal, oil and natural gas are the main fossil fuel resources and are limited in supply. Fuel rich combustion devices used in the past led to incomplete combustion of fuels, thus leading to high levels of fuel consumption, pollutant formation and greenhouse gas emissions. In the last two decades, the main concerns arising from fossil fuel burning were nitrous oxide and sulphur oxide emission, which led to ozone layer depletion, smog and acid rain. However, now it is widely accepted that greenhouse emissions are one of the key factors adversely affecting the environment and causing global warming. According to recent reports by the Intergovernmental Panel on Climate Change [74] and the International Energy Agency [75], combustion of fossil fuels in the industrial, energy, transport and domestic sectors contribute approximately 71% of the total greenhouse gas emissions. It has been agreed by many countries under the United Nations Framework Convention on Climate Change that more research and development is required to reduce greenhouse gas emissions, and that ongoing investment in cleaner energy sources is required [84]. While renewable energy sources such as solar, wind and tidal energy provide an alternative for energy production, combustion of fossil or alternative fuels (such as bio-fuels or hydrogen) will remain the main source of energy for the foreseeable future [73, 117].

Lean premixed combustion is one of the avenues available to reduce greenhouse gas emissions and increase fuel efficiency. In lean premixed combustion a homogeneous mixture of fuel and excess oxidiser is used, thus significantly reducing the

pollutant emissions while improving the fuel efficiency of the combustion device [51]. The use of lean premixed combustion in combustion devices is at an early stage; recently lean premixed combustion has been adopted for stationary land based gas turbine engines in the energy sector [78]. The adoption of lean premixed combustion for aircraft engines is more difficult due to the use of liquid fuels, as these fuels have to be vapourised and can lead to problems like autoignition or flashback [51]. Although due to the recent advances in technology, it is anticipated that aircraft engines are likely to switch to lean premixed combustion [52, 77, 106, 136]. In the automotive sector, the current generation of reciprocating engines such as spark ignition [169] and compression ignition engines [165] burn inhomogeneous mixtures that are lean over all. In such scenarios, the premixed combustion mode still plays an important role in determining the flame characteristics [162]. This implies that a fundamental understanding of premixed turbulent combustion is required. Although lean premixed combustion is appealing from the economic and environmental point of view, it is very susceptible to instabilities due to changes in fuel composition and weak reaction fronts in highly dynamic fluid flows [142]. These instabilities can lead to excessive strains on the engine and can significantly reduce lifetime of the engine. Hence more accurate mathematical models are required to predict correct flame behaviour in the engine development phase. The development of models for turbulent premixed combustion applicable to a wide range of combustion conditions is an area of intensive research by the combustion community [16, 19, 117, 161]. Significant progress has been made in modelling premixed turbulent combustion; however a lot still remains to be done. A few examples include accurate prediction of flame noise, pollutant emission, flame turbulence interaction, prediction of flame instability limits etc.

1.1 Computational Fluid Dynamics in combustion

Computational Fluid Dynamics (CFD) is widely used to design many engineering devices, such as cars, internal combustion engines, gas turbines etc. CFD greatly reduces the time and economic costs of the design process by providing a shorter

turn around time. There are several different approaches available in CFD to calculate the flow field; these include Direct Numerical Simulation (DNS), Large Eddy Simulation (LES) and Reynolds Averaged Navier-Stokes (RANS).

DNS represents one extreme of the computational spectrum, as it provides a good representation of the fluid flow problem (all scales of the flow are resolved), however it is computationally expensive for turbulent combustion due to the inclusion of detailed chemical kinetics and transport processes. Even with the state of the art computational resources DNS calculations are usually limited to typically a few cubic centimetres. In order to circumvent the need to resolve all the scales different modelling strategies are employed. These modelling strategies involve mathematical techniques such as averaging or filtering of the governing equations.

LES is one of the modelling strategies available in CFD. In LES governing equations of filtered quantities representing the dynamics of energy containing large scale motions of turbulent flow are solved [155]. The small scale is modelled by using appropriate modelling strategies. Although LES provides a good representation of the turbulent scales, but still requires models for the chemical scales as flames of practical interest always remain smaller than the smallest scales of turbulence. RANS on the other hand provides the least computationally expensive strategy. In RANS average quantities in the governing equations are solved, and statistical models are employed to approximate the unclosed correlations of turbulence and thermochemical quantities.

It should be noted that most models for LES applications are developed as extensions to the RANS models [118]. This implies that RANS models play a critical role in turbulent combustion modelling. This thesis makes some progress in this regard, and the main objectives and outline of the thesis is given in the next section.

1.2 Objectives and outline of the thesis

Future combustion system design would be influenced by the emphasis on reducing the green house gas emissions [10]. Mathematical models and CFD are going to play an important role in this process [10, 12]. New models are needed which

rely on less expensive computational requirements, and are reliable enough to be used for designing new combustors. Current models lack the detailed modelling of important physical processes such as flame turbulence interaction.

There are many theoretical concepts which try to address the problem of flame turbulence interaction and one such concept is scalar dissipation. The scalar dissipation determines how quickly the scalar fluctuations decay and denotes the rate of scalar mixing. Veynante and Vervisch [161] have shown that scalar dissipation is linked to the fundamental quantities in turbulent combustion such as the mean reaction rate and the prediction of pollutant emissions. Many modelling approaches use scalar dissipation rate to model premixed flames, as proposed for example by Pope [119], Bray [19], Kolla et al [85, 87, 88], Robin et al [112, 132, 134] and Bilger [11]. In premixed combustion the scalar dissipation appears as an explicit function of flame turbulence interaction. Flame turbulence interaction is not a well understood phenomenon, although some advances have recently been made in this regard [40, 44, 45, 151].

The main objective of this thesis is to replicate the effect of flame turbulence interaction in premixed combustion through a simplified mathematical model, and also to reduce the complexity of the mathematics involved.

The outline of the thesis is as follows. The basic thermochemistry, governing equations, laws of mass transport and differences between the two main types of flames are discussed in chapter 2. The concept of turbulence, its physical meaning and its influence on cold flows is introduced in chapter 3. The discussion in chapter 3 describes the RANS averaging technique and also elaborates on some of the different models used to close the correlations of turbulence. Chapter 4 introduces the key parameters involved in turbulent premixed combustion, regime diagrams and the laminar flamelet concept used in many modelling strategies. The Bray Moss Libby (BML) modelling approach for premixed turbulent combustion is introduced in chapter 5. The governing equations and the associated models used in RANS simulations of premixed turbulent combustion under the BML framework are also presented. Chapter 6 focuses on a number of different scalar dissipation models and their development. The concept of flame surface density and its dependence on flame turbulence interaction is also discussed in chapter 6. In chapter 7 a laboratory scale turbulent premixed V-flame is simulated

by using the BML theory and scalar dissipation models discussed in preceding chapters. The results of the V-flame simulation are compared against Particle Image Velocimetry (PIV) data obtained from the experiment of Bell et al [9]. The shortfalls in the current scalar dissipation models are then identified and discussed with respect to the V-flame RANS simulations. The treatment of flame turbulence interaction in the current scalar dissipation models is identified as one of the major sources of error, and it is argued that a better formulation for flame turbulence interaction is required. Chapter 8 introduces the concept of the flame turbulence interaction (FTI) evolution equation. In chapter 8 an order of magnitude analysis (OMA) is performed on the flame turbulence interaction evolution equation to identify the leading order terms. These leading order terms are then studied in chapter 9 via a detailed interrogation of a DNS data set of a premixed V-flame. The details of the DNS data set and data processing techniques are discussed and then the closures for the leading order terms in the flame turbulence interaction evolution equation are proposed.

The conclusions are summarised in the last chapter along with avenues for future work.

2 Thermochemistry involved in combustion

This chapter focuses on the laws and equations which govern the rate and progress of reaction in combustion. Different ways of expressing the concentration of a reacting mixture will be discussed first. Then the thermochemistry involved in combustion is discussed leading to the reaction rate formulations. Laws of mass transport are described with reference to the molecular transport of species and heat. Finally the differences between premixed and non-premixed flames are described.

2.1 Different ways to express concentrations

The concentration of different species in a multicomponent reacting system can be expressed in a number of different ways. The most commonly used are; the mass fractions denoted by Y_k for $k = 1$ to N (where N is the number of species in the reacting mixture); and the molar concentration, denoted by C_k and; the mole fraction denoted by X_k .
The mass fractions are generally defined as [118]:

$$Y_k = \frac{m_k}{m}, \tag{2.1}$$

where m_k is the mass of species k per unit volume and m is the total mass [118]. The molar concentration is defined as [91]:

$$C_k = \frac{m_k}{W_k} = \rho \frac{Y_k}{W_k}, \tag{2.2}$$

and the mole fraction is defined as:

$$X_k = \frac{C_k}{C} = \frac{W}{W_k} Y_k, \tag{2.3}$$

where W is the mean molecular weight of the mixture and W_k is the atomic weight of species k. Now Y_k could also be defined as :

$$Y_k = \frac{\rho_k}{\rho}, \tag{2.4}$$

where ρ_k is the mass concentration of species k, and ρ is the total mass density of the solution [91]. C_k can also be expressed as [91]:

$$C_k = \frac{\rho_k}{W_k}. \tag{2.5}$$

2.2 Thermochemistry

Several variables can be used to represent the energy of a reacting flow. The most commonly used are internal energy (e_k), enthalpy (h_k), sensible energy (e_{sk}) and sensible enthalpy (h_{sk}) (enthalpies and energies are related by $e_k = h_k - \frac{p_k}{\rho_k}$ and $e_{sk} = h_{sk} - \frac{p_k}{\rho_k}$) [118]. The sensible energy (e_{sk}) and sensible enthalpy (h_{sk}) are respectively defined as [118]:

$$e_{sk} = \int_{T_0}^{T} C_{pk} dT - \frac{\Re^0 T_0}{W_k} \tag{2.6}$$

$$h_{sk} = \int_{T_0}^{T} C_{pk} dT, \tag{2.7}$$

where $\Re^0$ is the universal gas constant ($\Re^0 = 8.314 J/(molK)$), W_k is the atomic weight of species k and C_p is the specific heat capacity at constant pressure.
The energy (e_k) and enthalpy (h_k) are defined as [118]:

$$e_k = e_{sk} + \Delta h^0_{f,k} \tag{2.8}$$

$$h_k = h_{sk} + \Delta h^0_{f,k}, \tag{2.9}$$

where $\Delta h^0_{f,k}$ is the mass enthalpy of formation of species k at temperature T_0 [118]. In principle any value can be assigned to the reference temperature T_0(i.e. $T_0 = 0$) [118], but gathering experimental information for enthalpy of formation at $0\,K$ is difficult so a standard reference state is used, which is usually set to $T_0 = 298.15K$ [130]. Along with the reference value of temperature a reference value of enthalpy is also required. This is done by assuming that the enthalpy h_k is defined as [118]:

$$h_k = \int_{T_0}^{T} \underbrace{C_{pk} dT}_{Sensible} \quad + \quad \underbrace{\Delta h^0_{f,k}}_{Chemical}, \tag{2.10}$$

chosen so that the sensible enthalpy $h_{sk} = 0$ at $T = T_0$ for all substances [118], giving $h_k(T_0) = \int_{T_0}^{T_0} \Delta h^0_{f,k} = 0$.

2.3 Rates of reaction and their functional dependence

Chemical reactions take place at a rate which depends on the conditions of the reacting system. When a system of N species react through M reactions, the forward and reverse reaction is symbolically expressed as [118]:

$$\sum_{k=1}^{N} \nu_k^{'} M_k \rightleftharpoons \sum_{k=1}^{N} \nu_k^{''} M_k, \tag{2.11}$$

where M_k represents the symbol for species k, $\nu_k^{'}$ and $\nu_k^{''}$ are the molar stoichiometric coefficients of species k, and N is the total number of species involved [118]. It should be noted that $\nu_k^{'}$ is the stoichiometric coefficient of reactants, and $\nu_k^{''}$ is the stoichiometric coefficient of the products.

A single-step forward reaction can be represented by using eq. (2.11) and rewriting it as [91, 96]:

$$\sum_{k=1}^{N} \nu_k^{'} M_k \rightarrow \sum_{k=1}^{N} \nu_k^{''} M_k. \tag{2.12}$$

If a species represented by M_k does not exist as a reactant, then $\nu_k^{'} = 0$; if the

species (M_k) does not exist as a product, then $\nu_k^{''} = 0$ [91].
The law of mass action is [91]:

> *"The rate of disappearance of a chemical species is proportional to the products of the concentrations of the reacting chemical species, each concentration being raised to a power equal to the value of the corresponding stoichiometric coefficient"* .

Thus, the reaction rate $\dot{\omega}_k$ is given by [96]:

$$\dot{\omega}_k = \Gamma \prod_{k=1}^{N} (C_k)^{\nu_k^{'}}, \tag{2.13}$$

where Γ is the proportionality constant known as the specific reaction-rate constant and C_k is the concentration of species k. Eq. (2.13) makes use of the view that the reaction rate is based on the collision frequency, which is proportional to the product of species concentration raised to the power of the stoichiometric coefficient of reactants [96, 164]. Generally in a given chemical reaction, Γ is independent of C_k and depends only on temperature, and so can be written as [91]:

$$\Gamma = BT^a exp\left(-\frac{E}{RT}\right), \tag{2.14}$$

where BT^a represents the collision frequency and the exponential term represents the Boltzmann factor [91].

2.4 The Arrhenius law

According to this law only the molecules which possess energy greater than the activation energy E_a will react and lead to the formation of products [91, 96]. The expression for the Arrhenius law is [96]:

$$\Gamma = A\, exp\left(-\frac{E_a}{RT}\right). \tag{2.15}$$

It can be seen that eq. (2.14) and eq. (2.15) are quite similar to each other, and in essence they are the same equations. In Eq. (2.15) it is assumed that

A includes the effect of the collision terms, the steric factor associated with the orientation of the colliding molecules, and the mild temperature dependence of the preexponential factor [91]. A in eq. (2.15) corresponds to BT^a in eq. (2.14), the value of a lies between 0 and 1 [91].

2.5 Laws of mass transport

Ficks law of diffusion

According to Ficks law of diffusion, particles always move from regions of high concentration to regions of low concentration [91]. Fick's law relates diffusion velocity to concentration gradients and can be expressed in terms of both the molar flux and the mass flux.
The molar flux in binary systems is expressed as [91]:

$$J_k^* = -CD_{kl}\nabla X_k, \tag{2.16}$$

where subscript k denotes fluid of species k and D_{kl} describes diffusion between species k and l, and C represents the molar concentration. For mass fluxes, Fick's law is expressed as [118]:

$$J_k = -\rho D_{kl}\nabla Y_k. \tag{2.17}$$

Note that for most combustion processes thermodiffusion is assumed to be small and is neglected in the Ficks law.

Fourier's law of heat conduction

According to the Fourier's law of heat conduction the heat flux should be proportional to the negative temperature gradient as[91, 118]:

$$q_j = -\lambda\,\nabla T + \sum_{k=1}^{N} h_k J_k, \tag{2.18}$$

where λ is the thermal conductivity, T represents the temperature and the second term on the right-hand side is associated with the diffusion of species with different enthalpies which is specific to multi species gas. Note that Dufour effects are

assumed to be small and have been neglected in eq. (2.18) [91].

2.6 Governing equations

The equations governing flows with chemical reactions are the mass, the species transport, the momentum and the energy conservation equations. A solution of these equation leads to all the information required in a reacting flow. These conservation equations are discussed in this section.

2.6.1 Mass and species

The mass conservation equation is written as [163]:

$$\frac{\partial \rho}{\partial t} + \frac{\partial \rho u_i}{\partial x_i} = 0, \tag{2.19}$$

and the mass conservation for species k is written as [91]:

$$\frac{\partial \rho Y_k}{\partial t} + \frac{\partial}{\partial x_i}\left(\rho\left(u_i + V_{k,i}\right) Y_k\right) = \dot{\omega}_k \qquad for \qquad k = 1, N\,, \tag{2.20}$$

where $V_{k,i}$ is the i^{th} component of the diffusion velocity $\mathbf{V}_k$ of species k, and $\dot{\omega}_k$ is the reaction rate of species k. By definition $\sum_{k=1}^{N} Y_k V_{k,i} = 0$ and $\sum_{k=1}^{N} \dot{\omega}_k = 0$ [91, 118]. The expression for species diffusion velocity, after ignoring the Soret effects is very complicated and usually the simplification proposed by Curtiss and Hirschfelder [53] is used. Thus leading to the Fickian form :

$$V_{k,i} = -D_k \frac{1}{Y_k} \nabla Y_k, \tag{2.21}$$

where D_k is the equivalent diffusivity, defined as :

$$D_k = \frac{1 - Y_k}{\sum_{l \neq k} X_l / D_{lk}}. \tag{2.22}$$

2.6.2 Momentum

The momentum equation is given as [91]:

$$\frac{\partial \rho u_i}{\partial t} + \frac{\partial \rho u_j u_i}{\partial x_j} = \frac{\partial \sigma_{ij}}{\partial x_j} + \rho \left(\sum_{k=1}^{N} Y_k f_k \right)_i , \tag{2.23}$$

where u_i and x_i are velocities and position respectively, t is the time, ρ is density, σ_{ij} is the stress tensor and $\rho \left(\sum_{k=1}^{N} Y_k f_k \right)_i$ represents the body force [91].

2.6.3 Navier Stokes equations

In order to define the Navier Stokes equations the stress tensor in eq. (2.23) has to be closed with a constitutive relation. In the case of Newtonian fluids the stress tensor can be expressed as the sum of pressure and viscous tensor as:

$$\sigma_{ij} = -p\delta_{ij} + \left(\mu^{'} - \frac{2}{3}\mu \right) S_{kk}\delta_{ij} + 2\mu S_{ij}, \tag{2.24}$$

where p is the applied pressure μ is the dynamic viscosity, $\mu^{'}$ is the bulk viscosity and δ_{ij} is the Kronecker delta. The bulk viscosity is 0 for monatomic gas mixtures [91]. S_{ij} in eq. (2.24) is the strain rate tensor and is defined as :

$$S_{ij} = \frac{1}{2} \left(\frac{\partial u_i}{\partial x_j} + \frac{\partial u_j}{\partial x_i} \right). \tag{2.25}$$

The stress tensor in eq. (2.24) can thus be simplified to give [91]:

$$\sigma_{ij} = -p\delta_{ij} + \mu \left(\left(\frac{\partial u_i}{\partial x_j} + \frac{\partial u_j}{\partial x_i} \right) - \frac{2}{3}\delta_{ij} \frac{\partial u_k}{\partial x_k} \right). \tag{2.26}$$

The stress tensor in eq. (2.26) is introduced into the momentum equation to give the Navier Stokes equation [91]:

$$\begin{aligned} \frac{\partial \rho u_i}{\partial t} + \frac{\partial \rho u_j u_i}{\partial x_j} &= \frac{\partial}{\partial x_j} \left[-p\delta_{ij} + \left(-\frac{2}{3}\mu \right) \frac{\partial u_k}{\partial x_k}\delta_{ij} + \mu \left(\frac{\partial u_i}{\partial x_j} + \frac{\partial u_j}{\partial x_i} \right) \right] + \rho \left(\sum_{k=1}^{N} Y_k f_k \right)_i \\ &= -\frac{\partial p}{\partial x_i} + \frac{\partial \tau_{ij}}{\partial x_j} + \rho \left(\sum_{k=1}^{N} Y_k f_k \right)_i , \end{aligned} \tag{2.27}$$

where τ_{ij} is the viscous tensor defined as [91]:

$$\tau_{ij} = \mu \left(\frac{\partial u_i}{\partial x_j} + \frac{\partial u_j}{\partial x_i} \right) - \frac{2}{3} \mu \frac{\partial u_k}{\partial x_k} \delta_{ij}. \tag{2.28}$$

Note that if the flow is assumed to be incompressible, the dilation term vanishes. In combustion, the density variations are non trivial, so the variable density form of the equation is used [91].

2.6.4 Energy

The energy equation can be written in terms of enthalpy, internal energy or temperature. The most common from used is [91, 118]:

$$\frac{\partial \rho e}{\partial t} + \frac{\partial \rho u_j e}{\partial x_j} = -\frac{\partial q_j}{\partial x_j} - \sigma_{ij} \frac{\partial u_j}{\partial x_i} + \rho \left(\sum_{k=1}^{N} Y_k f_k . V_k \right)_i + \dot{Q}, \tag{2.29}$$

where q_j is closed by the Fourier's law of heat conduction mentioned in eq. 2.18, and $\dot{Q}$ is the heat source term, which includes the effects such as ignition sources, radiative flux etc. The expression in eq. (2.29) can be converted into enthalpy or internal energy by using eq. (2.9) and eq. (2.8) respectively.

2.7 Molecular transport of species and heat

Heat diffusion coefficients, viscosity and diffusion coefficients play an important role in combustion problems, as they determine the way in which the reactants diffuse towards the reaction zone [91, 118]. Conservation equations for fluid flow problems are often written in terms of dimensionless ratios of various transport coefficients [91]. The mass diffusivity D is usually characterised in terms of a Lewis number as [164]:

$$Le = \frac{\lambda}{\rho C_p D} = \frac{\alpha_T}{D} = \frac{rate\, of\, energy\, transport}{rate\, mass\, transport}, \tag{2.30}$$

where $\alpha_T = \frac{\lambda}{(\rho C_p)}$ and is the heat diffusivity coefficient [118]. In essence, the Lewis number compares the relative diffusion rates of heat and chemical species; it is

an important parameter in laminar flames [118].
The Prandtl number Pr is used to compare momentum and heat transport and is expressed as [164]:

$$Pr = \frac{\mu C_p}{\lambda} = \frac{C_p \rho \left(\mu/\rho\right)}{\lambda} = \frac{rate\, of\, momentum\, transport}{rate\, of\, conduction}. \tag{2.31}$$

The Schmidt number, Sc is used to compare momentum diffusion and molecular diffusion; it is expressed as [164]:

$$Sc = \frac{\nu}{D} = \frac{rate\, of\, momentum\, transport}{rate\, of\, mass\, transport}. \tag{2.32}$$

It should be noted that Le and Sc can be defined for each species in a multicomponent mixture [91], making use of the equations eq. (2.31) and eq. (2.32), the Lewis number can be written as [91]:

$$Le = \frac{Sc}{Pr}. \tag{2.33}$$

Changes in Lewis number can significantly influence the flame stability by altering the flame speed [118]. Although simplifications to chemistry and transport have to be made to tackle more complex questions on the fluid mechanics level, especially in the case of turbulent combustion [118]. In many systems, Le is very close to unity and it is frequently assumed $Le = 1$ for theoretical combustion analysis [91, 164].

2.8 Types of flames

In general there are two types of flames; premixed flames and diffusion/non-premixed flames. The differences in premixed and diffusion flames are profound [35, 91, 117, 118]. The fuels, oxidisers, the underlying chemical mechanisms and the molecular transport processes are identical [35, 91, 117, 118]. The only difference lies in how the fuel and oxidisers are introduced into the system. These differences along with different properties of the two flames are discussed here.

2.8.1 Premixed-flame

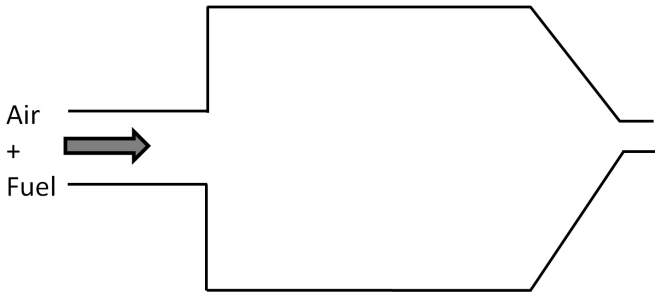

Figure 2.1: Premixed flame configuration

In this type of flame, reactants are perfectly mixed before the reaction [91] as shown in figure 2.1, the mixture is introduced into the combustion chamber and the reaction occurs as [118]:

$$\nu_F^{'} F + \nu_O^{'} O \rightarrow Products. \tag{2.34}$$

Under stoichiometric conditions the mass fractions of fuel and oxidiser are represented as [118]:

$$\left(\frac{Y_O}{Y_F}\right)_{st} = \frac{\nu_O^{'} W_O}{\nu_F^{'} W_F} = s, \tag{2.35}$$

where s is the mass stoichiometric ratio. Now the equivalence ratio of a given mixture can be written as [118]:

$$\phi = s\,\frac{Y_F}{Y_O} = \left(\frac{Y_F}{Y_O}\right) / \left(\frac{Y_F}{Y_O}\right)_{st}, \tag{2.36}$$

further simplification of eq. (2.36) gives [118]:

$$\phi = s\,\frac{\dot{m}_F}{\dot{m}_O}, \tag{2.37}$$

where $\dot{m}_O$ and $\dot{m}_F$ are the mass flow rates of oxidiser and fuel, respectively. In premixed gases, the equivalence ratio is of central importance, as it controls the flame structure and the flame stability limits [118]. In rich combustion regimes $\phi > 1$, which implies that fuel is in excess; and for lean regimes $\phi < 1$, which

implies that the oxidiser is in excess [118].

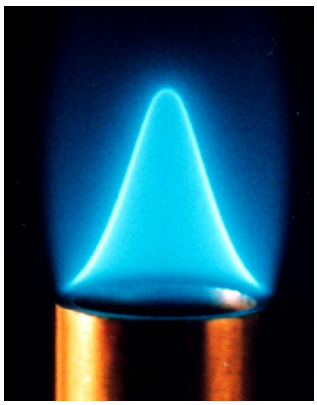

(a) Laminar premixed flame

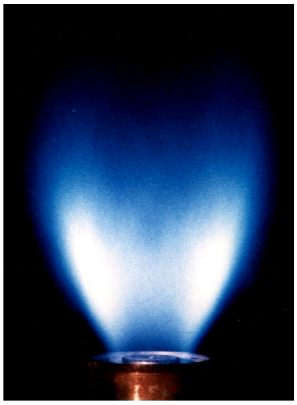

(b) Turbulent premixed flame

Figure 2.2: Premixed flames (used with permission from Professor H. Bockhorn) [14]

Typical laboratory scale laminar and turbulent premixed flames can be seen in figure 2.2. One of the most important characteristic of premixed flames is that the flame moves spontaneously in a direction normal to itself in order to consume the available reactant mixture [35, 117, 118]. It can be seen in figure 2.2a that the laminar premixed flame is a tight, sharply defined cone formed at the surface. The cone forms where the speed of propagation of the flame is equal to the normal velocity component of the on coming reactants [35, 117]. The light blue colour in premixed flames is caused by the chemiluminesence from radical species formed within the thin reaction layer [35]. It should be noted that in principle the mixing between fuel and oxidiser should be complete to the molecular level before combustion occurs, although there is some degree of inhomogeneity in practical combustion devices.

2.8.2 Diffusion/non-premixed flame

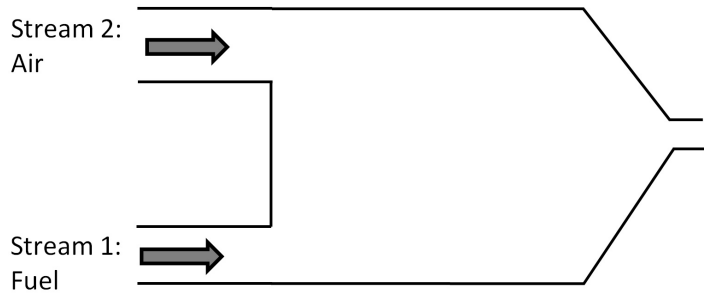

Figure 2.3: Diffusion flame configuration

In this type of flame, reactants diffuse into each other during the chemical reaction [91] as shown in figure 2.3, fuel and oxidiser enter separately into the combustion chamber. The mass fractions and flow rates are controlled separately at the inlets [118]. The mass fractions at inlets are given as Y_F^1 for fuel and Y_O^2 for the oxidiser, the superscripts 1 and 2 denote inlets 1 and 2, respectively. The equivalence ratio for diffusion flames is defined as:

$$\phi = s\,\frac{Y_F^1}{Y_O^2}. \tag{2.38}$$

This ratio gives the local structure of the flames at the point when the fuel and oxidiser streams interact with each other, but it does not give the overall behaviour of the combustor and a global equivalence ratio ϕ_g is also used, which is given as [118]:

$$\phi_g = s\,\frac{\dot{m}_F^1}{\dot{m}_O^2}, \tag{2.39}$$

where $\dot{m}_F^1$ and $\dot{m}_O^2$ are the respective flow rates of fuel and the oxidiser at the respective inlets. ϕ_g and ϕ are linked by the following expression:

$$\phi_g = \phi\,\frac{\dot{m}^1}{\dot{m}^2}, \tag{2.40}$$

where $\dot{m}^1$ and $\dot{m}^2$ are the respective flow rates entering inlets 1 and 2 as shown in figure 2.3. Generally $\phi_g = \phi$ for premixed combustion, as the fuel and oxidiser are carried in the same stream i.e. $\dot{m}^1 = \dot{m}^2$ [118].

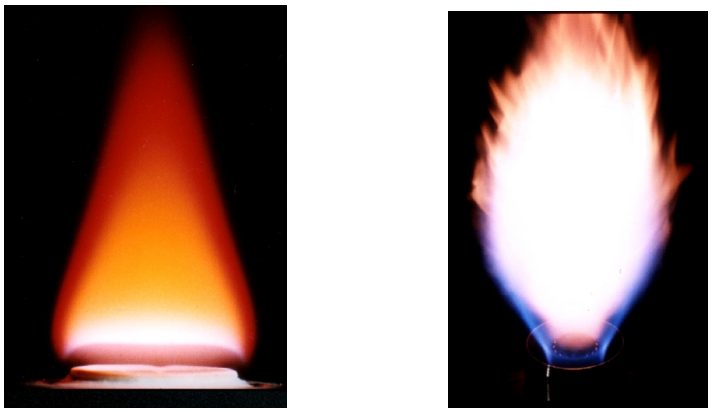

(a) Laminar diffusion flame

(b) Turbulent diffusion flame

Figure 2.4: Diffusion flames (used with permission from Professor H. Bockhorn) [14]

Typical laboratory scale laminar and turbulent diffusion flames can be seen in figure 2.4. Diffusion flames in contrast to premixed flames cannot propagate and instead remain attached to the stoichiometric surface between the fuel and the oxidiser, although the stoichiometric surface may be convected from place to place by the local flow field [35]. Diffusion flames are large and move slowly due to buoyant convection, and glow with a bright yellow light as shown in figure 2.4. The bright yellow colour is due to the thermal radiation from the incandescent soot particles formed on the rich side of the stoichiometric surface [35].

3 Turbulence in combustion

Turbulence in combustion is an important phenomenon as almost all flows of practical engineering interest are turbulent [65, 91, 123, 163]. It is important to gain an understanding of the concepts of turbulence and its effects on combustion, as turbulence alters the dynamics and structure of the flame. In this chapter the differences between laminar and turbulent flows are discussed. Then the properties of turbulent flows are discussed, along with the averaging procedure of Reynolds [129]. Finally different modelling strategies for closing the turbulent correlations (appearing due to the averaging technique) are discussed.

3.1 Differences in turbulent and laminar flows

Laminar Flow

Both the laminar and turbulent flow are types of viscous fluid flow. In laminar flows the adjacent layers of fluid (i.e. the streamlines) slide past each other in an orderly and smooth manner; mixing occurs due to molecular diffusion [163].

Turbulent Flow

At high Reynolds numbers, the inertial forces in the fluid overcome the viscous stresses, causing the laminar flow to become unstable. The motion of the fluid becomes three dimensional and unsteady, causing rapid velocity and pressure fluctuations [163].

3.2 General properties of turbulence

Turbulent flows are random and unsteady in nature [123]. Eddies in the fluid move randomly within and across the fluid layers; and the fluid velocity field varies significantly in both position and time [123]. At most points in a turbulent flow, a plot of the velocity as a function of time appears random as shown in figure 3.1. This makes it difficult to find solutions to turbulent flow problems, and statistical methods have to be used to obtain a solution. One of the intrinsic properties of turbulence is that it enhances diffusivity. In this process, rapid mixing occurs and higher rates of momentum, mass and heat transfer can be observed [65].

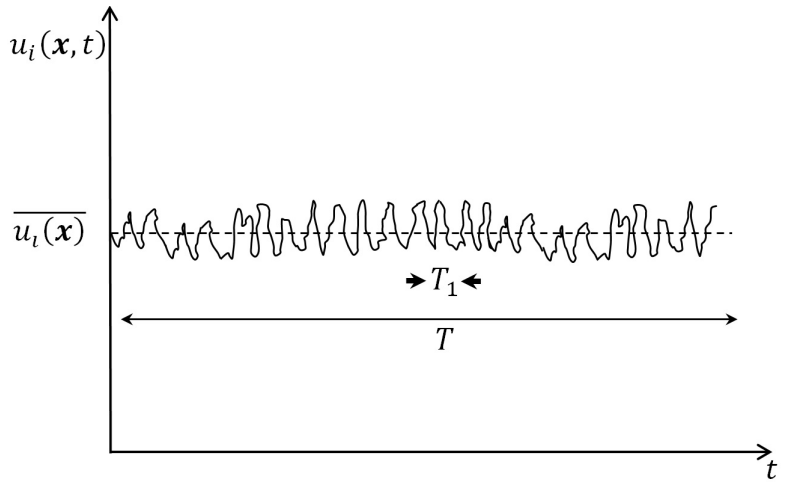

Figure 3.1: Time averaging for stationary turbulence

Turbulence consists of a continuous spectrum of scales. These scales range from largest (almost the size of the flow geometry) known as the integral length scale l_t to the smallest length scale (size of the smallest eddy) known as the Kolmogorov scale η [123]. To visualise a turbulent flow over a spectrum of scales, the physics are often discussed in terms of eddies. An eddy is assumed as a local swirling motion whose characteristic dimension provides the local turbulence scale [163]. The size of the smallest scales is very small but far larger than any molecular length scale [90].

Generally eddies overlap in space, and large eddies carry smaller eddies, as

shown in figure 3.2. Turbulence features a cascade process, as it decays the kinetic energy transfers from larger eddies to smaller eddies [65, 163]. The large eddies of size l_t are unstable and breakup into smaller eddies, and the kinetic energy is transferred to the small eddies. Ultimately, the kinetic energy carried by the smallest eddies dissipate into heat through the action of molecular viscosity [131]. Dissipation of kinetic energy is an important property of turbulent flows and is denoted by ϵ [35]. Generally the rate of dissipation of kinetic energy is equal to the rate of transfer of kinetic energy from large to the small eddies [35, 163] and is usually estimated as:

$$\epsilon \sim \frac{u'^3}{l_t} \tag{3.1}$$

Kolmogorov proposed that the statistics of small scale motions have a universal isotropic form, unlike the large eddies (which are anisotropic and directional in nature) [90]. The isotropic form of the small scale motions can be uniquely determined by velocity (u_η) and dissipation (ϵ) scales. Length (η), time (τ_η) and velocity scales can be deduced for the small eddies by dimensional analysis as [90]:

$$\eta_\eta = \left(\frac{\nu^3}{\epsilon}\right)^{\frac{1}{4}} \quad , \quad \tau_\eta = \left(\frac{\nu}{\epsilon}\right)^{\frac{1}{2}} \quad , \quad u_\eta = (\nu\epsilon)^{\frac{1}{4}} \tag{3.2}$$

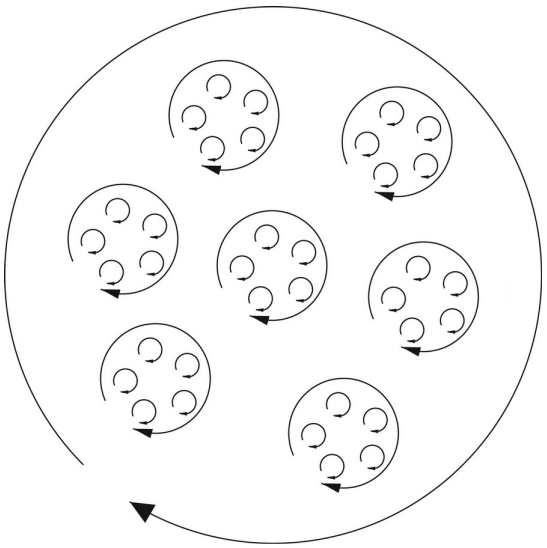

Figure 3.2: Schematic of large eddies containing smaller eddies

3.3 Reynolds averaging

One of the classical statistical methods used to analyse the complex behaviour of turbulence was introduced by Reynolds and involves averaging [129, 163]. The averaged equations are generally known as Reynolds averaged equations. The ensemble averaged form of Reynolds averaging is commonly used for flows that vary in time. In this form of averaging, every variable can be written as the sum of ensemble averaged value and a fluctuation about the mean value [65]; the instantaneous velocity $u_i(\boldsymbol{x}, t)$ can be written as [163]:

$$u_i(\boldsymbol{x}, t) = \overline{u_i(\boldsymbol{x}, t)} + u_i^{'}(\boldsymbol{x}, t), \tag{3.3}$$

where $u_i^{'}(\boldsymbol{x}, t)$ is the fluctuating part and $\overline{u_i(\boldsymbol{x}, t)}$ is the mean velocity [163]. In the case of ensemble averaging the mean velocity, for example, is calculated as [163]:

$$\overline{u_i\left(\boldsymbol{x}, t\right)} = \lim_{N\to\infty} \frac{1}{N} \sum_{n=1}^{N} u_{i,n}\left(\boldsymbol{x}, t\right), \tag{3.4}$$

where $u_{i,n}$ is the value of u_i on the n^{th} repetition out of N independent realisations. When this averaging is used in the conservation equations of mass (eq. (2.19)) and momentum (eq. (2.27) without the body forces) the following equations arise (note that the density is treated as a constant in the following equations) [123, 163] :

Conservation of mass

$$\rho \frac{\partial \overline{u}_i}{\partial x_i} = 0. \tag{3.5}$$

Conservation of momentum

$$\rho \frac{\partial \overline{u}_i}{\partial t} + \rho \frac{\partial}{\partial x_j}\left(\overline{u}_i \overline{u}_j + \overline{u_i^{'} u_j^{'}}\right) = -\frac{\partial \overline{p}}{\partial x_i} + \frac{\partial}{\partial x_j}\left(\overline{\tau}_{ij}\right). \tag{3.6}$$

The unclosed term $\overline{u_i^{'} u_j^{'}}$ is introduced by the averaging into the equations, and is known as the Reynolds stress tensor.

3.4 The closure problem

In a three dimensional flow, there are four unknowns in the instantaneous equation; three velocity components and the pressure component [123]. In modelling turbulence statistically, six Reynolds stress components are introduced, thus increasing the number of unknown quantities to ten. As a consequence, these equations are said to be unclosed [123]. In order to solve these equations, suitable models for the Reynolds stresses are required [163]. Many models have been developed to close the equations and a number are explored in section 3.6.

3.5 RANS simulation of turbulent combustion

Reynolds averaging applied to variable density flows introduces many other unclosed correlations between the dependent variables (denoted as Q) and density variations of the form $\overline{\rho' Q'}$. In order to reduce the number of unclosed terms, mass-weighted averages are usually used (known as **Favre averages** [63, 64]). The definition for the Favre averaging is [63, 64]:

$$\widetilde{Q} = \frac{\overline{\rho Q}}{\overline{\rho}}. \tag{3.7}$$

By using the expression in eq. (3.7) any dependent quantity Q can be split into mean and fluctuating components as:

$$Q = \widetilde{Q} + Q'' \qquad \text{with} \qquad \widetilde{Q''} = 0. \tag{3.8}$$

Using eq. (3.8) Favre averaged equations for variable density flows can be written as follows [91, 118]:

Mass

$$\frac{\partial \overline{\rho}}{\partial t} + \frac{\partial}{\partial x_i}\left(\overline{\rho}\widetilde{u}_i\right) = 0. \tag{3.9}$$

Momentum

$$\frac{\partial \overline{\rho}\widetilde{u}_i}{\partial t} + \frac{\partial}{\partial x_i}\left(\overline{\rho}\widetilde{u}_i\widetilde{u}_j\right) + \frac{\partial \overline{p}}{\partial x_j} = \frac{\partial}{\partial x_j}\left(\widetilde{\tau}_{ij} - \overline{\rho}\widetilde{u_i'' u_j''}\right). \tag{3.10}$$

Chemical species

$$\frac{\partial\left(\overline{\rho}\widetilde{Y_k}\right)}{\partial t}+\frac{\partial}{\partial x_i}\left(\overline{\rho}\widetilde{u_i}\widetilde{Y_k}\right)=-\frac{\partial}{\partial x_i}\left(\overline{V_{k,i}Y_k}+\overline{\rho}\widetilde{u_i''Y_k''}\right)+\overline{\dot{\omega}}_k \qquad for \qquad k=1,2,....N. \tag{3.11}$$

It should be noted here that Favre averaging removes the density fluctuations from the averaged equations, but it does not remove the effects of density fluctuations on turbulence. Hence it is a mathematical simplification and does not represent any physical phenomenon [163].

3.6 Turbulence models

In order to close the averaged equations, models are required for the Reynolds stresses. Many models are available in the literature with different levels of complexity and accuracy [69, 70, 72, 94, 145]. The simplest models are known as the eddy viscosity models (EVM), and are based on the turbulence viscosity approximation introduced by Boussinesq [18]. According to this assumption, the Reynolds stresses are proportional to the mean rate of strain and written as [18]:

$$\overline{\rho}\widetilde{u_i''u_j''}=-\mu_t\left(\frac{\partial\widetilde{u}_i}{\partial x_j}+\frac{\partial\widetilde{u}_j}{\partial x_i}-\frac{2}{3}\delta_{ij}\frac{\partial\widetilde{u}_k}{\partial x_k}\right)+\frac{2}{3}\overline{\rho}\widetilde{k}\delta_{ij}, \tag{3.12}$$

where μ_t is the eddy viscosity and k is the turbulence kinetic energy, defined as [123]:

$$\widetilde{k}=\frac{\widetilde{u_i''u_i''}}{2}. \tag{3.13}$$

The eddy viscosity is a product of a length and a velocity scale and represents the ratio of the turbulent quantities (Reynolds stresses) to mean flow quantities (mean shear) [163]. It should be noted that μ_t is not a fluid property, instead it depends on the geometry and the turbulent eddies present in the flow. A suitable way of defining the eddy viscosity is required and different models are proposed.

3.6.1 Zero equation model

The simplest form of EVM was proposed by Prandtl and is known as the zero equation or mixing length model [124]. According to this model the eddy viscosity

is approximated in terms of a mixing length [124]. According to this model the Favre averaged form of the eddy viscosity can be expressed as:

$$\mu_t = l_{mix}^2 \overline{\rho} \left\| \widetilde{S} \right\|, \tag{3.14}$$

where l_{mix} is the mixing length and is usually defined by an algebraic expression which varies according to the local flow conditions [155]. $\left\| \widetilde{S} \right\|$ is the strain invariant and is defined as :

$$\left\| \widetilde{S} \right\| = \sqrt{2\widetilde{S_{ij}S_{ij}}}. \tag{3.15}$$

Note that l_{mix} provides a length scale for turbulence. The model in eq. (3.14) is computationally inexpensive, but has a number of shortcomings, i.e. it gives a zero value for the turbulent viscosity whenever the velocity gradients go to zero [163]. Additionally, prescribing the mixing length for complex flows is difficult as l_{mix} is different for each flow configuration, and must be specified a priori to obtain a correct solution [163]. The model also fails to accurately predict flows with separation and recirculation [155].

3.6.2 One equation model

Turbulence energy equation models have been developed to include non-local and flow history effects through the eddy viscosity formulation, as the eddy viscosity is no longer based solely on a set mixing length. One of these models (proposed by Prandtl [125]) requires the solution to a modelled equation for the turbulence kinetic energy $\widetilde{k}$, in addition to the local mean velocity. According to this model the turbulent viscosity is calculated as [125]:

$$\mu_t = C\overline{\rho}\sqrt{\widetilde{k}}l_t, \tag{3.16}$$

where l_t is a turbulence length scale and C is a constant. In order to calculate $\widetilde{k}$ a transport equation is required [125]:

$$\frac{\partial \overline{\rho}\widetilde{k}}{\partial t} + \frac{\partial \overline{\rho}\widetilde{u_i k}}{\partial x_i} = \overline{\rho}\widetilde{u_i' u_j'}\frac{\partial \widetilde{u}_i}{\partial x_j} - \overline{\rho}\widetilde{\epsilon} + \frac{\partial}{\partial x_j}\left[\left(\mu + \frac{\mu_t}{\sigma_k}\right)\frac{\partial \widetilde{k}}{\partial x_j}\right], \tag{3.17}$$

where σ_k is the turbulent Schmidt number. Now in order to close the $\widetilde{k}$ equation a closure for $\widetilde{\epsilon}$ is needed [125]:

$$\widetilde{\epsilon} = C_l \frac{\widetilde{k}^{3/2}}{l_t}, \tag{3.18}$$

where C_l is a constant. It should be noted here that the turbulence length scale l_t still needs to be prescribed and is difficult for complex flows for similar reasons to those mentioned before.

3.6.3 Two equation models

In recirculating flows where production and destruction of turbulence are significantly different due to convection and diffusion, more complex models are required. Two equation models are considered to be complete models, as they do not require any prior knowledge of turbulent structures in order to predict properties of a given flow [163]. These models use transport equations for both length and velocity scales. Most of these models solve the transport equation for $\widetilde{k}$, and for some other quantity in order to calculate eddy viscosity. The differences between these models lie in the choice of the second variable. Here only the $k-\epsilon$ model is discussed in detail.

3.6.3.1 The $k-\epsilon$ model

The most common form of the model was developed by Jones and Launder [81] and is known as the standard form of the $k-\epsilon$ model. This model considers the dynamics of turbulence and focuses on the mechanisms which affect the turbulent kinetic energy [155]. This model uses k and ϵ to define a time scale (τ_t) and a length scale (l_t) which represent the large scale turbulence as:

$$\tau_t = \frac{\widetilde{k}}{\widetilde{\epsilon}} \text{ and } l_t = \frac{\widetilde{k}^{3/2}}{\widetilde{\epsilon}}. \tag{3.19}$$

It is assumed that at high Reynolds numbers, the rate at which large eddies extract energy from the mean flow is approximately equal to the rate of transfer of energy to the small (dissipating) eddies, assuming that the flow does not change too rapidly [155]. Applying dimensional analysis to the time and length scales

the following expression for eddy viscosity can be obtained [81]:

$$\mu_t = C_\mu \overline{\rho} \frac{\widetilde{k}^2}{\widetilde{\epsilon}}, \tag{3.20}$$

where C_μ is an empirical dimensionless constant [81]. The turbulent kinetic energy $\left(\widetilde{k}\right)$ and its dissipation rate $(\widetilde{\epsilon})$ in eq. (3.20) can be described by the two balance equations; one for $\widetilde{k}$ (mentioned in eq. (3.17)) and the other for $\widetilde{\epsilon}$, written as [81, 93]:

$$\frac{\partial \overline{\rho}\widetilde{\epsilon}}{\partial t} + \frac{\partial \overline{\rho}\widetilde{u_i}\widetilde{\epsilon}}{\partial x_i} = \frac{\partial}{\partial x_i}\left[\left(\mu + \frac{\mu_t}{\sigma_\epsilon}\right)\frac{\partial \widetilde{\epsilon}}{\partial x_i}\right] - C_{\epsilon 1}\overline{\rho}\widetilde{u_i'u_j'}\frac{\widetilde{\epsilon}}{\widetilde{k}}\frac{\partial \overline{u}_i}{\partial x_j} - C_{\epsilon 2}\overline{\rho}\frac{\widetilde{\epsilon}^2}{\widetilde{k}}. \tag{3.21}$$

It should be noted that the exact equation for $\widetilde{\epsilon}$ is more complicated than that for the $\widetilde{k}$ equation. Although an exact equation can be derived from the Navier Stokes equations, it is not useful as it involves many unknown double and triple correlations for velocities and pressure [123]. The modelled $\widetilde{\epsilon}$ equation is best viewed as being entirely empirical [123]. The terms containing σ_k and σ_ϵ in eq. (3.17) and eq. (3.21) represent the respective turbulent transport of $\widetilde{k}$ and $\widetilde{\epsilon}$. The model constants $C_\mu, C_{\epsilon 1}$ and $C_{\epsilon 2}$ in eq. (3.17) and eq. (3.21) are given in table 3.1. These coefficients are estimated from experimental data, such as decaying grid turbulence and homogeneous flows [123].

C_μ	σ_k	σ_ϵ	$C_{\epsilon 1}$	$C_{\epsilon 2}$
0.09	1.0	1.3	1.44	1.92

Table 3.1: Values of the empirical constants in the $k-\epsilon$ model

The standard $k-\epsilon$ model is one of the most widely used and validated turbulence models [155]. It has been shown to work well in flows with simple two-dimensional thin shear where the mean curvature and local pressure gradients are small [123]. The model is simple and effective in terms of computational costs but there are a number of problems. These include prediction of flows in the near wall (boundary layer) regions at low Reynolds numbers [123], and the underestimation of velocity fluctuations induced by low frequency motions associated with intermittency and flapping. These flows are not predicted accurately by the standard $k-\epsilon$ model and require more sophisticated modelling [123].

However, it should be noted that the standard $k-\epsilon$ model does provide length and time scale information that can be used in the modelling of additional processes such as combustion [123]. Furthermore, as statistically steady two dimensional shear flows have been investigated in this thesis, the use of the standard $k-\epsilon$ model is justified. A detailed comparison of turbulence modelling is beyond the scope of this thesis, and more details on turbulence models can be found in [61, 68, 70, 92, 93, 95, 123, 145, 163].

4 Premixed turbulent combustion

Different properties of premixed combustion are discussed in this chapter. The idea of laminar flame thickness and laminar flame speed is introduced, followed by adiabatic flame temperature and the progress variable. Different regimes of turbulent combustion are then discussed, leading to the laminar flamelet concept.

4.1 Laminar flame thickness

A flame thickness is usually required for combustion simulations; it is used as a reference length scale, in order to determine the mesh resolution, to distinguish between combustion regimes (discussed later) and also for modelling scalar dissipation (discussed later) [35, 118]. There are several approaches available in the literature to define the thickness for premixed flames, but it is very difficult to define the thickness with accuracy [35]. Two approaches are usually used to define the thickness of the flame. One approach makes use of variables such as temperature (useful in the case of simplified chemistry treatments). The other approach is to make use of a length scale corresponding to the radicals, which is mostly confined to detailed chemistry approaches [118]. Only the simple chemistry approach is discussed here.

An approximate estimate for the flame thickness is shown in figure 4.1. One approach is to use the temperature profile and take the inverse of the normalised maximum temperature gradient thus giving the thermal thickness as [35, 118]:

$$\delta_L^0 = \frac{T_P - T_R}{max\left(\frac{\partial T}{\partial x}\right)}. \tag{4.1}$$

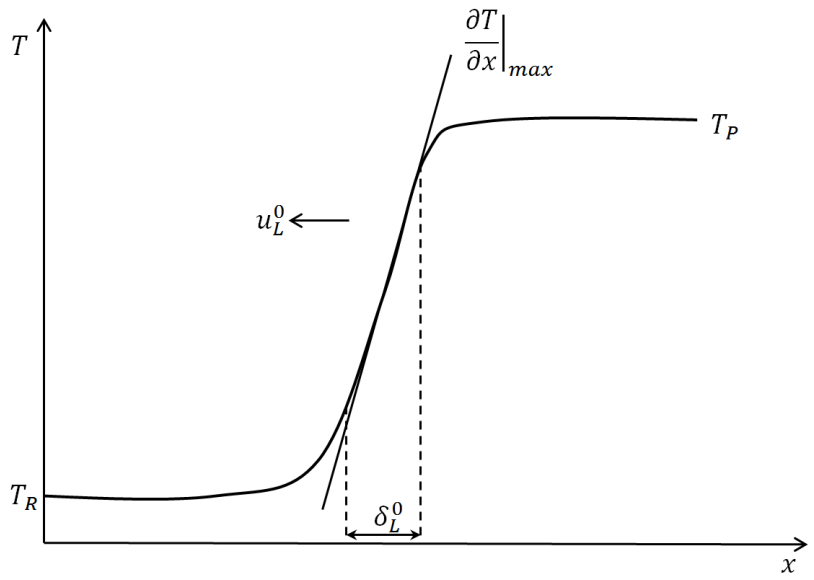

Figure 4.1: Laminar premixed flame thickness

Another approach based on order of magnitude analysis can be adopted and yields the diffusive thickness [118]. This approach makes use of the thermal properties of the flame and relates the flame thickness to the laminar burning velocity (discussed later) [117]:

$$\delta_L = \frac{\lambda}{\rho C_p u_L^0}, \tag{4.2}$$

where λ is the heat conductivity and C_p is the specific heat capacity at constant pressure, u_L^0 is the laminar burning velocity. In the case of unit Lewis number, eq. (4.2) can be expressed as [35, 117]:

$$\delta_L = \frac{\nu_R}{u_L^0}, \tag{4.3}$$

where ν_R is the kinematic viscosity of the reactants. This approach does not make use of any details of the local flame profile, so the values for λ, C_p and ν_R must be chosen carefully. These quantities vary strongly within the flame structure [35].

The thermal flame thickness and the diffusive flame thickness can be correlated as [13]:

$$\delta_L^0 = 2\delta_L \left(\frac{T_P}{T_R}\right)^{0.7}. \tag{4.4}$$

The expression in eq. (4.4) gives a fairly good estimate of the thermal flame thickness δ_L^0, given that the final temperature T_P is known before the calculation [118].

4.2 Burning velocities

In premixed flames, the laminar and turbulent burning velocities are of paramount interest [117]. These quantities give information about the velocities at which the flame front propagates normal to itself and the rate at which the flame can convert reactants into products [35].

4.2.1 Laminar burning velocity

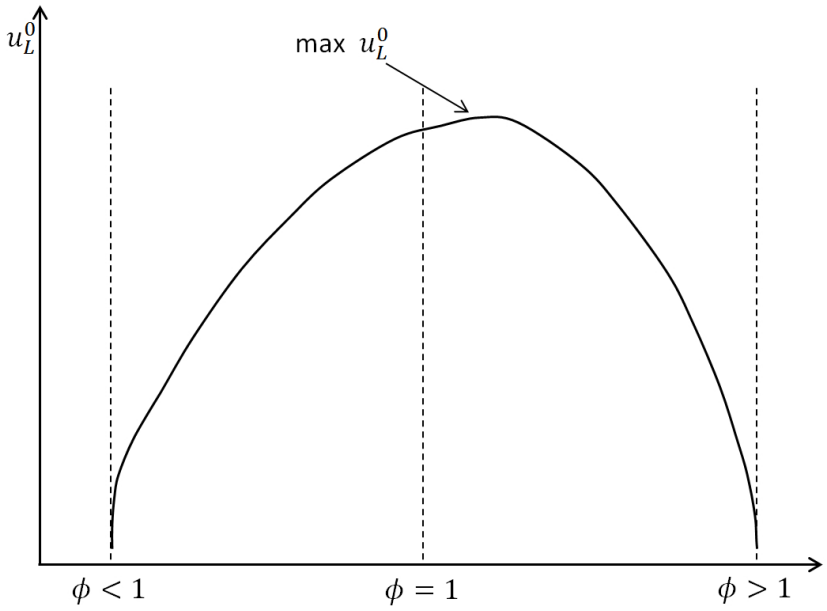

Figure 4.2: Change in laminar burning velocity with change in equivalence ratio

The laminar burning velocity u_L^0 is a thermochemical quantity and depends on the equivalence ratio ϕ, the temperature and the pressure of the unburnt mixture. Detailed measurements for different fuels and conditions have been carried out for the laminar burning velocity, which is usually less than $1m/s$ [35]. Experimental data on laminar flame speeds for different fuels and equivalence ratios can be

found in [67, 108]. The general trends for laminar burning velocity with change in equivalence ratio are shown in figure 4.2.

4.2.2 Turbulent burning velocity

The turbulent burning velocity u_T is defined by Cant and Mastorakos as [35]:

> *"The velocity with which the turbulent flame brush advances relative to the reactants, in the direction normal to itself and towards the reactants"* .

Turbulent burning velocity is not entirely dependent on the thermochemistry, but also depends on the properties of turbulence.

Damköhler [54] proposed that a mathematical expression can be obtained in case of one dimensional turbulent flame propagation, by making use of the chemical species transport equation in the reference frame of the flame and making use of continuity:

$$\rho_R u_T \frac{\partial \widetilde{Y_F}}{\partial x_i} = -\frac{\partial}{\partial x_i}\left(\overline{V_{F,i} Y_F} + \overline{\rho} \widetilde{u_i'' Y_F''}\right) + \overline{\dot{\omega}}_F, \tag{4.5}$$

where Y_F is the mass fraction of fuel and V_F is the diffusion velocity of fuel. Integrating the expression in eq. (4.5) between $x = -\infty$ to $x = \infty$ inside a control volume leads to [118]:

$$A \rho_R Y_F^R u_T = -\int_{-\infty}^{\infty} \dot{\omega}_F dV, \tag{4.6}$$

where $\dot{\omega}_F$ is the local reaction rate of the fuel, ρ_R and Y_F^R are the density and fuel mass fraction in the reactants respectively. A is the cross sectional area of the control volume which contains the flame as shown in figure 4.3. In eq. (4.6) it is assumed that the turbulent flame is statistically stationary, and that all the fuel entering the control volume is consumed entirely by combustion [118]. Damköhler proposed that the local reaction rate per unit area can be represented as $\rho_R Y_F^R u_L^0$, if it is assumed that locally the flame propagates at the laminar flame speed u_L^0

[54], thus giving [118]:

$$-\int_{-\infty}^{\infty} \dot{\omega}_F dV = A_T \rho_R Y_F^R u_L^0, \tag{4.7}$$

where A_T is the surface area of the wrinkled laminar flame. Now substituting eq. (4.6) in eq. (4.7) gives [54]:

$$\frac{u_T}{u_L^0} = \frac{A_T}{A}. \tag{4.8}$$

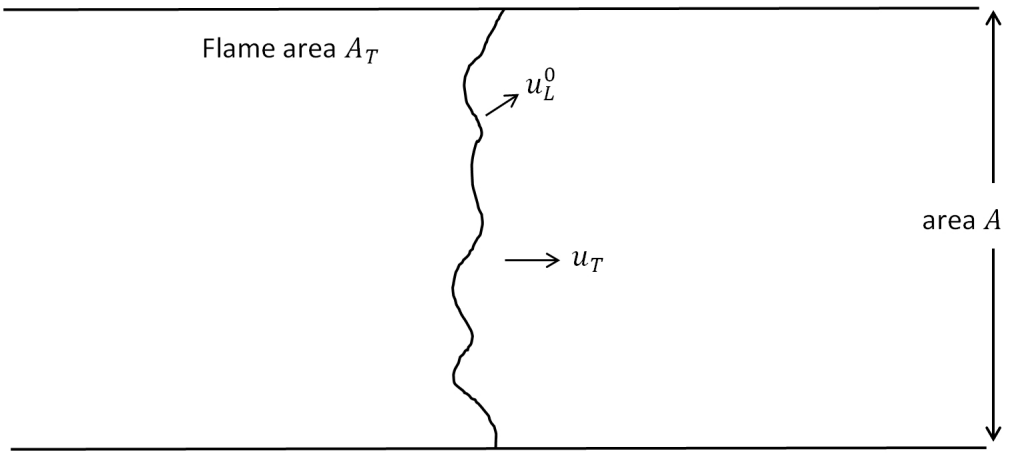

Figure 4.3: Turbulent flame speed using Damköhler's analysis

The expression in eq. (4.8) shows that, when there is an increase in the total flame surface area A_T, the consumption rate increases for the same cross section A. This increases the turbulent flame speed u_T, compared to the laminar flame speed u_L^0. The ratio A_T/A is the flame wrinkling factor, and is the ratio of the available flame area to its projection in the propagating direction [118]. It is important to note that Damköhler's hypothesis assumes that the internal structure of the wrinkled laminar flame remains unchanged in the presence of turbulence [54], thus giving a base for flamelet modelling of turbulent premixed flames.

Attempts have been made by Peters [116], and Abdel-Gayed et al [2, 1] to relate the magnitude of the velocity fluctuations of fresh gases and turbulent flame speed, one example is [2, 1] :

$$\frac{u_T}{u_L^0} \approx 1 + \hat{C} \left(\frac{u'}{u_L^0} \right)^n, \tag{4.9}$$

where $\hat{C}$ is a constant and depends on the integral length scale l_t, and n is a constant determined experimentally.

All the correlations in literature show almost the same trend [91]; u_T first increases almost linearly with $u^{'}$, then it levels out, before total quenching occurs for intense turbulence, as shown in figure 4.4.

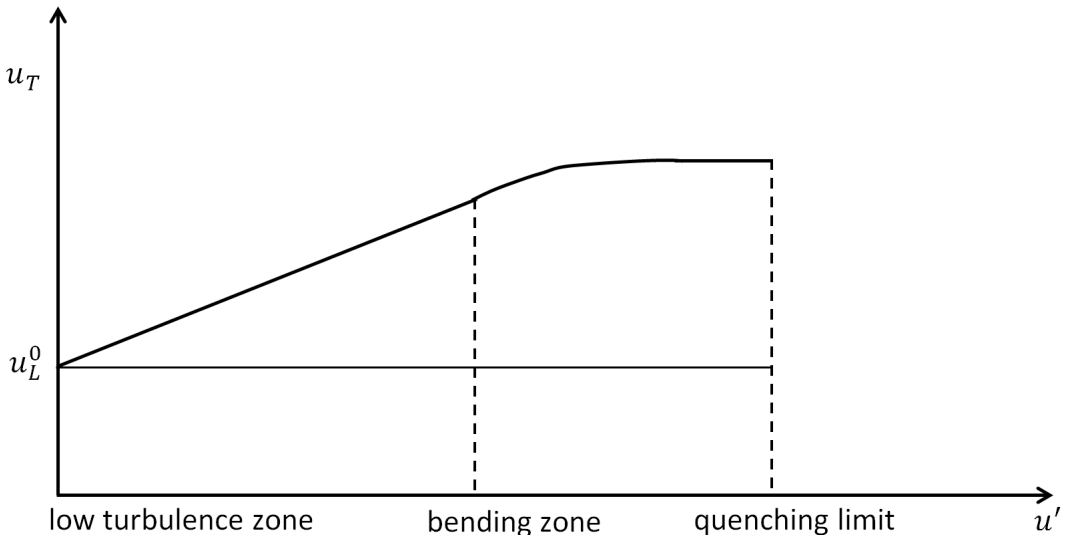

Figure 4.4: Turbulent flame speed plotted against magnitude of turbulent intensity

It can be observed in eq. (4.9) that when A_T/A increases with an increase in the Reynolds number the turbulent flame speed also increases [91, 117]. However, it is hard to predict the bending of the curve in figure 4.4 and determining the quenching limit is even harder [118].

4.3 Adiabatic flame temperature

If an air fuel mixture is considered to be burnt completely at constant pressure and if no external heat or work transfer takes place, then all the energy released by the chemical reaction heats the products [91, 96]. This forms the basis of the adiabatic flame temperature assumption.

- It is assumed that all species have the same molecular weight ($W_k = W$), equal specific heat capacities ($C_{p,k} = C_p$) and equal diffusion coefficients

($D_k = D$). This implies that the Lewis numbers for all species are equal ($Le_k = Le$), and the species and heat diffuse in the same manner.

- Chemistry proceeds through one irreversible reaction.
- The reaction rate $\dot{\omega}_F$ of the reaction in eq. (2.12) is assumed to be limited by the fuel mass fraction; oxidiser mass fraction is not considered.

Now using the mass fraction of fuel in the reference frame of the flame for a steady flame (i.e. flame moving at the laminar flame speed u_L^0) gives [118]:

$$\rho u = const = \rho_R u_L^0, \tag{4.10}$$

$$\rho_R u_L^0 \frac{dY_F}{dx} = \frac{d}{dx}\left(\rho D \frac{dY_F}{dx}\right) + \dot{\omega}_F, \tag{4.11}$$

$$\rho_R C_p u_L^0 \frac{dT}{dx} = \frac{d}{dx}\left(\lambda \frac{dT}{dx}\right) - Q\dot{\omega}_F. \tag{4.12}$$

In eq. (4.11) and eq. (4.12) diffusive terms on both sides of the flame are zero, as $\lim_{x\to\infty} \frac{\partial Y_F}{\partial x} \to 0$. The inlet speed is equal to the laminar flame speed so that the following expressions are obtained [118]:

$$\rho_R u_L^0 Y_F^R = -\int_{-\infty}^{+\infty} \dot{\omega}_F dx = \Omega_F, \tag{4.13}$$

$$\rho_R C_p u_L^0 \left(T_P - T_R\right) = -Q \int_{-\infty}^{+\infty} \dot{\omega}_F dx = Q\Omega_F, \tag{4.14}$$

where Ω_F is the total fuel consumption in the flame and Q is the heat release due to complete combustion. The expression in eq. (4.13) shows that all the fuel entering the domain $\left(\rho_R Y_F^R u_L^0\right)$ is burnt downstream in the flame front due to Ω_F [118]. The expression in eq. (4.14) shows that the power released by the combustion ($Q\Omega_F$) is completely converted into sensible energy, which increases the temperature of the gas ($\rho_R C_p u_L^0$) from T_R to T_P. An expression for the adiabatic flame temperature can be obtained by equating eq. (4.13) and eq. (4.14) :

$$C_p \left(T_P - T_R\right) = Q Y_F^R, \tag{4.15}$$

rearranging eq. (4.15) gives:

$$T_P = T_R + \frac{QY_F^R}{C_p}. \tag{4.16}$$

4.4 Progress variable

The expressions in eq. (4.12) and eq. (4.11) can be further simplified by introducing reduced variables [118]:

$$Y = \frac{Y_F}{Y_F^R}, \tag{4.17}$$

and

$$c = \frac{C_p\left(T - T_R\right)}{QY_F^R} = \frac{T - T_R}{T_P - T_R}, \tag{4.18}$$

where Y is the reduced mass fraction of fuel and c is the progress variable. The reduced mass fraction of fuel Y changes from 1 in the fresh gases to 0 in the burnt gases, whereas c changes from 0 in the fresh gases to 1 in the burnt gases. Now, using eq. (4.11), eq. (4.12) and substituting T_P from eq. (4.16) gives [118]:

$$\rho_R u_L^0 \frac{dY}{dx} = \frac{d}{dx}\left(\rho D \frac{dY}{dx}\right) + \frac{\dot{\omega}_F}{Y_F^R}, \tag{4.19}$$

$$\rho_R u_L^0 \frac{dc}{dx} = \frac{d}{dx}\left(\frac{\lambda}{C_p}\frac{dc}{dx}\right) - \frac{\dot{\omega}_F}{Y_F^R}. \tag{4.20}$$

Adding eq. (4.19) and eq. (4.20) under the unit Lewis number assumption gives:

$$\rho_R u_L^0 \frac{d}{dx}\left(c + Y\right) = \frac{d}{dx}\left[\rho D \frac{d}{dx}\left(c + Y\right)\right]. \tag{4.21}$$

The expression in eq. (4.21) has no source term and is a passive scalar equation. As $c + Y = 1$ in both burnt and fresh gases, the only valid solution is [118]:

$$c + Y = 1. \tag{4.22}$$

It is an important property of premixed flames and can also be explained by stating that the total enthalpy of the mixture is constant everywhere. In case of incompressible (low Mach number) flows with unit Lewis number and adia-

batic conditions at the boundaries the temperature and mass fractions are not independent of each other. They are in fact linked through chemical and sensible enthalpies. As the mass fraction of fuel decreases the chemical enthalpy decreases, and as the temperature increases the sensible enthalpy increases [118].

4.5 Premixed turbulent combustion regimes

A direct approach to model the mean reaction rates based on the Arrhenius law cannot be used because of the large number of unclosed quantities i.e. the correlations between species concentrations and temperature fluctuations (the term on the right side of eq. (2.15)) [118]. The derivation of models is based on physical analysis and the comparison of various length and time scales involved in combustion. These length and time scales can conveniently be represented on a combustion regime diagram [35, 117, 118]. Various regimes can be identified by using non dimensional parameters [118]. These diagrams define combustion regimes in terms of length and velocity scales, i.e. integral length scale, turbulent kinetic energy and its dissipation rate. The diagrams indicate if the flow contains flamelets (thin reaction zones) or pockets/distributed reaction zones [118]. All of the above mentioned information is necessary in order to build a combustion model. These diagrams are based on intuitive arguments and make use of order of magnitude arguments rather than exact numbers [35].

4.5.1 Dimensionless numbers for turbulent premixed combustion

Turbulent premixed combustion can be described as the interaction of a flame front with an ensemble of eddies representing turbulence [35]. The flame front depends on the flame thickness δ_L^0 and laminar flame speed u_L^0 [118]. The eddy sizes range from the Kolmogorov scales η to the integral scales l_t [35]. The characteristic velocities also range from the Kolmogorov velocities u_η to the integral scale velocities $u^{'}$. If the turbulence is assumed to be homogeneous and isotropic,

then the velocity $u^{'}$ and eddy size l_t can be linked as [118, 35]:

$$\epsilon \approx \frac{u^{'3}}{l_t}, \tag{4.23}$$

where ϵ is the local dissipation rate of turbulent kinetic energy. The characteristic time scale of an eddy of size l_t is defined as [118]:

$$\tau_t = \frac{l_t}{u^{'}} = \left(\frac{l_t^2}{\epsilon}\right)^{1/3}. \tag{4.24}$$

The time scale for a typical flame is defined as the time needed for the flame to move a distance corresponding to its own thickness (it can also be referred to as diffusion time scale). It is represented as [118]:

$$\tau_c = \frac{\delta_L^0}{u_L^0}. \tag{4.25}$$

When eq. (4.24) is divided by eq. (4.25), Damköhler number is obtained [35, 164]:

$$Da = \frac{\tau_t}{\tau_c} = \frac{\tau_t}{\tau_c} = \frac{l_t}{\delta_L^0}\frac{u_L^0}{u^{'}}. \tag{4.26}$$

Da is defined for the largest eddies, and is the ratio of integral time scale τ_t to the chemical time scale τ_c [120].

Basically there are two parameters in which the value of l_t is relevant in controlling the flame structure. One of the parameters is the Damköhler number, and the second parameter is the Karlovitz number Ka [118]. The Karlovitz number is defined for the smallest eddies, and is the ratio of the chemical time scale τ_c to the Kolmogorov time scale [118, 35, 31]:

$$Ka = \frac{\tau_c}{\tau_\eta} = \frac{u^{'}}{u_L^0}\frac{\delta_L^0}{\eta}. \tag{4.27}$$

The Karlovitz number can also be written as [118, 35, 115]:

$$Ka = \left(\frac{l_t}{\delta_L^0}\right)^{-1/2}\left(\frac{u^{'}}{u_L^0}\right)^{3/2} = \left(\frac{\delta_L^0}{\eta}\right)^2 = \frac{\sqrt{\frac{\epsilon}{\nu}}}{\frac{u_L^0}{\delta_L^0}}. \tag{4.28}$$

4.5.2 The regime diagram

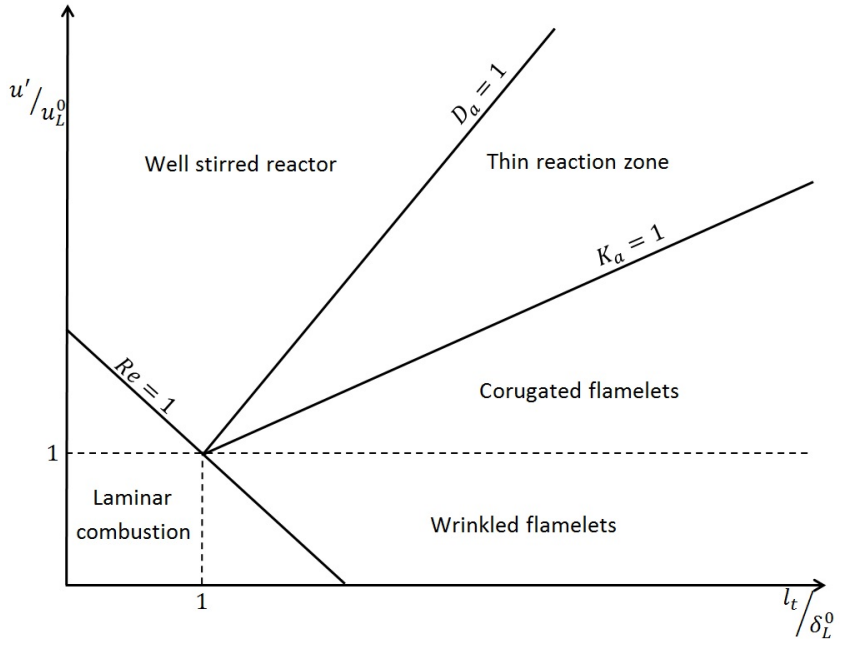

Figure 4.5: Classical turbulent combustion diagram

Different flame behaviour can be summarised on a regime diagram also known as the Borghi diagram, as it was first proposed by Borghi [15]. The regimes can be plotted on a combustion diagram as a function of non-dimensionalised length (l_t/δ_L^0) and non-dimensional velocity $\left(u^{'}/u_L^0\right)$ [118]. This is shown in figure 4.5. The diagram is divided into distinct regions by lines representing Reynolds number, Damköhler number and Karlovitz number.

4.5.3 Laminar flame regime

The laminar flame exists in the region where the Reynolds number is low, i.e. the flow field is laminar.

4.5.4 Thin flamelet regime

When Da is large ($Da \gg 1$) and ($Ka \ll 1$), the chemical time scale is small compared to the eddy time scale, and turbulence does not significantly affect the

inner structure of the flame [35, 118]. In this case the flame remains close to a laminar flame, but wrinkled by turbulent motions [35, 117, 118]. The flame thickness is smaller than the smallest turbulent scale. This regime can be further divided into two regions depending on the velocity ratio $u^{'}/u_L^0$ [117, 118].

4.5.4.1 Wrinkled flamelet regime

This occurs when $u^{'} < u_L^0$ the speed of the turbulent motion is small, so the flame sheet is slightly wrinkled by turbulence [117].

4.5.4.2 Corrugated flamelet regime

This occurs when $u^{'} > u_L^0$ the speed of the turbulent motion becomes larger than the flame speed, thus the flame sheet is strongly wrinkled [35]. This leads to the formation of pockets of fresh and burnt gases [118].

4.5.5 Thin reaction zone regime

In this regime the turbulent integral time scale is larger than the chemical time scale ($Ka > 1$ also $Da > 1$) [35, 118]. But the Kolmogorov scales are smaller than the flame thickness, thus the inner flame structure is modified by these scales [118, 35]. The flame front is no longer laminar, but is still a wrinkled flame [118]. It can be noticed in eq. (4.28) that when the stretch induced by Kolmogorov scale becomes larger than the critical flame stretch (u_L^0/δ_L^0), it leads to flame quenching [118].

4.5.6 Well stirred reactor limit

When $Da < 1$ the turbulent characteristic time scale is shorter than the chemical reaction time scale τ_c [118]. In this regime mixing is fast and the over all reaction is limited by chemistry [117].

4.6 Laminar flamelet concept

Premixed combustion of practical interest has fast (but it is not infinitely fast) chemistry, so molecular transport and chemistry are strongly coupled on short

length scales within the flame [35]. This gives the flame a sheet like structure. In flames which are not strongly distorted by turbulence, the local structure of the flame sheet is almost the same as that of a laminar flame [31]. In this case, chemistry can be separated from turbulence, and laminar flame properties can be used to calculate the reaction rates and transport properties. The mean flow features can be calculated by the turbulence model [35].

Flamelets consist of a thin and highly wrinkled interface which separates reactants and products [115]. This interface contains all the combustion chemistry and the associated heat release, it also includes the related molecular transport effects [35]. In case of premixed flames the flame front can propagate normal to itself, hence the interaction between flamelets and the mean flow are quite strong [115].

4.6.1 Classical turbulence models and the flamelet regime

In classical turbulence models, equations for the moments of dependent variables are derived on the basis of general balance equations [115]. Usually the equations cannot be closed and empirical closures are needed, so the higher moments are related to lower moments. These assumptions are not valid for combustion, as additional length and time scales are introduced via the chemistry, and which are required for the solution [98, 115]. Consequently, additional probability density functions (PDF) are used to obtain moments for reacting flows [115, 119]. A PDF can be calculated at each point in the flow field by making use of a transport equation, but it requires closures for the fluctuating pressure gradient and the molecular diffusion terms [115]. This method is useful as the nonlinear chemical source term does not require any models in case of reactions occurring in thin layers [115, 117]. In this case the molecular diffusion and reaction are closely linked together and the problem shifts towards the modelling of molecular diffusion term [115].

Another approach that gives a more detailed description of the physics involved is the presumed probability density function (PPDF) approach. The idea behind the PPDF approach is that well defined structures pass over a point of observation and contribute to the PDF in a quasi-deterministic way [115]. The occurrence of these structures can be usually represented by a bimodal PDF in

case of premixed combustion provided that the flame remains thin. A presumed PDF can be constructed by making use of certain properties of the structure and the randomness in the flow field [115]. This PDF depends on a number of parameters and can be related to moments of fluctuating variables. This approach forms the basis for the Bray Moss Libby (BML) modelling approach, which is explained in the next chapter.

5 Bray Moss Libby model

Turbulent premixed flames are usually analysed on the basis of an infinitely thin flame front. This makes use of the flamelet regime in figure 4.5. A model for thermochemistry in the flamelet regime was proposed by Bray and Moss [27]. The basic formulation is based on the reduced variable temperature/ progress variable c [118], defined as 0 in the unburned reactants, and 1 in the fully burned products [27]. The progress variable can be related to a particular species mass fraction Y_k as [35]:

$$c = \frac{Y_P}{Y_{PP}} \tag{5.1}$$

where Y_P is the mass fraction of products and Y_{PP} is the mass fraction of products in fully burned product gases. The progress variable can also be related through the adiabatic flame temperature formulation given in section 4.3. The basic assumptions of the analysis are [27]:

- Only two chemical species are to be considered, namely reactants $(1 - c)$ and products (c).
- A single step reaction occurs i.e. $reactants \rightarrow products$, and the rate is determined by the global reaction rate.
- Reactants and products are treated as ideal gases.
- The specific heat at constant pressure is represented by C_p and remains constant. It is the same for both reactants and products.
- Thermal and pressure diffusion effects are considered negligible and binary diffusion is represented by Fick's law.
- The Lewis number is considered to be unity for both reactants and products.

- The Mach number of the flow is much less than unity, so that the pressure and viscous dissipation terms in the enthalpy equation can be neglected.
- Pressure fluctuations are considered small and hence neglected.
- The flow is adiabatic and steady far upstream of the combustion zone.

The BML model based on the adiabatic flame temperature is not useful for compressible flows, flows with heat losses or with non unity Lewis number [35, 100].

5.1 BML probability density function

The BML formulation requires a probability density function (PDF) for c to be specified. The PDF is based on physical arguments. The flame is considered to be made up of thin flamelets; if a probe is inserted into the flame brush at a fixed point then it would pick up reactants for some time and products for the rest of the time [35]. Since the flamelet is very thin the reacting gas crosses the probe only for a very short time interval [35]. The PDF can thus be defined as [27]:

$$P(c;\mathbf{x},t) = \alpha(\mathbf{x},t)\delta(c) + \beta(\mathbf{x},t)\delta(1-c) + \gamma\left(\mathbf{x},t\right) f\left(c;\mathbf{x},t\right) \tag{5.2}$$

where $\delta\left(c\right)$ is the Dirac delta function, $\alpha(\mathbf{x},t)$ is the probability of finding reactants, $\beta(\mathbf{x},t)$ is the probability of finding products and $\gamma(\mathbf{x},t)$ is the probability of finding reacting gas [27]. α , β and γ are non-negative functions of position $(\mathbf{x})$ and time (t) [35]. The function $f(c;\mathbf{x})$ is a continuous function of the progress variable c and satisfies the condition [27]:

$$\int_0^1 f\left(c;\mathbf{x}\right) dc = 1 \tag{5.3}$$

Now integrating the expression in eq. (5.2) with respect to c (i.e. over c space):

$$1 = \int_0^1 \alpha(\mathbf{x},t)\delta(c)dc + \int_0^1 \beta(\mathbf{x},t)\delta(1-c)dc + \int_0^1 \gamma(\mathbf{x},t)f(c;\mathbf{x},t)dc \tag{5.4}$$

The delta functions on the right side of eq. (5.4) integrate individually to unity at $c = 0$ and at $c = 1$, which gives [27]:

$$\alpha(\mathbf{x}, t) + \beta(\mathbf{x}, t) + \gamma(\mathbf{x}, t) = 1 \tag{5.5}$$

where [27]:

$$0 \leq \alpha(\mathbf{x}, t),\ \beta(\mathbf{x}, t),\ \gamma(\mathbf{x}, t) \leq 1 \tag{5.6}$$

The delta functions can be identified at $c = 0$ and $c = 1$ as shown in figure 5.1. The function $f\,(c; \mathbf{x})$ represents the interior distribution of c. It should be noted here that according to the flamelet assumption (explained in section 4.6) the value of $\gamma \ll 1$, thus giving [118]:

$$\alpha(\mathbf{x}, t) + \beta(\mathbf{x}, t) + O(\gamma) = 1 \tag{5.7}$$

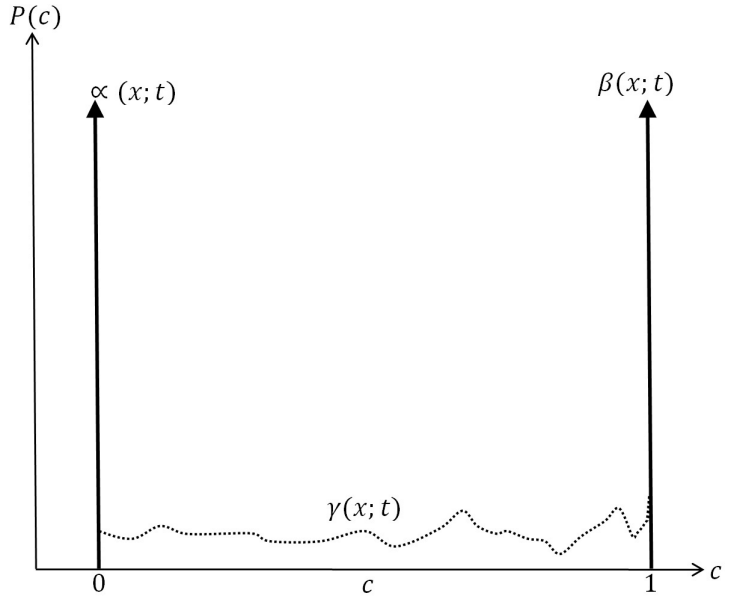

Figure 5.1: BML PDF including Dirac delta functions at $c = 0$ and $c = 1$

5.2 Thermochemistry

In the BML formulation the main thermodynamic variables are related to the reaction progress variable c. This is done by assuming that the enthalpy remains

constant, under which the density can be expressed as [27]:

$$\frac{\rho}{\rho_R} = \frac{1}{1+\tau c}, \tag{5.8}$$

where τ is the heat release parameter and is defined from the first law of thermodynamics for open systems as :

$$\tau = \frac{\rho_R}{\rho_P} - 1. \tag{5.9}$$

At constant enthalpy, the temperature is given as :

$$T = T_R\left(1+\tau c\right). \tag{5.10}$$

Applying Favre averaging to eq. (5.8) and eq. (5.10) gives [26, 117, 35]:

$$\frac{\overline{\rho}}{\rho_R} = \frac{1}{1+\tau\widetilde{c}} \tag{5.11}$$

and

$$\widetilde{T} = T_R\left(1+\tau\widetilde{c}\right), \tag{5.12}$$

respectively. A more detailed derivation for the thermochemistry involved in the BML approach is given in appendix A.

5.3 Evaluation of the BML coefficients

The coefficients $\alpha(\mathbf{x};t)$ and $\beta(\mathbf{x};t)$ can be calculated in terms of the heat release parameter τ and the Favre averaged progress variable $\widetilde{c}$ by making use of eq. (5.2) and eq. (5.7). The Favre averaged progress variable can be defined as :

$$\begin{aligned}\widetilde{c} &= \int_0^1 \frac{\rho c}{\overline{\rho}} P(c;\mathbf{x},t)dc \\ &= \int_0^1 \frac{\rho c}{\overline{\rho}} \alpha\left(\mathbf{x},t\right)\delta(c)dc + \int_0^1 \frac{\rho c}{\overline{\rho}} \beta\left(\mathbf{x},t\right)\delta\left(1-c\right)dc + O(\gamma),\end{aligned} \tag{5.13}$$

as $c = 0$ in reactants, eq. (5.13) reduces to:

$$\widetilde{c} = \frac{\rho_P}{\overline{\rho}} \beta \left(\mathbf{x}; t \right). \tag{5.14}$$

Now making use of the definition of heat release parameter in eq. (A.22) in appendix A gives [19, 27]:

$$\beta \left(\mathbf{x}; t \right) = \frac{\left(1 + \tau \right) \widetilde{c}}{1 + \tau \widetilde{c}} + O(\gamma), \tag{5.15}$$

using eq. (A.22) in appendix A and eq. (5.7) gives [19, 27]:

$$\alpha(\mathbf{x}; t) = \frac{1 - \widetilde{c}}{1 + \tau \widetilde{c}} + O(\gamma). \tag{5.16}$$

The Reynolds average progress variable can also be evaluated as [19]:

$$\begin{aligned} \overline{c} &= \int_0^1 cP \left(c; \mathbf{x}, t \right) dc \\ &= \int_0^1 c\alpha \left(\mathbf{x}, t \right) \delta(c) dc + \int_0^1 c\beta \left(\mathbf{x}, t \right) \delta(c) dc + O(\gamma), \end{aligned} \tag{5.17}$$

as $c = 0$ in reactants

$$\overline{c} = \beta(\mathbf{x}; t), \tag{5.18}$$

and

$$\overline{c} = 1 - \alpha(\mathbf{x}; t). \tag{5.19}$$

A relation between the Reynolds averaging and Favre averaging can be formulated by using $\beta(\mathbf{x}; t)$, as :

$$1 - \beta(\mathbf{x}; t) = \alpha(\mathbf{x}; t) = 1 - \overline{c}, \tag{5.20}$$

further simplification of eq. (5.20) gives [117]:

$$\overline{c} = \frac{\left(1 + \tau \right) \widetilde{c}}{1 + \tau \widetilde{c}}. \tag{5.21}$$

5.4 Favre variance of reaction progress variable

Means and higher moments can be calculated by using the BML formulation. One example of this is Favre variance of c, required for closures of several equations in RANS modelling of premixed combustion. This can be done as [21, 26]:

$$\begin{aligned}\frac{\overline{\rho c'' c''}}{\overline{\rho}} &= \int_0^1 \frac{\rho\,(c-\widetilde{c})}{\overline{\rho}} P\,(c;\mathbf{x},t)\,dc \\ &= \int_0^1 \frac{\rho\,(c-\widetilde{c})}{\overline{\rho}} \alpha\,(\mathbf{x},t)\,\delta(c)dc + \int_0^1 \frac{\rho\,(c-\widetilde{c})}{\overline{\rho}} \beta\,(\mathbf{x},t)\,\delta(1-c)dc + O(\gamma) \\ &= \widetilde{c}\,(1-\widetilde{c}) + O(\gamma). \end{aligned} \tag{5.22}$$

The Favre variance of c can be expressed as a simple function of Favre averages through the BML formulation [35]. Similarly higher moments can be calculated [26]:

$$\begin{aligned}\frac{\overline{\rho c'' c'' c''}}{\overline{\rho}} &= \int_0^1 \frac{\rho\,(c-\widetilde{c})^3}{\overline{\rho}} P\,(c;\mathbf{x},t)\,dc \\ &= \int_0^1 \frac{\rho\,(c-\widetilde{c})^3}{\overline{\rho}} \alpha\,(\mathbf{x},t)\,\delta(c)dc + \int_0^1 \frac{\rho\,(c-\widetilde{c})^3}{\overline{\rho}} \beta\,(\mathbf{x},t)\,\delta(1-c)dc + O(\gamma) \\ &= \widetilde{c}\,(1-\widetilde{c})\,(1-2\widetilde{c}) + O(\gamma). \end{aligned} \tag{5.23}$$

It can thus be seen that BML has reduced the statistical order of the problem in eq. (5.22) and eq. (5.23).

5.5 Joint probability density functions

In order to deal with different statistical quantities involving velocities, the single variable PDF defined in eq. (5.2) can be extended to include the velocity component $u_i(\mathbf{x},t)$ [26, 99]:

$$\begin{aligned} P(c,u_i;\mathbf{x},t) &= \alpha(\mathbf{x},t)\delta(c)P_R(0,u_i;\mathbf{x},t) + \beta(\mathbf{x},t)\delta(1-c)P_P(1,u_i;\mathbf{x},t) \\ &\quad +\gamma\,(\mathbf{x},t)\,f\,(u_i,c;\mathbf{x},t)\,, \end{aligned} \tag{5.24}$$

where $P_R(0, u_i; \mathbf{x}, t)$ and $P_P(1, u_i; \mathbf{x}, t)$ are conditional PDFs with-in the reactants and products respectively. The function $f(u_i, c; \mathbf{x}, t)$ is the joint distribution in the interior of the reacting gas. If the two conditional PDFs and $f(u_i, c; \mathbf{x}, t)$ are normalised individually they integrate to unity, thus satisfying eq. (5.7) [26]. This implies that eq. (5.15) and eq. (5.16) determine the strength of the PDF [26, 99]. As explained earlier $\gamma \ll 1$. The shape of the joint PDF is shown in figure 5.2.

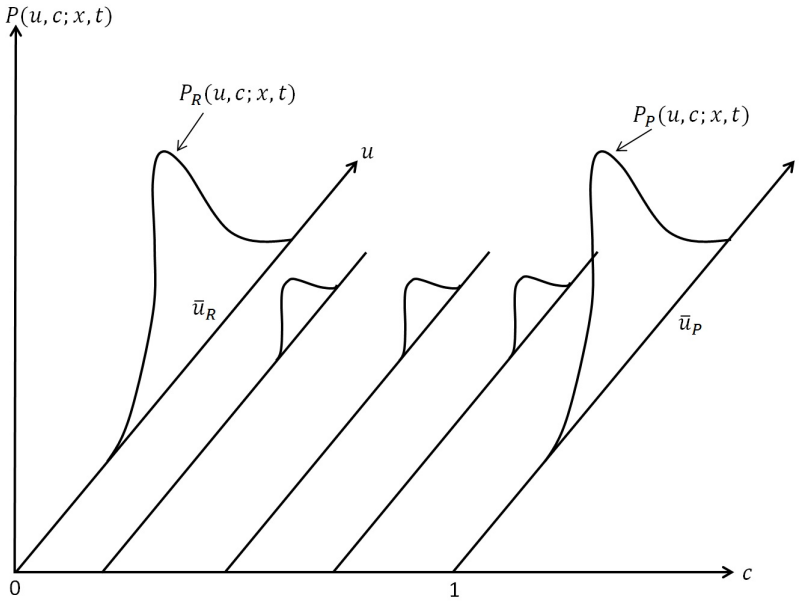

Figure 5.2: Joint PDF of velocity and product concentration in the BML framework

Now making use of the joint PDF expressed in eq. (5.24) to calculate the Favre averaged velocity component gives [99]:

$$\begin{aligned}
\widetilde{u}_i &= \int_{-\infty}^{\infty}\int_0^1 \left(\frac{\rho u_i}{\overline{\rho}}\right) P(c, u_i; \mathbf{x}, t)\, du_i dc \\
&= \int_{-\infty}^{\infty}\int_0^1 \left(\frac{\rho u_i}{\overline{\rho}}\right) \alpha(\mathbf{x}, t)\delta(c) P_R du_i dc + \int_{-\infty}^{\infty}\int_0^1 \left(\frac{\rho u_i}{\overline{\rho}}\right) \beta(\mathbf{x}, t)\delta(1-c) P_P du_i dc + O(\gamma) \\
&= (1 - \widetilde{c})\, \overline{u}_{i,R} + \widetilde{c}\overline{u}_{i,P} + O(\gamma), \qquad (5.25)
\end{aligned}$$

where

$$\overline{u}_{i,R} = \int_{-\infty}^{\infty} u_i P_R(0, u_i; \mathbf{x}, t) du_i, \qquad (5.26)$$

and

$$\overline{u}_{i,P} = \int_{-\infty}^{\infty} u_i P_P(1, u_i; \mathbf{x}, t) du_i. \tag{5.27}$$

A bar is used instead of a tilde to denote conditioned averages, as these averages correspond to constant density ρ_R for $\overline{(\,)}_R$ and $\rho_R/(1+\tau)$ for $\overline{(\,)}_P$ [99]. It should be noted that as a result of the normalisation of the conditional PDFs the conditional quantities do not vanish when $\widetilde{c} \to 0, 1$. As $\widetilde{c} \to 0$, $\overline{u}_{i,R} \to \overline{u}_i$ and $\overline{u}_{i,P} \neq 0$, while as $\widetilde{c} \to 1$, $\overline{u}_{i,P} \to \overline{u}_i$ and $\overline{u}_{i,R} \neq 0$ [26].

5.6 Conservation equations used for the BML model

The conservation equations used for the BML model in RANS calculations are [26, 33]:

Continuity

$$\frac{\partial \overline{\rho}}{\partial t} + \frac{\partial}{\partial x_k}\left(\overline{\rho}\widetilde{u}_k\right) = 0. \tag{5.28}$$

Momentum

$$\frac{\partial\left(\overline{\rho}\widetilde{u}_i\right)}{\partial t} + \frac{\partial}{\partial x_k}\left(\overline{\rho}\widetilde{u}_k\widetilde{u}_i\right) = -\frac{\partial \overline{p}}{\partial x_i} - \frac{\partial}{\partial x_k}\overline{\rho u_k'' u_i''}. \tag{5.29}$$

Progress variable

$$\frac{\partial\left(\overline{\rho}\widetilde{c}\right)}{\partial t} + \frac{\partial}{\partial x_k}\left(\overline{\rho}\widetilde{u}_k\widetilde{c}\right) = -\frac{\partial}{\partial x_k}\overline{\rho u_k'' c''} + \overline{\dot{\omega}}_c. \tag{5.30}$$

Variance of the progress variable

$$\frac{\partial \overline{\rho}\widetilde{c''^2}}{\partial t} + \frac{\partial \overline{\rho}\widetilde{u}_i\widetilde{c''^2}}{\partial x_i} = -\frac{\partial}{\partial x_i}\left(\overline{\rho u_i'' c''^2}\right) - 2\overline{\rho D_c}\widetilde{\frac{\partial c''}{\partial x_k}\frac{\partial c''}{\partial x_k}} - 2\overline{\rho u_i'' c''}\frac{\partial \widetilde{c}}{\partial x_i} + 2\overline{c''\dot{\omega}_c''}. \tag{5.31}$$

5.7 Closures from the BML framework

BML model provides simple algebraic closures for the unclosed terms in the above equations. In order to close eq. (5.30)- eq. (5.31) the following closures are usually

used.

5.7.1 Turbulent transport in BML

Turbulent scalar transport in premixed flames is an important topic. In case of RANS simulations it is usually modelled using the gradient transport assumption. Gradient transport of the mean turbulent flux of a scalar c (progress variable in this case) is generally defined as [97]:

$$\overline{\rho}\widetilde{u_i'' c''} = \frac{-\overline{\rho}\nu_t}{\sigma_c}\frac{\partial \tilde{c}}{\partial x_i}. \tag{5.32}$$

Although eddy viscosity/gradient transport models are used for many types of turbulent flows, they are hard to justify on the basis of physical phenomena [20]. Most arguments regarding turbulent flux are based on flows with constant density. In combustion there are mutual interactions between the flow field and the flame, due to fluctuations in density [21]. Thus giving rise to a new type of turbulent transport mechanism in flames, which leads to net turbulent fluxes in the counter gradient direction [24]. This physical phenomenon is also supported by experimental data [66, 110]. DNS studies have shown that interaction of flames with low turbulence show counter gradient diffusion (CGD), whereas flames interacting with high turbulence levels show gradient diffusion (GD) [160]. DNS studies done by Chakraborty and Cant show the effect of Lewis number on the scalar flux [39] and studies done by Veynante and Poinsot [159] show the effects of pressure gradient on the turbulent transport of the progress variable.

The CGD phenomenon can be explained by dividing the flame into pockets of fully burned products and pockets of cold reactants. The pockets of fully burned products have high temperature and low density, and pockets of cold reactants have high density and low temperature. These pockets are separated by thin zones where the chemical reactions occur [20]. Flames without an externally induced pressure gradient (i.e. open premixed flames) have a self induced mean pressure drop due to heat release [20, 31]. This pressure gradient causes the low density products to accelerate towards the fully burned side of the flame, as well as causing the high density reactants to move towards the unburned side of the flame i.e. $\overline{u}_{i,P} > \overline{u}_{i,R}$ [31, 35] as shown in figure 5.3.

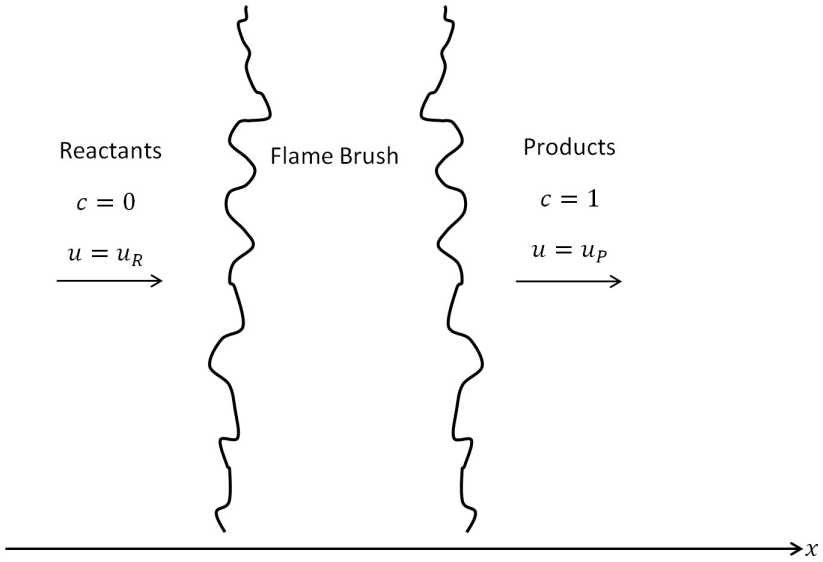

Figure 5.3: Turbulent transport in premixed flames

Interactions between mean pressure and density inhomogeneities are attributed to the buoyancy mechanism [24]. Additional turbulence is generated at values of heat release of practical interest; this is due to interaction of burnt and unburnt pockets of gas with in the flame [24], and leads to a phenomenon which counters the decrease of turbulence energy due to dilatation [21]. If the effects of pressure gradient induced by the hydrodynamics are considered, the interactions are going to result in mean turbulent fluxes different in sign and magnitude from the fluxes predicted by the gradient transport [20]. The physics in this phenomenon is not represented by the standard gradient transport modelling, so more detailed models are required.

By making use of the BML joint probability density function an expression for the Reynolds flux of c can be obtained [97]:

$$\begin{aligned}
\overline{\rho u_i'' c''} &= \int_{-\infty}^{\infty}\int_{0}^{1} \rho\left(u_i - \widetilde{u}_i\right)\left(c - \widetilde{c}\right) P\left(c, u_i; \mathbf{x}, t\right) du_i dc \\
&= \int_{-\infty}^{\infty}\int_{0}^{1} \rho\left(u_i - \widetilde{u}_i\right)\left(c - \widetilde{c}\right) \alpha\left(x,t\right) P_R(0, u_i; \mathbf{x}, t) du_i dc \\
&+ \int_{-\infty}^{\infty}\int_{0}^{1} \rho\left(u_i - \widetilde{u}_i\right)\left(c - \widetilde{c}\right) \beta\left(x,t\right) P_P(1, u_i; \mathbf{x}, t) du_i dc \\
&= \overline{\rho}\widetilde{c}\left(1 - \widetilde{c}\right)\left(\overline{u}_{i,P} - \overline{u}_{i,R}\right). \qquad (5.33)
\end{aligned}$$

Note that according to the gradient transport assumption in eq. (5.32), $\overline{\rho u'' c''} < 0$ and hence, from eq. (5.33) $\overline{u}_{i,P} < \overline{u}_{i,R}$. However, the density of products is typically less than that of the reactants, and the pressure drop across the flame leads to $\overline{\rho u'' c''} > 0$ and $\overline{u}_{i,P} > \overline{u}_{i,R}$ (a result given by eq. (5.33)) [97]. Now, using eq. (5.25) and eq. (5.33) expressions for $\overline{u}_{i,R}$ and $\overline{u}_{i,P}$ can be obtained [97]:

$$\overline{u}_{i,R} = \widetilde{u}_i - \frac{\overline{\rho u_i'' c''}}{\overline{\rho}\,(1-\widetilde{c})} + O(\gamma)\,, \tag{5.34}$$

and

$$\overline{u}_{i,P} = \widetilde{u}_i - \frac{\overline{\rho u_i'' c''}}{(\overline{\rho}\widetilde{c})} + O(\gamma)\,. \tag{5.35}$$

hence

$$\overline{u}_{iP} - \overline{u}_{iR} = \frac{\overline{\rho u_i'' c''}}{\overline{\rho}\widetilde{c}\,(1-\widetilde{c})}. \tag{5.36}$$

Note that $(\overline{u}_{i,P} - \overline{u}_{i,R})$ in eq. (5.36) is known as the slip velocity, and is an important quantity for determining the GD or CGD behaviour in premixed flames. In the DNS studies done by Veynante et al [160], the slip velocity is found to be strongly correlated with the turbulent transport of $\widetilde{c}$. These studies also show that the sign of the slip velocities is a good indication of the occurrence of GD or CGD turbulent transport [160]. This implies that the slip velocity provides a strong base for the physical description of the turbulent diffusion process.

The flame surface averaged flow velocity can be approximated as a weighted average of the mean unburnt and burnt gas velocities :

$$\langle u_i \rangle = (1-K)\,\overline{u}_{iR} + K\overline{u}_{iP}, \tag{5.37}$$

where K is a constant related to the location of the flame, and $\langle u_i \rangle$ is the surface averaged flow velocity. Eq. (5.37) assumes a linear variation of mean flow velocity across the flame [160]. Making use of the BML framework, the unconditional statistics can be related to conditional statistics by eq. (5.25), and by combining eq. (5.25) and eq. (5.37) the following expression is obtained:

$$\langle u_i'' \rangle = \langle u_i \rangle - \widetilde{u} = (K - \widetilde{c})\,(\overline{u}_{iP} - \overline{u}_{iR})\,. \tag{5.38}$$

Eq. (5.38) is combined with eq. (5.33) to give a relation between turbulent diffusion velocity and turbulent flux of $\widetilde{c}$ [160]:

$$\langle u_i^{''} \rangle = \frac{(K - \widetilde{c})}{\widetilde{c}\,(1 - \widetilde{c})} \widetilde{u_i^{''} c^{''}}. \tag{5.39}$$

The expression in eq. (5.39) can now be used to estimate the turbulent flux $\widetilde{u_i^{''} c^{''}}$, through a model for surface averaged velocity fluctuation $\langle u_i^{''} \rangle$.

The following analysis is based on a one dimensional statistical flame. In this case, the flame front remains smooth at low levels of turbulence [49]. The change in velocity of fresh and burnt gases is determined by thermal expansion, and the value is close to that obtained in a planar laminar flame [49]:

$$\overline{u}_P - \overline{u}_R \approx \tau u_L^0. \tag{5.40}$$

Now if a freely propagating turbulent flame without externally imposed pressure gradient is considered, the expression in eq. (5.38) can be re-written as [160]:

$$\langle u^{''} \rangle = (K - \widetilde{c})\, \tau u_L^0. \tag{5.41}$$

In case of high levels of turbulence, the flame front motion is controlled by the turbulent eddies [160]. If it is assumed that $\langle u^{''} \rangle$ varies linearly in $\widetilde{c}$ space then [160]:

$$\langle u^{''} \rangle = -2\,(K - \widetilde{c})\, e u^{'}, \tag{5.42}$$

where $u^{'}$ is the root mean square velocity taken upstream of the flame, e is the efficiency factor. The efficiency factor is included to account for the varying degree of flame distortion/wrinkling produced by turbulent eddies [160]; it ranges from unity for large turbulent eddies to zero in small turbulent eddies (i.e. turbulent length scales are too small to distort the flame front). The reason for this range of e is that the small eddies are strongly affected by viscous dissipation and flame curvature effects, and have too short a life time to exert a significant effect on flame wrinkling [160]. Combining eq. (5.41) and eq. (5.42) [160] gives:

$$\langle u^{''} \rangle = (K - \widetilde{c}) \left(\tau u_L^0 - 2 e u^{'} \right), \tag{5.43}$$

and combining eq. (5.39) and eq. (5.43) gives [160]:

$$\widetilde{u''c''} = \underbrace{\widetilde{c}\,(1-\widetilde{c})\,\tau u_L^0}_{a} - \underbrace{\widetilde{c}\,(1-\widetilde{c})\,2eu'}_{b}. \tag{5.44}$$

5.7.1.1 Criterion for GD/CGD turbulent transport

CGD occurs at positive values of the turbulent transport. This implies that eq. (5.44) should give :

$$\tau u_L^0 - 2eu' \geqslant 0. \tag{5.45}$$

The transition criterion which separates CGD from GD is the Bray number [23, 160]:

$$N_B = \frac{\tau u_L^0}{2eu'}. \tag{5.46}$$

CGD transport is indicated by $N_B \gg 1$; GD transport is indicated by $N_B \ll 1$ [39, 160]. GD becomes less likely with an increase in the heat release τ [160].

The algebraic expression in eq. (5.44) is now compared with standard closure models based on the eddy viscosity concept. The gradient for $\widetilde{c}$ can be written in terms of the thickness δ_B of the turbulent flame brush :

$$\frac{\partial \widetilde{c}}{\partial x} \approx 4\frac{\widetilde{c}\,(1-\widetilde{c})}{\delta_B}. \tag{5.47}$$

Term b in eq. (5.44) can be written as :

$$\widetilde{c}\,(1-\widetilde{c})\left(2 - eu'\right) = \frac{e}{2}\delta_B\sqrt{\widetilde{k}}\frac{\partial \widetilde{c}}{\partial x}, \tag{5.48}$$

where $\widetilde{k}$ is the Favre averaged turbulent kinetic energy. The flame brush thickness δ_B is of the same order as that of the integral length scale l_t upstream of the flame. If δ_B is also taken as the mixing length, then the expression in eq. (5.48) becomes similar to the one equation model described in section 3.6.2 [160]:

$$\widetilde{c}\,(1-\widetilde{c})\left(2eu'\right) = e\frac{\mu_t}{\overline{\rho}\sigma_c}\frac{\partial \widetilde{c}}{\partial x}, \tag{5.49}$$

where σ_c is a turbulent Schmidt number, and the turbulent viscosity ν_t can be obtained by (say) a two equation model. The expression in eq. (5.44) can now

be written as :

$$\widetilde{u''c''} = \widetilde{c}\,(1-\widetilde{c})\,\tau u_L^0 - e\frac{\mu_t}{\overline{\rho}\sigma_c}\frac{\partial\widetilde{c}}{\partial x}. \tag{5.50}$$

The second term in eq. (5.50) is similar to the gradient approximation. The only difference is the introduction of an efficiency function.

This analysis implies that the closure models developed for turbulent non-reactive flows can not be directly used for turbulent reactive flows, and have to be modified to include the flame surface effects.

In this thesis, the turbulent transport of $\widetilde{c}$ in eq. (5.30) is closed by a gradient transport model. The use of this closure is questionable as counter gradient transport is known to occur in premixed flames of practical interest as demonstrated above. The algebraic model discussed in this section makes use of the Bray number, thus introducing uncertainty in modelling via the specification of the efficiency factor (e in eq. (5.50)) involved in the Bray number definition.

In order to avoid the uncertainty introduced by the efficiency factor involved in the Bray number a gradient transport model is used here to close the turbulent transport of $\widetilde{c}$, as the relative behaviour of closures of quantities such as scalar dissipation and their effect on the reaction rate closure can be studied if the model for turbulent transport is kept the same [3, 85, 88, 89, 133, 139].

5.7.2 Reynolds stresses

The Reynolds stresses appearing in eq. (5.29) are usually calculated by using the eddy viscosity type models mentioned in section 3.6. The $k-\epsilon$ model is used in this thesis as explained earlier in section 3.6.3.1. The variable density form of the $k-\epsilon$ model is written as:

Turbulent kinetic energy

$$\frac{\partial\overline{\rho}\widetilde{k}}{\partial t} + \frac{\partial\overline{\rho}\widetilde{u}_i\widetilde{k}}{\partial x_i} = \frac{\partial}{\partial x_j}\left[\left(\mu+\frac{\mu_t}{\sigma_k}\right)\frac{\partial\widetilde{k}}{\partial x_j}\right] - \overline{\rho}\widetilde{u_i''u_j''}\frac{\partial\widetilde{u}_i}{\partial x_j} - \overline{u_i''}\frac{\partial\overline{p}}{\partial x} + \overline{p'\frac{\partial u_k''}{\partial x_k}} - \overline{\rho}\widetilde{\epsilon}. \tag{5.51}$$

Turbulent dissipation

$$\frac{\partial\overline{\rho}\widetilde{\epsilon}}{\partial t} + \frac{\partial\overline{\rho}\widetilde{u}_i\widetilde{\epsilon}}{\partial x_i} = \frac{\partial}{\partial x_i}\left[\left(\mu+\frac{\mu_t}{\sigma_\epsilon}\right)\frac{\partial\widetilde{\epsilon}}{\partial x_i}\right] - C_{\epsilon1}\frac{\widetilde{\epsilon}}{\widetilde{k}}\overline{\rho}\widetilde{u_i''u_j''}\frac{\partial\widetilde{u}_i}{\partial x_j} - C_{\epsilon2}\overline{\rho}\frac{\widetilde{\epsilon}^2}{\widetilde{k}} + C_{\epsilon1}\frac{\widetilde{\epsilon}}{\widetilde{k}}\overline{u_i''}\frac{\partial\overline{p}}{\partial x_i}. \tag{5.52}$$

It can be observed by comparing eq. (5.51) and eq. (3.17) that pressure work and pressure dilatation terms appear in eq. (5.51) because of the density variation effects caused by the heat release. These effects are missing from the standard form of the $k-\epsilon$ model.

5.7.2.1 Pressure work

The pressure work term in eq. (5.51) requires modelling of flame generated turbulence represented by $\overline{u_i''}$. Note that the density variations across the flame brush in case of unit Lewis number flames can be found as [26]:

$$\rho = \frac{\rho_R}{(1+\tau c)} \tag{5.53}$$

where τ the heat release parameter, c is the mass fraction of one species and ρ_R is the density corresponding to $c = 0$. Now making use of eq. (5.53) and the BML framework an expression for $\overline{u_i''}$ can be obtained as [24, 41, 114]:

$$\overline{u_i''} = \frac{\tau\overline{\rho u_i'' c''}}{\overline{\rho}\,(1+\tau\widetilde{c})} \tag{5.54}$$

5.7.2.2 Pressure dilatation

The pressure dilatation term in eq. (5.51) is usually modelled by using a closure proposed by Zhang and Rutland [168] based on their DNS study of a premixed flame. In this model the dilatation effects are approximated as $\tau u_L^0 |\nabla c|$ and it is assumed that the pressure fluctuations depend on $\widetilde{c}$, thus leading to :

$$\overline{p'\frac{\partial u_k''}{\partial x_k}} = \frac{1}{2}\widetilde{c}\left(\tau u_L^0\right)^2\overline{\dot{\omega}}_c. \tag{5.55}$$

Following earlier studies of Bray [26] and Jones [79, 80], the pressure dilatation term has been included in the turbulent kinetic energy transport equation, but not in the turbulent dissipation transport equation as its influence is assumed to be relatively small in magnitude when compared to the other terms in the turbulent dissipation transport equation [26, 79, 80, 88].

5.7.3 Variance of the progress variable

The BML approximation for variance in eq. (5.22) is only valid for a high Damköhler number limit whereas eq. (5.31) allows for departures from the strict BML limit, thus giving a useful degree of flexibility in scalar dissipation and reaction rate modelling. A transport equation for the variance of the progress variable can thus be used instead of the algebraic closure obtained from the BML model.

The turbulent transport term in eq. (5.31) is closed using gradient diffusion assumption as [118]:

$$\overline{\rho u_i'' c''^2} = -\frac{\mu_t}{\sigma_c}\frac{\partial \widetilde{c''^2}}{\partial x_i}, \tag{5.56}$$

and the production term in eq. (5.31) is also closed using the gradient diffusion assumption as [118]:

$$2\overline{\rho u_i'' c''}\frac{\partial \widetilde{c}}{\partial x_i} = -\frac{\mu_t}{\sigma_c}\frac{\partial \widetilde{c}}{\partial x_i}\frac{\partial \widetilde{c}}{\partial x_i}. \tag{5.57}$$

The reaction source term in eq. (5.31) can be closed by using the BML framework as [21]:

$$\overline{\dot{\omega}_c'' c''} = (C_m - \widetilde{c})\,\overline{\dot{\omega}}_c \tag{5.58}$$

Closures for the scalar dissipation term in eq. (5.31) are discussed in detail later.

5.7.4 Reaction rate modelling

In order to close the source term in eq. (5.30) models for the reaction rate are needed and are discussed below.

5.7.4.1 The Eddy Break Up (EBU) model

The Eddy Break Up (EBU) model is used for the analysis of turbulent combustion under the assumption that the Reynolds number is high i.e. $Re \gg 1$ [118]. It is assumed that the reaction rate is controlled by turbulent motion and chemistry does not play any important role in the reaction rate [29, 103]. The reaction zone is considered as a collection of unburnt and burnt gaseous pockets transported by turbulent eddies, and the mean reaction rate depends on a characteristic turbulent

mixing time τ_t [144]. The general expression used is [143]:

$$\overline{\dot{\omega}}_c = C_{EBU}\overline{\rho}\frac{\widetilde{c''^2}}{\tau_{EBU}} \tag{5.59}$$

where C_{EBU} is a constant, and $\widetilde{c''^2}$ represents the fluctuations of the progress variable. The turbulence time τ_t is calculated from the turbulent kinetic energy k and its dissipation rate ϵ and is expressed as :

$$\tau_{EBU} = \frac{\widetilde{k}}{\widetilde{\epsilon}} \tag{5.60}$$

The scalar fluctuations require an estimate and are calculated under the assumption that the flame is infinitely thin [118]. There are some adjustments available for the model constant C_{EBU} to include chemical effects [137]. An improved version of the model has been proposed by Magnussen and Hjertager [103] and is useful for non-premixed combustion.

The eddy break up model is very useful but has an obvious limitation, as it does not include any effects of chemical kinetics [118]. The EBU model has the advantages of being simple and easy to implement with low computational costs. However, since it yields non-zero reaction rates even at low temperatures [118], it overestimates the reaction rate in strained regions where the ratio $\widetilde{\epsilon}/\widetilde{k}$ is high [118]. These regions include flame-holder wakes, walls etc [118]. The accuracy of the EBU model decreases further as the chemical time scale becomes significant with reference to the turbulent time scale.

5.7.4.2 Flamelet surface density model

In case of the thin flamelet assumption the reaction rate can be modelled as the product of flame surface density Σ and the consumption rate per unit of flame area [22]:

$$\overline{\dot{\omega}}_c = \rho_R u_L^0 I_0 \Sigma, \tag{5.61}$$

where Σ is the flamelet surface to volume ratio, u_L^0 is the unstrained laminar flame speed and I_0 is a factor which includes the effects of strain and curvature on the local burning velocity [35, 100]. Note that in eq. (5.61), the effects of

turbulence are included in the reaction rate through Σ, as this quantity measures the flame front convolutions [118]. The higher the flame surface density at a given location, the higher the reaction rate at that location. This approach separates the complex chemistry features (embodied in $u_L^0 I_0$) from turbulence/combustion interactions (modelled by Σ) [118]. The details of closing Σ are discussed in section 6.4.

5.7.4.3 Enhanced EBU model involving scalar dissipation

A reaction rate model based on the scalar dissipation of the progress variable has been proposed by Bray [21] under the BML framework, written as :

$$\overline{\dot{\omega}}_c \backsimeq \frac{1}{2C_m - 1} \overline{\rho} \widetilde{\epsilon}_c, \tag{5.62}$$

where [19]

$$C_m = \frac{\int c\dot{\omega} f(c).dc}{\int \dot{\omega} f(c).dc}, \tag{5.63}$$

and usually for lean hydrocarbons has the value $C_m = 0.75$. $\widetilde{\epsilon}_c$ in eq. (5.62) is known as the scalar dissipation, and is a sink term in eq. (5.31). Note that the effects of turbulence in eq. (5.62) are represented by $\widetilde{\epsilon}_c$, as this quantity represents the mixing rate of the fluid [35]. This approach like the flame surface density approach separates the complex chemistry (represented by C_m) from turbulence/combustion interactions (represented by $\widetilde{\epsilon}_c$). It can be observed in eq. (5.62) that the problem of modelling the mean reaction rate has been reduced to that of modelling the scalar dissipation. Closures for the scalar dissipation $\widetilde{\epsilon}_c$ are discussed in the next chapter.

6 Scalar dissipation in premixed flames

The scalar dissipation rate is one of the most important quantities in combustion modelling. It is one of the key mathematical tools in turbulent combustion and is often a stumbling block in modelling [161]. The scalar dissipation determines the rate at which the scalar fluctuations decay, and it is a measure of the rate at which mixing occurs [35]. It is an important quantity for turbulent reacting flows, as it is directly related to the heat release and species concentration/temperature [19, 105]. In case of turbulent non-premixed flames, scalar dissipation denotes the mixing rate of fuel and oxidiser, whereas in case of premixed flames it represents the rate of mixing of hot and cold fluids on the flame surface required to sustain combustion.

In premixed flames scalar dissipation is strongly coupled with turbulence, chemical and diffusion processes [149]. Experimental studies have shown that scalar dissipation is low in turbulent premixed flames compared with laminar premixed flames [47, 48], the reasons are still unknown and are being studied [149].

Mathematically scalar dissipation rate is defined as [35]:

$$\overline{\rho N_c} = \overline{\rho D_c}\left(\frac{\partial \widetilde{c}}{\partial x_i}\frac{\partial \widetilde{c}}{\partial x_i}\right) + \overline{2\rho D_c \frac{\partial c''}{\partial x_i}\frac{\partial \widetilde{c}}{\partial x_i}} + \overline{\rho D_c \frac{\partial c''}{\partial x_i}\frac{\partial c''}{\partial x_i}} \tag{6.1}$$

where c is the progress variable and D_c is the diffusivity of the progress variable. Usually in turbulent mixing studies, the scalar dissipation is based on the gradients of the fluctuations, as the gradient of the mean progress variable is negligible compared to the gradients of fluctuations; $\overline{\rho N_c} \approx \overline{\rho}\widetilde{\epsilon}_c$, where

$$\widetilde{\epsilon}_c = D_c\left(\widetilde{\frac{\partial c''}{\partial x_i}\frac{\partial c''}{\partial x_i}}\right). \tag{6.2}$$

The scalar dissipation $\widetilde{\epsilon}_c$ appears explicitly in the transport equation for the variance of the progress variable $\widetilde{c''^2}$ in eq. (5.31), and is one half of the dissipation rate of $\widetilde{c''^2}$. Modelling of $\widetilde{\epsilon}_c$ with the turbulent time scale alone is insufficient for premixed flames, as there is strong coupling between turbulence, chemical, and molecular-diffusion processes [40, 86, 104, 149].

Transport equations for $\widetilde{\epsilon}_c$ were developed for buoyancy driven mixing layers and for high Reynolds number turbulent flows involving mean scalar gradients by Zeman and Lumley [167] and Jones and Musonge [82], but did not take chemical effects into account. Balance equations for $\widetilde{\epsilon}_c$ with chemical effects have been studied by Mantel and Borghi [105] and Mura and Borghi [111], but the fluid density has been treated as a constant, thus ignoring the effects of heat release. Recently a balance equation has been developed by Swaminathan and Bray [149], which includes the effects of heat release and the associated thermal expansion and is discussed in the next section.

6.1 Transport equation for scalar dissipation

A transport equation for the instantaneous scalar dissipation rate N_c can be written as [149]:

$$\rho\frac{DN_c}{Dt} = \frac{\partial}{\partial x_i}\left(\rho D_c\frac{\partial N_c}{\partial x_i}\right) - 2\rho D_c D_c\frac{\partial}{\partial x_i}\left(\frac{\partial c}{\partial x_j}\right)\frac{\partial}{\partial x_i}\left(\frac{\partial c}{\partial x_j}\right) - 2\rho D_c\frac{\partial c}{\partial x_i}S_{ij}\frac{\partial c}{\partial x_j} - 2D_c\frac{\dot{\omega}_c + \frac{\partial}{\partial x_n}\left(D_c\frac{\partial c}{\partial x_n}\right)}{\rho}\frac{\partial c}{\partial x_j}\frac{\partial \rho}{\partial x_j} + 2D_c\frac{\partial c}{\partial x_j}\frac{\partial \dot{\omega}_c}{\partial x_j} \tag{6.3}$$

A transport equation for the Favre averaged scalar dissipation can be obtained by using the expressions in eq. (6.1) and eq. (6.3), thus leading to [149]:

$$\frac{\partial \overline{\rho}\widetilde{\epsilon}_c}{\partial t} + \frac{\partial}{\partial x_i}\left(\overline{\rho}\widetilde{u}_i\widetilde{\epsilon}_c\right) = \underbrace{\frac{\partial}{\partial x_i}\left(\overline{\rho D_c}\frac{\partial \widetilde{\epsilon}_c}{\partial x_i}\right)}_{D_1} \underbrace{-\overline{2\rho D_c D_c\left(\frac{\partial}{\partial x_i}\left(\frac{\partial c''}{\partial x_j}\right)\frac{\partial}{\partial x_i}\left(\frac{\partial c''}{\partial x_j}\right)\right)}}_{D_2} + T_1 + T_2 + T_3 + T_4 \tag{6.4}$$

where

$$T_1 = \underbrace{-\frac{\partial \overline{\rho u_i'' \epsilon_c}}{\partial x_i}}_{T_{11}} \underbrace{-2\overline{\rho D_c}\left(\widetilde{u_i'' \frac{\partial c''}{\partial x_j}}\right)\frac{\partial^2 \widetilde{c}}{\partial x_i \partial x_j}}_{T_{12}} \tag{6.5}$$

$$T_2 = 2\overline{\rho}\widetilde{\epsilon_c}\frac{\partial \widetilde{u}_l}{\partial x_l} + \overline{2\rho D_c\left(\left(\frac{\partial}{\partial x_i}\left(\frac{\partial c''}{\partial x_j}\right)\frac{\partial}{\partial x_i}\left(\frac{\partial c''}{\partial x_j}\right)\right)\frac{\partial u_l''}{\partial x_l}\right)} = 2\overline{\rho\epsilon_c}\frac{\partial u_l}{\partial x_l} \tag{6.6}$$

$$T_3 = \underbrace{-2\overline{\rho D_c}\frac{\partial \widetilde{c}}{\partial x_i}\left(\widetilde{\frac{\partial c''}{\partial x_j}\frac{\partial u_i''}{\partial x_j}}\right)}_{T_{31}} \underbrace{-2\overline{\rho D_c}\left(\widetilde{\frac{\partial c''}{\partial x_i}S_{ij}''\frac{\partial c''}{\partial x_j}}\right)}_{T_{32}}$$
$$\underbrace{-2\overline{\rho D}_c\left(\widetilde{\frac{\partial c''}{\partial x_i}\frac{\partial c''}{\partial x_j}}\right)\widetilde{S_{ij}}}_{T_{33}} \tag{6.7}$$

$$T_4 = 2\left(\overline{D_c\frac{\partial c''}{\partial x_j}\frac{\partial \dot{\omega}_c''}{\partial x_j}}\right) \tag{6.8}$$

The terms on left-hand side of eq. (6.4) represent the temporal and convective terms. Term D_1 represents the molecular diffusion effects and term D_2 represents the dissipation of $\widetilde{\epsilon}_c$. Term T_{11} represents the turbulent transport of $\widetilde{\epsilon}_c$ and term T_{12} represents the influence of curvature of the mean scalar field. Term T_2 represents dilatation and appears due to the density change across the flame front; this term is absent in the scalar dissipation transport equation proposed by Mantel and Borghi [105]. Term T_{31} represents the effects of mean scalar gradient on flame turbulence interaction, term T_{32} represents interaction between turbulent strain and scalar gradients and term T_{33} represents the effects of mean strain on flame turbulence interaction. Term T_4 represents the chemical effects. In non reacting flows the dilatation and the reaction rate are zero, thus terms $T_2 = T_4 = 0$ in eq. (6.4) in the case of cold scalar mixing of non-reacting turbulent flows [167].

6.2 Order of magnitude analysis

An order of magnitude analysis under the large Damköhler and Reynolds number limit has been carried out by Swaminathan and Bray [149]. The details for the order of magnitude analysis (OMA) are given in section 8.2. When applied to eq. (6.4) (details can be found in appendix B) the following leading order terms are obtained :

$$T_2 + T_{32} + T_4 - D_2 \backsimeq 0. \tag{6.9}$$

6.3 Models for $\mathcal{O}(1)$ terms in scalar dissipation transport equation and the algebraic models

Simple algebraic models for $\widetilde{\epsilon}_c$ can be obtained by considering the leading order ($\mathcal{O}(1)$) terms. Several algebraic models of varying complexity have been proposed by Mantel and Borghi [17, 105], Mura and Borghi [111], Swaminathan and Bray [149], Kolla et al [85, 86] and Vervisch et al [157]. Some of these models and the closures used for the $\mathcal{O}(1)$ terms in eq. (6.4) are discussed below.

6.3.1 Swaminathan and Bray model

An algebraic model based on the closures for the leading order terms in eq. (6.9) has been proposed by Swaminathan and Bray. The closures for the leading order terms used in this model are discussed below.

6.3.1.1 Model for term T_2

Term T_2 represents the effect of dilatation due to heat release in the scalar dissipation transport equation. The importance of T_2 has been demonstrated by Chakraborty et al [44, 45] in case of both high and low Da flames. Thus signifying the importance of T_2.

The model for T_2 proposed by Swaminathan and Bray [149] makes use of the Bray Moss Libby Model [26]. This in turn postulates that dilatation should be zero everywhere other than the flame front, so T_2 must be proportional to γ in

eq. (5.2), thus giving [149]:

$$\begin{aligned} T_2 = 2\overline{\rho\epsilon_c \frac{\partial u_l}{\partial x_l}} &= 2\gamma \int_0^1 \rho\epsilon_c \left(\nabla.u\right) f(c)dc \\ &= 2K_c\overline{\dot{\omega}}_c \left(\frac{u_L^0}{\delta_L^0}\right) \\ &= \frac{4K_c}{(2C_m - 1)} \left(\frac{u_L^0}{\delta_L^0}\right) \overline{\rho}\widetilde{\epsilon}_c, \end{aligned} \tag{6.10}$$

where K_c is the ratio of the dilatation due to scalar dissipation to the unstrained reaction rate (both for laminar flames) [149]

$$K_c = \left(\frac{\delta_L^0}{u_L^0}\right) \frac{\int \{\rho N \left(\nabla.\boldsymbol{u}\right)\}_L^0 f(c)dc}{\int \dot{\omega}_L^0 f(c)dc}. \tag{6.11}$$

$\{\}_L^0$ denotes quantities corresponding to an unstrained laminar flame. K_c and C_m include the effects of chemistry and have constant values for a given fuel [21].

6.3.1.2 Model for Term T_{32}

Term T_{32} represents the flame turbulence interaction in the scalar dissipation transport equation. A model for T_{32} has been proposed by Mantel and Borghi [105]:

$$T_{32} = -2\overline{\rho D_c} \left(\widetilde{\frac{\partial c''}{\partial x_i} S''_{ij} \frac{\partial c''}{\partial x_j}}\right) = A_e \overline{\rho} \left(\frac{\widetilde{\epsilon}}{\widetilde{k}}\right) \widetilde{\epsilon}_c. \tag{6.12}$$

This model is based on a scalar interacting with turbulence under the cold flow conditions. The constant A_e represents the ratio of turbulence to scalar time scale and is based on the notion that the decay rate of scalar fluctuations is proportional to the decay rate of the velocity fluctuations. Pope [119] has questioned the universality of the value for A_e, especially in the case of a scalar field in decaying grid turbulence. It has been confirmed by Eswaran and Pope [62] in their DNS study that A_e tends to a value of about 1. Although the model has been applied to various scenarios in combustion, it is only valid for passive scalar transport in incompressible turbulence. In combustion applications, A_e must change according to local flow conditions; this is discussed in detail in section 6.3.1.4.

6.3.1.3 Model for Term T_4^*

T_4^* represents the combined effects of reaction (T_4), dissipation (D_2) and molecular diffusion (D_1) and is defined as [105, 111, 40]:

$$T_4^* = \underbrace{2\left(\overline{D_c \frac{\partial c''}{\partial x_j}\frac{\partial \dot{\omega}_c''}{\partial x_j}}\right)}_{T_4} + \underbrace{\frac{\partial}{\partial x_j}\left(\overline{\rho D_c}\frac{\partial \widetilde{\epsilon}_c}{\partial x_j}\right)}_{D_1} \underbrace{- 2\overline{\rho D_c D_c\left(\frac{\partial}{\partial x_j}\left(\frac{\partial c''}{\partial x_k}\right)\frac{\partial}{\partial x_j}\left(\frac{\partial c''}{\partial x_k}\right)\right)}}_{D_2} \tag{6.13}$$

Borghi and co-workers [105, 111] assume that D_1 plays an important role in the evolution of $\widetilde{\epsilon}_c$ and model T_4^* instead of $T_4 - D_2$, and propose the closure :

$$T_4^* = -\frac{2}{3}\beta\overline{\rho}\frac{\widetilde{\epsilon}_c^2}{\widetilde{c''^2}}\left(\frac{3}{2} - C_{\epsilon_c}\frac{u_L^0}{\sqrt{\widetilde{k}}}\right) \tag{6.14}$$

where $\beta = 4.2$ and $C_{\epsilon_c} = 0.1$ are model constants. Note that the positive part of eq. (6.14) represents the combined effects of molecular diffusion and decreases with increasing Da, which is consistent with the scaling laws of Swaminathan and Bray [149]. The negative part of eq. (6.14) represents the dissipation process for the scalar dissipation transport equation [40] and plays an important role in the evolution of $\widetilde{\epsilon}_c$ [40, 105, 111].

6.3.1.4 Algebraic model

An algebraic model for $\widetilde{\epsilon}_c$ can be obtained by using the individual closures for the leading order terms in eq. (6.9). Note that $T_4 - D_2$ has been replaced by T_4^* in this model, leading to [149]:

$$\widetilde{\epsilon}_c \backsimeq \left(1 + \frac{2}{3}C_{\epsilon_c}\frac{u_L^0}{\sqrt{\widetilde{k}}}\right)\left(C_{D_c}\frac{u_L^0}{\delta_L^0} + C_D\frac{\widetilde{\epsilon}}{\widetilde{k}}\right)\widetilde{c''^2}, \tag{6.15}$$

where C_{D_c} is the ratio of $4K_c$ to $(2C_m - 1)\,\beta$ and C_D is the ratio of turbulence time scale ($\widetilde{k}/\widetilde{\epsilon}$) to the scalar time scale ($\widetilde{c''^2}/\widetilde{\epsilon}_c$) (i.e. A_e/β) [139, 150, 157]. The expression in eq. (6.15) incorporates a dependence of scalar dissipation rate on chemical time scales [149]. Swaminathan and Bray have shown that $C_D = 0.25$ via DNS data of a planar flame; where as Vervisch et al [157] have shown that

C_D reaches around 2 at some locations in their DNS of a V-flame. Lindstedt and Vaos [101] argue that the time scale ratio should not be smaller than 1 to obtain a stable solution in case of Bunsen flames. Thus, although the time scale ratio C_D is an important quantity in this model, there is no universally agreed value for the time scale ratio C_D [35, 139]. The model in eq. (6.15) is referred to as SDR-1 in the subsequent chapters.

6.3.2 Kolla et al model

Kolla et al [85, 86] have proposed improvements to the $\widetilde{\epsilon}_c$ model in eq. (6.15) in response to the observations of both Swaminathan and Grout [151] and of Chakraborty and Swaminathan [44] that the heat release and change in Damköhler number effect $\widetilde{\epsilon}_c$ via a strong influence on flame turbulence interaction, which is controlled by the competition between the dilatation rate and the turbulent strain rate in the regions of intense heat release. To take this phenomenon into account, Chakraborty et al [43] introduced a time scale for the dilatation rate based on the local Damköhler number (Da_L) and heat release in their modelling approach for flame turbulence interaction. These modelling strategies are discussed in the following subsections.

6.3.2.1 Modelling of term T_2

As mentioned before the dilatation is zero everywhere other than in the flame brush, so T_2 must be proportional to γ and Swaminathan and Bray [149] proposed a closure mentioned in eq. (6.6). The value of K_c in eq. (6.6) can not be chosen arbitrarily once the internal flame structure has been specified [86, 135]. It is argued by Kolla et al [86] and Rogerson and Swaminathan [135] that this sensitivity is not desirable from a modelling point of view and a new model has been proposed [86, 135]:

$$T_2 = 2\overline{\rho\epsilon_c\frac{\partial u_l}{\partial x_l}} = 2K_c^*\left(\frac{u_L^0}{\delta_L^0}\right)\overline{\rho}\widetilde{\epsilon}_c, \tag{6.16}$$

where

$$K_c^* = \left(\frac{\delta_L^0}{u_L^0}\right)\frac{\int\{\rho N\left(\nabla.\boldsymbol{u}\right)\}_L^0 f(c)dc}{\int\{\rho N\}_L^0 f(c)dc}. \tag{6.17}$$

Note that this model is similar to the earlier model in eq. (6.6), the only difference is that $\{\rho N\}_L^0$ replaces $\dot{\omega}_L^0$ in eq. (6.16) leading to a different model constant K_c^*. This new constant includes the effects of heat release and is less sensitive to the changes in equivalence ratio. For hydrocarbon-air flames K_c^* is usually calculated as $K_c^* = 0.85\tau$ [85].

6.3.2.2 Modelling of flame turbulence interaction T_{32}

This term describes the interaction of turbulence and scalar gradients. T_{32} can be re-expressed by using the eigendecomposition and written as [40, 86]:

$$T_{32} = -2\overline{\rho D_c}\left(\widetilde{\frac{\partial c''}{\partial x_i}S''_{ij}}\frac{\partial c''}{\partial x_j}\right) = \overline{-2\rho\epsilon_c\left(e_\alpha\cos^2\theta_\alpha + e_\beta\cos^2\theta_\beta + e_\gamma\cos^2\theta_\gamma\right)}, \tag{6.18}$$

where e_α, e_β and e_γ are the eigenvalues of the turbulent strain rate tensor S''_{ij}.

The eigenvalues are ranked as $e_\alpha > e_\beta > e_\gamma$ with e_α being the most extensive principal strain rate and e_γ being the most compressive principal strain rate; the three eigenvalues are orthogonal to one another [40]. It can be seen in eq. (6.18) that the source or sink behaviour of T_{32} is dependent on the statistics of the alignment angles between the scalar gradient and the directions of the principal strain rates [40, 86]. It is well known that in case of the cold turbulence the scalar gradient preferentially aligns with the most compressive principal strain rate e_γ [7, 8], thus giving a source contribution from T_{32}. In flows with intense heat release, it has been shown by Chakraborty and Swaminathan [44] and Swaminathan and Grout [151] that the scalar gradient preferentially aligns with the most extensive principal strain rate e_α and thus produces a net sink from T_{32}.

This variation between the alignment characteristics is due to the competition between dilation rate and turbulent strain rate [151]. This implies that turbulence produces scalar gradients by bringing isoscalar surfaces closer and this production is balanced by the molecular diffusion process [40]. In case of strong heat release, the dilatation usually occurring in the flame normal direction overcomes the turbulence effects thus causing the scalar gradient to align with the most extensive strain rate e_α [40]; T_{32} becomes negative and dissipates the scalar gradient [39, 71, 83]. This effect is not modelled by the earlier models proposed by Mantel

and Borghi [105].

In order to capture the correct behaviour of T_{32}, Kolla et al [86, 85] have proposed that the turbulent strain rate effect is modelled as :

$$[T_{32}]_{turb} = C_3 \overline{\rho}\widetilde{\epsilon_c} \left(\frac{\widetilde{\epsilon}}{\widetilde{k}} \right), \tag{6.19}$$

and the strain rate due to heat release is modelled as [86, 85]:

$$[T_{32}]_{\tau} = -\tau C_4 \overline{\rho}\widetilde{\epsilon_c} \left(\frac{u_L^0}{\delta_L^0} \right), \tag{6.20}$$

where C_3 and C_4 are scaling factors in eq. (6.19) and eq. (6.20). Combining eq. (6.19) and eq. (6.20) gives a model for T_{32} as [85, 86]:

$$T_{32} = [C_3 - \tau C_4 Da_L] \left(\frac{\widetilde{\epsilon}}{\widetilde{k}} \right) \overline{\rho}\widetilde{\epsilon_c}, \tag{6.21}$$

where Da_L is the local Damkohler number and is defined as :

$$Da_L = \frac{(u_L^0/\delta_L^0)}{\left(\widetilde{\epsilon}/\widetilde{k}\right)}. \tag{6.22}$$

C_3 and C_4 in eq. (6.19) and eq. (6.20) are empirical scaling factors and are calculated as [85, 88]:

$$C_3 = 1.5 \left(\frac{\sqrt{Ka_L}}{(1+\sqrt{Ka_L})} \right), \tag{6.23}$$

$$C_4 = \left(\frac{1.1}{(1+Ka_L)} \right)^{0.4}. \tag{6.24}$$

Ka_L is the local Karlovitz number and is defined as [85, 88]:

$$Ka_L = \left\{ \frac{\left(u^{'}/u_L^0\right)^3 (\delta_L^0/l_t)}{\left[2\left(1+\tau\right)\right]^{0.7}} \right\}^{0.5}, \tag{6.25}$$

where

$$u^{'} = \sqrt{\frac{2\widetilde{k}}{3}}, \tag{6.26}$$

and

$$l_t = \frac{u^{'3}}{\widetilde{\epsilon}}. \tag{6.27}$$

6.3.2.3 Modelling of $(T_4 - D_2)$

In the earlier studies of Mantel and Borghi [105], Mura and Borghi [111] and Swaminathan and Bray [149] $T_4 - D_2 + D_1$ is related to the flame front curvature contributions, hence the algebraic models were proposed accordingly using the flamelet theories. However, D_1 is already a closed term and the order of magnitude analysis shows that it is not one of the leading order terms. A new model based on the DNS data analysis of planar flames has been proposed by Chakraborty et al [43] . The new model excludes the term D_1 :

$$\begin{aligned}(T_4 - D_2) &= \underbrace{2\left(\overline{D_c \frac{\partial c''}{\partial x_j}\frac{\partial \dot{\omega}_c''}{\partial x_j}}\right)}_{T_4} - \underbrace{2\overline{\rho D_c D_c \left(\frac{\partial}{\partial x_j}\left(\frac{\partial c''}{\partial x_k}\right)\frac{\partial}{\partial x_j}\left(\frac{\partial c''}{\partial x_k}\right)\right)}}_{D_2} \\ &= -\beta^{'}\overline{\rho}\frac{\widetilde{\epsilon}_c^2}{\widetilde{c}(1-\widetilde{c})}.\end{aligned} \tag{6.28}$$

In case of high Da flames, $\widetilde{c}(1-\widetilde{c}) \approx \widetilde{c''^2}$ and the expression in eq. (6.28) can be written as :

$$(T_4 - D_2) = -\beta^{'}\overline{\rho}\frac{\widetilde{\epsilon}_c^2}{\widetilde{c''^2}} \tag{6.29}$$

The analysis of Chakraborty et al [43] shows that D_2 is a dissipative term and overwhelms the contribution from T_4 thus making the term $(T_4 - D_2)$ negative through out the flame. This justifies the negative sign in eq. (6.28) and (6.29) [85, 86]. The model constant $\beta^{'}$ in eq. (6.29) usually takes the value of 6.7 under the thin flame front assumption ($Da >> 1$). However, under higher levels of turbulence the typical value of $\beta^{'}$ over estimates the scalar dissipation rate by more than 30% [113]. Nikolaou and Swaminathan [113] have proposed a new value of $\beta^{'} \approx 8.7$ based on a detailed chemistry DNS data set. In order to reduce the uncertainty in the approximation of $\beta^{'}$ Chakraborty and Swaminathan [46] have recently proposed an empirical model for $\beta^{'}$:

$$\beta^{'} = 3.9 + 2.8erf\left(\frac{Re_{l_t}}{10}\right), \tag{6.30}$$

where Re_{l_t} is the local turbulent Reynolds number defined as:

$$Re_{l_t} = \frac{\widetilde{k}^2}{\nu_R \widetilde{\epsilon}}, \tag{6.31}$$

and ν_R is the kinematic viscosity of the unburnt gases.

6.3.2.4 Algebraic model

An algebraic model for $\widetilde{\epsilon}_c$ is achieved by using eq. (6.16), eq. (6.21) and eq. (6.29) in eq. (6.9) [85, 86]:

$$\widetilde{\epsilon}_c \backsimeq \frac{1}{\beta'} \left(2K_c^* \frac{u_L^0}{\delta_L^0} + [C_3 - \tau C_4 Da_L] \frac{\widetilde{\epsilon}}{\widetilde{k}} \right) \widetilde{c''^2}. \tag{6.32}$$

Eq. (6.32) includes the chemical time scale, which is important for correct prediction of combustion process [149]. Eq. (6.32) can be further simplified by using the definition of the local Damköler number to give:

$$\widetilde{\epsilon}_c \backsimeq \frac{1}{\beta'} \left([2K_c^* - \tau C_4] \frac{u_L^0}{\delta_L^0} + C_3 \frac{\widetilde{\epsilon}}{\widetilde{k}} \right) \widetilde{c''^2}. \tag{6.33}$$

The algebraic model in eq. (6.33) is referred to as the SDR-2 model in the subsequent chapters.

6.3.3 Vervisch et al model

A model for scalar dissipation has been proposed by Vervisch et al [157], in which it is assumed that $\overline{\rho \epsilon_c}$ is proportional to the product $\rho_R u_L^0 \overline{|\nabla c|}$, where ρ_R is the density in fresh gases [157].

In order to simplify the modelling, Veynante and Vervisch [161] propose a surface average, defined as:

$$\langle a \rangle = \frac{\overline{a \, |\nabla c|}}{\overline{|\nabla c|}}. \tag{6.34}$$

This leads to a modified scalar dissipation definition [157]:

$$\begin{aligned}\overline{\rho}\widetilde{\epsilon}_c &= \overline{\rho D_c \left|\nabla c\right|^2} = \left\langle \rho D_c \left|\nabla c\right| \right\rangle \overline{\left|\nabla c\right|} \\ &= \left\langle \rho D_c \left|\nabla c\right| \right\rangle \Xi \left|\nabla \overline{c}\right|, \end{aligned} \tag{6.35}$$

where Ξ is the flame wrinkling factor, and is defined as:

$$\Xi = \frac{\overline{\left|\nabla c\right|}}{\left|\nabla \overline{c}\right|}. \tag{6.36}$$

In eq. (6.35), the average turbulent mixing rate appears as $\left\langle \rho D_c \left|\nabla c\right| \right\rangle$ [157]. $\overline{\left|\nabla c\right|}$ is the integral of the flame surface density function Σ [122, 156]:

$$\overline{\left|\nabla c\right|} = \int_0^1 \Sigma(c) dc = \Xi \left|\nabla \overline{c}\right|. \tag{6.37}$$

The main advantage of using eq. (6.35) is that it explicitly includes a flame wrinkling length scale ($\Xi \left|\nabla \overline{c}\right|$) in the approximation of $\widetilde{\epsilon}_c$.

The reaction rate $\overline{\dot{\omega}}_c$ is related to $\overline{\left|\nabla c\right|}$ as:

$$\overline{\rho\dot{\omega}}_c \approx \rho_R u_L^0 \overline{\left|\nabla c\right|}. \tag{6.38}$$

Eq. (6.38) does not allow for the estimation of intermediate species and pollutants, for which some information on micro-mixing and scalar dissipation rate is essential [157]. In the high Da limit, the turbulent micro-mixing rate $\left\langle \rho D_c \left|\nabla c\right| \right\rangle$ is expected to be proportional to $\rho_R u_L^0$ [157]. An exact form of $\left\langle \rho D_c \left|\nabla c\right| \right\rangle$ can be obtained by using eq. (6.34) and eq. (6.35) [157]:

$$\begin{aligned}\overline{\rho\dot{\omega}_c} &= \left\langle \frac{\rho\dot{\omega}_c}{\left|\nabla c\right|} \right\rangle \overline{\left|\nabla c\right|} \\ &= \frac{\left\langle \frac{\rho\dot{\omega}_c}{\left|\nabla c\right|} \right\rangle}{\left\langle \rho D_c \left|\nabla c\right| \right\rangle} \overline{\rho}\widetilde{\epsilon}_c. \end{aligned} \tag{6.39}$$

Using the BML reaction rate closure from eq. (5.62) gives [157]:

$$\frac{\left\langle \frac{\rho\dot{\omega}_c}{|\nabla c|} \right\rangle}{\langle \rho D_c \left|\nabla c\right| \rangle} \approx \frac{2}{2C_m - 1}. \tag{6.40}$$

The turbulent mixing speed can be approximated by using eq. (6.35) eq. (5.62) and eq. (6.38) as [157]:

$$\langle \rho D_c \left|\nabla c\right| \rangle \approx \frac{1}{2} \left(2C_m - 1\right) \rho_R u_L^0. \tag{6.41}$$

Thus giving the scalar dissipation rate as [157]:

$$\begin{aligned} \overline{\rho}\widetilde{\epsilon}_c &= \overline{\rho D_c \left|\nabla c\right|^2} \\ &\approx \frac{1}{2} \left(2C_m - 1\right) \rho_R u_L^0 \Xi \left|\nabla \overline{c}\right| \left(\frac{\widetilde{c''^2}}{\widetilde{c}\left(1 - \widetilde{c}\right)} \right). \end{aligned} \tag{6.42}$$

In RANS applications under the thin flamelet assumption $\Xi \left|\nabla \overline{c}\right| \approx \Sigma$ [161], thus leading to :

$$\overline{\rho}\widetilde{\epsilon}_c \approx \frac{1}{2} \left(2C_m - 1\right) \rho_R u_L^0 \Sigma \left(\frac{\widetilde{c''^2}}{\widetilde{c}\left(1 - \widetilde{c}\right)} \right). \tag{6.43}$$

The ratio $\widetilde{c''^2}/\widetilde{c}(1-\widetilde{c})$ in the above equation represents the normalised variance of the progress variable [19], this ratio is close to unity in a thin flame front ($Da > 1$) and reduces as the combustion regime changes, thus relaxing the BML limit and allowing the model to include a wider range of combustion regimes.

The scalar dissipation model in eq. (6.43) reduces the problem of modelling scalar dissipation to closing the flame surface density (Σ), which is discussed in the next section. The model in eq. (6.43) is referred to as the SDR-3 model in the subsequent chapters.

6.4 Flame surface density in premixed flames

The flame surface density (Σ) is an important quantity in premixed turbulent combustion since, as shown in section 5.7.4.2, the mean reaction rate can be expressed as a function of Σ. It has been shown by Borghi [17], that $\widetilde{\epsilon}_c$ is related

to the flame surface density as :

$$\widetilde{\epsilon}_c = K_\Sigma u_L^0 \Sigma, \tag{6.44}$$

where $K_\Sigma = \rho_R \left(2C_m - 1\right)/2$ is a constant. This implies that $\widetilde{\epsilon}_c$ and Σ represent the same physical phenomenon. In case of RANS approaches and the thin flamelet assumption Σ is defined as $\Sigma = \overline{|\nabla c|}$. In this section, different modelling strategies for flame surface density are explored. Different approaches have been used to model Σ including algebraic models and modelled transport equations. These techniques are discussed in the following sections.

6.4.1 Algebraic models for Σ

Algebraic expressions have been proposed by Cant and Bray [34], and Cant et al [36] and Bray and Swaminathan [28]. The simplest model is based on the flame brush crossing a probe at a single spatial location, which captures the time varying signal [25]. The graph of reaction progress variable versus time can be approximated as a square wave, where the flat portions of the graph correspond to either reactants or products [25, 35]. This approximation gives an expression for Σ as [37]:

$$\Sigma = \frac{g\overline{c}\left(1-\overline{c}\right)}{|\hat{\sigma}_y|\,\hat{L}_y}, \tag{6.45}$$

where g is a constant, and $|\hat{\sigma}_y|$ is the orientation factor, evaluated using experimental data. The usual values are $g \approx 1$ and $|\hat{\sigma}_y| \approx 0.5$ [35, 118]. $\hat{L}_y$ is the integral length scale of wrinkling, and can be related to the integral length scale of turbulence as :

$$\hat{L}_y = c_L l_t \left(\frac{u^{'}}{u_L}\right)^n, \tag{6.46}$$

where $c_L \approx 1.0$ and $n \approx 1.0$ [35].

6.4.2 Transport equation approach to Σ

A transport equation for Σ can also be solved and has been proposed by Pope [121], Candel and Poinsot [30], Trouvé and Poinsot [153], and Vervisch et al [156].

The exact equation is written as [35, 118, 121]:

$$\underbrace{\frac{\partial \Sigma}{\partial t}}_{a} + \underbrace{\frac{\partial}{\partial x_i}\left(\langle u_i \rangle \Sigma\right)}_{b} + \underbrace{\frac{\partial}{\partial x_i}\left[\langle s_d n_i \rangle \Sigma\right]}_{c} = \underbrace{\left\langle \left(\delta_{ij} - n_i n_j\right) \frac{\partial u_i}{\partial x_j} \right\rangle \Sigma}_{d} + \underbrace{\left\langle s_d \frac{\partial n_i}{\partial x_i} \right\rangle \Sigma}_{e}, \tag{6.47}$$

where s_d is the propagation speed of the flame relative to the reactants, the subscript <> represents the surface average and n_i is the component of the unit vector normal to the flame surface. The unit normal vector is represented as [35, 118]:

$$\mathbf{n} = -\frac{\nabla c}{|\nabla c|}. \tag{6.48}$$

The negative sign in eq. (6.48) implies that $\mathbf{n}$ is pointing to the the reactants [35].

Term a in eq. (6.47) represents the unsteady effects. Term b represents the flame surface convection by the flow field. Term c represents the normal propagation of the flame. Term d represents the action of tangential strain rate on the flame surface. Term e represents the combined flame propagation and curvature effects. The sum of terms d and e encompass the stretch rate $\langle \kappa \rangle_s$ acting on the flame surface. Note that term c in eq. (6.47) is generally neglected under the assumption that the propagation velocity in the $\langle s_d n_i \rangle$ is of the order of the laminar flame speed and is negligible when compared to the convection velocity [31, 118].

The flame surface density transport equation in eq. (6.47) is decomposed using the Favre decomposition to give :

$$\frac{\partial \Sigma}{\partial t} + \frac{\partial \widetilde{u}_i \Sigma}{\partial x_i} = -\frac{\partial}{\partial x_i}\left(\left\langle u_i^{''} \right\rangle \Sigma\right) + \kappa_m \Sigma + \kappa_t \Sigma + \kappa_c \Sigma. \tag{6.49}$$

κ_m in eq. (6.49) is the tangential strain rate acting due to the mean flow, defined as :

$$\kappa_m = \left(\delta_{ij} - \langle n_i n_j \rangle\right) \frac{\partial \widetilde{u}_i}{\partial x_j}. \tag{6.50}$$

κ_t in eq. (6.49) is the tangential strain rate acting due to the turbulent motion of the flow, defined as :

$$\kappa_t = \left\langle (\delta_{ij} - n_i n_j) \frac{\partial u_i''}{\partial x_j} \right\rangle. \tag{6.51}$$

Eq. (6.51) can be expanded to give:

$$\kappa_t = \left\langle \frac{\partial u_i''}{\partial x_i} \right\rangle - \left\langle \frac{\partial u_i''}{\partial x_j} \right\rangle \widetilde{n}_i \widetilde{n}_j - \left\langle \frac{\partial u_i''}{\partial x_j} n_j'' \right\rangle \widetilde{n}_i - \left\langle \frac{\partial u_i''}{\partial x_j} n_i'' \right\rangle \widetilde{n}_j - \left\langle \frac{\partial u_i''}{\partial x_j} n_i'' n_j'' \right\rangle. \tag{6.52}$$

In case of thin flamelets $\frac{\partial \widetilde{c}}{\partial x_k} << \frac{\partial c''}{\partial x_k}$, thus simplifying eq. (6.52) to :

$$\kappa_t = \left\langle \frac{\partial u_i''}{\partial x_i} - \frac{c_{,i}'' S_{ij}'' c_{,j}''}{\left| c_{,i}'' c_{,i}'' \right|} \right\rangle. \tag{6.53}$$

Note that the first term on the right-hand side of eq. (6.53) represents dilatation and the second term on the right-hand side of eq. (6.53) represents the flame turbulence interaction. κ_c in eq. (6.49) represents the combined effects flame propagation and curvature, and is defined as :

$$\kappa_c = \left\langle s_d \frac{\partial n_i}{\partial x_i} \right\rangle. \tag{6.54}$$

κ_m, κ_t and κ_c in eq. (6.50), eq. (6.53) and eq. (6.54) need to be closed. There are several closures available in literature for all the terms in eq. (6.49) including closures proposed by Cant et al [36], Duclos et al [55], Mantel and Borghi [105], Veynante et al [158], Cheng and Diringer [50]. The most common form of the closed transport equation is [118, 153]:

$$\frac{\partial \Sigma}{\partial t} + \frac{\partial \widetilde{u}_i \Sigma}{\partial x_i} = \frac{\partial}{\partial x_i} \left(\frac{\nu_t}{\sigma_\Sigma} \frac{\partial \Sigma}{\partial x_i} \right) + \kappa_t \Sigma + \kappa_c \Sigma, \tag{6.55}$$

where κ_t is closed as :

$$\kappa_t \approx A_0 \frac{\widetilde{\epsilon}}{\widetilde{k}} \Sigma, \tag{6.56}$$

and κ_c is closed as :

$$\kappa_c \approx -B_0 \left\langle s_c \right\rangle_s \frac{\Sigma^2}{1 - \widetilde{c}}. \tag{6.57}$$

Note that in eq. (6.55) contributions from κ_m have been ignored, as these contributions are assumed to be small when compared with other terms under the

high Reynolds number limit.

In eq. (6.55) the turbulent transport of Σ is expressed using a gradient diffusion assumption, ν_t represents the turbulent viscosity and σ_Σ is the turbulent Schmidt number. A negative sign is used in the closure for κ_c, as κ_c is mainly responsible for the destruction of Σ. The contributions from κ_t are generally positive and without a destruction term the flame surface density transport equation would predict an infinite growth of flame area [118]. It is still unknown whether κ_c represents only the curvature effects or it also includes additional features like flame front interactions [118]. A_0 and B_0 in eq. (6.55) are model constants and have the following values $A_0 = 1.7$ and $B_0 = 1.0$ [126]. $\langle s_c \rangle$ in eq. (6.57) represents the consumption speed computed by detailed chemistry mechanisms. The focus of this study is on flame turbulence interaction, hence the detailed chemistry is not used here; instead the consumption speed is assumed to equal the unstrained laminar flame speed u_L^0. The assumption $\langle s_c \rangle \approx u_L^0$ is valid as a first order approximation [35, 56, 118].

7 RANS simulation of a laboratory scale premixed V-flame

The laboratory-scale turbulent rod stabilised premixed V-flame of Bell et al [9] has been investigated. In the V-flame configuration, a stationary, non-planar flame is produced which is oblique to the mean flow, and subject to mean shear, strong tangential convection by the mean flow and flow divergence [58]. This type of configuration is characterised by a continuously developing flame in a statistically two dimensional mean flow field; the turbulence intensity along the leading edge of the flame brush decreases significantly while the individual flame elements are convected in the stream wise direction [58].

The experimental results are used here as a benchmark to compare the RANS calculations. A similar type of configuration has been studied by Kolla et al [85, 89] and Robin et al [132, 133] using different RANS modelling approaches; the principal novelty of this study lies in the comparison of several scalar dissipation models in context of the BML approach.

7.1 Experimental configuration

A methane air mixture with equivalence ratio of $\phi = 0.7$ is used. The mixture exits a $50mm$ diameter nozzle with a mean axial velocity of $3m/s$. Turbulence is introduced by using a perforated plate $90mm$ upstream of the nozzle exit. The flame is stabilised by a $2mm$ diameter rod spanning the nozzle exit. The flame in the experiment is in the corrugated flamelet regime [9] on the regime diagram in figure 4.5. The experimental setup is shown in figure 7.1 and additional details

of the experimental configuration can be found in [9].

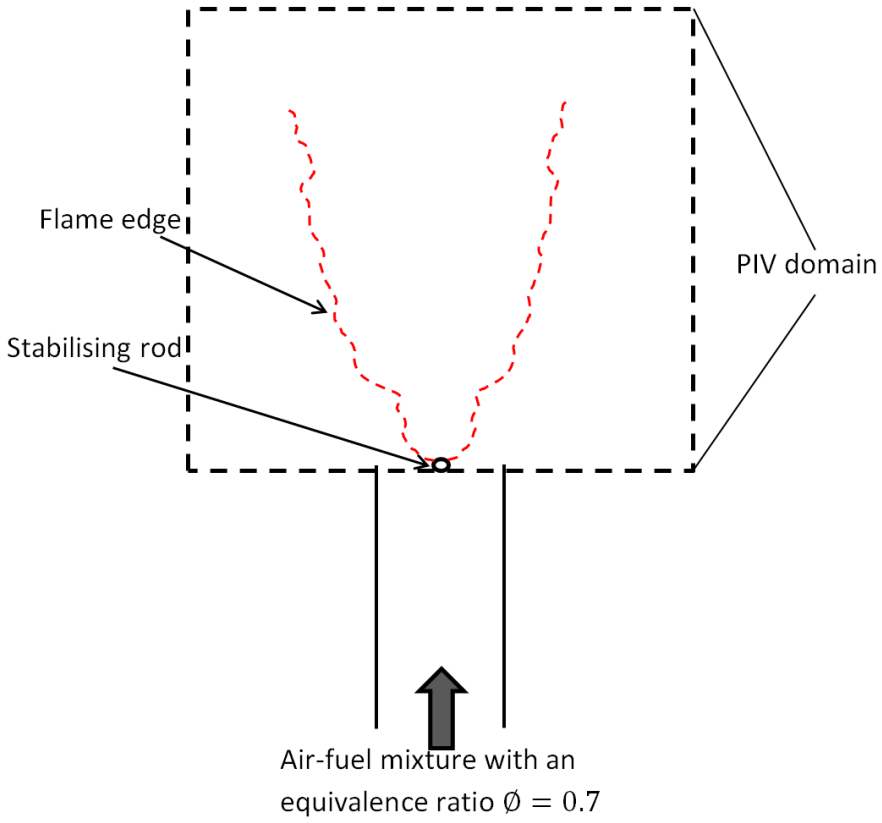

Figure 7.1: Schematic of the experimental setup for the V-flame

7.2 Numerical configuration

The computational domain for the simulation is shown in figure 7.2. The flow is statistically two-dimensional, and the width of the domain in the x direction in figure 7.2 accounts for the entrainment of ambient air. The experimental data is reported in a $120\,mm \times 120\,mm$ plane downstream of the stabilising rod. In the experiment, the flame can be observed up to $150mm$ downstream of the stabilising rod [9]; in order to account for the extended length of the flame the computational domain is extended up to $320mm$ in the mean flow (y) direction.

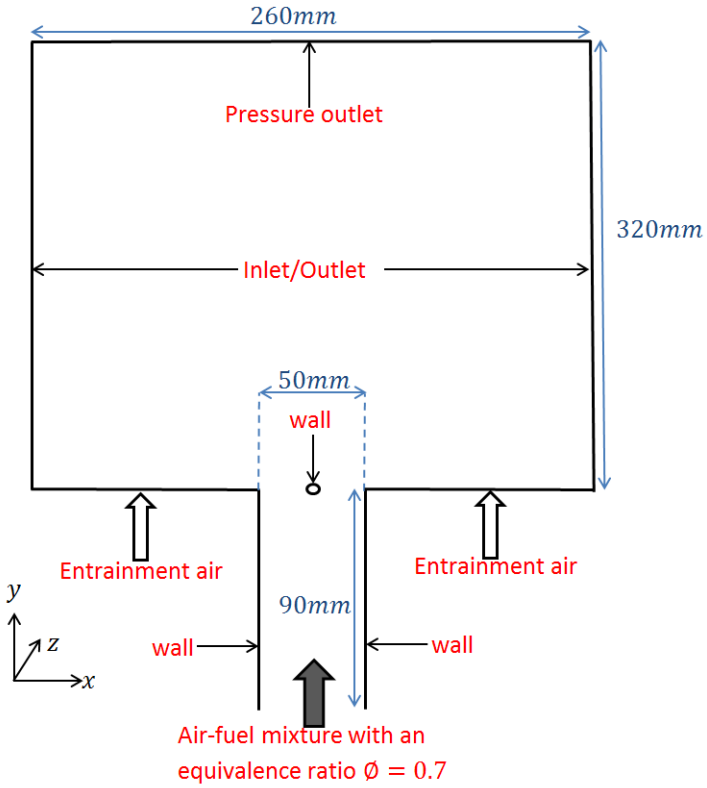

Figure 7.2: Dimensions of the computational domain for the V-flame (figure not to scale)

The experiment considered in this chapter is of an open flame in a large laboratory. It is not possible to simulate the entire laboratory, hence an inlet/outlet condition has been used at the boundaries in the transverse (x) direction. Similar inlet/outlet boundary conditions have been used to represent entrainment of air by Robin et al [132, 133] and by Sapa [140]. In order to mimic the stabilisation mechanism used in the experiment the flame is anchored numerically by using a region of 4 cells in the upper half of the rod with burnt conditions $\widetilde{c} = 1$.

A fully structured grid of 160172 cells has been used and the region near the stabilising rod is shown in figure 7.3. It is made sure that the mean flame structure is resolved with at least 10 grid points. A standard wall function is used to resolve the flow near the walls, and it is made sure that the mesh has a minimum non-dimensional distance from the wall (y^*) of approximately 30. The mesh has a skewness of 1 for approximately 94% of the cells in the computational domain, where 0 corresponds to a highly skewed cell and 1 represents a perfect

cube [5]. The global thermochemical parameters used in the simulation are; planar unstrained laminar flame speed $u_L^0 = 0.19\,m/s$ and laminar flame thermal thickness $\delta_L^0 = 0.6\,mm$ as reported by Bell et al [9].

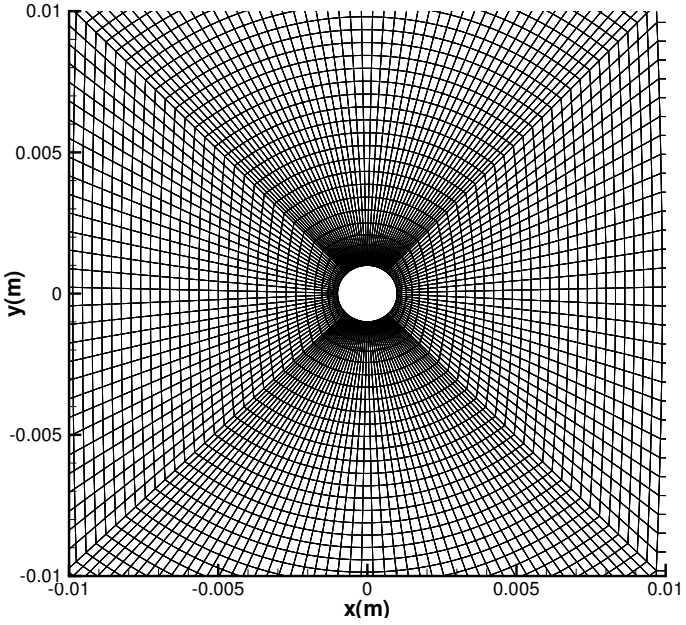

Figure 7.3: The mesh used near the stabilising rod in the V-flame calculation

7.3 Treatment of entrainment air and inlet conditions

The fluid density can be influenced by both combustion and also by mixing of the entraining fluid. In order to take mixing into account, a formulation proposed by Kolla and Swaminathan [89] is used. A transport equation for the mean mixture fraction $\widetilde{\xi}$ is solved [85, 89] :

$$\frac{\partial\left(\overline{\rho}\widetilde{\xi}\right)}{\partial t} + \frac{\partial}{\partial x_k}\left(\overline{\rho}\widetilde{u}_k\widetilde{\xi}\right) = -\frac{\partial}{\partial x_k}\overline{\rho u_k'' \xi''}, \tag{7.1}$$

where ξ is defined as [11]

$$\xi = \frac{Z_i - Z_{i2}}{Z_{i1} - Z_{i2}}, \tag{7.2}$$

and Z_i is the mass fraction of any element i. The subscripts 1 and 2 denote the two different feeds for the reacting mixture and the ambient air, respectively. The inlet values are specified as $\widetilde{\xi} = 1$ in the reacting mixture and $\widetilde{\xi} = 0$ in the regions with ambient air. The turbulent transport in eq. (7.1) is modelled by the gradient diffusion model. The formulation proposed by Kolla and Swaminathan [89] assumes that the flame brush does not interact with the entrainment air. The mean density is calculated as [85, 89] :

$$\overline{\rho} = \left[\frac{\left(1 - \widetilde{\xi}\right)}{\rho_{air}} + \frac{\widetilde{\xi}}{\rho_{reac}} \right]^{-1} \tag{7.3}$$

where ρ_{air} is the density of the ambient air and ρ_{reac} is the density of the reacting mixture obtained from the BML model. The inlet conditions used for the simulation are listed in table 7.1.

Density of the reacting mixture $\rho_{reac}(kg/m^3)$	1.170
Density of the air $\rho_{air}(kg/m^3)$	1.1455
Kinematic viscosity $\nu(m^2/s)$	1.6×10^{-5}
Temperature in unburned gases $T_R(K)$	300
Equivalence ratio ϕ	0.7
inlet velocity for the reacting mixture (m/s)	3.0
inlet velocity for air (m/s)	0.3
$u^{'}$ at the inlet for reacting mixture(m/s)	0.18
l_t at the inlet for the reacting mixture (mm)	3.5

Table 7.1: Inlet conditions used for RANS simulation of the V-flame

The solution is sensitive to the entrainment air velocity at the inlet and a number of entrainment air velocities for laboratory scale V-flames have been used in the literature. Bell et al [9] have used the co-flow velocity of $1.5m/s$ in their DNS for the same V-flame as used in this study, while Kolla et al [85, 89] used approximately 10% of the inlet velocity of the jet carrying the air-fuel mixture. Both approaches have been tested, and it is found that the approach proposed by Kolla et al [85, 89] leads to results closer to the experimental values. Hence a co-flow velocity of $0.3m/s$ has been used.

7.4 Solution algorithm

Calculations for this work have been performed using the unstructured finite volume code *Code_Saturne* [6]. *Code_Saturne* is a parallel, general purpose, three dimensional, low Mach number CFD code, based on a collocated discretization [6]. The code solves the turbulent Navier Stokes equations for Newtonian incompressible flows with a fractional step method based on a prediction-correction algorithm for pressure/velocity coupling (SIMPLEC) and a Rhie and Chow interpolation to avoid pressure oscillations [6]. The details of the numerics used in *Code_Saturne* are given in appendix C.

The BML model along with all the scalar dissipation models discussed in chapter 6 have been implemented in *Code_Saturne* as part of this thesis. The solution is time advanced using a time step of $8\mu s$ for all equations. This leads to a maximum CFL number of 0.65 within the computational domain. The simulations are run until a steady solution is observed.

7.5 Results and discussion

The mean axial and transverse velocities at different locations downstream of the stabilising rod for different scalar dissipation rate models are reported in figures 7.4 and 7.5, respectively. It can be seen in figure 7.4 that the experiments show a decrease in the centre line velocity at $x \approx 0.02m$ and $x \approx 0.04m$ whereas predictions from almost all the $\widetilde{\epsilon}_c$ models show an increase in the velocity, thus producing an anomalous jet at the centre-line. This is due to the the simple approximation of the complex rod stabilisation process in the simulations. The simulated flame is anchored at the top of the stabilising rod, whereas in the experiment the flame is stabilised in the shear layer between the the recirculation region and the reacting flow [141]. Anomalous behaviour in this region has been reported in earlier numerical studies of Bell et al [9], Kolla et al [89, 85] and Robin et al [132, 133]. The velocity decay in the experiment is a consequence of the flow recirculation induced by the rod, which is not captured properly by the the $k-\epsilon$ model. Generally models based on Boussinesq's approximation have problems in swirling flows and flows with large rapid strain (i.e.curved boundary layers), as the normal stresses are not represented properly [155]. It is usually argued that this

does not influence results in the far wake of the stabilisation region as the bulk of the flame lies outside of the wake region and the flame dynamics are determined by the flame interacting with the reactant flow turbulence [9, 60]. Dunstan et al [60] have carried out a statistical analysis for their Direct Numerical Simulation (DNS) of a V-flame to show that the flame behaviour is not effected by the shortfalls of the stabilisation mechanism in the far wake of the stabilisation region. This implies that the flame behaviour in the far wake of the stabilisation region should not be influenced by the shortfalls of the $k-\epsilon$ model at the stabilisation region.

Contours of the progress variable $\overline{c}$ are shown in figures 7.6a- 7.12a for different scalar dissipation rate models. It can be observed that the spread rate of the simulated V-flame is not in agreement with the experimental data. One of the many reasons for the variation in the spread rate of the V-flame is the closure for pressure dilatation term $\overline{p' \frac{\partial u_i''}{\partial x_i}}$, as it is an explicit source term in the turbulent kinetic energy $\widetilde{k}$ transport equation eq. (5.51). Salehi and Bushe [139] have shown the influence of pressure dilatation on the production of turbulent kinetic energy, and it has also been shown in [139] that the closure used here (eq. (5.55)) over predicts the turbulent kinetic energy for the reaction rate mechanism used in their study. It is argued here that the closure for $\overline{p' \frac{\partial u_i''}{\partial x_i}}$ relies on the closure for $\overline{\dot{\omega}}_c$ and eventually on the choice of the closure used for $\widetilde{\epsilon}_c$, hence the performance of the closure for pressure dilatation is going to be influenced by the choice of the $\widetilde{\epsilon}_c$ model. The details of model performance for alternative closures of $\widetilde{\epsilon}_c$ are discussed in the following sub-sections.

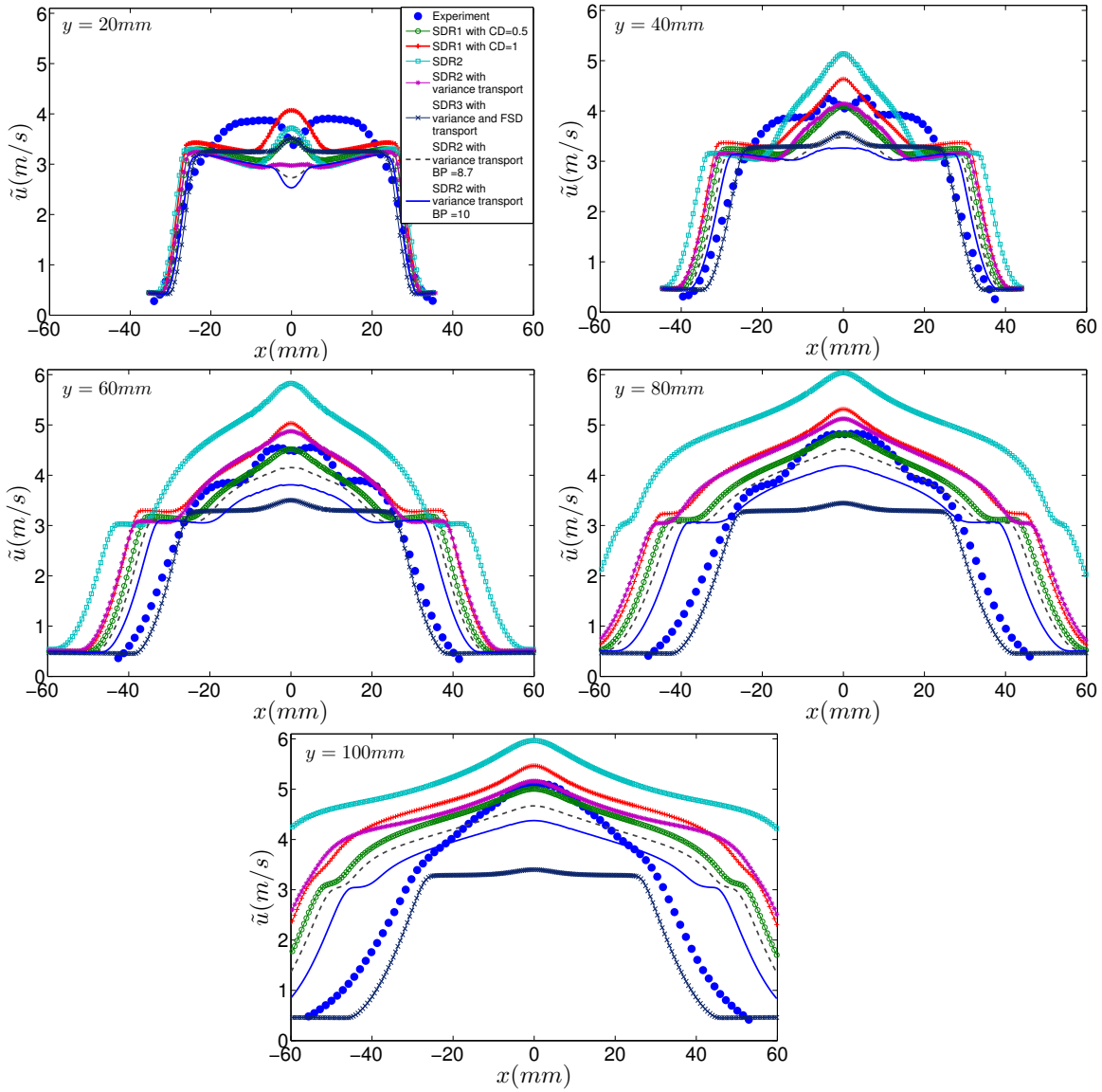

Figure 7.4: Mean axial velocities at different locations downstream of the stabilising rod in the V-flame calculation

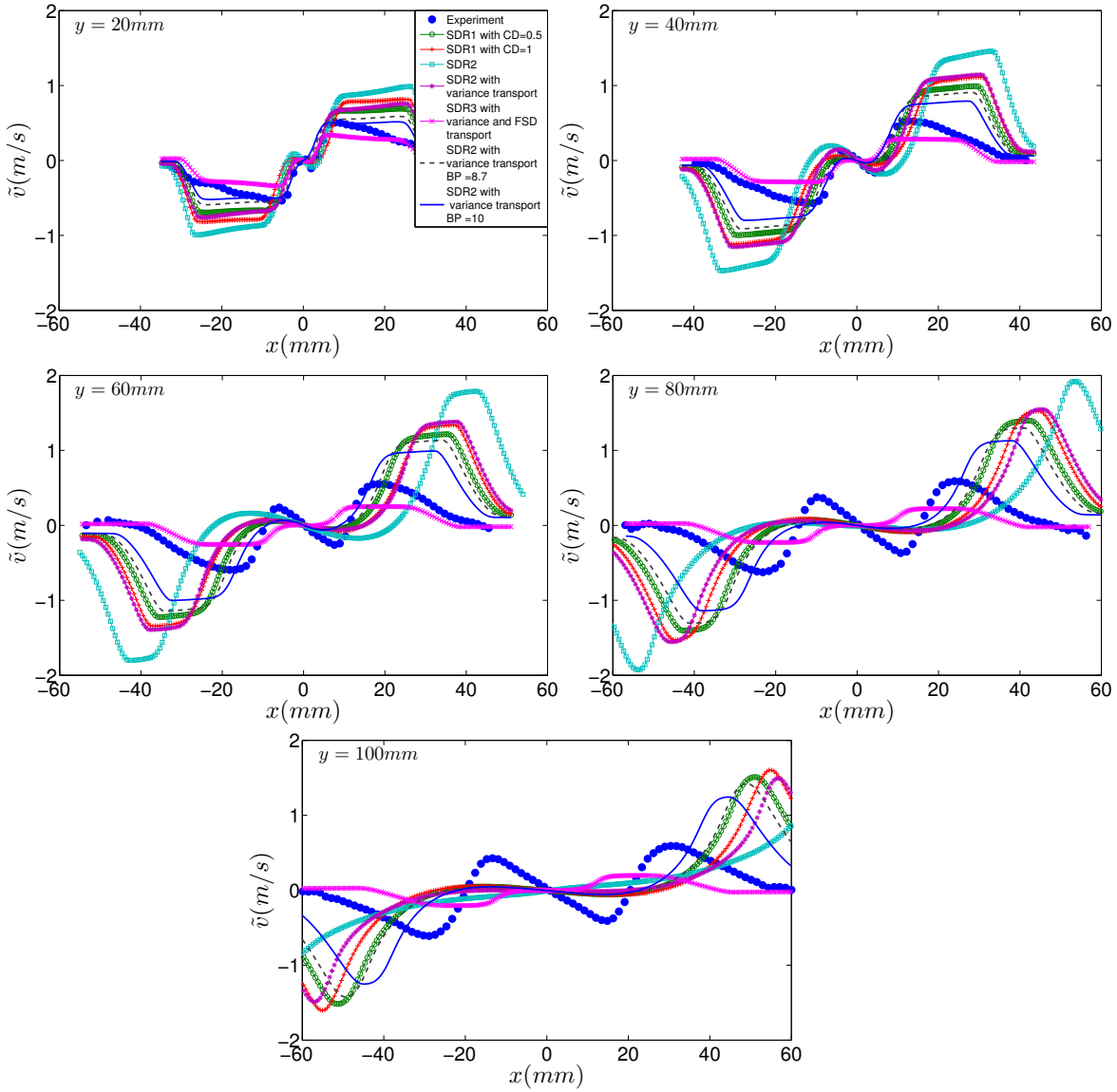

Figure 7.5: Mean transverse velocities at different locations downstream of the stabilising rod V-flame calculation

7.5.1 SDR-1 model

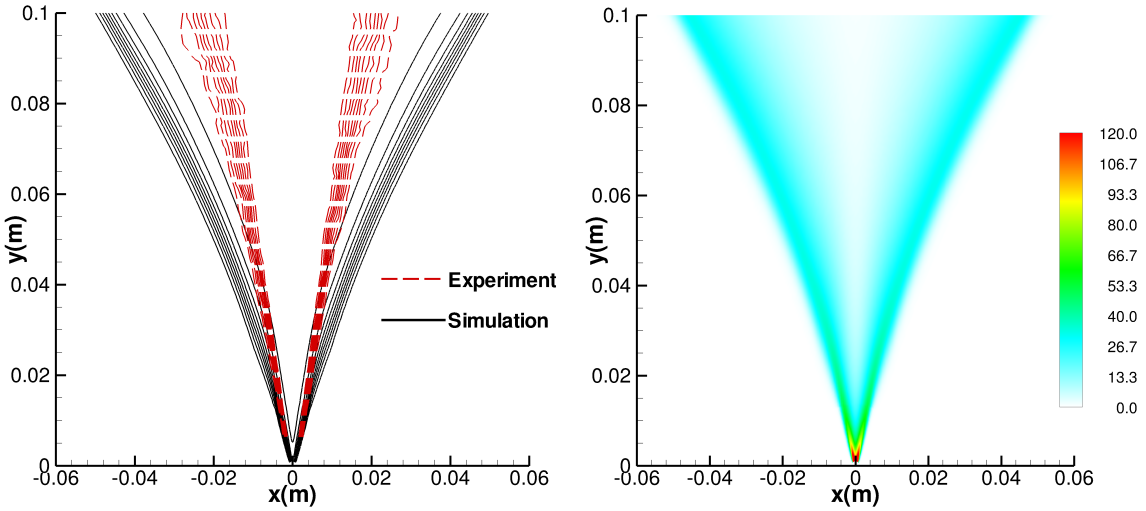

(a) $0.1 \leq \bar{c} \leq 0.9$ contours

(b) $\overline{\dot{\omega}}_c\,(kg/m^3s)$

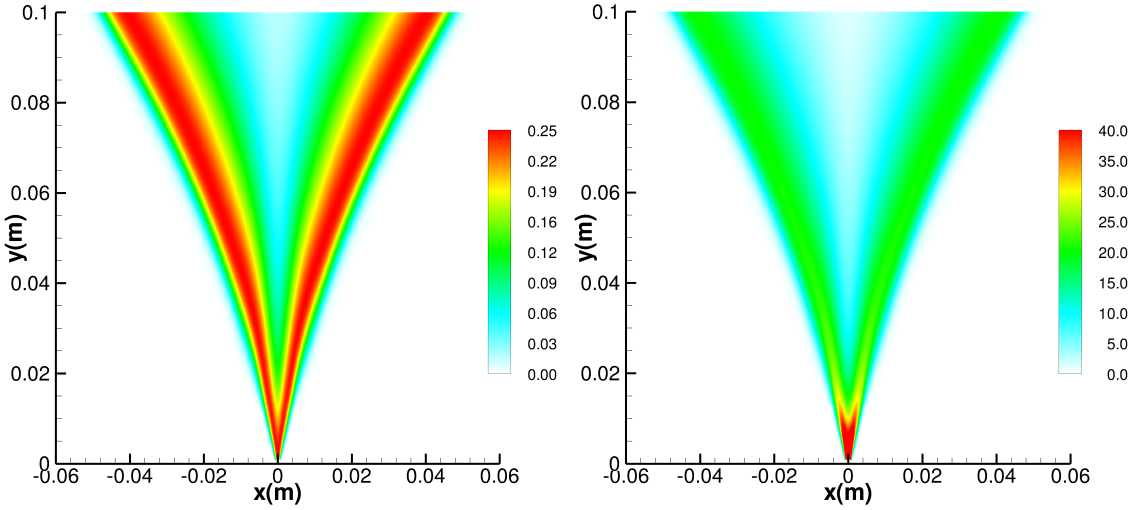

(c) $\widetilde{c}(1-\widetilde{c})$

(d) $\widetilde{\epsilon}_c\,(1/s)$

Figure 7.6: SDR-1 model ($C_D = 0.5$)

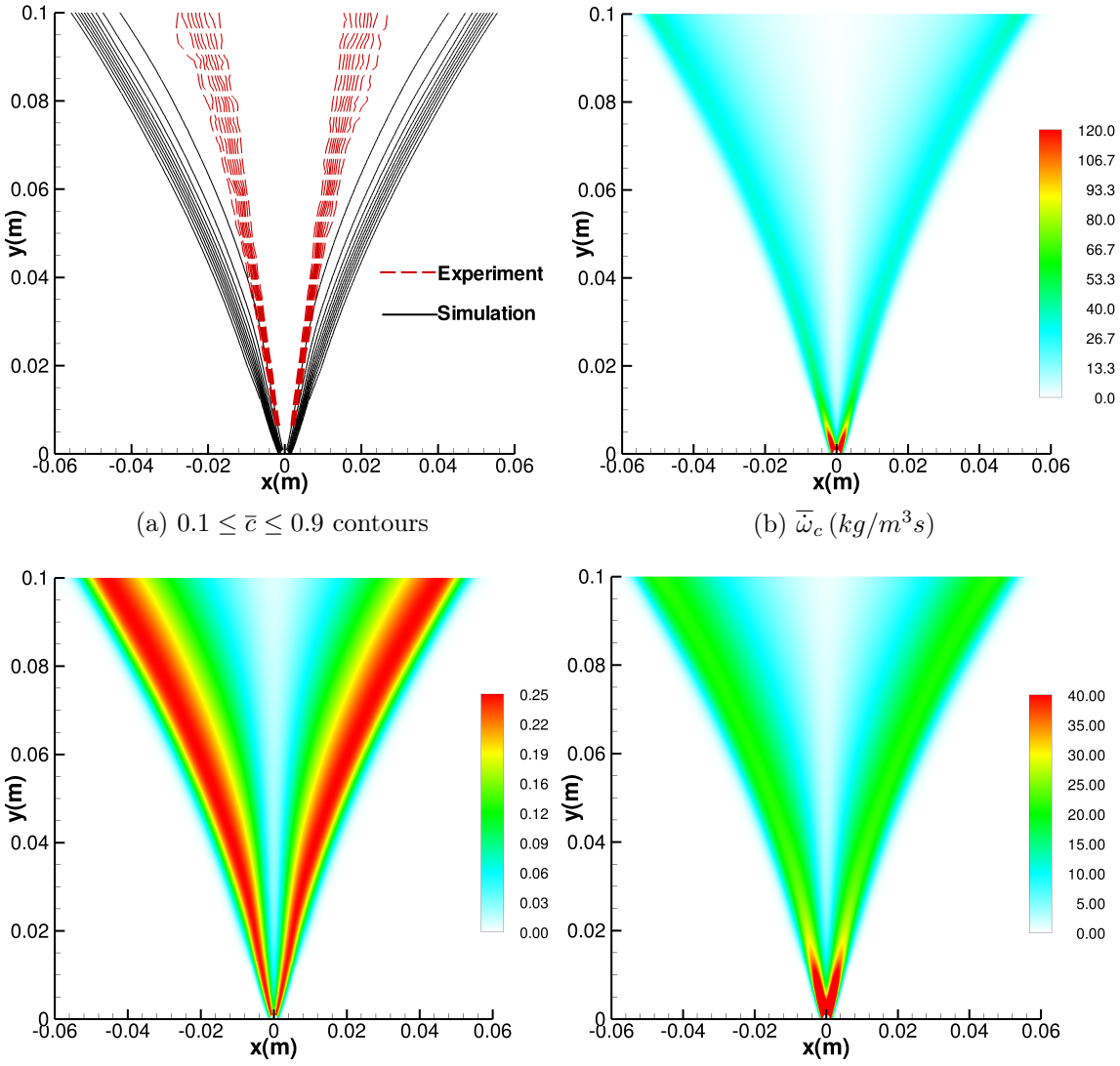

(a) $0.1 \leq \overline{c} \leq 0.9$ contours

(b) $\overline{\dot{\omega}}_c\,(kg/m^3 s)$

(c) $\widetilde{c}\,(1-\widetilde{c})$

(d) $\widetilde{\epsilon}_c\,(1/s)$

Figure 7.7: SDR-1 model ($C_D = 1$)

Figures 7.6a and 7.7a show the contours of $\overline{c}$ obtained from the SDR-1 model with the time scale ratios parametrised by $C_D = 0.5$ and $C_D = 1$, respectively. In this thesis the variance of the progress variable for the SDR-1 model is calculated by the BML algebraic closure, hence the variance is predicted under the strict BML limit as shown in figure 7.6c and figure 7.7c for different values of C_D. It can be seen in figures 7.6a and 7.7a that the change in the value of the time scale ratio has an influence on the prediction of the scalar dissipation $\widetilde{\epsilon}_c$ and the resulting

reaction rate, thus changing the location of the flame and affecting the resulting mean axial and transverse velocities as shown in figures 7.4 and 7.5. It can be observed that the lower value of C_D tends to improve the results by reducing the flame speed and the spread rate of the flame. The solution is very sensitive to the value of C_D used in the SDR-1 model, and there seems to be no accurate way of prescribing it in the context of RANS approaches.

The sensitivity of the model constant K_c to the heat release and equivalence ratio of the air fuel mixture also contributes to the higher spread rate of the V-flame predicted by the SDR-1 model; K_c influences C_{D_c} [149], which is associated with the modelling of dilatation.

The SDR-1 model relies on the classical approximation for flame turbulence alignment, which is based on the alignment of scalar gradient aligning with the most compressive strain rate eigenvector. This assumption ignores the changes in the alignment characteristics of the scalar gradient and the strain rate eigenvectors in the regions of intense heat release. This error in the modelling approach leads to wrong predictions of the scalar dissipation and the associated reaction rate.

7.5.2 SDR-2 model

The sensitivity of the SDR-2 model to alternative closures for $\widetilde{c''^2}$ and different values for β' has been tested. Initially $\beta' = 6.7$ is used, figures 7.8a and 7.9a show the contours of $\bar{c}$ obtained by using the BML closure for $\widetilde{c''^2}$ and with $\widetilde{c''^2}$ transport equation, respectively. The results show an improvement (a reduction in the spread rate) when the BML closure for variance is replaced by the transport equation for the variance of the progress variable $\widetilde{c''^2}$. This improvement is due to the explicit dependence of the $\widetilde{c''^2}$ transport equation on $\widetilde{\epsilon}_c$ in eq. 5.31, as using the transport equation for $\widetilde{c''^2}$ relaxes the strict BML limit, thus extending the range of applicability of the BML model. It can be observed in figures 7.8c and 7.9c that the BML closure for $\widetilde{c''^2}$ predicts higher levels of variance when compared with the results obtained from the variance transport equation. This leads to higher values of $\widetilde{\epsilon}_c$ (figures 7.8d and 7.9d) and consequently the associated reaction rates (figures 7.8b and 7.9b) predicted by the SDR-2 model. The flame locations predicted by both versions of the SDR-2 model start to deviate from the experimental results as the distance from the stabilisation rod increases. The

mean axial and transverse velocities in figure 7.4 and figure 7.5 respectively show that the velocities are over predicted by both versions of the SDR-2 model as the distance from the stabilisation region increases ($y > 0.04m$). The higher velocities are a result of an over estimation of the scalar dissipation rate and the resulting reaction rate calculated by using either forms of the SDR-2 model.

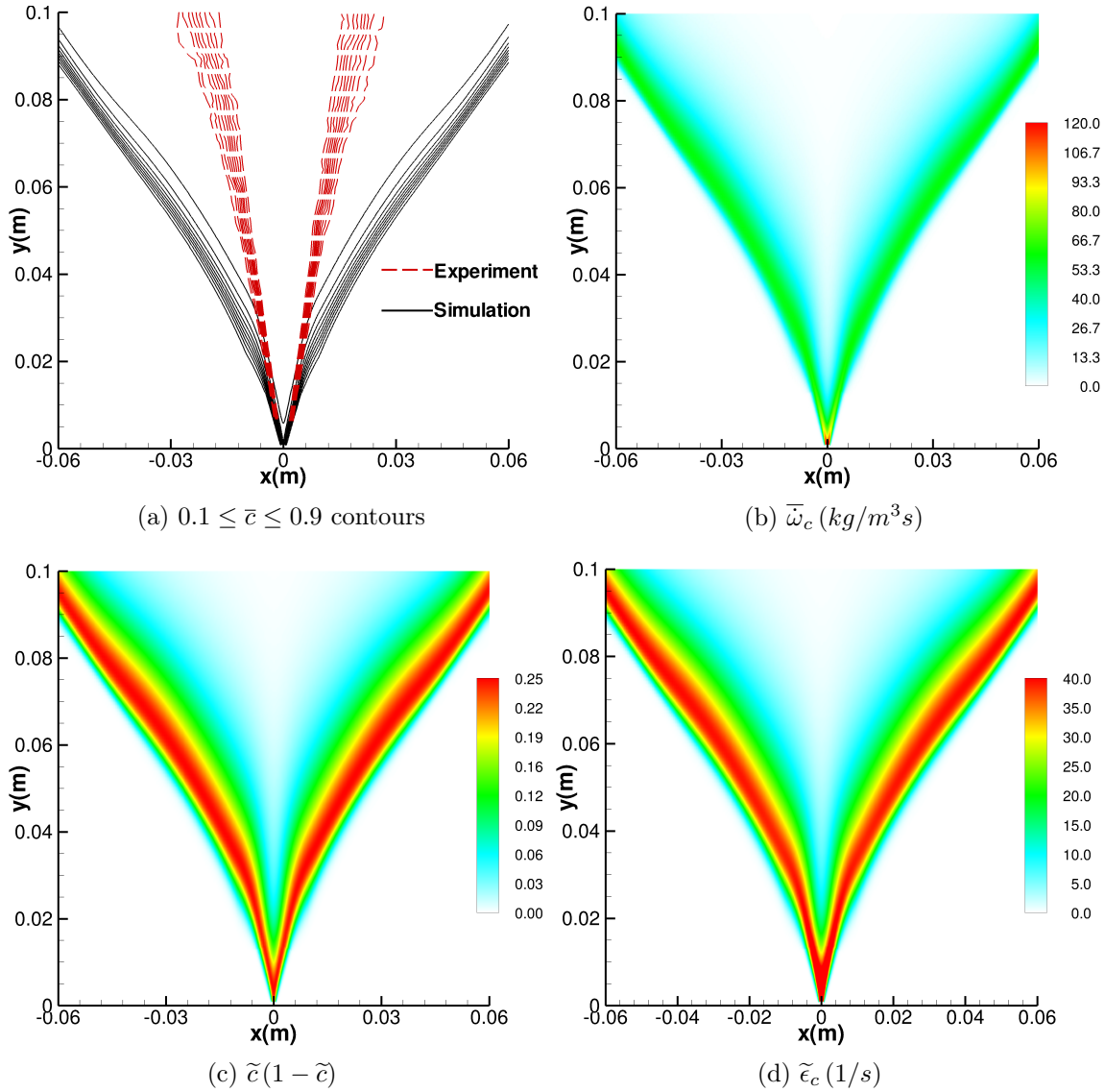

(a) $0.1 \leq \bar{c} \leq 0.9$ contours

(b) $\overline{\dot{\omega}}_c\,(kg/m^3s)$

(c) $\widetilde{c}(1-\widetilde{c})$

(d) $\widetilde{\epsilon}_c\,(1/s)$

Figure 7.8: SDR-2 model

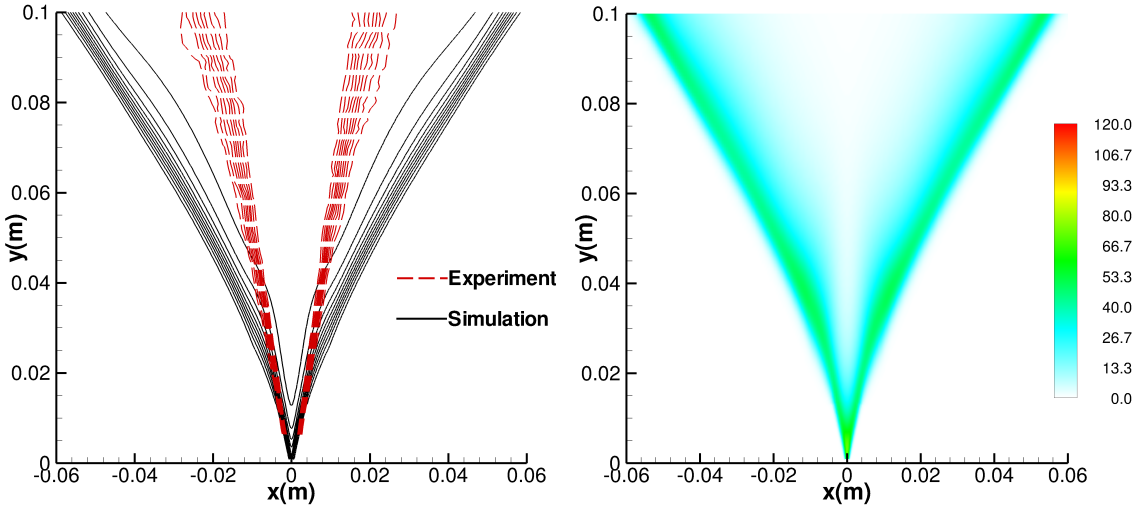

(a) $0.1 \leq \overline{c} \leq 0.9$ contours

(b) $\overline{\dot{\omega}}_c\,(kg/m^3 s)$

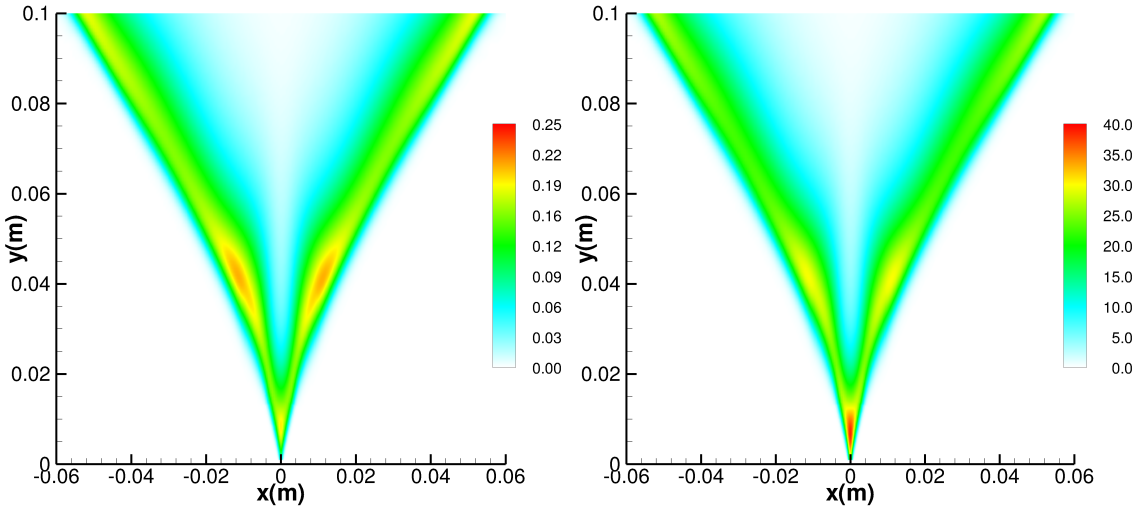

(c) $\widetilde{c''^2}$

(d) $\widetilde{\epsilon}_c\,(1/s)$

Figure 7.9: SDR-2 model with $\widetilde{c''^2}$ transport

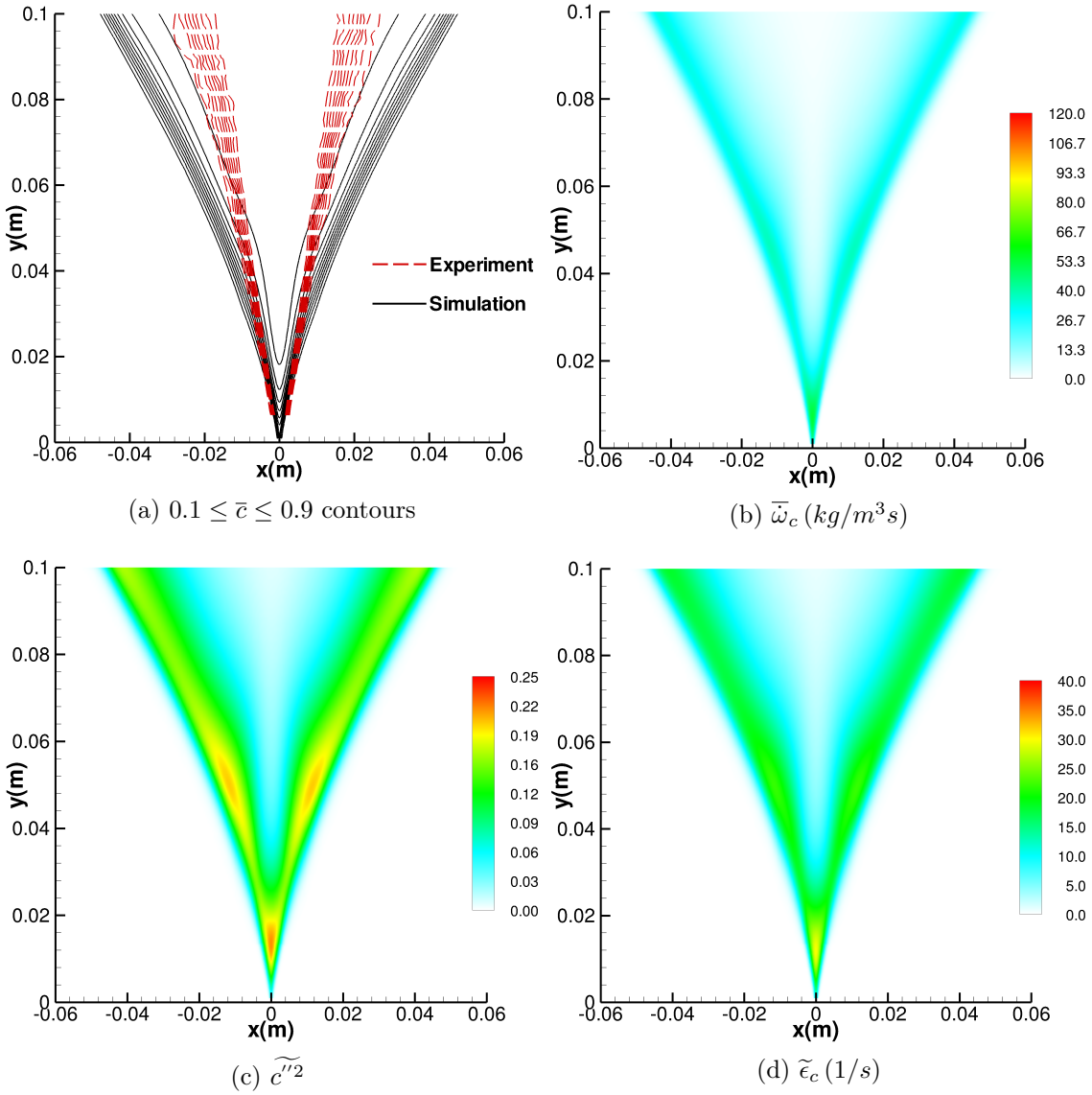

(a) $0.1 \leq \overline{c} \leq 0.9$ contours

(b) $\overline{\dot{\omega}}_c\,(kg/m^3s)$

(c) $\widetilde{c''^2}$

(d) $\widetilde{\epsilon}_c\,(1/s)$

Figure 7.10: SDR-2 model with $\widetilde{c''^2}$ transport and $\beta' = 8.7$

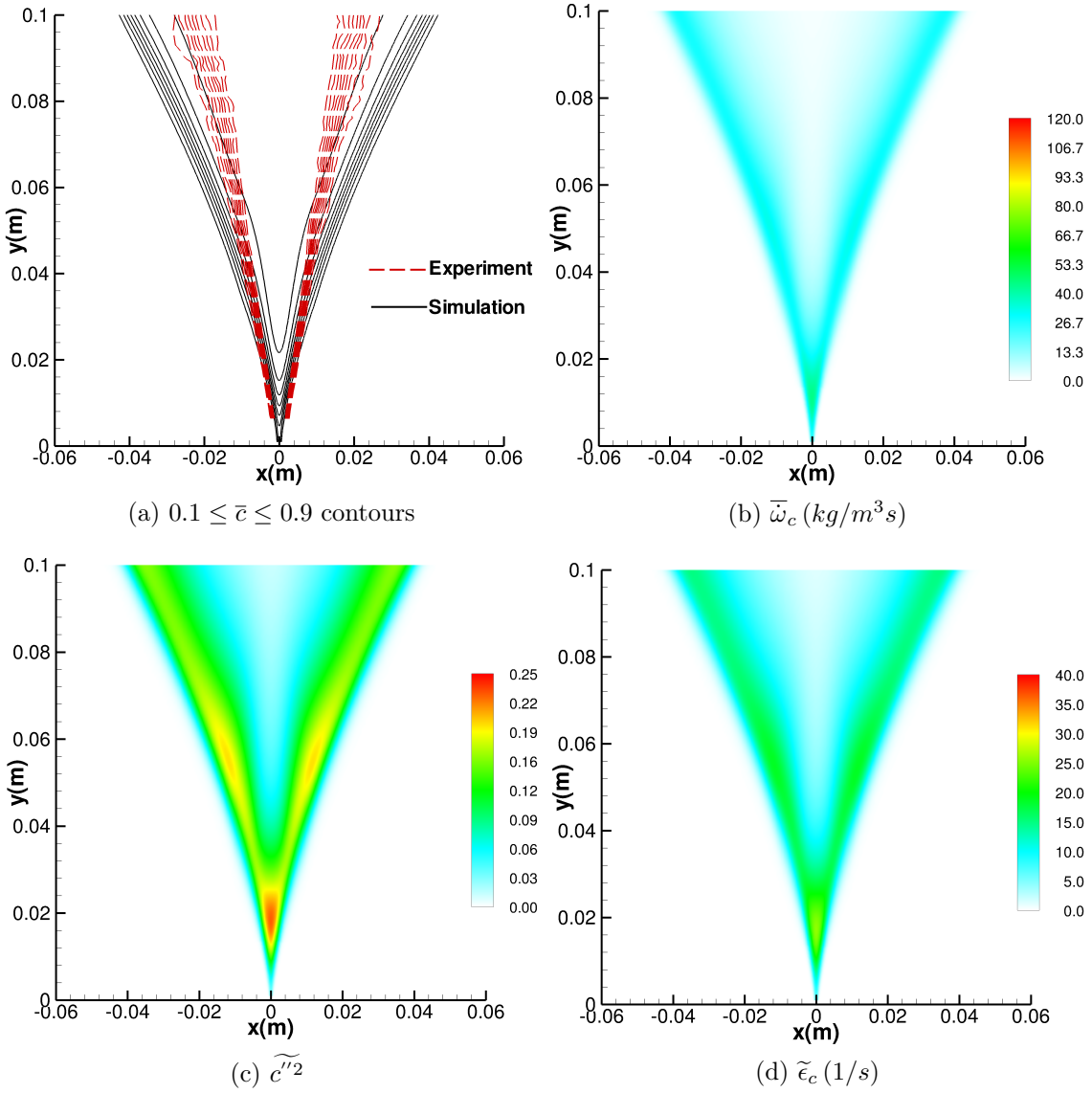

(a) $0.1 \leq \overline{c} \leq 0.9$ contours

(b) $\overline{\dot{\omega}}_c\,(kg/m^3 s)$

(c) $\widetilde{c''^2}$

(d) $\widetilde{\epsilon}_c\,(1/s)$

Figure 7.11: SDR-2 model with $\widetilde{c''^2}$ transport and $\beta' = 10$

In order to reduce the predicted scalar dissipation rate, the changes proposed for the constant β' by Chakraborty and Swaminathan [46] and Nikolaou and Swaminathan [113] have been tested. It has been found that the functional form of β' in eq. (6.30) gives similar results to that predicted by $\beta' = 6.7$, hence the results are not shown here. When $\beta' = 8.7$ is used it leads to an improvement of the flame location predicted by the SDR-2 model as shown in figure 7.10a. A higher value of $\beta' = 10$ has also been tested and it has been found that it

leads to a better agreement between the experimental data and the simulation as shown in figure 7.11a. A decrease in scalar dissipation rate can be observed by comparing figure 7.10d and figure 7.11d, thus leading to a decrease in the reaction rate as shown in figure 7.10b and figure 7.11b. The velocities predicted by the SDR-2 model with the new values of $\beta^{'}$ still deviate from the experimental data as shown in figure 7.4 and figure 7.5. Although it should be noted that the new values of $\beta^{'}$ improve the prediction of the mean axial velocity, and the velocity profiles start to follow the experimental trends.

Another reason for the deviation of the predictions of the SDR-2 model from the experimental data is the approximation for flame turbulence interaction term in the SDR-2 model. The scaling factors C_3 and C_4 used in the approximation for flame turbulence interaction in the SDR-2 model are sensitive to the choice of the laminar flame thickness used (i.e. thermal flame thickness or diffusive flame thickness) [59], thus the prediction of flame turbulence interaction is affected by the calibration of these scaling factors. Minamoto et al [109] have reported that the flame turbulence interaction approximation used in the SDR-2 model shows deviations from the DNS data and under predicts this quantity in the case of V-flames, this is due to the fact that the actual modelling strategies for T_{32} were developed for planar flames and the scaling factors are not tuned to take account of the changes in the flame geometry. Improvements to the flame turbulence interaction approximation are thus needed to improve the SDR-2 model. The lack of experimental data for the flame turbulence interaction term does not allow for a direct comparison of the RANS simulations to be made for this term.

7.5.3 SDR-3 model

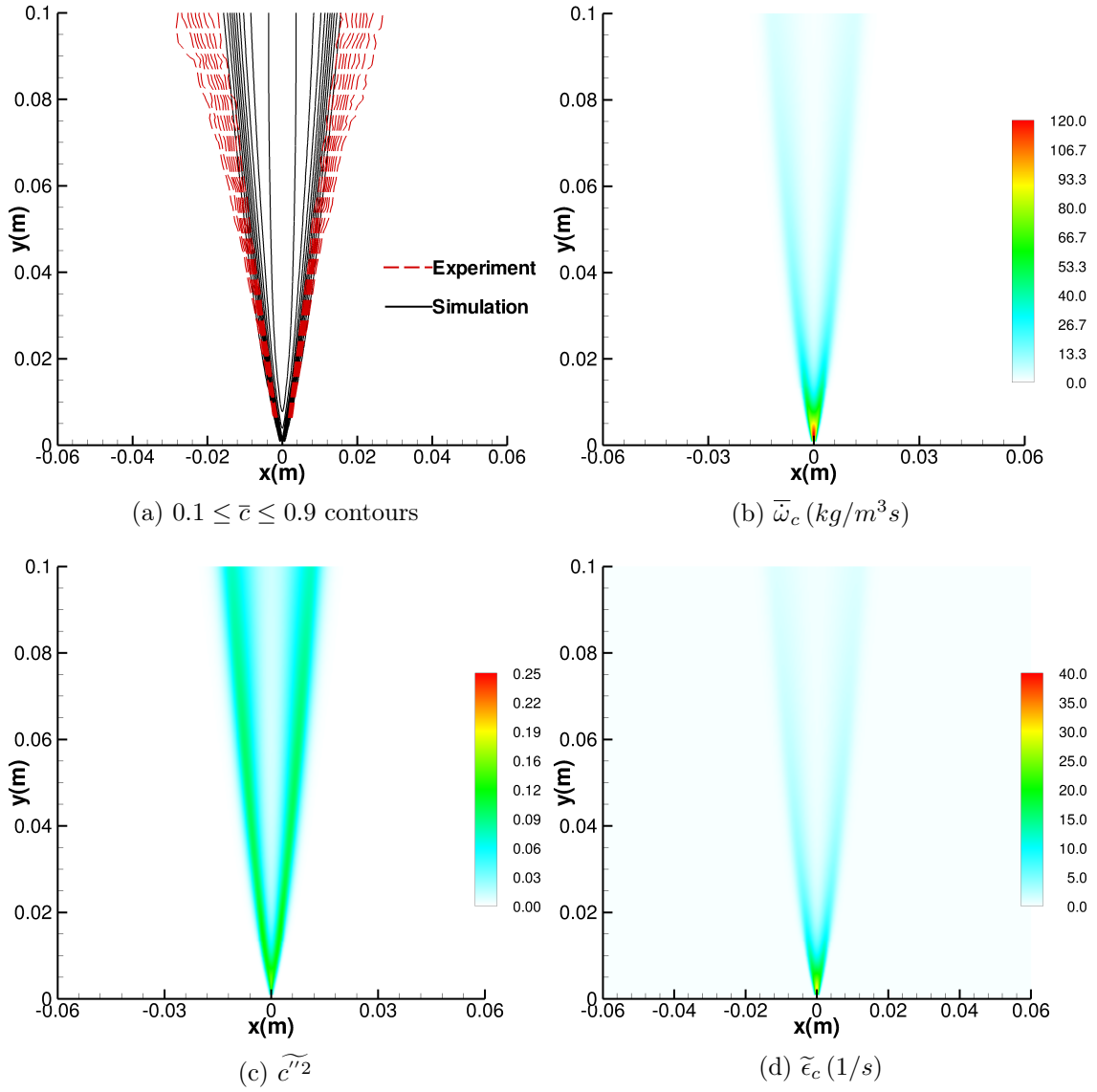

(a) $0.1 \leq \overline{c} \leq 0.9$ contours

(b) $\overline{\dot{\omega}}_c\,(kg/m^3 s)$

(c) $\widetilde{c''^2}$

(d) $\widetilde{\epsilon}_c\,(1/s)$

Figure 7.12: SDR-3 model with with $\widetilde{c''^2}$ and modelled Σ transport

The SDR-3 model makes use of the transport equation for Σ, hence the degree of accuracy for this model relies on the accuracy of the modelled Σ transport equation. The Σ transport equation enables the $\widetilde{\epsilon}_c$ model to account for the flow history effects on tangential strain rate and flame curvature. Figure 7.12a shows the contours of $\overline{c}$ obtained by using the SDR-3 model with modelled Σ

transport equation. It can be seen in figure 7.12a that the flame location is in good agreement up to $y \approx 0.05m$ with the experimental data. The flame location starts to deviate from the experiments for $y > 0.05m$, as the spread rate of the V-flame is under predicted. This is due to the lower predicted values of scalar dissipation rate (figure 7.12d) and the associated reaction rate (figure 7.12b). It can be seen in figure 7.12b that the reaction rate becomes small as the distance from the stabilisation rod increases ($y > 0.05m$). The effect of the SDR-3 model on variance transport can be seen in figure 7.12c. The value of $\widetilde{c''^2}$ decreases as the reaction rate decreases, this is due to the decrease in the reaction term in eq. 5.31 which leads to lower values of scalar dissipation and consequently $\widetilde{c''^2}$.

The decrease in scalar dissipation rate and the associated reaction rate away from the stabilisation rod leads to mean axial and transverse velocities being under predicted when compared with the experiment. This implies that the SDR-3 model with the modelled Σ transport equation predicts a shorter flame than the one reported in the experiment. Hence the mean axial and transverse velocities do not change beyond $y \approx 0.06m$ as shown in figure 7.4 and figure 7.5. The shortfalls of the SDR-3 model can be explained by the approximations made in the modelled Σ transport equation. The destruction term in the Σ transport equation only includes the flame curvature effects, and additional mechanisms might be involved in the destruction process [118]. Further more the modelled Σ transport equation also lacks the dilatation effects arising from the tangential strain acting on the flame surface. It should also be noted that the strain rate modelling used in the Σ transport equation (eq. (6.55)) relies on the classical model for the flame turbulence interaction phenomenon and does not include any effects of heat release and the associated changes in the flame turbulence alignment behaviour.

7.6 Summary and preliminary conclusions

In the RANS simulations, the flame behaviour is dominated by the choice of scalar dissipation model used for the calculations. The SDR-1 model has been used with two different time scale ratios. It has been found that the solution is very sensitive to the choice of the value used for the time scale ratio, which affects

the flame location and the resulting mean and axial velocities predicted by the model.

The SDR-2 model has been used with different closures for the variance of the progress variable $\widetilde{c''^2}$, and it has been found that the SDR-2 model performs better when the transport equation for $\widetilde{c''^2}$ is solved instead of using the algebraic closure obtained from the BML theory. The sensitivity of the SDR-2 model to different values of β' has also been tested. It has been found that the model tends to perform better when higher values of β' are used. A new value of $\beta' \approx 10$ has been proposed for V-flame calculations. It is argued here that the disagreement between the experimental data and the predicted values from the model (with $\beta' \approx 10$) is due the approximation of the flame turbulence interaction term. The lack of experimental data for the flame turbulence interaction does not allow for a direct comparison of the RANS simulations to be made for this term.

The SDR-3 model has been used with a modelled flame surface density transport equation. The results obtained by the model in the immediate wake region of the stabilisation rod are in good agreement with the experimental data. However, a shorter flame is predicted by the model, additionally affecting the mean velocities in the far wake region of the stabilising rod. The shortfalls in the SDR-3 model can be explained by the assumptions made in modelling the Σ transport equation. The destruction term in the Σ transport equation only includes the flame curvature effects and additional mechanisms might be involved in the destruction process [56, 118]. Further more the modelled Σ transport equation also lacks the dilatation effects arising from the tangential strain acting on the flame surface. The strain rate modelling used in the Σ transport equation relies on the classical form of scalar turbulence interaction and does not include any effects of heat release and the associated changes in the flame turbulence alignment behaviour.

In order to improve the modelling for the flame turbulence interaction a new transport equation has been proposed and is discussed in the subsequent chapters.

8 An evolution equation for flame turbulence interaction in premixed turbulent flames

The flame turbulence interaction phenomenon presents a major difficulty in obtaining an accurate closure for both the scalar dissipation $\widetilde{\epsilon}_c$ and the flame surface density Σ, and thus the mean reaction rate $\overline{\dot{\omega}}_c$. Earlier studies have shown that this term represents the production (or dissipation) of scalar gradients in flows with chemical reactions [40, 71]. Swaminathan and Grout [151] and Chakraborty and Swaminathan [44, 45] have shown that the effect of strain rate on the transport of $\widetilde{\epsilon}_c$ is dominated by the interaction between the fluctuating scalar gradients and the fluctuating strain rate. These fluctuations represent the flame turbulence interaction phenomenon. Here, an alternative way for the prediction of flame turbulence interaction in premixed flames is presented by proposing a transport equation for $\widetilde{D_c \nabla c^{''} S_{ij}^{''} \nabla c^{''}}$. This equation provides a detailed insight into the flame turbulence interaction phenomenon and provides a more flexible approach to model the important physics represented by $\widetilde{D_c \nabla c^{''} S_{ij}^{''} \nabla c^{''}}$.

8.1 Flame turbulence interaction evolution equation

In the case of statistically multidimensional flames $\overline{\rho D_c \nabla c^{''} S_{ij}^{''} \nabla c^{''}}$ can be decomposed using an eigendecomposition and written as :

$$\overline{\rho D_c \nabla c^{''} S_{ij}^{''} \nabla c^{''}} = \overline{\rho D_c \left|\nabla c^{''}\right|^2 \left(e_\alpha \cos^2\theta_\alpha + e_\beta \cos^2\theta_\beta + e_\gamma \cos^2\theta_\gamma\right)}, \tag{8.1}$$

where e_α, e_β and e_γ are the eigenvalues of the turbulent strain rate tensor S''_{ij}. The eigenvalues are ranked as $e_\alpha > e_\beta > e_\gamma$, with e_α being the most extensive principal strain rate and e_γ being the most compressive principal strain rate. The angle between scalar gradient and the eigenvector associated with the e_α strain rate is denoted by θ_α.

An evolution equation for $\widetilde{D_c \nabla c'' S''_{ij} \nabla c''}$ can be used to represent the degree of misalignment between the gradient of the scalar and the eigenvectors of the strain rate. The details of the physics represented by the change in alignment of the flame gradient and the strain rate eigenvectors has been discussed earlier in section 6.3.2.2.

The evolution equation can be found by taking the total derivative of

$$\rho \frac{D}{Dt}\left(D_c \frac{\partial c}{\partial x_i} S_{ij} \frac{\partial c}{\partial x_j}\right), \tag{8.2}$$

where D_c is assumed to be constant. Applying the Reynolds decomposition to eq. (8.2) and Favre averaging leads to:

$$\begin{aligned}\overline{\rho \frac{D}{Dt}\left(D_c \frac{\partial c}{\partial x_i} S_{ij} \frac{\partial c}{\partial x_j}\right)} = \overline{\rho} \frac{D}{Dt} \Bigg[&\underbrace{\widetilde{D_c \frac{\partial c''}{\partial x_i} S''_{ij} \frac{\partial c''}{\partial x_j}}}_{\text{Term 1}} + \underbrace{\widetilde{D_c \frac{\partial c''}{\partial x_i} \frac{\partial c''}{\partial x_j}}\, \widetilde{S_{ij}}}_{\text{Term 2}} + \underbrace{\widetilde{D_c \frac{\partial c''}{\partial x_j} S''_{ij}}\, \frac{\partial \widetilde{c}}{\partial x_i}}_{\text{Term 3}} \\ &+ \underbrace{\widetilde{D_c \frac{\partial c''}{\partial x_i} S''_{ij}}\, \frac{\partial \widetilde{c}}{\partial x_j}}_{\text{Term 4}} + \underbrace{\overline{D_c} \frac{\partial \widetilde{c}}{\partial x_i} \widetilde{S_{ij}} \frac{\partial \widetilde{c}}{\partial x_j}}_{\text{Term 5}} \Bigg]\end{aligned} \tag{8.3}$$

An order of magnitude analysis under the joint assumptions of high Re_{l_t} and Da is used to find the leading order terms in eq. (8.3). It is important here to understand the different arguments used in the order of magnitude analysis.

8.2 Order of magnitude analysis arguments

In previous studies OMA has been developed for the $\widetilde{\epsilon}_c$ transport equations to reduce their complexity. In this section the OMA rules are discussed in detail. The classical rules for OMA proposed by Tennekees and Lumley [152] are discussed, then the improvements proposed by Mantel and Borghi [105] are discussed and finally the recently proposed OMA rules by Swaminathan and Bray [149] are discussed.

8.2.1 OMA scaling arguments of Tennekes and Lumley

The classical rules for OMA have been proposed by Tennekes and Lumley [152]:

- The spatial derivatives of mean quantities are scaled by the integral length scale l_t.
- The spatial derivatives of fluctuating quantities are scaled by the Taylor micro-scale λ_T (as it is assumed that mixing occurs at the Taylor micro-scale).
- The time derivatives of mean quantities are scaled by using the turbulent time scale $\tau_t = l_t/u^{'}$.
- The velocity is scaled by the root-mean square velocity $u^{'}$.

According to these scaling laws all the terms being analysed scale in terms of a turbulent Reynolds number (Re_{l_t}). Note that the scaling rules of Tennekes and Lumley [152] do not include any effects of combustion, heat release and the associated density variations. These rules rely only on the effects from cold flow turbulence, and also do not account for the second-order derivatives of scalar fluctuations.

8.2.2 OMA scaling arguments of Mantel and Borghi

A new scaling rule under the joint assumption of high turbulent Reynolds (Re_{l_t}) and Damkhöler (Da) number has been proposed by Mantel and Borghi [105]. The effects due to combustion are included via the inclusion of the high Da limit, as

the flow field can be divided into a flamelet and non-flamelet region. The scaling arguments proposed by Mantel and Borghi are [105]:

- The spatial derivatives of mean quantities are scaled by the integral length scale l_t.
- The spatial derivatives of the fluctuating quantities are scaled by the Taylor micro-scale λ_T.
- The velocity is scaled by the root-mean square velocity $u^{'}$.
- The spatial derivatives of the fluctuating progress variable are scaled by the unstretched laminar flame thermal thickness δ_L^0.
- The time derivatives of mean quantities are scaled by using the turbulent time scale $\tau_t = l_t/u^{'}$.

In the scaling arguments of Mantel and Borghi [105] terms in a given transport equation scale as functions of Re_{l_t} and Da. The contributions in the non-flamelet part do not depend on Da thus Re_{l_t} is retained in the scaling arguments of Mantel and Borghi [105]. In these scaling rules the effects of combustion are explicitly included by introducing the chemical length and time scales, but the density is treated as a constant.

8.2.3 OMA scaling arguments of Swaminathan and Bray

Swaminathan and Bray have proposed improvements to the scaling rules proposed by Mantel and Borghi [105]. The scaling arguments proposed by Swaminathan and Bray are [149]:

- The spatial derivatives of mean quantities are scaled by the integral length scale l_t.
- The time derivatives are scaled by the ratio of the integral length scale and the root mean square velocity $\tau_t = l_t/u^{'}$.
- The density is scaled by the density of the reactants ρ_R.
- The mean velocities are scaled by a reference velocity u_{ref}.

- The thermal diffusivity of the mixture is scaled by the laminar flame scales $u_L^0 \delta_L^0$, where u_L^0 is the unstretched laminar flame speed and δ_L^0 is the laminar flame thermal thickness.

Note that in Swaminathan and Bray's scaling the laminar flame scales are used to scale the quantities involving (or multiplied) by the gradients of the fluctuating part of the progress variable c. As in case of thin flames, the gradient of c is zero outside the flame. These scaling rules take account of the dilatation effects, and only rely on one length scale of turbulence unlike the earlier scaling arguments proposed by Mantel and Borghi [105] and Tennekees and Lumley [152].

Although the aforementioned OMA rules have been developed for the analysis of $\widetilde{\epsilon}_c$ transport equations, OMA rules proposed by Swaminathan and Bray [149] have been used for the flame turbulence interaction transport equation, as these scaling laws include the effects of dilatation due to heat release, and thus include the effects of flame straining due to dilatation.

According to the scaling laws the terms in eq. (8.3) scale as:
Term 1 scales as:

$$\overline{\rho D_c} \widetilde{\frac{\partial c''}{\partial x_i} S''_{ij} \frac{\partial c''}{\partial x_j}} \backsimeq \mathcal{O}\left(\rho_R \left(\frac{u_L^0}{\delta_L^0} \right)^2 ; 1 \right) \tag{8.4}$$

Term 2 scales as:

$$\overline{\rho D_c} \widetilde{\frac{\partial c''}{\partial x_i} \frac{\partial c''}{\partial x_j}} \widetilde{S_{ij}} \backsimeq \mathcal{O}\left(\rho_R \left(\frac{u_L^0}{\delta_L^0} \right)^2 ; \left(\frac{u' Da}{u_{ref}} \right)^{-1} \right) \tag{8.5}$$

Term 3 scales as:

$$\overline{\rho D_c} \widetilde{\frac{\partial c''}{\partial x_j} S''_{ij}} \frac{\partial \widetilde{c}}{\partial x_i} \backsimeq \mathcal{O}\left(\rho_R \left(\frac{u_L^0}{\delta_L^0} \right)^2 ; (Re_{l_t} Da)^{-1/2} \right) \tag{8.6}$$

Term 4 scales as:

$$\overline{\rho D_c} \widetilde{\frac{\partial c''}{\partial x_i} S''_{ij}} \frac{\partial \widetilde{c}}{\partial x_j} \backsimeq \mathcal{O}\left(\rho_R \left(\frac{u_L^0}{\delta_L^0} \right)^2 ; (Re_{l_t} Da)^{-1/2} \right) \tag{8.7}$$

Term 5 scales as:

$$\overline{\rho D_c}\left(\frac{\partial\widetilde{c}}{\partial x_i}\widetilde{S_{ij}}\frac{\partial\widetilde{c}}{\partial x_j}\right) \backsimeq \mathcal{O}\left(\rho_R\left(\frac{u_L^0}{\delta_L^0}\right)^2;\left(\frac{Re_{l_t}Da^2u^{'}}{u_{ref}}\right)^{-1}\right) \tag{8.8}$$

The above order of magnitude analysis suggests that in the thin flamelet limit, $\overline{\rho}\left(\overline{D_c c_{,i}^{''} S_{ij}^{''} c_{,j}^{''}}\right)$ is a dominant term, and, thus an evolution equation for $\overline{\rho}\left(\overline{D_c c_{,i}^{''} S_{ij}^{''} c_{,j}^{''}}\right)$ will provide a useful leading order approximation.

8.3 Flame turbulence interaction evolution equation development

Introducing the definition:

$$\overline{\rho}\widetilde{\Delta}_c \equiv \overline{\rho D_c \frac{\partial c^{''}}{\partial x_i} S_{ij}^{''} \frac{\partial c^{''}}{\partial x_j}}. \tag{8.9}$$

The total derivative of the fluctuating part of flame turbulence interaction term is:

$$\begin{aligned}\overline{\rho}\frac{D}{Dt}\left(\overline{D_c\frac{\partial c^{''}}{\partial x_i}S_{ij}^{''}\frac{\partial c^{''}}{\partial x_j}}\right) &= \overline{\rho D_c}\left[\overline{\frac{\partial c^{''}}{\partial x_i}S_{ij}^{''}\frac{D}{Dt}\left(\frac{\partial c^{''}}{\partial x_j}\right)} + \overline{\frac{\partial c^{''}}{\partial x_j}\frac{\partial c^{''}}{\partial x_i}\frac{D}{Dt}\left(S_{ij}^{''}\right)}\right. \\ &\quad \left. + \overline{\frac{\partial c^{''}}{\partial x_j}S_{ij}^{''}\frac{D}{Dt}\left(\frac{\partial c^{''}}{\partial x_i}\right)}\right]\end{aligned} \tag{8.10}$$

Using the definition of $S_{ij}^{''}$ and some algebraic simplification leads to:

$$\overline{\rho}\frac{D}{Dt}\left(\overline{D_c\frac{\partial c^{''}}{\partial x_i}S_{ij}^{''}\frac{\partial c^{''}}{\partial x_j}}\right) = 2\underbrace{\overline{\rho D_c}\overline{\frac{\partial c^{''}}{\partial x_i}S_{ij}^{''}\frac{D}{Dt}\left(\frac{\partial c^{''}}{\partial x_j}\right)}}_{\text{Term 1}} + \underbrace{\overline{\rho D_c}\overline{\frac{\partial c^{''}}{\partial x_j}\frac{\partial c^{''}}{\partial x_i}\frac{D}{Dt}\left(\frac{\partial u_i^{''}}{\partial x_j}\right)}}_{\text{Term 2}} \tag{8.11}$$

Terms 1 and 2 in eq. (8.11) can be simplified to give the final transport equation for $\widetilde{\Delta}_c$. In order to resolve the first term in eq. (8.11), a transport equation for

the gradient of $c^{''}$ is required. That can be achieved by recalling the definition

$$\rho D_c \frac{D}{Dt}\left(\frac{\partial c^{''}}{\partial x_i}\right) = \rho D_c \frac{D}{Dt}\left(\frac{\partial c}{\partial x_i} - \frac{\partial \widetilde{c}}{\partial x_i}\right).$$

The general transport equation for c is :

$$\rho \frac{Dc}{Dt} = \dot{\omega}_c + \frac{\partial}{\partial x_n}\left(\rho D_c \frac{\partial c}{\partial x_n}\right). \tag{8.12}$$

Taking the derivative of eq. (8.12) in the x_j direction leads to

$$\begin{aligned}\rho \frac{\partial}{\partial t}\left(\frac{\partial c}{\partial x_j}\right) + \frac{\partial}{\partial x_j}\left(\rho u_n \frac{\partial c}{\partial x_n}\right) + \rho \frac{\partial c}{\partial x_n}\frac{\partial u_n}{\partial x_j} + \frac{\partial \rho}{\partial x_j}\left(\frac{\frac{\partial}{\partial x_n}\left(\rho D_c \frac{\partial c}{\partial x_n}\right) + \dot{\omega}_c}{\rho}\right) \\ = \frac{\partial}{\partial x_j}\left(\frac{\partial}{\partial x_n}\left(\rho D_c \frac{\partial c}{\partial x_n}\right)\right) + \frac{\partial \dot{\omega}_c}{\partial x_j}.\end{aligned} \tag{8.13}$$

Following earlier studies [148] the dilatation term can be expressed as

$$\frac{\partial \rho}{\partial x_j}\frac{\left(\dot{\omega}_c + \frac{\partial}{\partial x_n}\left(\rho D_c \frac{\partial c}{\partial x_n}\right)\right)}{\rho} = -\rho \frac{\partial c}{\partial x_j}\left(\frac{\partial u_l}{\partial x_l}\right), \tag{8.14}$$

and simplification and multiplication with D_c leads to :

$$\begin{aligned}\rho D_c \frac{\partial}{\partial t}\left(\frac{\partial c}{\partial x_j}\right) + \rho D_c u_n \frac{\partial}{\partial x_n}\left(\frac{\partial c}{\partial x_j}\right) = D_c \frac{\partial}{\partial x_j}\left(\frac{\partial}{\partial x_n}\left(\rho D_c \frac{\partial c}{\partial x_n}\right)\right) \\ + \frac{\partial \dot{\omega}_c}{\partial x_j} - \rho \frac{\partial c}{\partial x_n}\frac{\partial u_n}{\partial x_j} + \rho \frac{\partial c}{\partial x_j}\left(\frac{\partial u_l}{\partial x_l}\right).\end{aligned} \tag{8.15}$$

Applying the Reynolds decomposition and Favre averaging to eq. (8.15) provides:

$$\begin{aligned}\overline{\rho D_c}\frac{\partial}{\partial t}\left(\frac{\partial \widetilde{c}}{\partial x_j}\right) + \frac{\partial}{\partial x_n}\left(\overline{\rho D_c}\widetilde{u}_n \frac{\partial \widetilde{c}}{\partial x_j}\right) = \frac{\partial}{\partial x_j}\left(\frac{\partial}{\partial x_n}\left(\overline{\rho D_c D_c}\frac{\partial \widetilde{c}}{\partial x_n}\right)\right) - \frac{\partial}{\partial x_n}\left(\overline{\rho D_c}\widetilde{u_n^{''}\frac{\partial c^{''}}{\partial x_j}}\right) \\ + \overline{D_c}\frac{\partial}{\partial x_j}\overline{\dot{\omega}_c} + \overline{\rho D_c \frac{\partial c^{''}}{\partial x_j}\frac{\partial u_l^{''}}{\partial x_l}} + \overline{\rho D_c}\frac{\partial \widetilde{c}}{\partial x_j}\frac{\partial \widetilde{u}_l}{\partial x_l} - \overline{\rho D_c \frac{\partial c^{''}}{\partial x_n}\frac{\partial u_n^{''}}{\partial x_j}} + \overline{\rho D_c}\frac{\partial \widetilde{c}}{\partial x_n}\frac{\partial \widetilde{u}_n}{\partial x_j}.\end{aligned} \tag{8.16}$$

Subtracting eq. (8.16) from eq. (8.15), then multiplying the resulting equation with $\frac{\partial c^{''}}{\partial x_i} S^{''}_{ij}$ and Favre averaging leads to:

$$\begin{aligned}
\overline{\rho D_c} \widetilde{\frac{\partial c^{''}}{\partial x_i} S^{''}_{ij} \frac{D}{Dt}\left(\frac{\partial c^{''}}{\partial x_j}\right)} &= \overline{\frac{\partial c^{''}}{\partial x_i} S^{''}_{ij} \frac{\partial}{\partial x_j}\left(\frac{\partial}{\partial x_n}\left(\rho D_c D_c \frac{\partial c^{''}}{\partial x_n}\right)\right)} \\
&+ \widetilde{\frac{\partial c^{''}}{\partial x_i} S^{''}_{ij}} \frac{\partial}{\partial x_n}\left(\overline{\rho D_c} \widetilde{u^{''}_n \frac{\partial c^{''}}{\partial x_j}}\right) - \overline{\rho D_c} \widetilde{\frac{\partial c^{''}}{\partial x_i} S^{''}_{ij} u^{''}_n \frac{\partial}{\partial x_n}\left(\frac{\partial c^{''}}{\partial x_j}\right)} \\
&- \overline{\rho D_c} \widetilde{\frac{\partial c^{''}}{\partial x_i} S^{''}_{ij} u^{''}_n} \frac{\partial}{\partial x_n}\left(\frac{\partial \widetilde{c}}{\partial x_j}\right) + \overline{D_c \frac{\partial c^{''}}{\partial x_i} S^{''}_{ij} \frac{\partial}{\partial x_j} \dot{\omega}^{''}_c} \\
&+ \overline{\rho D_c} \widetilde{\frac{\partial c^{''}}{\partial x_i} S^{''}_{ij} \frac{\partial c^{''}}{\partial x_j} \frac{\partial u^{''}_l}{\partial x_l}} + \overline{\rho D_c} \frac{\partial \widetilde{u}_l}{\partial x_l} \widetilde{\frac{\partial c^{''}}{\partial x_i} S^{''}_{ij} \frac{\partial c^{''}}{\partial x_j}} \\
&+ \overline{\rho D_c} \frac{\partial \widetilde{c}}{\partial x_j} \widetilde{\frac{\partial c^{''}}{\partial x_i} S^{''}_{ij} \frac{\partial u^{''}_l}{\partial x_l}} - \overline{\rho D_c} \widetilde{\frac{\partial c^{''}}{\partial x_j} \frac{\partial u^{''}_l}{\partial x_l}} \widetilde{\frac{\partial c^{''}}{\partial x_i} S^{''}_{ij}} \\
&- \overline{\rho D_c} \widetilde{\frac{\partial c^{''}}{\partial x_i} S^{''}_{ij} \frac{\partial c^{''}}{\partial x_n} \frac{\partial u^{''}_n}{\partial x_j}} - \overline{\rho D_c} \widetilde{\frac{\partial c^{''}}{\partial x_i} S^{''}_{ij} \frac{\partial c^{''}}{\partial x_n}} \frac{\partial \widetilde{u}_n}{\partial x_j} \\
&- \overline{\rho D_c} \frac{\partial \widetilde{c}}{\partial x_n} \widetilde{\frac{\partial c^{''}}{\partial x_i} S^{''}_{ij} \frac{\partial u^{''}_n}{\partial x_j}} + \overline{\rho D_c} \widetilde{\frac{\partial c^{''}}{\partial x_n} \frac{\partial u^{''}_n}{\partial x_j}} \widetilde{\frac{\partial c^{''}}{\partial x_i} S^{''}_{ij}} \,. \qquad (8.17)
\end{aligned}$$

Term 2 of eq. (8.11) can be obtained by using the transport equation for the gradient of $u^{''}_i$, which can be obtained as:

$$\rho D_c \frac{D}{Dt}\left(\frac{\partial u^{''}_i}{\partial x_j}\right) = \rho D_c \frac{D}{Dt}\left(\frac{\partial u_i}{\partial x_j} - \frac{\partial \widetilde{u}_i}{\partial x_j}\right). \qquad (8.18)$$

The instantaneous part of eq. (8.18) can be obtained by using general transport equation for u_i. The general transport equation for u_i can be written as:

$$\rho \frac{D u_i}{Dt} = -\frac{\partial p}{\partial x_i} + \frac{\partial \tau_{in}}{\partial x_n}, \qquad (8.19)$$

where τ_{in} represents the viscous tensor. Taking the derivative of eq. (8.19) in the x_j direction and multiplying the resulting equation by D_c leads to :

$$\rho D_c \frac{\partial}{\partial t}\left(\frac{\partial u_i}{\partial x_j}\right) + \frac{\partial}{\partial x_n}\left(\rho D_c u_n \frac{\partial u_i}{\partial x_j}\right) = -D_c \frac{\partial}{\partial x_i}\left(\frac{\partial p}{\partial x_j}\right) + D_c \frac{\partial}{\partial x_n}\left(\frac{\partial \tau_{in}}{\partial x_j}\right) - \rho D_c \frac{\partial u_n}{\partial x_j}\frac{\partial u_i}{\partial x_n} - D_c \frac{\partial \rho}{\partial x_j}\left(-\frac{\partial p}{\partial x_i} + \frac{\partial \tau_{in}}{\partial x_n}\right)\frac{1}{\rho}. \tag{8.20}$$

Applying the Reynolds decomposition and Favre averaging eq. (8.20) leads to:

$$\overline{\rho D_c}\frac{\partial}{\partial t}\left(\frac{\partial \widetilde{u}_i}{\partial x_j}\right) + \frac{\partial}{\partial x_n}\left(\overline{\rho D_c}\widetilde{u}_n \frac{\partial \widetilde{u}_i}{\partial x_j}\right) = -\overline{D_c}\frac{\partial}{\partial x_i}\left(\frac{\partial \overline{p}}{\partial x_j}\right) - \frac{\partial}{\partial x_n}\left(\widetilde{\overline{\rho D_c} u_n'' \frac{\partial u_i''}{\partial x_j}}\right) + \overline{D_c}\frac{\partial}{\partial x_n}\left(\frac{\partial \overline{\tau_{in}}}{\partial x_j}\right) - \overline{\rho D_c}\widetilde{\frac{\partial u_n''}{\partial x_j}\frac{\partial u_i''}{\partial x_n}} - \overline{\rho D_c}\frac{\partial \widetilde{u}_n}{\partial x_j}\frac{\partial \widetilde{u}_i}{\partial x_n} + \frac{\partial \overline{\rho D_c}}{\partial x_j}\frac{\partial \overline{p}}{\partial x_i}\frac{1}{\overline{\rho}} - \frac{\partial \overline{\rho D_c}}{\partial x_j}\frac{\partial \overline{\tau_{in}}}{\partial x_n}\frac{1}{\overline{\rho}}. \tag{8.21}$$

Subtracting eq. (8.21) from eq. (8.20) then multiplying the resulting equation with $\frac{\partial c''}{\partial x_i}\frac{\partial c''}{\partial x_j}$ and Favre averaging leads to:

$$\begin{aligned}
&\overline{\rho D_c}\,\widetilde{\frac{\partial c''}{\partial x_i}\frac{\partial c''}{\partial x_j}\frac{D}{Dt}\left(\frac{\partial u_i''}{\partial x_j}\right)} = -\overline{\rho D_c}\,\widetilde{\frac{\partial c''}{\partial x_i}\frac{\partial c''}{\partial x_j}u_n''\frac{\partial}{\partial x_n}\left(\frac{\partial u_i''}{\partial x_j}\right)} \\
&-\overline{\rho D_c}\,\widetilde{\frac{\partial c''}{\partial x_i}\frac{\partial c''}{\partial x_j}u_n''}\,\frac{\partial}{\partial x_n}\left(\frac{\partial \widetilde{u}_i}{\partial x_j}\right) - \overline{D_c\frac{\partial c''}{\partial x_i}\frac{\partial c''}{\partial x_j}\frac{\partial}{\partial x_i}\left(\frac{\partial p'}{\partial x_j}\right)} \\
&+\overline{D_c\frac{\partial c''}{\partial x_i}\frac{\partial c''}{\partial x_j}\frac{\partial}{\partial x_n}\left(\frac{\partial \tau_{in}''}{\partial x_j}\right)} + \widetilde{\frac{\partial c''}{\partial x_i}\frac{\partial c''}{\partial x_j}}\,\frac{\partial}{\partial x_n}\left(\widetilde{\overline{\rho D_c}\,u_n''\frac{\partial u''}{\partial x_j}}\right) \\
&-\overline{\rho D_c}\,\widetilde{\frac{\partial c''}{\partial x_i}\frac{\partial c''}{\partial x_j}\frac{\partial u_n''}{\partial x_j}\frac{\partial u_i''}{\partial x_n}} - \overline{\rho D_c}\,\widetilde{\frac{\partial c''}{\partial x_i}\frac{\partial c''}{\partial x_j}\frac{\partial u_n''}{\partial x_j}}\,\frac{\partial \widetilde{u}_i}{\partial x_n} \\
&-\overline{\rho D_c}\frac{\partial \widetilde{u}_n}{\partial x_j}\,\widetilde{\frac{\partial c''}{\partial x_j}\frac{\partial c''}{\partial x_i}\frac{\partial u_i''}{\partial x_n}} + \overline{\rho D_c}\,\widetilde{\frac{\partial c''}{\partial x_i}\frac{\partial c''}{\partial x_j}}\,\widetilde{\frac{\partial u_n''}{\partial x_j}\frac{\partial u_i''}{\partial x_n}} \\
&+\overline{D_c\frac{\partial \rho}{\partial x_j}\frac{\partial P'}{\partial x_i}\frac{\partial c''}{\partial x_j}\frac{\partial c''}{\partial x_i}\frac{1}{\rho}} - \overline{D_c\frac{\partial \rho}{\partial x_j}\frac{\partial \tau_{in}''}{\partial x_n}\frac{\partial c''}{\partial x_i}\frac{\partial c''}{\partial x_j}\frac{1}{\rho}}.
\end{aligned} \tag{8.22}$$

Replacing terms 1 and 2 in eq. (8.11) leads finally to the $\widetilde{\Delta}_c$ transport equation. After much algebra, the transport equation for $\widetilde{\Delta}_c$ can be obtained as:

$$\overline{\rho}\frac{D\widetilde{\Delta}_c}{Dt} = -\frac{\partial}{\partial x_n}\left(\overline{\rho D_c}\,\overbrace{u_n''\frac{\partial c''}{\partial x_i}S_{ij}''\frac{\partial c''}{\partial x_j}}\right)\underbrace{+2\overline{\frac{\partial c''}{\partial x_i}S_{ij}''\frac{\partial}{\partial x_j}\left(\frac{\partial}{\partial x_n}\left(\rho D_c D_c\frac{\partial c''}{\partial x_n}\right)\right)}}_{D_{f1}}$$
$$\underbrace{+\overline{D_c\frac{\partial c''}{\partial x_i}\frac{\partial c''}{\partial x_j}\frac{\partial}{\partial x_n}\left(\frac{\partial \tau_{in}''}{\partial x_j}\right)}}_{D_{f2}} + F_1 + F_2 + F_3 + F_4 + F_5. \tag{8.23}$$

where D_{f1} and D_{f2} represent the diffusion terms, F_1 represents the source terms due to pressure gradient and the reaction rate :

$$F_1 = \underbrace{2\overline{D_c\frac{\partial c''}{\partial x_i}S_{ij}''\frac{\partial \dot{\omega}_c''}{\partial x_j}}}_{F_{11}}\underbrace{-\overline{D_c\frac{\partial c''}{\partial x_i}\frac{\partial c''}{\partial x_j}\frac{\partial}{\partial x_i}\left(\frac{\partial p'}{\partial x_j}\right)}}_{F_{12}}, \tag{8.24}$$

F_2 represents the terms arising due to the turbulent transport :

$$F_2 = \underbrace{2\overline{\rho D_c}\,\overbrace{\frac{\partial c''}{\partial x_i}S_{ij}''}\,\overbrace{u_n''\frac{\partial}{\partial x_n}\left(\frac{\partial c''}{\partial x_j}\right)}}_{F_{21}}\underbrace{-2\overline{\rho D_c}\,\overbrace{\frac{\partial c''}{\partial x_i}S_{ij}''u_n''}\,\frac{\partial}{\partial x_n}\left(\frac{\partial \widetilde{c}}{\partial x_j}\right)}_{F_{22}}$$
$$\underbrace{+\overline{\rho D_c}\,\overbrace{\frac{\partial c''}{\partial x_i}\frac{\partial c''}{\partial x_j}}\,\overbrace{u_n''\frac{\partial}{\partial x_n}\left(\frac{\partial u_i''}{\partial x_j}\right)}}_{F_{23}}\underbrace{-\overline{\rho D_c}\,\overbrace{\frac{\partial c''}{\partial x_i}\frac{\partial c''}{\partial x_j}u_n''}\,\frac{\partial}{\partial x_n}\left(\frac{\partial \widetilde{u}_i}{\partial x_j}\right)}_{F_{24}}, \tag{8.25}$$

F_3 represents the dilatation terms:

$$
\begin{aligned}
F_3 = & \underbrace{2\overline{\rho\alpha_T}\,\overbrace{\frac{\partial c''}{\partial x_i}S''_{ij}\frac{\partial c''}{\partial x_j}\frac{\partial u''_l}{\partial x_l}}}_{F_{31}} \underbrace{+2\overline{\rho D_c}\frac{\partial \widetilde{u}_l}{\partial x_l}\widetilde{\Delta}_c}_{F_{32}} \\
& \underbrace{+2\overline{\rho D_c}\frac{\partial \widetilde{c}}{\partial x_j}\overbrace{\frac{\partial c''}{\partial x_i}S''_{ij}\frac{\partial u''_l}{\partial x_l}}}_{F_{33}} \underbrace{-2\overline{\rho D_c}\overbrace{\frac{\partial c''}{\partial x_j}\frac{\partial u''_l}{\partial x_l}}\overbrace{\frac{\partial c''}{\partial x_i}S''_{ij}}}_{F_{34}} \\
& \underbrace{+\overline{D_c\frac{\partial \rho}{\partial x_j}\frac{\partial p'}{\partial x_i}\frac{\partial c''}{\partial x_j}\frac{\partial c''}{\partial x_i}\frac{1}{\rho}}}_{F_{35}} \underbrace{-\overline{D_c\frac{\partial \rho}{\partial x_j}\frac{\partial \tau''_{in}}{\partial x_n}\frac{\partial c''}{\partial x_i}\frac{\partial c''}{\partial x_j}\frac{1}{\rho}}}_{F_{36}},
\end{aligned}
\tag{8.26}
$$

F_4 represents turbulent straining terms :

$$
\begin{aligned}
F_4 = & \underbrace{-2\overline{\rho D_c}\,\overbrace{\frac{\partial c''}{\partial x_i}S''_{ij}\frac{\partial c''}{\partial x_n}\frac{\partial u''_n}{\partial x_j}}}_{F_{41}} \underbrace{-2\overline{\rho D_c}\,\overbrace{\frac{\partial c''}{\partial x_i}S''_{ij}\frac{\partial c''}{\partial x_n}}\frac{\partial \widetilde{u}_n}{\partial x_j}}_{F_{42}} \\
& \underbrace{-2\overline{\rho D_c}\frac{\partial \widetilde{c}}{\partial x_n}\overbrace{\frac{\partial c''}{\partial x_i}S''_{ij}\frac{\partial u''_n}{\partial x_j}}}_{F_{43}} \underbrace{+2\overline{\rho D_c}\,\overbrace{\frac{\partial c''}{\partial x_n}\frac{\partial u''_n}{\partial x_j}}\overbrace{\frac{\partial c''}{\partial x_i}S''_{ij}}}_{F_{44}} \\
& \underbrace{-\overline{\rho D_c}\,\overbrace{\frac{\partial c''}{\partial x_i}\frac{\partial c''}{\partial x_j}\frac{\partial u''_n}{\partial x_j}\frac{\partial u''_i}{\partial x_n}}}_{F_{45}} \underbrace{-\overline{\rho D_c}\,\overbrace{\frac{\partial c''}{\partial x_i}\frac{\partial c''}{\partial x_j}\frac{\partial u''_n}{\partial x_j}}\frac{\partial \widetilde{u}_i}{\partial x_n}}_{F_{46}} \\
& \underbrace{-\overline{\rho D_c}\frac{\partial \widetilde{u}_n}{\partial x_j}\overbrace{\frac{\partial c''}{\partial x_i}\frac{\partial c''}{\partial x_j}\frac{\partial u''_i}{\partial x_n}}}_{F_{47}} \underbrace{+\overline{\rho D_c}\,\overbrace{\frac{\partial c''}{\partial x_i}\frac{\partial c''}{\partial x_j}}\overbrace{\frac{\partial u''_n}{\partial x_j}\frac{\partial u''_i}{\partial x_n}}}_{F_{48}},
\end{aligned}
\tag{8.27}
$$

and F_5 represents the dilatation due to turbulent transport :

$$
F_5 = \overline{D_c\frac{\partial c''}{\partial x_i}S''_{ij}\frac{\partial c''}{\partial x_j}\frac{\partial}{\partial x_n}(\rho u''_n)}. \tag{8.28}
$$

In order to reduce the complexity of the transport equation an order of magnitude analysis is carried out for the $\widetilde{\Delta}_c$ transport equation.

8.4 OMA for the flame turbulence interaction $\left(\widetilde{\Delta}_c\right)$ evolution equation

A number of simplifications have been made while carrying out the OMA for the flame turbulence interaction transport equation. It is assumed that under the high Re limit the contributions from the viscous tensor would be small. Hence it is assumed that $\tau_{in} \approx 2\mu S_{in}$, $\mu \approx \rho D_c$ and the spatial gradients of density associated with τ_{in} are very small when compared with other terms.

The first term on the left-hand side of eq. (8.23) can be decomposed into two parts as :

$$\overline{\rho}\frac{D}{Dt}\left(\overline{D_c\frac{\partial c^{''}}{\partial x_i}S^{''}_{ij}\frac{\partial c^{''}}{\partial x_j}}\right) = \underbrace{\frac{\partial}{\partial t}\left(\overline{\rho D_c}\,\overline{\frac{\partial c^{''}}{\partial x_i}S^{''}_{ij}\frac{\partial c^{''}}{\partial x_j}}\right)}_{\text{Term 1}} + \underbrace{\frac{\partial}{\partial x_n}\left(\overline{\rho D_c}\widetilde{u}_n\,\overline{\frac{\partial c^{''}}{\partial x_i}S^{''}_{ij}\frac{\partial c^{''}}{\partial x_j}}\right)}_{\text{Term 2}}, \tag{8.29}$$

where the terms on the right-hand side scales as

$$\backsimeq \quad \mathcal{O}\left(\rho_R\left(\frac{u^0_L}{\delta^0_L}\right)^3; Da^{-1}\right), \tag{8.30}$$

and

$$\backsimeq \quad \mathcal{O}\left(\rho_R\left(\frac{u^0_L}{\delta^0_L}\right)^3; \left(\frac{u^{'}Da}{u_{ref}}\right)^{-1}\right), \tag{8.31}$$

respectively. The turbulent transport of $\widetilde{\Delta}_c$ scales as:

$$\frac{\partial}{\partial x_n}\left(\overline{\rho D_c u^{''}_n\frac{\partial c^{''}}{\partial x_i}S^{''}_{ij}\frac{\partial c^{''}}{\partial x_j}}\right) \backsimeq \mathcal{O}\left(\rho_R\left(\frac{u^0_L}{\delta^0_L}\right)^3; (Re_{l_t}Da)^{-1/2}\right) \tag{8.32}$$

Term D_{f1} represents the diffusion terms arising from the scalar part of the $\widetilde{\Delta}_c$ transport equation. Term D_{f1} can be expanded and simplified based on the

assumption that the second gradient of ρ is small compared with the other terms, thus leading to:

$$\overline{\frac{\partial c''}{\partial x_i} S''_{ij} \frac{\partial}{\partial x_j}\left(\frac{\partial}{\partial x_n}\left(\rho D_c D_c \frac{\partial c''}{\partial x_n}\right)\right)} = \underbrace{\frac{\partial}{\partial x_n}\left(\overline{\rho D_c}\frac{\partial}{\partial x_n}\left(\overline{D_c \frac{\partial c''}{\partial x_i} S''_{ij} \frac{\partial c''}{\partial x_j}}\right)\right)}_{Df11}$$
$$\underbrace{-\overline{\rho D_c D_c \frac{\partial}{\partial x_n}\left(\frac{\partial c''}{\partial x_j}\right)\frac{\partial}{\partial x_n}\left(\frac{\partial c''}{\partial x_i} S''_{ij}\right)}}_{Df12} \underbrace{-\overline{\rho D_c D_c \frac{\partial}{\partial x_n}\left(\frac{\partial c''}{\partial x_i}\frac{\partial c''}{\partial x_j}\frac{\partial}{\partial x_n} S''_{ij}\right)}}_{Df13}$$
$$\underbrace{-\overline{\rho D_c D_c \frac{\partial}{\partial x_n}\left(\frac{\partial c''}{\partial x_j} S''_{ij}\frac{\partial}{\partial x_n}\left(\frac{\partial c''}{\partial x_i}\right)\right)}}_{Df14} \tag{8.33}$$

Terms D_{f1i} scale as :

$$D_{f11} = \frac{\partial}{\partial x_n}\left(\overline{\rho D_c}\frac{\partial}{\partial x_n}\left(\overline{D_c \frac{\partial c''}{\partial x_i} S''_{ij} \frac{\partial c''}{\partial x_j}}\right)\right)$$
$$\backsimeq \mathcal{O}\left(\rho_R \left(\frac{u_L^0}{\delta_L^0}\right)^3 ; \left(Dau'\right)^{-1}\right) \tag{8.34}$$

$$D_{f12} = -\overline{\rho D_c D_c \frac{\partial}{\partial x_n}\left(\frac{\partial c''}{\partial x_j}\right)\frac{\partial}{\partial x_n}\left(\frac{\partial c''}{\partial x_i} S''_{ij}\right)}$$
$$\backsimeq \mathcal{O}\left(\rho_R \left(\frac{u_L^0}{\delta_L^0}\right)^3 ; 1\right) \tag{8.35}$$

$$D_{f13} = -\overline{\rho D_c D_c \frac{\partial}{\partial x_n}\left(\frac{\partial c''}{\partial x_i}\frac{\partial c''}{\partial x_j}\frac{\partial}{\partial x_n} S''_{ij}\right)}$$
$$\backsimeq \mathcal{O}\left(\rho_R \left(\frac{u_L^0}{\delta_L^0}\right)^3 ; 1\right) \tag{8.36}$$

$$D_{f14} = -\overline{\rho D_c D_c \frac{\partial}{\partial x_n}\left(\frac{\partial c''}{\partial x_j} S''_{ij} \frac{\partial}{\partial x_n}\left(\frac{\partial c''}{\partial x_i}\right)\right)}$$
$$\backsimeq \mathcal{O}\left(\rho_R \left(\frac{u_L^0}{\delta_L^0}\right)^3 ; 1\right) \tag{8.37}$$

Term D_{f2} represents the diffusion from the momentum part of the $\widetilde{\Delta}_c$ transport equation and scales as :

$$D_{f2} = \overline{D_c \frac{\partial c''}{\partial x_i}\frac{\partial c''}{\partial x_j}\frac{\partial}{\partial x_n}\left(\frac{\partial \tau''_{in}}{\partial x_j}\right)}$$
$$\backsimeq \mathcal{O}\left(\rho_R \left(\frac{u_L^0}{\delta_L^0}\right)^3 ; 1\right) \tag{8.38}$$

Terms F_{1i} representing the source terms scale as :

$$F_{11} = \overline{D_c \frac{\partial c''}{\partial x_i} S''_{ij} \frac{\partial \dot{\omega}''_c}{\partial x_j}}$$
$$\backsimeq \mathcal{O}\left(\rho_R \left(\frac{u_L^0}{\delta_L^0}\right)^3 ; 1\right) \tag{8.39}$$

$$F_{12} = \overline{D_c \frac{\partial c''}{\partial x_j}\frac{\partial c''}{\partial x_i}\frac{\partial}{\partial x_i}\left(\frac{\partial p'}{\partial x_j}\right)}$$
$$\backsimeq \mathcal{O}\left(\rho_R \left(\frac{u_L^0}{\delta_L^0}\right)^3 ; 1\right) \tag{8.40}$$

Terms F_{2i} representing the terms arising due to the turbulent transport of $\widetilde{\Delta}_c$ scale as :

$$F_{21} = \overline{\rho D_c} \overbrace{\frac{\partial c''}{\partial x_i} S''_{ij}} \overbrace{u''_n \frac{\partial}{\partial x_n} \left(\frac{\partial c''}{\partial x_j} \right)} \\ \backsimeq \mathcal{O} \left(\rho_u \left(\frac{u_L^0}{\delta_L^0} \right)^3 ; 1 \right) \tag{8.41}$$

$$F_{22} = \overline{\rho D_c} \overbrace{\frac{\partial c''}{\partial x_i} S''_{ij} u''_n} \frac{\partial}{\partial x_n} \left(\frac{\partial \widetilde{c}}{\partial x_j} \right) \\ \backsimeq \mathcal{O} \left(\rho_R \left(\frac{u_L^0}{\delta_L^0} \right)^3 ; (Re_{l_t} Da)^{-1/2} \right) \tag{8.42}$$

$$F_{23} = \overline{\rho D_c} \overbrace{\frac{\partial c''}{\partial x_i} \frac{\partial c''}{\partial x_j}} \overbrace{u''_n \frac{\partial}{\partial x_n} \left(\frac{\partial u''_i}{\partial x_j} \right)} \\ \backsimeq \mathcal{O} \left(\rho_R \left(\frac{u_L^0}{\delta_L^0} \right)^3 ; 1 \right) \tag{8.43}$$

$$F_{24} = \overline{\rho D_c} \overbrace{\frac{\partial c''}{\partial x_i} \frac{\partial c''}{\partial x_j} u''_n} \frac{\partial}{\partial x_n} \left(\frac{\partial \widetilde{u}_i}{\partial x_j} \right) \\ \backsimeq \mathcal{O} \left(\rho_R \left(\frac{u_L^0}{\delta_L^0} \right)^3 ; \left(\frac{u' Da^{3/2} Re_{l_t}^{-1/2}}{u_{ref}} \right)^{-1} \right) \tag{8.44}$$

Terms F_{3i} representing the dilatation terms scale as :

$$F_{31} = \overline{\rho D_c} \overbrace{\frac{\partial c''}{\partial x_i} S''_{ij} \frac{\partial c''}{\partial x_j} \frac{\partial u''_l}{\partial x_l}} \\ \backsimeq \mathcal{O} \left(\rho_R \left(\frac{u_L^0}{\delta_L^0} \right)^3 ; 1 \right) \tag{8.45}$$

$$F_{32} = \overline{\rho D_c} \frac{\partial \widetilde{u}_l}{\partial x_l} \overline{\frac{\partial c''}{\partial x_i} S''_{ij} \frac{\partial c''}{\partial x_j}}$$
$$\backsimeq \mathcal{O}\left(\rho_R \left(\frac{u_L^0}{\delta_L^0}\right)^3 ; \left(\frac{u' Da}{u_{ref}}\right)^{-1}\right) \tag{8.46}$$

$$F_{33} = \overline{\rho D_c} \frac{\partial \widetilde{c}}{\partial x_j} \overline{\frac{\partial c''}{\partial x_i} S''_{ij} \frac{\partial u''_l}{\partial x_l}}$$
$$\backsimeq \mathcal{O}\left(\rho_R \left(\frac{u_L^0}{\delta_L^0}\right)^3 ; (Re_{l_t} Da)^{-1/2}\right) \tag{8.47}$$

$$F_{34} = \overline{\rho D_c} \overline{\frac{\partial c''}{\partial x_j} \frac{\partial u''_l}{\partial x_l}} \overline{\frac{\partial c''}{\partial x_i} S''_{ij}}$$
$$\backsimeq \mathcal{O}\left(\rho_R \left(\frac{u_L^0}{\delta_L^0}\right)^3 ; 1\right) \tag{8.48}$$

$$F_{35} = \overline{D_c \frac{\partial \rho}{\partial x_j} \frac{\partial p'}{\partial x_i} \frac{\partial c''}{\partial x_i} \frac{\partial c''}{\partial x_j} \frac{1}{\rho}}$$
$$\backsimeq \mathcal{O}\left(\rho_R \left(\frac{u_L^0}{\delta_L^0}\right)^3 ; 1\right) \tag{8.49}$$

$$F_{36} = \overline{D_c \frac{\partial \rho}{\partial x_j} \frac{\partial \tau''_{in}}{\partial x_n} \frac{\partial c''}{\partial x_j} \frac{\partial c''}{\partial x_i} \frac{1}{\rho}}$$
$$\backsimeq \mathcal{O}\left(\rho_R \left(\frac{u_L^0}{\delta_L^0}\right)^3 ; 1\right) \tag{8.50}$$

Terms F_{4i} representing the turbulent straining terms scale as :

$$F_{41} = \overline{\rho D_c} \overline{\frac{\partial c^{''}}{\partial x_i} S_{ij}^{''} \frac{\partial c^{''}}{\partial x_n} \frac{\partial u_n^{''}}{\partial x_j}}$$
$$\backsimeq \mathcal{O}\left(\rho_R \left(\frac{u_L^0}{\delta_L^0}\right)^3 ; 1\right) \tag{8.51}$$

$$F_{42} = \overline{\rho D_c} \overline{\frac{\partial c^{''}}{\partial x_i} S_{ij}^{''} \frac{\partial c^{''}}{\partial x_j}} \frac{\partial \widetilde{u}_n}{\partial x_j}$$
$$\backsimeq \mathcal{O}\left(\rho_R \left(\frac{u_L^0}{\delta_L^0}\right)^3 ; \left(\frac{u^{'} Da}{u_{ref}}\right)^{-1}\right) \tag{8.52}$$

$$F_{43} = \overline{\rho D_c} \frac{\partial \widetilde{c}}{\partial x_n} \overline{\frac{\partial c^{''}}{\partial x_i} S_{ij}^{''} \frac{\partial u_n^{''}}{\partial x_j}}$$
$$\backsimeq \mathcal{O}\left(\rho_R \left(\frac{u_L^0}{\delta_L^0}\right)^3 ; (Re_{l_t} Da)^{-1/2}\right) \tag{8.53}$$

$$F_{44} = \overline{\rho D_c} \overline{\frac{\partial c^{''}}{\partial x_n} \frac{\partial u_n^{''}}{\partial x_j}} \overline{\frac{\partial c^{''}}{\partial x_i} S_{ij}^{''}}$$
$$\backsimeq \mathcal{O}\left(\rho_R \left(\frac{u_L^0}{\delta_L^0}\right)^3 ; 1\right) \tag{8.54}$$

$$F_{45} = \overline{\rho D_c} \overline{\frac{\partial c^{''}}{\partial x_j} \frac{\partial c^{''}}{\partial x_i} \frac{\partial u_n^{''}}{\partial x_j} \frac{\partial u_i^{''}}{\partial x_n}})$$
$$\backsimeq \mathcal{O}\left(\rho_R \left(\frac{u_L^0}{\delta_L^0}\right)^3 ; 1\right) \tag{8.55}$$

$$F_{46} = \overline{\rho D_c} \overbrace{\frac{\partial c''}{\partial x_i} \frac{\partial c''}{\partial x_j} \frac{\partial u_n''}{\partial x_j}} \frac{\partial \widetilde{u}_i}{\partial x_n}$$
$$\backsimeq \mathcal{O}\left(\rho_R \left(\frac{u_L^0}{\delta_L^0}\right)^3 ; \left(\frac{u' Da}{u_{ref}}\right)^{-1}\right) \tag{8.56}$$

$$F_{47} = \overline{\rho D_c} \frac{\partial \widetilde{u}_n}{\partial x_j} \overbrace{\frac{\partial c''}{\partial x_j} \frac{\partial c''}{\partial x_i} \frac{\partial u_i''}{\partial x_n}}$$
$$\backsimeq \mathcal{O}\left(\rho_R \left(\frac{u_L^0}{\delta_L^0}\right)^3 ; \left(\frac{u' Da}{u_{ref}}\right)^{-1}\right) \tag{8.57}$$

$$F_{48} = \overline{\rho D_c} \overbrace{\frac{\partial c''}{\partial x_i} \frac{\partial c''}{\partial x_j}} \overbrace{\frac{\partial u_n''}{\partial x_j} \frac{\partial u_i''}{\partial x_n}}$$
$$\backsimeq \mathcal{O}\left(\rho_R \left(\frac{u_L^0}{\delta_L^0}\right)^3 ; 1\right) \tag{8.58}$$

Term F_5 scales as :

$$F_5 = \overline{D_c \frac{\partial c''}{\partial x_i} S_{ij}'' \frac{\partial c''}{\partial x_j} \frac{\partial}{\partial x_n} (\rho u_n'')}$$
$$\backsimeq \mathcal{O}\left(\rho_R \left(\frac{u_L^0}{\delta_L^0}\right)^3 ; 1\right) \tag{8.59}$$

8.5 Leading order terms in $\widetilde{\Delta}_c$ evolution equation

According to the above order of magnitude analysis under the joint assumptions of high Re_{l_t} and Da limit, the leading order terms in eq. (8.23) are :

$$D_f + F_1 + F_D + F_{TS} + F_5 + F_{21} + F_{23} \backsimeq 0, \tag{8.60}$$

where F_D represents the leading order dilatation terms as:

$$F_D = F_{31} + F_{34} + F_{35} + F_{36}, \tag{8.61}$$

and F_{TS} represents the leading order turbulent straining terms:

$$F_{TS} = F_{41} + F_{44} + F_{45} + F_{48}. \tag{8.62}$$

All the terms in eq. (8.60) represent a unique physical phenomenon and require modelling. In order to understand fully the physics represented by the leading order terms in the $\widetilde{\Delta}_c$ evolution equation a DNS data set is used, and appropriate closures for the leading order terms are proposed in the next chapter.

9 Closures for the leading order terms in the flame turbulence interaction evolution equation

The leading order terms identified in eq. (8.60) are unclosed and require appropriate modelling. In this chapter, the leading order terms are studied by using a DNS data set and are then closed by suitable approximations. This is achieved via detailed interrogation of a Direct Numerical Simulation (DNS) data set of a turbulent premixed V-flame in the corrugated flamelet regime. The details of the DNS data set are given in the next section, followed by the alignment statistics of the flame gradients with the strain rate. Finally, proposals for closing the leading order terms in eq. (8.62) are made.

9.1 Direct Numerical Simulation data

The DNS data produced by Dunstan et al [60] for a turbulent premixed V-flame has been used. The V-flame in the DNS is representative of a lean, unit Lewis number flame with pre-heated reactants. The combustion kinetics are approximated by a single step reaction [58, 60]. DNS of the V-flame was carried out using the code SENGA2, in which the conservation equations for mass, momentum, energy and reacting species are solved for compressible flow [32, 56, 58, 60, 76]. The spatial derivatives for interior grid points are calculated by using a 10th order central difference scheme, which gradually reduce to a 2nd order one sided scheme for all outflow boundaries, and 4th order one sided scheme at the inlet boundary. The solution is evolved in time by using a 4th order explicit Runge-Kutta scheme. The transport coefficients have a temperature dependence approximated

by 5th order polynomials following the CHEMKIN formats. Navier-Stokes Characteristic Boundary Conditions (NSCBC) have been applied to all non-periodic boundaries. The standard NSCBC has been modified to accommodate the steep thermal and compositional gradients when the flame crosses the boundary. This has been done to avoid large pressure perturbations which can have a significant influence on the interior solution. A detailed discussion on NSCBC is beyond the scope of this thesis and further details on the boundary conditions can be found in [60, 118, 127, 147, 166]. Similar DNS data sets have been used in several modelling studies for scalar dissipation rate, turbulent flame speed and flame generated noise in premixed turbulent combustion [57, 58, 60, 102].

The domain for the V-flame simulation is a cube of side $29.69\delta_L^0$. The domain is discretised by a $512 \times 512 \times 512$ node uniform grid, ensuring a resolution of about 10 grid points is maintained to resolve the laminar flame thickness δ_L^0. The flame is stabilised by a flame holder of radius $1.16\delta_L^0$ positioned at $3.49\delta_L^0$ from the inlet plane; this is achieved by fixing the mass fraction through a Gaussian weighting function and restricting velocities to their mean values (further details on the flame holder can be found in [58, 60]). The schematic of the computational domain is given in figure 9.1. The simulation is run for one flow through time, to allow for the transients to decay before collecting data for analysis.

The global thermochemical parameters used in the DNS are; planar, unstretched laminar flame speed $u_L^0 = 0.6034\,m/s$; laminar flame thermal thickness $\delta_L^0 = (T_P - T_R)/max|\nabla T| = 0.43\,mm$ (where $T_P = 2113.3\,K$ is the adiabatic flame temperature and $T_R = 600.0\,K$ is the inlet reactant temperature); heat release parameter $\tau = (T_P - T_R)/T_R = 2.52$; characteristic laminar flame time is given by $\tau_c = \delta_L^0/u_L^0 = 0.71\,ms$ and the laminar diffusive thickness $\delta_L = D_c/u_L^0 = 0.1207\,mm$. For the purpose of comparison with real air-fuel mixture flames, this is representative of a premixed methane-air flame with an equivalence ratio $\phi \approx 0.6$ [60].

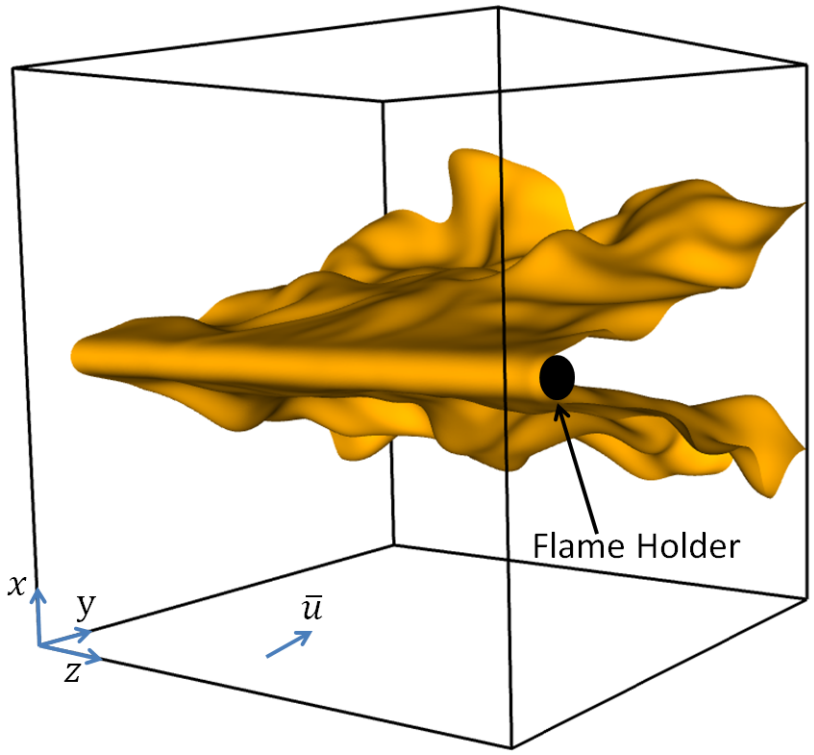

Figure 9.1: Computational domain for the V-flame DNS

The values of the turbulent Reynolds number (Re_{l_t}), Karlovitz number, (Ka) and Damköhler number, (Da) based on the diffusion flame thickness and inlet flow conditions are summarised in table 9.1, where $u^{'}_{in}$ is the rms velocity at the inlet, $\overline{u}_{in}$ is the mean inlet velocity in the $y-$direction as shown in figure 9.1, ν is the kinematic viscosity and l_t is the integral length scale.

$u^{'}_{in}/u^0_L$	$\overline{u}_{in}/u^0_L$	$Re_{l_t,in}$	$l_{t,in}/\delta^0_L$	Ka_{in}	Da_{in}
2.0	16.6	37	12.82	0.79	6.41

Table 9.1: DNS database parameters at inlet plane

Figure 9.2 show the contours of $0.1 \leq \widetilde{c} \leq 0.9$ in the V-flame DNS, where the x^+ and y^+ represent the directions normalised by the thermal thickness of the the flame δ^0_L.

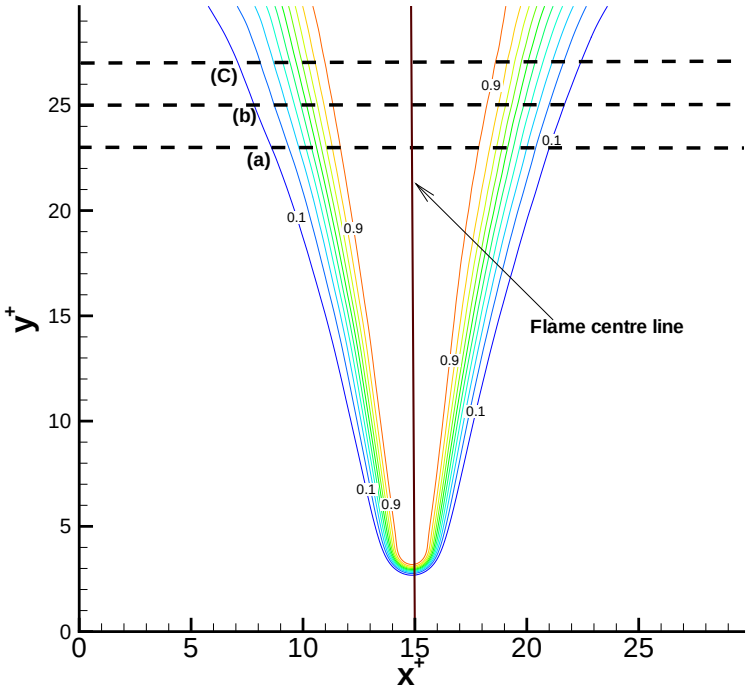

Figure 9.2: Favre averaged progress variable $\widetilde{c}$ contours $0.1 - 0.9$ in the V-flame DNS. The dashed lines represent the sampling locations, and the solid line represents the flame centre line.

During the post processing of the DNS, the data was averaged in time over 21 instantaneous realisations of the flow (over a sample time of one flow through), and space averaged in the periodic (z) direction. The averaging process for any variable $A\left(x, y, z, t\right)$ can be represented as:

$$\overline{A}(x, y) = \frac{1}{N_t N_z} \sum_{n=1}^{N_t} \sum_{m=1}^{N_z} A\left(x, y, n, m\right), \tag{9.1}$$

where N_t and N_z are the total number of snapshots and and total number of nodes in the periodic (z) direction, respectively. The Favre-average is then calculated as $\widetilde{A} = \overline{\rho A}/\overline{\rho}$. Spatial derivatives of fluctuating quantities required by the terms in eq. (8.60) are calculated using the same numerical algorithm as used in the DNS. The present analysis is restricted to $y^+ > 20$, beyond which the flame has sufficient time to develop after ignition at the flame holder [57, 60]. Three sampling locations downstream of the flame holder at $y^+ \approx 23$, $y^+ \approx 25$ and $y^+ \approx 27$ are

used, labelled as a, b, and c in figure 9.2. The flame is influenced by the level of turbulence upstream of the flame, hence non-dimensional parameters such as Ka, Da and $Re_{l_t}$are reported for all the sampling locations at $\widetilde{c} \approx 0.001$ in table 9.2. It can be observed from table 9.2 that flame lies in the corrugated flamelet regime, and Re_{l_t} remains close to approximately 20 at all the sampling locations used. All the results have been normalised using ρ_R,u_L^0 and δ_L^0. As the thickness of $\widetilde{c}$ changes along the mean flow direction and $\widetilde{c}$ varies monotonically from the flame centreline, $\widetilde{c}$ is used instead to denote the location inside the flame brush in the results discussed below.

Sampling location	$u^{'}/u_L^0$	Re_{l_t}	l_t/δ_L^0	Ka	Da
Region a	1.51	22.16	10.0	0.50	9.94
Region b	1.48	17.56	8.6	0.49	9.09
Region c	1.41	22.16	9.8	0.46	10.31

Table 9.2: DNS database parameters at the sampling locations

9.2 Eigenvector analysis and alignment statistics

The behaviour of the flame turbulence interaction depends on the alignment of the strain rate eigenvectors with the scalar gradient, hence an eigenvector analysis has been undertaken for the V-flame DNS. The eigenvectors for the strain rate have been calculated by using LAPACK libraries for FORTRAN [4]. Figures 9.3, 9.4 and 9.5 show the pdfs of direction cosines between the strain rate eigenvectors and the flame gradient at $y^+ \approx 23$, $y^+ \approx 25$ and $y^+ \approx 27$ respectively for different iso-surfaces of c. It can be observed in figures 9.3a, 9.4a and 9.5a that the most probable inner product tending towards unity is the inner product between e_α and ∇c, which implies that the extensive strain rate eigenvector aligns preferentially with the flame gradient for $0.3 \leq c \leq 0.7$ at all the sampling locations in the DNS. It should be noted here however that the direct interpretation of strain rate orientation from direction cosines can be obscured by the non-linearity of the cosine function. In case of a uniformly distributed angle between two vectors, the pdf of $cos\theta$ shows higher probabilities of unity [146], and caution must be taken when interpreting alignment pdfs based on direction cosines.

Steinberg et al [146] argue that the actual physical orientation of the strain

rate field with the flame gradient can be better represented by the pdfs of the angle between the two vectors directly. Figures 9.3b, 9.4b and 9.5b show the pdfs of the angles between the extensive strain rate eigenvector and the flame gradient at $y^+ \approx 23$, $y^+ \approx 25$ and $y^+ \approx 27$ respectively for different iso-surfaces of c. It can be observed that the most probable alignment between e_α and ∇c occurs at $0 \leq \theta_\alpha \leq 0.5$ for $0.3 \leq c \leq 0.7$ at all sampling locations, which again implies that e_α preferentially aligns with ∇c for $0.3 \leq c \leq 0.7$. This is in agreement with the earlier studies [44, 71] as the chemical reactions releasing heat compete with the local fluid dynamic processes, thus causing the flame gradient to align with the most extensive strain rate eigenvector.

The non-linearity induced by the cosine function can be noticed by comparing the pdfs of direction cosines between e_α and ∇c and the pdfs for the resulting angles between e_α and ∇c. The pdfs for the direction cosines between e_α and ∇c show a bias towards higher probability of unity as shown in figures 9.3a, 9.4a and 9.5a; whereas the pdfs for the associated angles show a range of angles with lower probability as shown in figures 9.3b, 9.4b and 9.5b.

Note that e_α and ∇c are not completely aligned for $c = 0.1$ and $c = 0.9$ iso-surfaces at all sampling locations. The dilatation due to heat release is low near $c = 0.1$ and $c = 0.9$ iso-surfaces, as shown in figure 9.6 for all the sampling locations in the V-flame. The mean shear overcomes the dilatation effects and enters the flame structure at $c = 0.1$ and $c = 0.9$, thus causing the flame gradients to move away from the extensive strain rate eigenvector and towards the compressive strain rate eigenvector as shown in figures 9.3b, 9.4b, 9.5b, 9.3f, 9.4f and 9.5f. This phenomenon has been noted in the earlier studies by Minamoto et al [109] in case of reacting flows and by Ashurst et al [7] in case of non reacting flows. These changes in alignment characteristics across the flame structure signify the importance of the transport equation for $\widetilde{\Delta}_c$, as the transport equation allows for a more flexible approach to incorporate the correct physics and flow history effects into the modelling strategy.

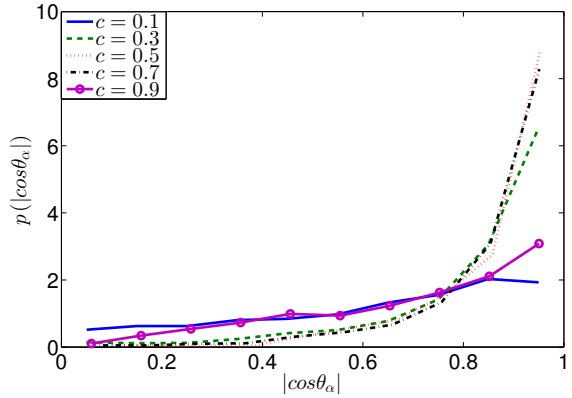

(a) Direction cosine between e_α and ∇c

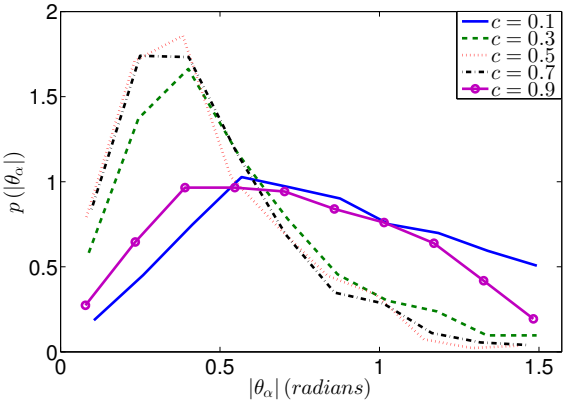

(b) The angle between e_α and ∇c

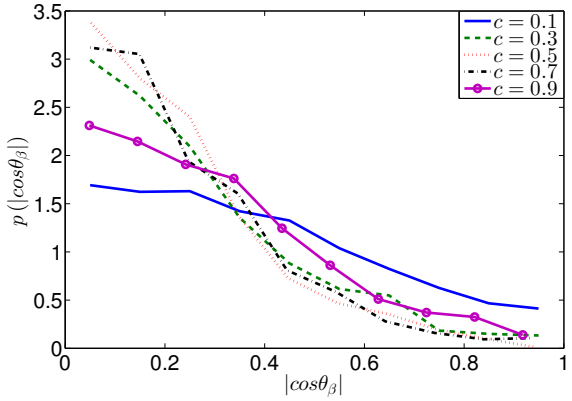

(c) Direction cosine between e_β and ∇c

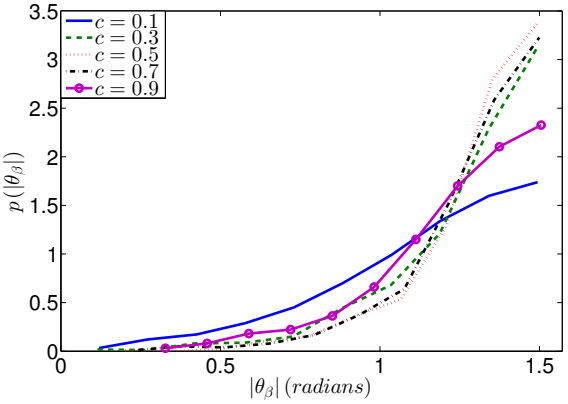

(d) The angle between e_β and ∇c

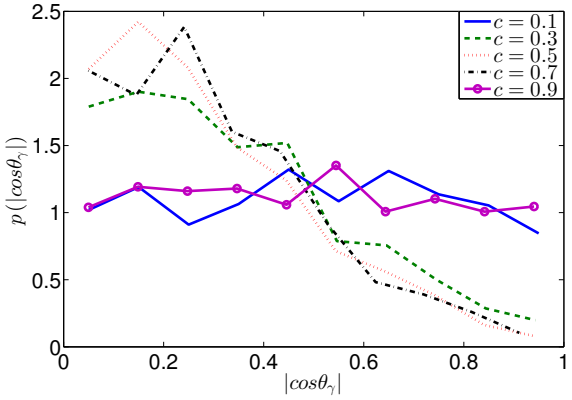

(e) Direction cosine between e_γ and ∇c

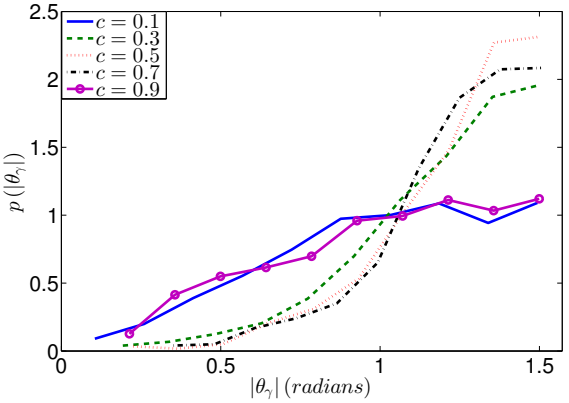

(f) The angle between e_γ and ∇c

Figure 9.3: Pdfs of the direction cosines and the associated angles at $y^+ \approx 23$ in the V-flame DNS

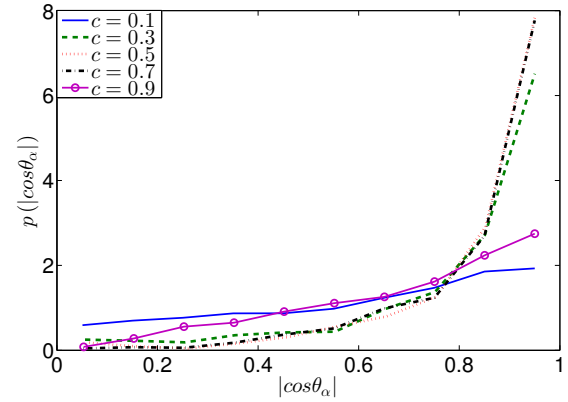

(a) Direction cosine between e_α and ∇c

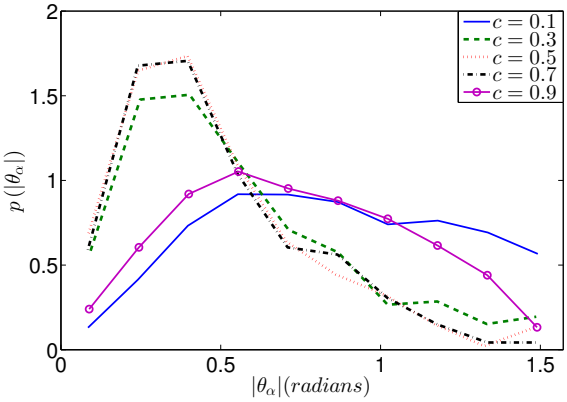

(b) The angle between e_α and ∇c

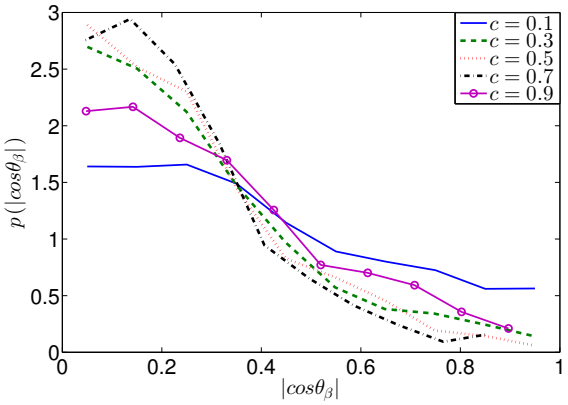

(c) Direction cosine between e_β and ∇c

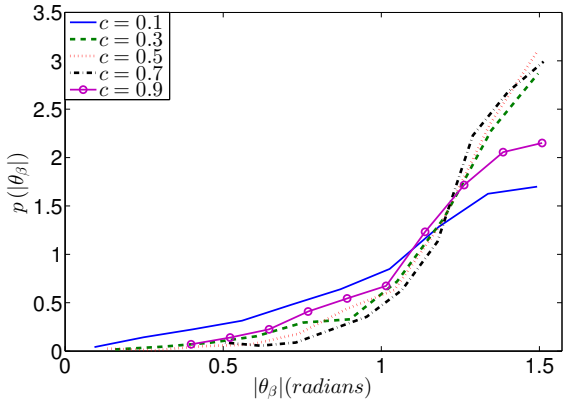

(d) The angle between e_β and ∇c

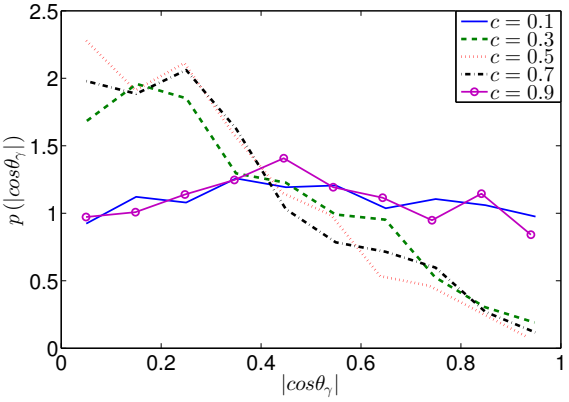

(e) Direction cosine between e_γ and ∇c

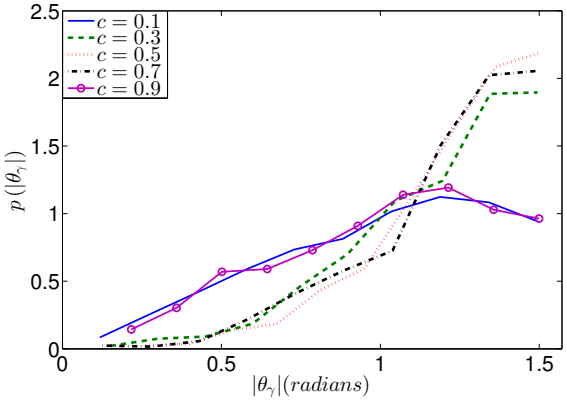

(f) The angle between e_γ and ∇c

Figure 9.4: Pdfs of the direction cosines and the associated angles at $y^+ \approx 25$ in the V-flame DNS

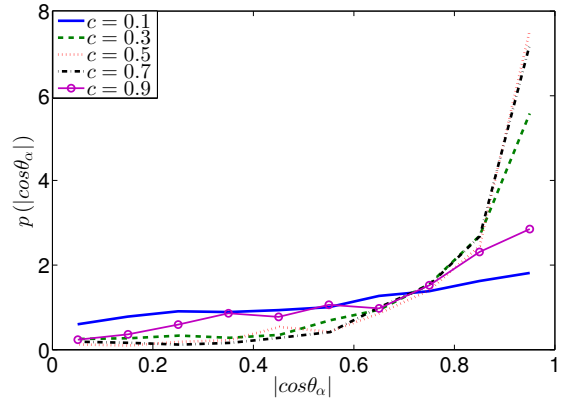

(a) Direction cosine between e_α and ∇c

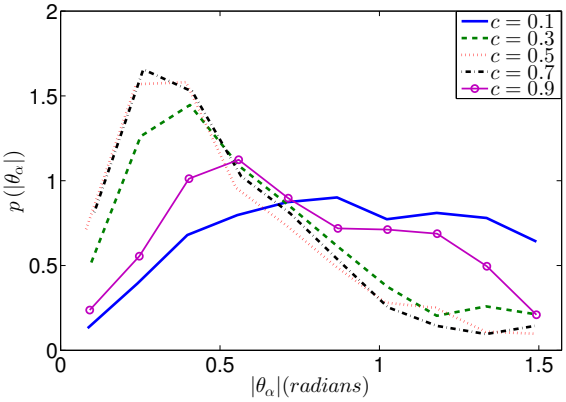

(b) The angle between e_α and ∇c

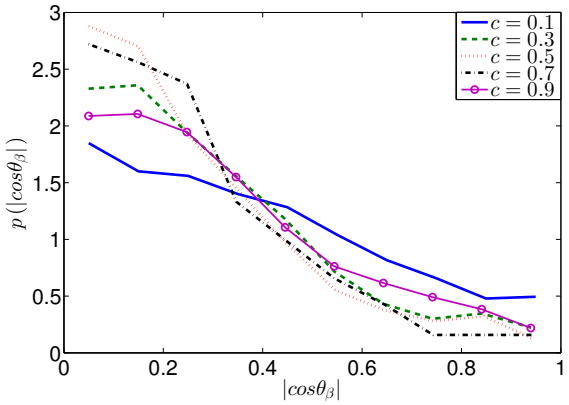

(c) Direction cosine between e_β and ∇c

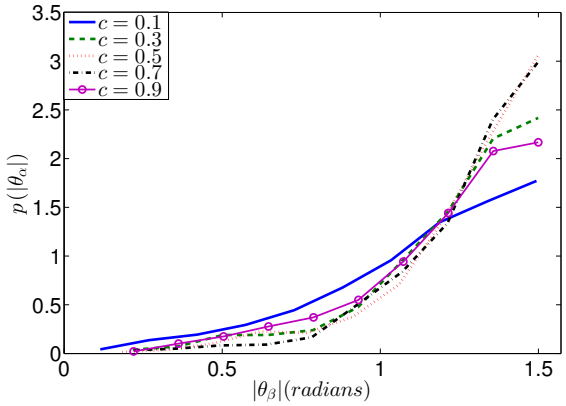

(d) The angle between e_β and ∇c

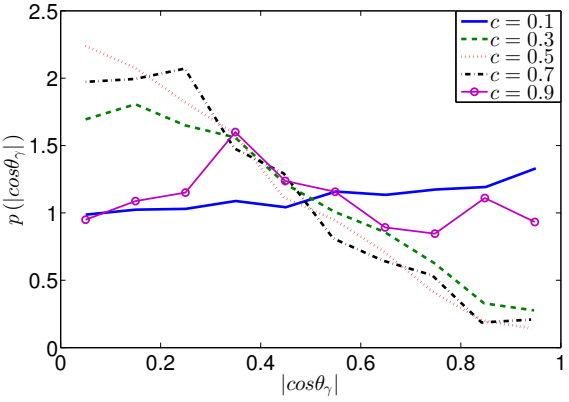

(e) Direction cosine between e_γ and ∇c

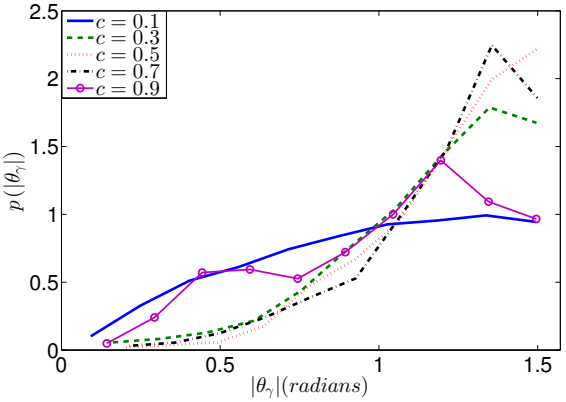

(f) The angle between e_γ and ∇c

Figure 9.5: Pdfs of the direction cosines and the associated angles at $y^+ \approx 27$ in the V-flame DNS

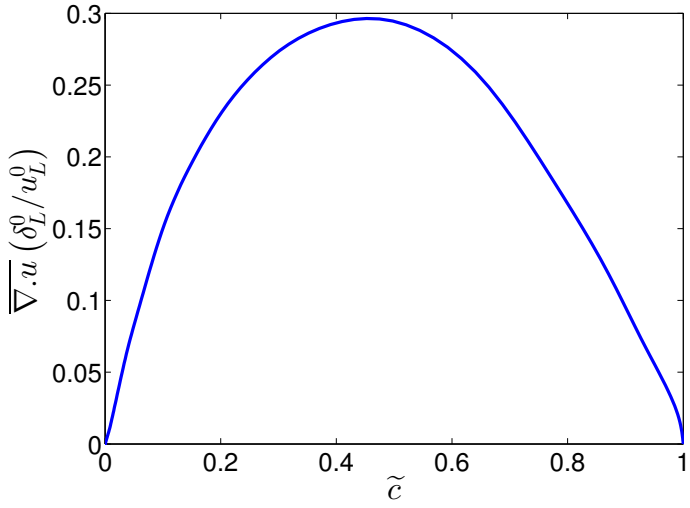

(a) $y^+ \approx 23$

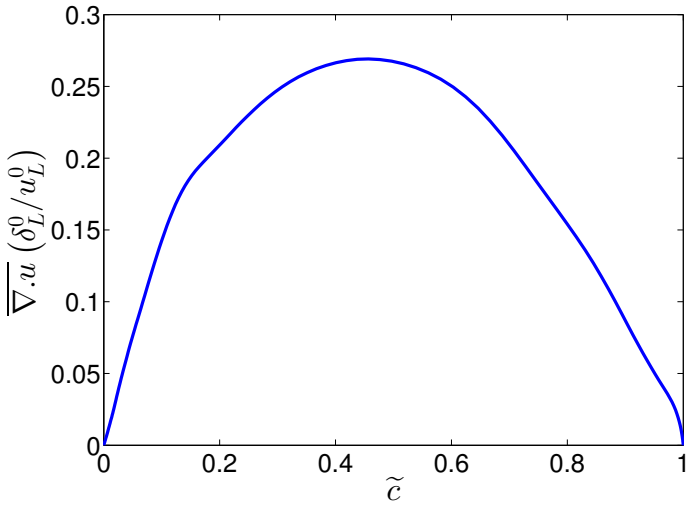

(b) $y^+ \approx 25$

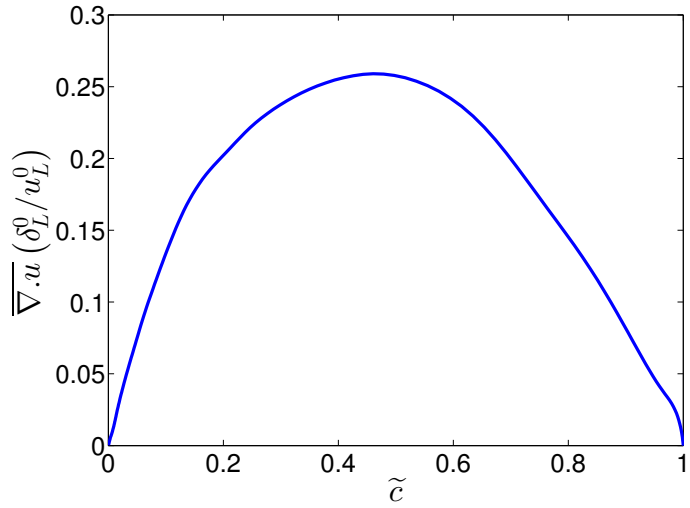

(c) $y^+ \approx 27$

Figure 9.6: Normalised dilatation in the V-flame DNS

9.3 Leading order terms in the $\widetilde{\Delta}_c$ evolution equation

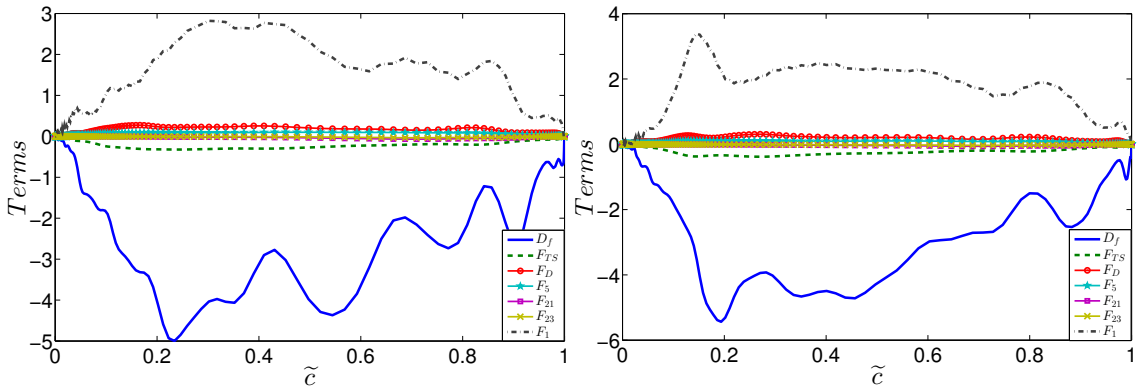

(a) $y^+ \approx 23$ (b) $y^+ \approx 25$

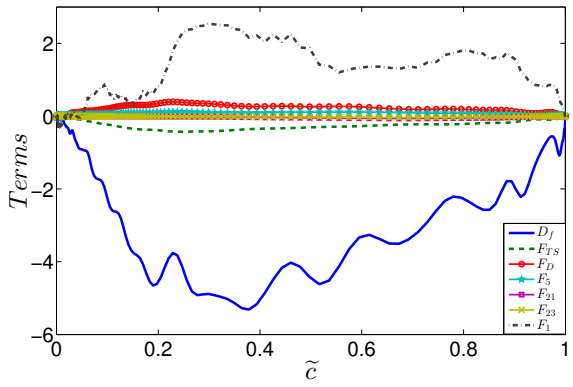

(c) $y^+ \approx 27$

Figure 9.7: Leading order terms for $\widetilde{\Delta}_c$ evolution equation in the V-flame DNS. The values are normalised using the respective ρ_R, u_L^0 and δ_L^0.

Figures 9.7(a) - 9.7(c) show the profiles for the leading order terms in the $\widetilde{\Delta}_c$ transport equation at $y^+ \approx 23$, $y^+ \approx 25$ and $y^+ \approx 27$. The overall behaviour of $\widetilde{\Delta}_c$ transport equation is strongly controlled by a competition between the source terms (F_1), diffusion process (D_f), turbulent strain rate (F_{TS}) and the dilatation rate ($F_D + F_5$) as shown in figure 9.7.

It can be seen in figure 9.8 that there is a competition between the turbulent strain rate (F_{TS}) and the dilatation rate ($F_D + F_5$) at all the sampling locations,

which is in agreement with theories proposed in earlier studies [40, 151]. These earlier studies further suggest that the competition between F_{TS} and F_D significantly influences the evolution of $\widetilde{\Delta}_c$ and is considered to be an important phenomenon [40, 151]. We argue here that the source terms (F_1) and diffusion processes (D_f) are the main contributing terms in the evolution of $\widetilde{\Delta}_c$ as shown in figure 9.7. In the light of the current DNS data, terms F_{21} and F_{23} have been ignored in the analysis as they are relatively close to zero, however more DNS data with different turbulent and chemical conditions is required to investigate these terms further.

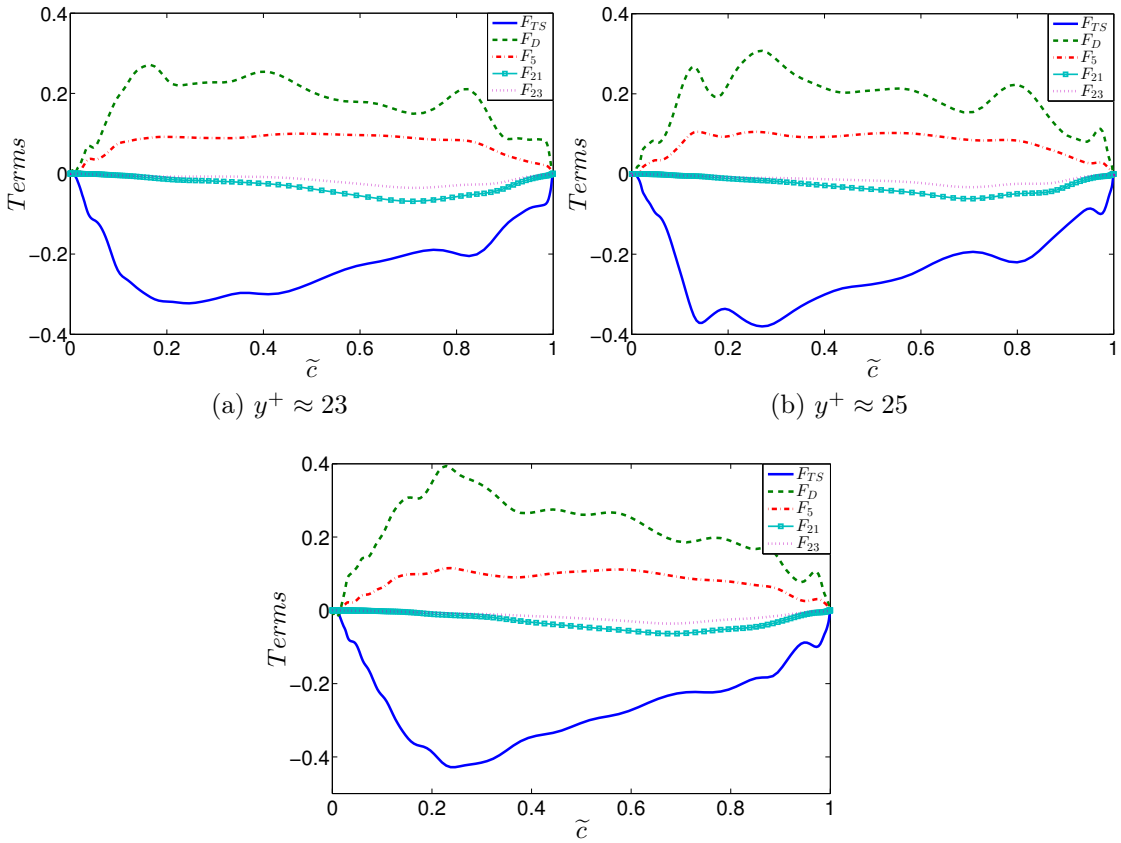

(a) $y^+ \approx 23$ (b) $y^+ \approx 25$

(c) $y^+ \approx 27$

Figure 9.8: Leading order terms without the diffusion and source terms for the $\widetilde{\Delta}_c$ evolution equation in the V-flame DNS. The values are normalised using the respective ρ_R, u_L^0 and δ_L^0.

It should be noted here that there is no prior theoretical or experimental know-

ledge available in the literature for any of the terms in eq. (8.62). It is argued in here that dimensional analysis and scaling arguments combined with the physical insight from the DNS data set can be used to model the individual terms in eq. (8.62).

9.4 Model for turbulent straining terms (F_{TS})

Expanding the expression for F_{TS} in eq. (8.62) leads to:

$$F_{TS} = \underbrace{\overline{\rho D_c}\,\widetilde{\frac{\partial c''}{\partial x_i} S''_{ij} \frac{\partial c''}{\partial x_n} \frac{\partial u''_n}{\partial x_j}}}_{F_{41}} \underbrace{+2\overline{\rho D_c}\,\widetilde{\frac{\partial c''}{\partial x_n} \frac{\partial u''_n}{\partial x_j} \frac{\partial c''}{\partial x_i} S''_{ij}}}_{F_{44}} \underbrace{-\overline{\rho D_c}\,\widetilde{\frac{\partial c''}{\partial x_i} \frac{\partial c''}{\partial x_j} \frac{\partial u''_n}{\partial x_j} \frac{\partial u''_i}{\partial x_n}}}_{F_{45}} \underbrace{+\overline{\rho D_c}\,\widetilde{\frac{\partial c''}{\partial x_i} \frac{\partial c''}{\partial x_j}} \widetilde{\frac{\partial u''_n}{\partial x_j} \frac{\partial u''_i}{\partial x_n}}}_{F_{48}}. \tag{9.2}$$

All the terms in eq. (9.2) require closures. The scalar gradient and strain rate contribution in F_{41} are assumed to scale as:

$$\rho D_c \frac{\partial c''}{\partial x_i} S''_{ij} \frac{\partial c''}{\partial x_n} \sim \overline{\rho} \widetilde{\Delta}_c,$$

and the turbulent straining represented by the fluctuating velocity gradients is scaled as:

$$\frac{\partial u''_n}{\partial x_j} \sim \frac{\widetilde{\epsilon}}{\widetilde{k}}.$$

Similar scaling arguments are used to scale the rest of the terms in eq. (9.2), thus leading to:

$$F_{TS} \approx C_b \overline{\rho} \frac{\widetilde{\epsilon}}{\widetilde{k}} \widetilde{\Delta}_c, \tag{9.3}$$

where C_b is a scaling factor for the model.

The value of C_b is of key importance. Following earlier modelling strategies of Chakraborty and Swaminathan [43, 45, 46] used in the $\widetilde{\epsilon}_c$ transport equation, several functions for C_b can be proposed based on Ka_L and Re_{l_t}:

$$C_{b1} = \frac{-6.4}{1 + \sqrt{Ka_L}}, \tag{9.4}$$

$$C_{b2} = \frac{-7.5}{0.8 + (1.6Ka_L)^{7/2}}, \tag{9.5}$$

$$C_{b3} = \frac{-2.6Re_{l_t}}{\sqrt{Ka_L + Re_{l_t}}}, \tag{9.6}$$

where Re_{l_t} is defined as:

$$Re_{l_t} = \frac{u^{'} l_t}{\nu_R},$$

and Ka_L is defined as:

$$Ka_L = \left(u^{'}/u_L^0\right)^{3/2} (\delta_L/l_t)^{1/2}. \tag{9.7}$$

Figure 9.9 shows the results obtained with different functions for C_b at all the sampling locations. It can be observed that the choice of the scaling factor used determines the accuracy of the proposed model. The functions in eq. (9.4) and eq. (9.5) only include the effects of the local Karlovitz number, whereas eq. (9.6) includes the effects of the local Karlovitz and turbulent Reynolds number. Chakraborty and Swaminathan [46] have recently reported that the changes in turbulent Reynolds number play a significant role in the evolution of $\widetilde{\epsilon}_c$. In the light of these findings it is argued here that the function represented by C_{b3} is used as the the scaling factor C_b in eq. (9.3).

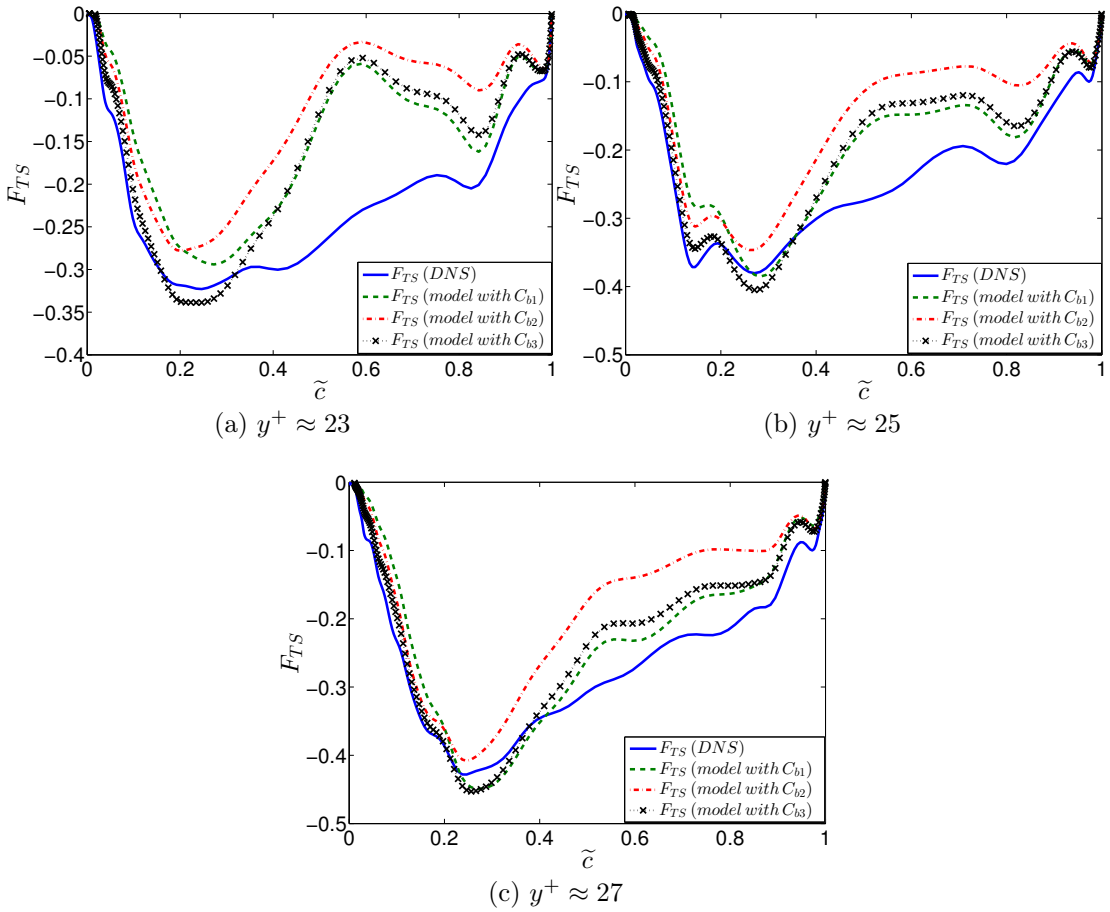

(a) $y^+ \approx 23$ (b) $y^+ \approx 25$

(c) $y^+ \approx 27$

Figure 9.9: Comparisons of F_{TS} model predictions and the V-flame DNS results. The values are normalised using the respective ρ_R, u_L^0 and δ_L^0.

It should be noted that the functions proposed for C_b are a few of several possible empirical relations which lead to a physically plausible result. Comparisons of the model against the DNS data set at all the sampling locations are given in figure 9.9. Throughout, the model performance improves as the distance of the sampling location from the flame holder increases. This is due to the fact that the numerical flame holder used in the DNS introduces a negative bias to the strain rate distribution immediately downstream of the flame holder [60]. It is argued by Dunstan et al [60] that the magnitude of the negative bias in the strain rate distribution is dependent on the inlet flow velocity, and diminishes as the distance from the flame holder increases.

9.5 Model for dilatation terms $(F_D + F_5)$

Term F_5 shows similar trends to that of the dilatation term (F_D) for all the sampling locations in the V-flame as shown in figure 9.10, hence in the light of the current DNS data term F_5 has been added to term F_D for modelling purposes.

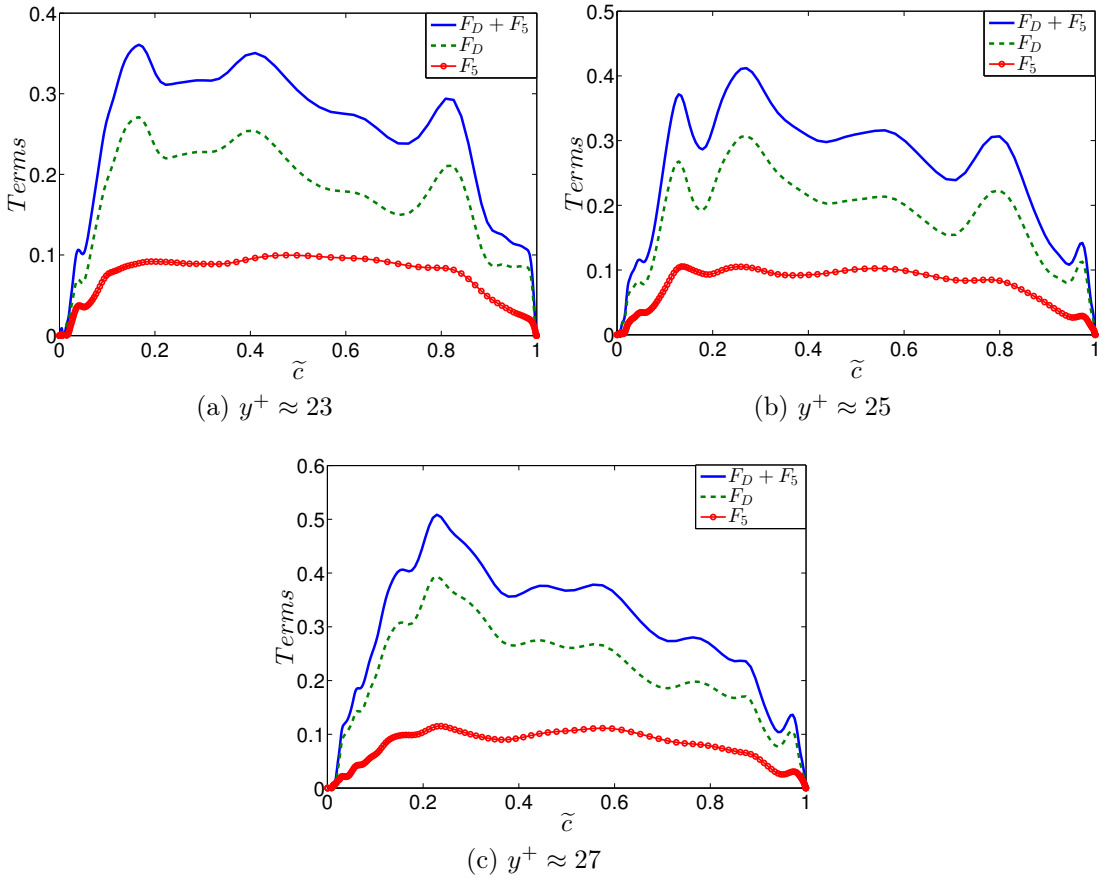

(a) $y^+ \approx 23$

(b) $y^+ \approx 25$

(c) $y^+ \approx 27$

Figure 9.10: Comparisons of F_5 and F_D in the the V-flame DNS. The values are normalised using the respective ρ_R, u_L^0 and δ_L^0.

From eq. (8.61) and eq. (8.28),

$$F_D + F_5 = \underbrace{2\overline{\rho D_c}\overbrace{\frac{\partial c^{''}}{\partial x_i}S^{''}_{ij}\frac{\partial c^{''}}{\partial x_j}\frac{\partial u^{''}_l}{\partial x_l}}}_{F_{31}} \underbrace{-2\overline{\rho D_c}\overbrace{\frac{\partial c^{''}}{\partial x_j}\frac{\partial u^{''}_l}{\partial x_l}}\overbrace{\frac{\partial c^{''}}{\partial x_i}S^{''}_{ij}}}_{F_{34}} \underbrace{+\overline{D_c\frac{\partial \rho}{\partial x_j}\frac{\partial p^{'}}{\partial x_i}\frac{\partial c^{''}}{\partial x_j}\frac{\partial c^{''}}{\partial x_i}\frac{1}{\rho}}}_{F_{35}}$$
$$\underbrace{-\overline{D_c\frac{\partial \rho}{\partial x_j}\frac{\partial \tau^{''}_{in}}{\partial x_n}\frac{\partial c^{''}}{\partial x_i}\frac{\partial c^{''}}{\partial x_j}\frac{1}{\rho}}}_{F_{36}} \underbrace{+\overline{D_c\frac{\partial c^{''}}{\partial x_i}S^{''}_{ij}\frac{\partial c^{''}}{\partial x_j}\frac{\partial}{\partial x_n}\left(\rho u^{''}_n\right)}}_{F_5}. \tag{9.8}$$

We propose here that the contributions involving the scalar gradients and the strain rate in F_{31} scale as:

$$\rho D_c\frac{\partial c^{''}}{\partial x_i}S^{''}_{ij}\frac{\partial c^{''}}{\partial x_j} \backsim \overline{\rho}\widetilde{\Delta}_c,$$

while the contributions involving the dilatation represented by the divergence of the velocity field scale as:

$$\frac{\partial u^{''}_l}{\partial x_l} \sim \tau Da_L\frac{u^0_L}{\delta_L},$$

where Da_L represents the local Damköhler number and is defined as:

$$Da_L = \frac{(u^0_L/\delta_L)}{\left(\widetilde{\epsilon}/\widetilde{k}\right)}. \tag{9.9}$$

Similar scaling arguments apply to F_{34}. F_{35} includes the effects of pressure gradient which is a source term for the transport of momentum. In the limiting case of statistically steady high Re_{l_t} flows the velocity gradients are generated by the pressure gradient. Under these conditions it can be assumed that the pressure gradient contains the effects of the strain rate and the density gradients include the effects of dilatation. Hence combining the two observations F_{35} can be scaled as:

$$D_c\frac{\partial \rho}{\partial x_j}\frac{\partial p^{'}}{\partial x_i}\frac{\partial c^{''}}{\partial x_j}\frac{\partial c^{''}}{\partial x_i}\frac{1}{\rho} \sim \overline{\rho}\widetilde{\Delta}_c\tau Da_L\frac{u^0_L}{\delta_L}.$$

F_{36} can be simplified by assuming that under the high Re_{l_t} the density variations associated with $\tau^{''}_{in}$ are small and substituting $\tau^{''}_{in}$ as $\tau^{''}_{in} \approx 2\mu S^{''}_{in}$, where $\mu \approx \rho\alpha$

from the Pr definition (eq. (2.31)), thus leading to:

$$-\overline{\rho D_c D_c \frac{\partial \rho}{\partial x_j} \frac{\partial S''_{in}}{\partial x_n} \frac{\partial c''}{\partial x_j} \frac{\partial c''}{\partial x_i} \frac{1}{\rho}}. \tag{9.10}$$

Following the earlier scaling arguments the expression in eq. (9.10) scales as:

$$\sim \overline{\rho} \widetilde{\Delta}_c \tau Da_L \frac{u'^0_L}{\delta_L}.$$

The contributions involving the scalar gradients and the strain rate in F_5 can be scaled as:

$$D_c \frac{\partial c''}{\partial x_i} S''_{ij} \frac{\partial c''}{\partial x_j} \sim \widetilde{\Delta}_c,$$

while the contributions from the density gradient and the divergence of the velocity field scale as:

$$\frac{\partial}{\partial x_n} \left(\rho u''_n \right) \sim \overline{\rho} \tau Da_L \frac{u'^0_L}{\delta_L}.$$

Thus leading to the model:

$$F_D + F_5 \approx C_c \tau Da_L \overline{\rho} \widetilde{\Delta}_c \frac{u'^0_L}{\delta_L}, \tag{9.11}$$

where C_c is a scaling factor for the model. The model proposed in eq. (9.11) has an explicit dependence on the heat release parameter τ and the local Damköhler number Da_L, thus allowing the model to account for the changes in heat release and turbulence and their influence on dilatation in the $\widetilde{\Delta}_c$ evolution. Furthermore, an explicit dependence of the model on τ allows the model to vanish in the limiting case of cold flow turbulence.

The accuracy of the model in eq. (9.11) relies on the choice of the scaling factor C_c. Following earlier modelling strategies of Chakraborty et al [40, 43, 45, 46] for the $\widetilde{\epsilon}_c$ transport equation, several functions for C_c based on Re_{l_t} and Ka_L can be obtained as:

$$C_{c1} = \frac{0.01 + (0.1 Ka_L)}{1 - Ka_L}, \tag{9.12}$$

and

$$C_{c2} = \frac{0.38 Re_{l_t}}{\left(Re_{l_t} - Ka_L\right)^2}. \tag{9.13}$$

Figure 9.11 shows the results obtained with different values for C_c.

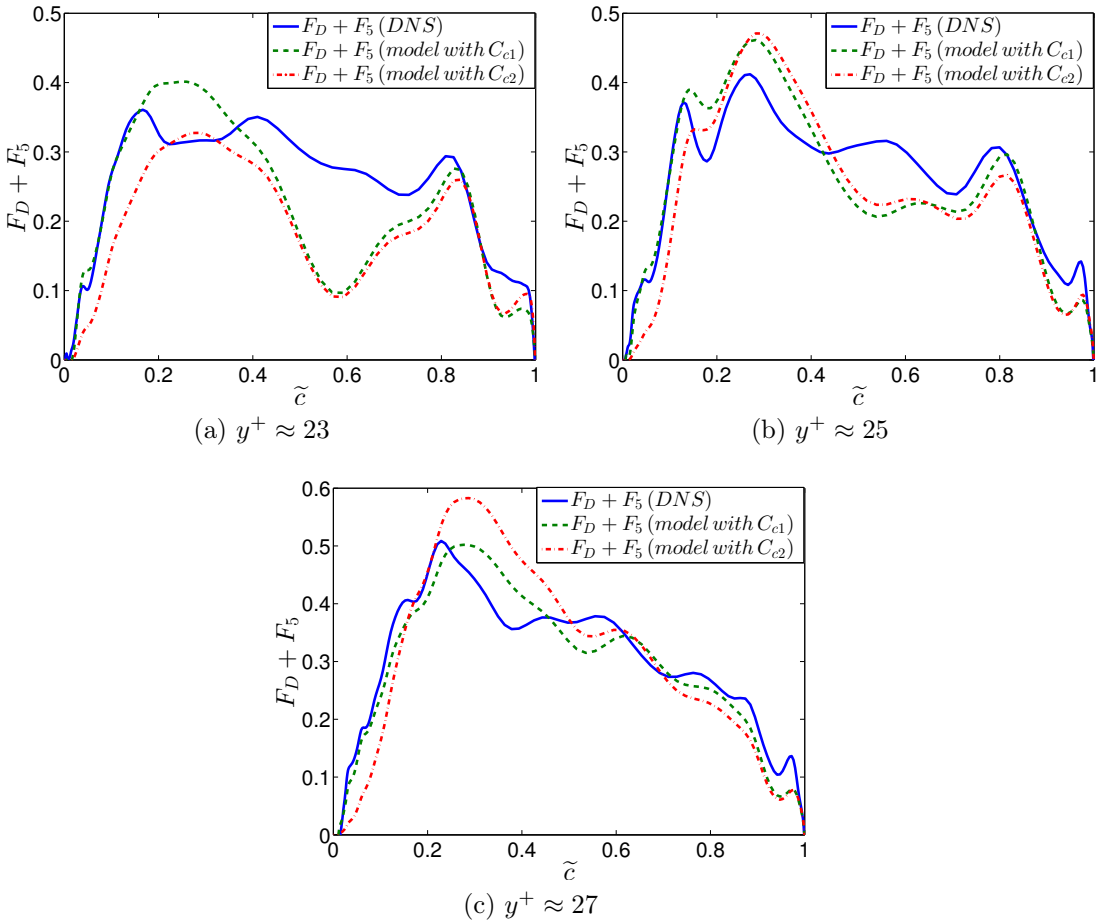

(a) $y^+ \approx 23$ (b) $y^+ \approx 25$

(c) $y^+ \approx 27$

Figure 9.11: Comparisons of $(F_D + F_5)$ model predictions and the the V-flame DNS results. The values are normalised using the respective ρ_R, u_L^0 and δ_L^0.

It is proposed here that the function represented by C_{c2} is used as the function for C_c in eq. (9.11), as C_{c2} involves the influence of the local Karlovitz number and the turbulent Reynolds number, thus accounting for changes in the local turbulent and chemical conditions. It should be noted that the functions in eq. (9.12) and eq. (9.13) are only calibrated for $Ka < 1$ combustion conditions, and more DNS data with different combustion conditions is required to extend the

range of C_c. The results from the model are in good agreement with the DNS data, and the model predictions improve as the distance from the flame holder increases.

9.6 Model for diffusion D_f and F_1 source terms

$$D_f + F_1 = \overline{-2\rho D_c D_c \frac{\partial}{\partial x_n}\left(\frac{\partial c''}{\partial x_j}\right)\frac{\partial}{\partial x_n}\left(\frac{\partial c''}{\partial x_i}S''_{ij}\right)} - \overline{2\rho D_c D_c \frac{\partial}{\partial x_n}\left(\frac{\partial c''}{\partial x_i}\frac{\partial c''}{\partial x_j}\frac{\partial S''_{ij}}{\partial x_n}\right)}$$
$$\overline{-2\rho D_c D_c \frac{\partial}{\partial x_n}\left(\frac{\partial c''}{\partial x_j}S''_{ij}\frac{\partial}{\partial x_n}\left(\frac{\partial c''}{\partial x_i}\right)\right)} + \overline{D_c \frac{\partial c''}{\partial x_i}\frac{\partial c''}{\partial x_j}\frac{\partial}{\partial x_n}\left(\frac{\partial \tau''_{in}}{\partial x_j}\right)}$$
$$\overline{+2D_c \frac{\partial c''}{\partial x_i}S''_{ij}\frac{\partial \dot{\omega}''_c}{\partial x_j}} - \overline{D_c \frac{\partial c''}{\partial x_i}\frac{\partial c''}{\partial x_j}\frac{\partial}{\partial x_i}\left(\frac{\partial p'}{\partial x_j}\right)}. \tag{9.14}$$

It can be seen in figure 9.7 that term F_1 is predominantly a source and D_f is predominantly a sink in the $\widetilde{\Delta}_c$ evolution. In order to model $D_f + F_1$, simple scaling arguments and physical insight gained from the DNS data set are used. The combined terms in eq. (9.14) scale as a product of flame normal strain rate $\widetilde{\Delta}_c/\widetilde{\epsilon}_c$ and flame turbulence interaction $\widetilde{\Delta}_c$ as:

$$\sim \widetilde{\Delta}_c^2/\widetilde{\epsilon}_c,$$

thus leading to:

$$D_f + F_1 \approx -C_a \overline{\rho}\frac{\widetilde{\Delta}_c^2}{\widetilde{\epsilon}_c}. \tag{9.15}$$

C_a is a scaling factor in eq. (9.15), and the negative sign is used due to the (over all) sink nature of $D_f + F_1$ as shown in figure 9.12. The sum of terms D_f and F_1 has a dominant effect on the $\widetilde{\Delta}_c$ evolution, thus the ratio $\widetilde{\Delta}_c^2/\widetilde{\epsilon}_c$ in eq. (9.15) represents the rate of change of flame turbulence interaction, $\widetilde{\Delta}_c^2/\widetilde{\epsilon}_c \approx d\widetilde{\Delta}_c/dt$.

The value of C_a in eq. (9.15) is a matter of calibration and is dependent on the DNS data set used for model calibration. Following earlier modelling strategies C_a can be expressed as

$$C_{a1} = 50 \tag{9.16}$$

$$C_{a2} = \frac{1.4Da_L}{0.1Ka_L} \tag{9.17}$$

$$C_{a3} = \frac{1.5Re_{l_t}}{0.1Ka_L} \tag{9.18}$$

Figure 9.12 shows the results obtained with different functions for C_a. It can be observed that all the scaling functions for C_a behave in a similar manner. Although it is recommended here that function C_{a3} is used as the recommended scaling factor in eq. (9.15), as C_{a3} rescales according to the turbulent Reynolds number and local Karlovitz number.

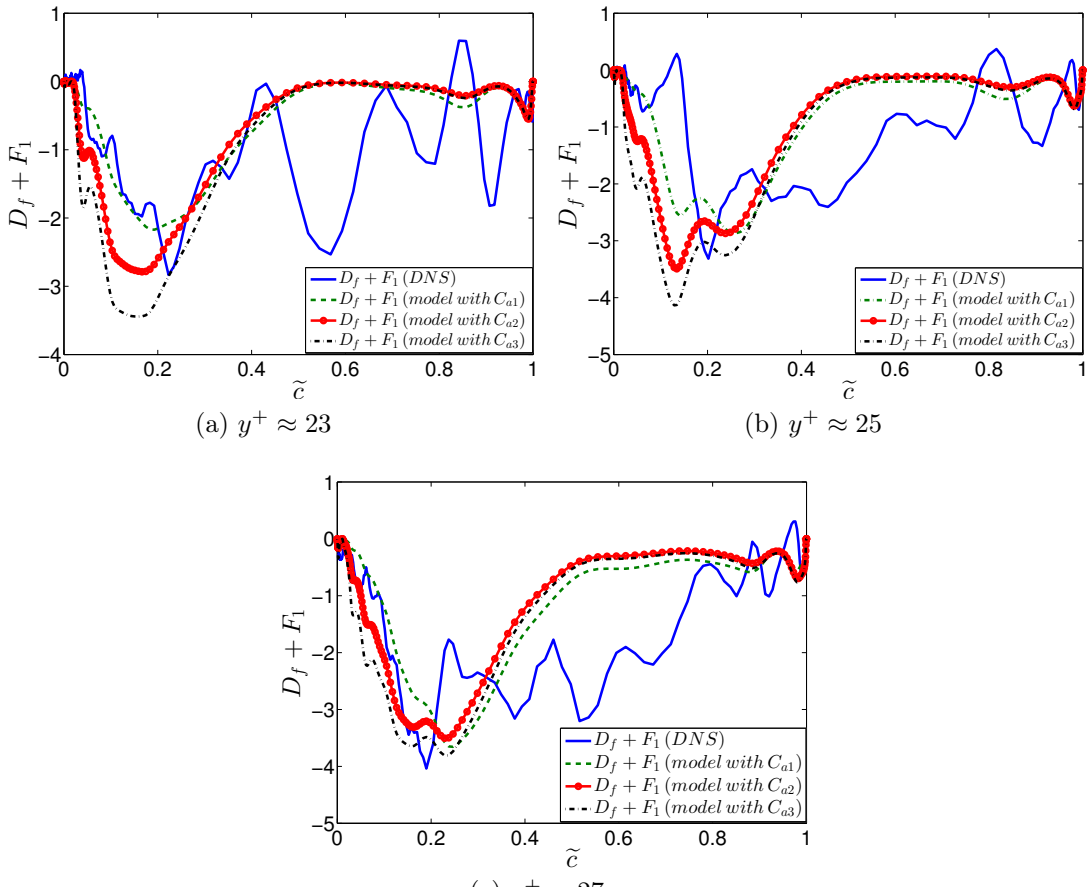

(a) $y^+ \approx 23$ (b) $y^+ \approx 25$

(c) $y^+ \approx 27$

Figure 9.12: Comparisons of $(D_f + F_1)$ model predictions and the V-flame DNS results. The values are normalised using the respective ρ_R, u_L^0 and δ_L^0.

The model proposed for $D_f + F_1$ is in qualitative agreement with the DNS data as shown in figure 9.12. One of the possible reasons for quantitative disagreement between the modelled and DNS values of $D_f + F_1$ is due to the numerical inaccuracies introduced into the pressure field. These inaccuracies are introduced primarily due the outlet boundary conditions used in the DNS. It is well known that the standard NSCBC fails to account for a flame crossing the boundary. These boundary conditions give rise to large unphysical pressure and velocity waves as flames cross the boundary [147]. Several solutions to this problem have been proposed in the literature [127, 128, 166, 147], and one of the solutions provided by Yoo and Im [166] has been used in the V-flame DNS [60]. It is argued here that the pressure statistics are still affected by the boundary conditions used. The error in the pressure field becomes apparent when the DNS results for term F_{12} (which contains the double derivative of the pressure) are analysed. The influence of the pressure waves from the boundaries on the pressure statistics can be observed in figure 9.13. It can be observed that there are sudden fluctuations in the DNS data. In order to overcome this problem improved boundary conditions are needed and are beyond the scope of this thesis.

In the absence of better boundary conditions the current DNS data set is believed to have provided approximately realistic results, and it is argued that even with the exact representation of the boundaries the results are not going to be significantly different from the ones obtained here.

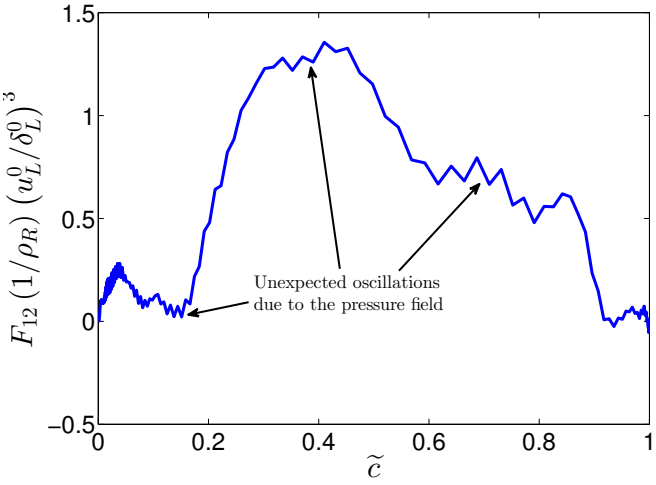

(a) $y^+ \approx 23$

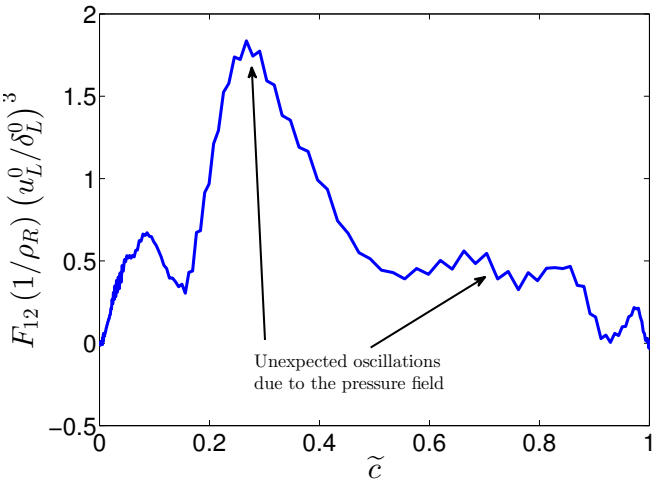

(b) $y^+ \approx 25$

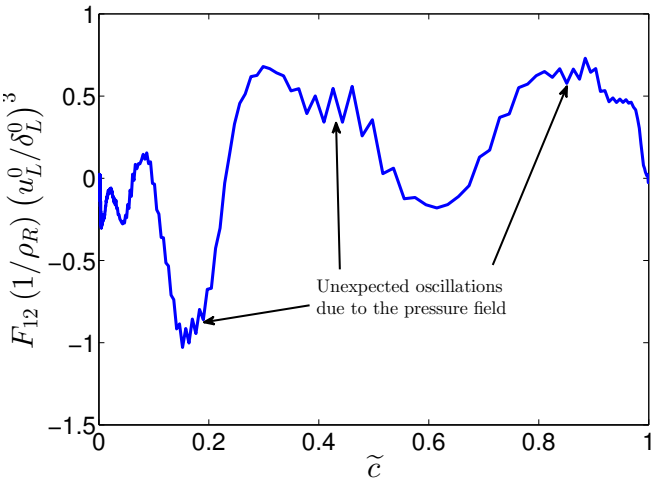

(c) $y^+ \approx 27$

Figure 9.13: Normalised F_{12} in the V-flame DNS

9.7 Time scale for flame turbulence interaction

A time scale for flame turbulence alignment behaviour can be obtained by combining the models for the leading order terms as:

$$-C_a\frac{\widetilde{\Delta}_c^2}{\widetilde{\epsilon}_c}+C_b\widetilde{\Delta}_c\frac{\widetilde{\epsilon}}{\widetilde{k}}+C_c\widetilde{\Delta}_c\tau Da_L\frac{u_L^0}{\delta_L}\backsimeq 0, \tag{9.19}$$

thus leading to :

$$\frac{\widetilde{\Delta}_c}{\widetilde{\epsilon}_c}\propto\frac{\widetilde{\epsilon}}{\widetilde{k}}+\tau Da_L\frac{u_L^0}{\delta_L}. \tag{9.20}$$

Eq. (9.20) implies that the flame normal strain rate is directly related to the competition between the dilatation rate and the turbulent strain rate. It can be observed in eq. (9.20) that in the limiting case of $u^{'}\rightarrow\infty$ and $Da\rightarrow 0$ the turbulent strain rate dominates the flame normal strain rate and the contributions from the dilatation rate vanish, whereas at lower levels of turbulence intensity there is a competition between the dilatation rate and the turbulent strain rate. A time scale for the change in the alignment characteristics of the flame turbulence interaction can be obtained from eq. (9.20). The time scale is represented as :

$$\tau_{FTI}=\frac{\widetilde{\epsilon}_c}{\widetilde{\Delta}_c}, \tag{9.21}$$

where τ_{FTI} represents the time taken by the scalar/flame gradient to change alignment from the compressive strain rate e_γ to the extensive strain rate e_α and vice-versa.

9.8 Algebraic model

It can be observed in eq. (9.19) that an algebraic expression for $\widetilde{\Delta}_c$ can easily be obtained as:

$$\widetilde{\Delta}_c\backsimeq\left(C_b\frac{\widetilde{\epsilon}}{\widetilde{k}}+C_c\tau Da_L\frac{u_L^0}{\delta_L}\right)\frac{\widetilde{\epsilon}_c}{C_a}. \tag{9.22}$$

Although the algebraic model for $\widetilde{\Delta}_c$ is mathematically consistent, it does not lead to a physically realisable result when compared against the DNS data. The reasons for this anomalous behaviour are unknown, and it is believed that more

robust scaling factors for the leading order terms are required. In order to improve the scaling factors in the leading order terms, more DNS data with different turbulent and chemical conditions is required.

9.9 Summary

Flame turbulence interaction is an important quantity in turbulent premixed combustion modelling. It has been shown in previous studies that the effect of strain rate on the transport of scalar dissipation is dominated by the interaction between the fluctuating scalar gradients and the fluctuating strain rate (here denoted by $\widetilde{\Delta}_c$). An accurate representation of the flame turbulence interaction can be obtained from the leading order terms in the evolution equation for $\widetilde{\Delta}_c$. An evolution equation for $\widetilde{\Delta}_c$ has been derived and an order of magnitude analysis under the joint assumption of high Reynolds and Damköhler numbers has been done to identify the leading order terms. The leading order terms have been analysed via the DNS results of Dunstan et al [60]. It has been found that the turbulent strain rate and the dilatation rate compete in $\widetilde{\Delta}_c$ evolution, which is in agreement with the theories proposed in earlier studies [40, 151]. It has also been found that there is also competition between the source terms (pressure gradient and reaction rate) and the diffusion processes. It is argued in this study that the overall behaviour of $\widetilde{\Delta}_c$ evolution equation is determined by the competition between source and diffusion terms.

Closures for the leading order terms have been proposed and compared against the DNS data set at different locations. The comparisons of modelled predictions and the DNS values are in good agreement for the combustion conditions considered here. In the light of a recent study by Chakarborty and Swaminathan [46], the closures for the leading order terms have been made functions of turbulent Reynolds and local Karlovitz numbers. It has also been shown here that the flame normal strain rate is dependent on the contributions from the turbulent strain rate and the dilatation rate. Thus, a new time scale representing the time required by the flame gradient to change alignment with the strain rate eigenvectors has been proposed. An algebraic model for $\widetilde{\Delta}_c$ has been obtained, although the algebraic model is mathematically consistent it does not lead to any

physically realisable results. The reasons for this anomalous behaviour are not know. However, it is argued here that improvements to the scaling factors for the models of the leading order terms with different DNS data sets are required to improve the algebraic model for $\widetilde{\Delta}_c$.

10 Conclusions and suggestions for future work

10.1 Summary and Conclusions

In this thesis, flame turbulence interaction in premixed turbulent combustion has been investigated. In the first part of the thesis, currently available scalar dissipation ($\widetilde{\epsilon}_c$) models for RANS formulation have been tested by using a laboratory scale turbulent premixed V-flame. Problems in the current $\widetilde{\epsilon}_c$ models have been identified, and one of the major problems identified in nearly all the $\widetilde{\epsilon}_c$ models is the correct representation of the flame turbulence interaction $\left(\widetilde{\Delta}_c\right)$. In order to rectify this problem, a new transport equation has been proposed.

Summaries and conclusions from the respective studies of the the different $\widetilde{\epsilon}_c$ models, and from the development of $\widetilde{\Delta}_c$ evolution equation are given in the following subsections.

RANS simulation of a laboratory scale V-flame

- In chapter 7, several scalar dissipation $\widetilde{\epsilon}_c$ models of varying complexity are used in conjunction with the Bray Moss Libby (BML) model, and a rod stabilised turbulent premixed V-flame has been used as a representative configuration. The effects of using different modelling approaches for $\widetilde{\epsilon}_c$ on the prediction of reaction rate have been studied. Algebraic models proposed by Swaminathan and Bray [149] (the SDR-1 model), Kolla et al [86, 85] (the SDR-2 model) and Vervisch et al [157] (the SDR-3 model) have been used. The RANS simulations were compared against the experimental data of Bell et al [9]. It was found that all the $\widetilde{\epsilon}_c$ models used tend to deviate from the experimental data in the far wake region of the stabilising

rod. All the $\widetilde{\epsilon}_c$ models are sensitive to the values of the constants used in the respective $\widetilde{\epsilon}_c$ models. The SDR-1 model is sensitive to the time scale ratio C_D, and there is no credible way of determining the value for RANS applications. In the SDR-2 model the scaling factors used for flame turbulence interaction are sensitive to the choice of flame thickness (thermal flame thickness or the diffusive flame thickness) used. The parameter $\beta^{'}$ (which controls the dissipation of the $\widetilde{\epsilon}_c$ evolution) in the SDR-2 model has to be calibrated for a given flame configuration and chemical properties. It has been found that higher values of $\beta^{'}$ lead to a better prediction of the scalar dissipation in the SDR-2 model, and an updated value of $\beta^{'} \approx 10$ has been proposed in case of the V-flame. In the SDR-3 model the modelled flame surface density transport equation needs to be improved to include the correct representation of the flame turbulence interaction phenomenon. In order to improve the current scalar dissipation modelling approaches a new transport equation for the flame turbulence interaction phenomenon has been proposed.

Evolution equation for flame turbulence interaction

- A new evolution equation for flame turbulence interaction ($\widetilde{\Delta}_c$) has been developed in chapter 8. In section 8.2 leading order terms for $\widetilde{\Delta}_c$ evolution equation were identified by using a suitable order of magnitude analysis. The leading order terms were then studied via the DNS results of Dunstan et al [60] in chapter 9. It has been found that the turbulent strain rate and the dilatation rate compete in the $\widetilde{\Delta}_c$ evolution, which is in agreement with earlier studies [40, 151]. It has also been found that there is competition between the source terms and the diffusion processes. It is argued here that the overall behaviour of the $\widetilde{\Delta}_c$ evolution equation is dominated by the competition between source and diffusion terms. Closures for the leading order terms have been proposed and compared against the DNS data set in chapter 9. The comparisons of modelled predictions and the DNS values are in good agreement for the combustion conditions considered. Although more investigations of DNS data sets with different combustion conditions and turbulent Reynolds number are needed to fully understand the be-

haviour of the leading order terms in the $\widetilde{\Delta}_c$ evolution equation. Some recommendations for the DNS studies have been made in the next section.

10.2 Suggestions for future work

DNS studies and modelling strategies for $\widetilde{\Delta}_c$ evolution equation

In order to understand fully the physics represented by the $\widetilde{\Delta}_c$ evolution equation and to extend the modelling strategies for the closures of the leading order terms. Several DNS studies with different combustion and turbulence conditions are required. Some of the proposed studies for future work are listed below.

- Investigations of DNS data sets with different turbulent Reynolds number are required to fully understand the effects of changes in turbulent Reynolds number on the $\widetilde{\Delta}_c$ evolution equation. Recently it has been shown by Chakraborty and Swaminathan [46] that changes in Re_{l_t} have a significant influence on the $\widetilde{\epsilon}_c$ evolution. In the light of the earlier studies for $\widetilde{\epsilon}_c$ it is expected that the behaviour of F_{TS} and $F_D + F_5$ is going to be significantly affected by the changes in the turbulent Reynolds number. The contributions from F_{TS} are expected to increase with increasing Re_{l_t} and the contributions from $F_D + F_5$ are expected to decrease with an increase in Re_{l_t}. The behaviour of $D_f + F_1$ with changes in the Re_{l_t} is not clear and needs to be investigated further.

- DNS investigations with different Damköhler numbers are needed to check the sensitivity of the flame turbulence interaction evolution under different chemical and turbulent conditions. It is well known from the earlier findings of Chakraborty and Swaminathan [44, 45] that the changes in Da alter the behaviour of the flame turbulence interaction alignment statistics. In the light of earlier studies it is expected that the behaviour of F_{TS} and $F_D + F_5$ is going to be significantly affected by the changes in Da. The contributions from F_{TS} are expected to decrease with increasing Da and the contributions from $F_D + F_5$ are expected to increase with an increase in Da. The influence of Da on $D_f + F_1$ is not known and needs to be investigated further.

- Effects of variations in Lewis number on the $\widetilde{\Delta}_c$ evolution equation need to be studied, as these effects have shown to significantly influence the flame turbulence interaction alignment statistics in the study of Chakraborty et al [42].

- The behaviour of F_{21} and F_{23} in the $\widetilde{\Delta}_c$ evolution equation should be investigated in different DNS data sets with varying turbulence and chemical parameters. These terms have been ignored here, as the magnitude of these terms is relatively close to zero in the V-flame DNS. The detailed DNS studies would elucidate the uncertainty regarding the contributions from F_{21} and F_{23}.

Use of $\widetilde{\Delta}_c$ evolution equation in industrial codes

The $\widetilde{\Delta}_c$ evolution equation is yet to be used for any of the RANS calculation. A few recommendations for future work in this regard have been made here, and are listed as follows:

- Implement the $\widetilde{\Delta}_c$ evolution equation into a RANS code and couple it with $\widetilde{\epsilon}_c$ models to check the influence of $\widetilde{\Delta}_c$ on the mean reaction rate and the flame location. The $\widetilde{\Delta}_c$ evolution equation can be coupled to Kolla et al [85, 86](the SDR-2) model as:

$$\widetilde{\epsilon}_c \backsimeq \left(2Kc^*\left(\frac{u_L^0}{\delta_L^0}\right) - 2\frac{\widetilde{\Delta}_c}{\widetilde{\epsilon}_c}\right)\frac{\widetilde{c''^2}}{\beta'}. \tag{10.1}$$

  It should be noted here that $\widetilde{\Delta}_c$ is divided by $\widetilde{\epsilon}_c$ in the second term on the right-hand side of eq. (10.1), and would lead to numerical instabilities. In order to avoid the numerical instabilities, a limiter can be used in the code such that $\widetilde{\Delta}_c/\widetilde{\epsilon}_c$ is zero outside the flame.

- Improve the scaling factors for the leading order terms in the $\widetilde{\Delta}_c$ evolution equation. These improvements would lead to a more robust algebraic model with physically realisable results for RANS applications. The expression for $\widetilde{\Delta}_c$ proposed in eq. (9.22) can be used as a basis for the improvement of the algebraic model for $\widetilde{\Delta}_c$. The new algebraic formulation of $\widetilde{\Delta}_c$ can be

included into the algebraic formulation of $\widetilde{\epsilon}_c$ in eq. (10.1) to obtain an improved algebraic model for $\widetilde{\epsilon}_c$.

- Similarly the $\widetilde{\Delta}_c$ evolution equation can be coupled with the Σ transport equation by changing the closure for the flame turbulence interaction term in the tangential strain rate term.

Improvement of the strained flamelet models

A strained flamelet formulation based on the scalar dissipation rate approach has recently been proposed by Kolla et al [85, 87, 88]. This approach relies on detailed chemical libraries to calculate the mean reaction rate. In the chemical libraries the mean reaction rate appears as a function of the mean progress variable, variance of the progress variable and the scalar dissipation. It is proposed here that the dimensions of the library can be increased by including the flame turbulence interaction. This would lead to a better prediction of the flame straining process and would explicitly include the strain rate into the strained flamelet formulation. The new formulation would improve the mean reaction rate prediction and would also lead to a better prediction of the pollutant formation.

RANS simulations for the laboratory scale V-flame

- Use the $\widetilde{\epsilon}_c$ models described in this thesis in conjunction with detailed chemistry approaches, such as the ones proposed by Kolla et al [85, 87, 88] and Salehi and Bushe [138, 139]. These chemical approaches would improve the predictive capabilities of the mean reaction rate and would also allow the prediction of pollutant formation.

- Use Vervisch et al [157] (the SDR-3) model with different closures for the modelled Σ transport equation for example closures proposed by Mantel and Borghi [105] and Cant et al [36]. This would lead to a better understanding of the sensitivity of the SDR-3 model to the choice of closures used in the modelled Σ transport equation.

Appendix A

Thermochemistry in BML

In the BML formulation, the main thermodynamic variables are related to the reaction progress variable c. This is done by assuming that the enthalpy remains constant [27]. The heat release parameter τ is defined from the first law of thermodynamics for open systems, which is [38]:

$$q - w = (h_2 - h_1) + \frac{1}{2}(v_2^2 - v_1^2) + g(z_2 - z_1) \tag{A.1}$$

where q is the heat flux , w is the work done on the system, h_2 and h_1 are the enthalpies at the two state points, v_2 and v_1 are the respective velocities at the two state points and z_2 and z_1 are the respective heights at the two state points (i.e. reactants and products) as shown in figure A.1.

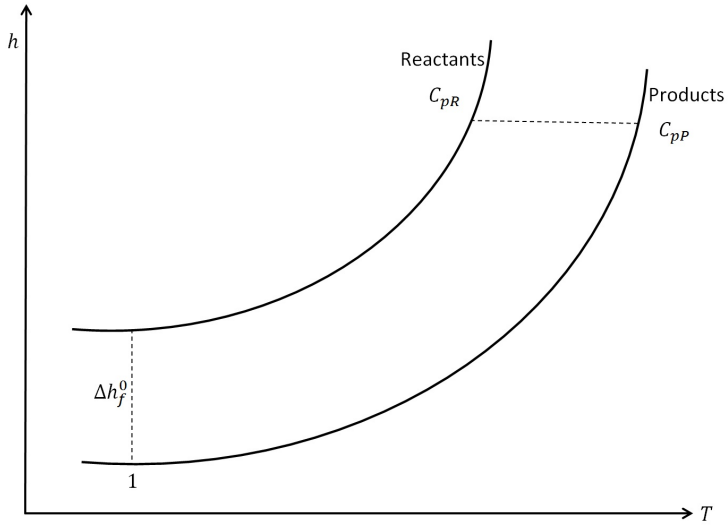

Figure A.1: enthalpy-temperature diagram

The expression in eq. (A.1) can be simplified as [38]:

$$\underset{\substack{no\\ external\\ work}}{q - w} = (h_2 - h_1) + \underset{\substack{no\\ change\ in\\ Kinetic\ energy}}{\tfrac{1}{2}(v_2^2 - v_1^2)} + \underset{\substack{no\\ change\ in\\ Potential\ energy}}{g(z_2 - z_1)} \tag{A.2}$$

so eq. (A.2) reduces to [38]

$$q = h_2 - h_1 \tag{A.3}$$

As there are no heat losses i.e. combustion is adiabatic $q = 0$.

Now using figure A.1 and starting from point 1 and assuming C_p to be linear :

$$h_P = C_{pP}\left(T_p - T_0\right) \tag{A.4}$$

and

$$h_R = \left(\Delta h^0_{f,R} Y_R\right) + C_{pR}\left(T_R - T_0\right) \tag{A.5}$$

where $\Delta h^0_{f,R}$ is the heat release per unit mass of fuel (i.e. chemical enthalpy). As the combustion is assumed to be adiabatic:

$$h_P = h_R \tag{A.6}$$

Now comparing expressions in eq. (A.4) and eq. (A.5) gives:

$$C_{pP}\left(T_p - T_0\right) = \left(\Delta h^0_{f,R} Y_R\right) + C_{pR}\left(T_R - T_0\right) \tag{A.7}$$

Assuming that :

$$C_{pP} = C_{pR} = C_p \tag{A.8}$$

and using eq. (A.7) gives:

$$C_p T_P - C_p T_0 = \left(\Delta h^0_{f,R} Y_R\right) + C_p T_R - C_p T_0 \tag{A.9}$$

simplifying eq. (A.9) gives:

$$\frac{T_P}{T_0} = \frac{\left(\Delta h^0_{f,R} Y_R\right)}{C_p T_0} + \frac{T_R}{T_0} \tag{A.10}$$

further simplification of eq. (A.10) leads to:

$$\frac{T_P}{T_R} = \frac{\left(\Delta h^0_{f,R} Y_R\right)}{C_p T_R} + 1 \tag{A.11}$$

In the case of adiabatic combustion:

$$\tau = \frac{\left(\Delta h^0_{f,R} Y_R\right)}{C_p T_R} \tag{A.12}$$

This leads to [19]:

$$\frac{T_P}{T_R} = 1 + \tau \tag{A.13}$$

Now using the thermal equation of state for reactants and products [38]:

$$p_R = \rho_R R_R T_R \tag{A.14}$$

and

$$p_P = \rho_P R_P T_P \tag{A.15}$$

where p_R and p_P are the respective reactant and product pressures, and R_R and R_P are the respective characteristic gas constants.

Now making T_R and T_P the subject in eq. (A.14) and eq. (A.15) respectively, and then dividing eq. (A.15) by eq. (A.14) gives [118]:

$$\frac{T_P}{T_R} = \frac{\rho_R R_R}{p_R} \frac{p_P}{\rho_P R_P}. \tag{A.16}$$

It is assumed that the pressure does not change thermodynamically, thus implying that $R_P = R_R$ [26, 117, 35]. This assumption leads to :

$$\frac{T_P}{T_R} = \frac{\rho_R}{\rho_P}. \tag{A.17}$$

Making use of the expression in eq. (A.13) an expression for the heat release in terms density can be obtained [26, 117, 35]:

$$\tau = \frac{\rho_R}{\rho_P} - 1 \tag{A.18}$$

So at constant enthalpy, the temperature is given by [27]:

$$T = T_R \left(1 + \tau c\right). \tag{A.19}$$

Multiplying eq. (A.19) by ρ and then applying Favre averaging gives:

$$\frac{\rho\widetilde{T}}{T_R} + \frac{\rho T''}{T_R} = \rho + \rho\tau\widetilde{c} + \rho\tau c'' \tag{A.20}$$

Time averaging and simplifying eq. (A.20) gives [26, 117, 35]

$$\widetilde{T} = T_R \left(1 + \tau\widetilde{c}\right). \tag{A.21}$$

By making use of the thermal equation of state an expression in terms of instantaneous density $\overline{\rho}$ is obtained [26, 117, 35]:

$$\frac{\overline{\rho}}{\rho_R} = \frac{1}{1 + \tau\widetilde{c}}. \tag{A.22}$$

Appendix B

Order of magnitude analysis of scalar dissipation transport equation

The transport equation for $\widetilde{\epsilon}_c$ is :

$$\frac{\partial \overline{\rho}\widetilde{\epsilon_c}}{\partial t} + \frac{\partial \overline{\rho}\widetilde{u}_j\widetilde{\epsilon_c}}{\partial x_j} - \underbrace{\frac{\partial}{\partial x_j}\left(\overline{\rho D_c}\frac{\partial \widetilde{\epsilon_c}}{\partial x_j}\right)}_{D_1} + \underbrace{2\overline{\rho D_c D_c\left(\frac{\partial}{\partial x_j}\left(\frac{\partial c''}{\partial x_k}\right)\left(\frac{\partial c''}{\partial x_k}\right)\right)}}_{D_2}$$
$$= T_1 + T_2 + T_3 + T_4 \tag{B.1}$$

where

$$T_1 = \underbrace{-\frac{\partial \overline{\rho u_j'' \epsilon_c}}{\partial x_j}}_{T_{11}} \underbrace{- 2\overline{\rho\alpha}\left(\widetilde{u_j''\frac{\partial c''}{\partial x_k}}\right)\frac{\partial}{\partial x_j}\left(\frac{\partial \widetilde{c}}{\partial x_j}\right)}_{T_{12}} \tag{B.2}$$

$$T_2 = 2\overline{\rho}\widetilde{\epsilon_c}\frac{\partial \widetilde{u}_l}{\partial x_l} + 2\overline{\rho D_c\left(\frac{\partial c''}{\partial x_x}\frac{\partial c''}{\partial x_x}\frac{\partial u_l''}{\partial x_l}\right)} = 2\overline{\rho\epsilon_c\frac{\partial u_l}{\partial x_l}} \tag{B.3}$$

$$T_3 = \underbrace{-2\overline{\rho D_c}\frac{\partial \widetilde{c}}{\partial x_j}\left(\widetilde{\frac{\partial c''}{\partial x_x}\frac{\partial u_j''}{\partial x_x}}\right)}_{T_{31}} \underbrace{-2\overline{\rho D_c}\left(\widetilde{\frac{\partial c''}{\partial x_j}S_{jk}''\frac{\partial c''}{\partial x_k}}\right)}_{T_{32}}$$
$$\underbrace{-2\overline{\rho D_c}\left(\frac{\partial c''}{\partial x_k}\frac{\partial c''}{\partial x_k}\right)\widetilde{S_{jk}}}_{T_{33}} \tag{B.4}$$

$$T_4 = 2\left(\overline{D_c\frac{\partial c''}{\partial x_k}\frac{\partial \dot{\omega}_c''}{\partial x_k}}\right) \tag{B.5}$$

B.1 The order of magnitude analysis of $\widetilde{\epsilon_c}$ transport equation

The details of the order of magnitude (OMA) scaling arguments are given in section 8.2.3. The details of the scaling of each term are as follows:

Unsteady term

$$\begin{aligned}\frac{\partial \overline{\rho}\widetilde{\epsilon_c}}{\partial t} &\simeq \mathcal{O}\left(\rho_R\frac{u'}{l_t}\times\frac{u_L^0}{\delta_L^0}\right)\\ &= \mathcal{O}\left(\rho_R\frac{u_L^0}{\delta_L^0}D_a^{-1}\frac{u_L^0}{\delta_L^0}\right)\\ &= \mathcal{O}\left(\rho_R\left(\frac{u_L^0}{\delta_L^0}\right)^2; D_a^{-1}\right)\end{aligned} \tag{B.6}$$

Convection term

$$\begin{aligned}\frac{\partial\overline{\rho}\widetilde{u_j}\widetilde{\epsilon_c}}{\partial x_j} &\backsimeq \mathcal{O}\left(\rho_R\frac{u_{ref}}{l_t}\frac{u_L^0}{\delta_L^0}\right)\\ &= \mathcal{O}\left(\rho_R\frac{u_{ref}}{\frac{\delta_L^0}{u_L^0}u'Da}\frac{u_L^0}{\delta_L^0}\right)\\ &= \mathcal{O}\left(\rho_R\frac{u_{ref}}{u'Da}\left(\frac{u_L^0}{\delta_L^0}\right)\right)\\ &= \mathcal{O}\left(\rho\left(\frac{u_L^0}{\delta_L^0}\right);\frac{u_{ref}}{u'Da}\right)\end{aligned} \tag{B.7}$$

Term D_1

$$\begin{aligned}\frac{\partial}{\partial x_j}\left(\overline{\rho D_c}\frac{\partial\widetilde{\epsilon_c}}{\partial x_j}\right) &\backsimeq \mathcal{O}\left(\rho_R\left(\frac{u_L^0}{l_t}\right)^2\right)\\ &= \mathcal{O}\left(\rho_R\left(\frac{u_L^0}{\delta_L^0}\right)^2\left(\frac{1}{DaRe}\right)\right)\\ &= \mathcal{O}\left(\rho_R\left(\frac{u_L^0}{\delta_L^0}\right);(DaRe_{l_t})^{-1}\right)\end{aligned} \tag{B.8}$$

Term D_2

$$\begin{aligned}\overline{\rho D_c D_c\left(\frac{\partial}{\partial x_j}\left(\frac{\partial c''}{\partial x_j}\right)\frac{\partial}{\partial x_j}\left(\frac{\partial c''}{\partial x_j}\right)\right)} &\backsimeq \mathcal{O}\left(\rho_R\frac{u_L^0}{\delta_L^0}\frac{u_L^0}{\delta_L^0}\right)\\ &= \mathcal{O}\left(\rho_R\left(\frac{u_L^0}{\delta_L^0}\right)^2;1\right)\end{aligned} \tag{B.9}$$

Term T_{11}

$$\begin{aligned}\frac{\partial \overline{\rho}\widetilde{u_j^{''}\epsilon_c}}{\partial x_j} &\backsimeq \mathcal{O}\left(\rho_R \frac{u^{'}}{l_t}\frac{u_L^0}{\delta_L^0}\right)\\ &= \mathcal{O}\left(\rho_R\left(\frac{u_L^0}{\delta_L^0}\right)^2 \times \frac{1}{Da}\right)\\ &= \mathcal{O}\left(\rho_R\left(\frac{u_L^0}{\delta_L^0}\right)^2; Da^{-1}\right)\end{aligned} \tag{B.10}$$

Term T_{12}

$$\begin{aligned}2\overline{\rho D_c}\left(\widetilde{u_j^{''}\frac{\partial c^{''}}{\partial x_k}}\right)\frac{\partial}{\partial x_j}\left(\frac{\partial \widetilde{c}}{\partial x_j}\right) &\backsimeq \mathcal{O}\left(\rho_R u_L^0 \delta_L^0\left(\frac{u_L^0}{\delta_L^0}\right)\left(\frac{1}{l_t^2}\right)\right)\\ &= \mathcal{O}\left(\rho_R\left(\frac{u_L^0}{l_t}\right)^2\right)\\ &= \mathcal{O}\left(\rho_R\left(\frac{u_L^0}{\delta_L^0}\frac{u_L^0}{\delta_L^0}\right)\left(\frac{1}{DaRe_{l_t}}\right)\right)\\ &= \mathcal{O}\left(\rho_R\left(\frac{u_L^0}{\delta_L^0}\right)^2; (DaRe_{l_t})^{-1}\right)\end{aligned} \tag{B.11}$$

Term T_2

$$\begin{aligned}\overline{2\rho\epsilon_c\left(\frac{\partial u_l}{\partial x_l}\right)} &\backsimeq \mathcal{O}\left(\rho_R\left(\frac{u_L^0}{\delta_L^0}\right)\left(\frac{u_L^0}{\delta_L^0}\right)\right)\\ &= \mathcal{O}\left(\rho_R\left(\frac{u_L^0}{\delta_L^0}\right)^2; 1\right)\end{aligned} \tag{B.12}$$

Term T_{31}

$$\begin{aligned}\overline{\rho D_c}\frac{\partial \widetilde{c}}{\partial x_j}\left(\widetilde{\frac{\partial c''}{\partial x_k}\frac{\partial u_j''}{\partial x_k}}\right) &\backsimeq \mathcal{O}\left(\rho_R u_L^0 \delta_L^0 \frac{1}{l_t}\left(\frac{1}{\delta_L^0}\frac{u_L^0}{\delta_L^0}\right)\right)\\ &= \mathcal{O}\left(\rho_R \frac{u_L^{0^2}}{l_t \delta_L^0}\right)\\ &= \mathcal{O}\left(\rho_R \frac{u_L^{0^2}}{\delta_L^{0^2}\sqrt{D_a Re}}\right)\\ &= \mathcal{O}\left(\rho_R \left(\frac{u_L^0}{\delta_L^0}\right)^2 ; (Re_{l_t} Da)^{-1/2}\right)\end{aligned} \tag{B.13}$$

Term T_{32}

$$\begin{aligned}2\overline{\rho D_c}\left(\widetilde{\frac{\partial c''}{\partial x_j}S_{jk}''\frac{\partial c''}{\partial x_k}}\right) &\backsimeq \mathcal{O}\left(\rho_R \frac{u_L^{0^2}}{\delta_L^{0^2}}\right)\\ &= \mathcal{O}\left(\rho_R \left(\frac{u_L^0}{\delta_L^0}\right)^2 ; 1\right)\end{aligned} \tag{B.14}$$

Term T_{33}

$$\begin{aligned}2\overline{\rho D_c}\left(\widetilde{\frac{\partial c''}{\partial x_j}\frac{\partial c''}{\partial x_k}}\right)\widetilde{S_{jk}} &\backsimeq \mathcal{O}\left(\rho_R \frac{u_L^0 u_{ref}}{\delta_L^0 l_t}\right)\\ &= \mathcal{O}\left(\rho_R \frac{u_L^0 u_{ref}}{\delta_L^0} / \frac{\delta_L^0}{u_L^0} u' Da\right)\\ &= \mathcal{O}\left(\rho_R \frac{u_L^0 u_{ref}}{\delta_L^0} \times \frac{u_L^0}{\delta_L^0 u' Da}\right)\\ &= \mathcal{O}\left(\rho_R \left(\frac{u_L^0}{\delta_L^0}\right)\left(\frac{u_{ref}}{u' Da}\right)\right)\\ &= \mathcal{O}\left(\rho_R \left(\frac{u_L^0}{\delta_L^0}\right)^2 ; \left(\frac{u' Da}{u_{ref}}\right)^{-1}\right)\end{aligned} \tag{B.15}$$

Term T_4

$$2\left(\overline{D_c \frac{\partial c''}{\partial x_k} \frac{\partial \dot{\omega}_c''}{\partial x_k}}\right) \backsimeq \mathcal{O}\left(u_L^0 \times \rho_R \frac{u_L^0}{\delta_L^0} \times \frac{1}{\delta_L^0}\right)$$
$$= \mathcal{O}\left(\rho_R \left(\frac{u_L^0}{\delta_L^0}\right)^2 ; 1\right) \tag{B.16}$$

Appendix C

Numerical procedure in *Code_Saturne*

Computational Fluid Dynamics (CFD) is a method of simulating and analysing fluid flows, heat transfer and chemical reactions using a numerical approach on a discretised mesh representing a fluid flow problem. The actual analysis is often carried out using computers, as the system of equations that need to be solved is often extremely large. CFD problems result in non linear coupled partial differential equations. These equations are hard to solve as very few analytical solutions exist, hence numerical methods are used in CFD to approximate a solution [65, 155]. The flow geometry, boundary conditions and governing equations have to be specified, as well as any models used to simulate turbulence in the fluid flow (and chemical reactions in combustion). This is a very powerful technique and is widely used in industrial and non-industrial applications [155]. There are many methods available in literature, and detailed reviews can be found in Ferziger and Perić [65], and Versteeg and Malalasekera [155].

Calculations for this work have been performed using an unstructured finite volume code, *Code_Saturne* [6]. The finite volume method is useful as it is inherently conservative and can be used with any kind of mesh (i.e. structured or unstructured). This section only provides a brief introduction to the numerics used in *Code_Saturne* and further details can be found in [6, 107].

C.1 The finite volume method

In the finite volume method the conservation of a flow variable (say ϕ) can be expressed as a balance between different processes tending to change it. The method divides the domain into control volumes over which the equations are integrated [65]. The general equation for the integral over control volume (V) for a variable (ϕ) is written as:

$$\int_V \frac{\partial \rho\phi}{\partial t} dV + \int_V \frac{\partial}{\partial x_j} \left(\rho u_j \phi\right) dV = \int_V \frac{\partial}{\partial x_j} \left(C_\Gamma \frac{\partial \phi}{\partial x_j} \right) dV + \int_V S dV \qquad \text{(C.1)}$$

where S is a source term, V is the volume of the cell and C_Γ is a diffusion coefficient. Now, by using Gauss's divergence theorem, the volume integrals of the convection and diffusion terms can be converted into surface integrals as:

$$\int_V \frac{\partial \rho\phi}{\partial t} dV + \int_A \rho\phi u_j n_i dA = \int_A C_\Gamma \frac{\partial \phi}{\partial x_j} n_i dA + \int_V S dV, \qquad \text{(C.2)}$$

where A is the area of the cell face and n_i is the face normal vector. The unsteady term is approximated as :

$$\frac{\partial}{\partial t} \int_V \rho\phi dV \approx \frac{\rho\phi_I V_I}{\Delta t}, \qquad \text{(C.3)}$$

where ϕ_I is the value of ϕ at the centre of gravity of the cell I, and V_I is the volume of the cell. The source term can be approximated in a similar way :

$$\int_V S dV \approx S_I V_I \qquad \text{(C.4)}$$

Code_Saturne is an unstructured code and cell faces are used as a frame of reference to calculate the diffusive and convective transport [6]. The general configuration of an internal face between two adjacent cells V_I and V_J is shown in figure C.1.

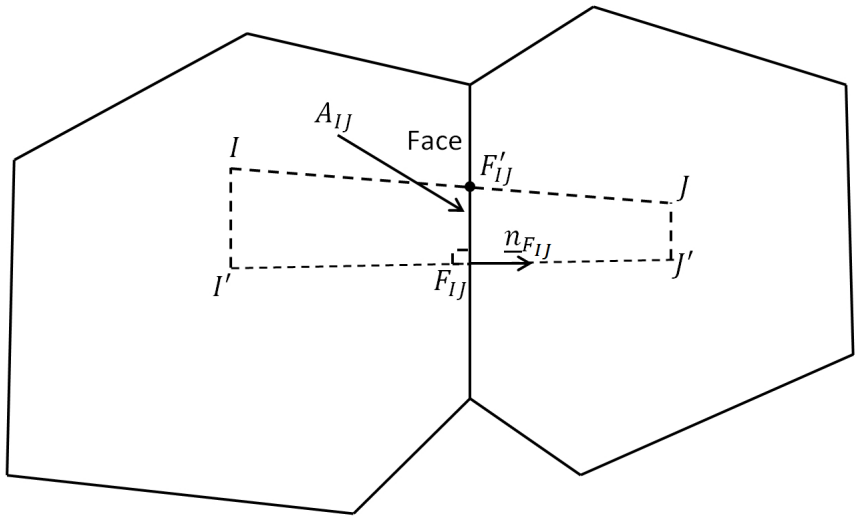

Figure C.1: general configuration of a face between two cells

Point F_{IJ} in figure C.1 is the centre of gravity of the cell face, and points I and J are the centres of mass of the two cells. The line joining points $J^{'}$ and $I^{'}$ represents the projection of the line joining points I and J on the vector normal to the common face between the two cells. Point F_{IJ} represents the point where the vector $\underline{IJ}$ intersects the cell face.

C.1.1 Convection term

The convection for a given cell can be calculated by summing the mass flux of the variable ϕ over each of the cell faces as :

$$\int_A \rho\phi\,(u_i.n_i)\,dA \approx \sum_{neighbour} \phi_{IJ} m_{IJ} \tag{C.5}$$

where m_{IJ} is the mass flux across the face between two adjacent cells.

Code_Saturne makes use of the collocated arrangement, so all the variables are stored at the cell centres. This means that the value of ϕ needs to be calculated at the cell face (point F_{IJ} in figure C.1). This is achieved by making use of different interpolation schemes discussed in the following sections [65].

C.1.2 Upwind differencing scheme (UDS)

Code_Saturne has the first order upwind differencing scheme (UDS). In this scheme the value of ϕ at a cell face is approximated as the value at the cell centre of the neighbouring cell upstream of the cell face [65]:

$$\phi_{IJ} = \begin{cases} \phi_I & \text{if} \quad \rho \underline{u}_I . \underline{n}_{F_{IJ}} \geq 0 \\ \phi_J & \text{if} \quad \rho \underline{u}_I . \underline{n}_{F_{IJ}} < 0 \end{cases} \tag{C.6}$$

This scheme is robust and satisfies the boundedness criterion (i.e. does not give oscillatory solutions). This scheme is numerically diffusive and would introduce errors on a coarse grid, or when the flow direction is oblique to the grid [65, 155].

C.1.3 Central differencing scheme (CDS)

Another way of approximating the value of ϕ at the cell face is linear interpolation between the two neighbouring cell centres as [65]:

$$\phi_{IJ} = \alpha_{I'J'} \phi_{J'} + (1 - \alpha_{I'J'}) \, \phi_{I'} \tag{C.7}$$

where $\alpha_{I'J'}$ is defined as [6]:

$$\alpha_{I'J'} = \frac{|\underline{I'F_{IJ}}|}{|\underline{I'J'}|} \tag{C.8}$$

This scheme is considered to be second order accurate.

C.1.4 Diffusion term

The third term on the right side of eq. (C.2) represents diffusion term. It is approximated as [6]:

$$\int_A C_\Gamma \frac{\partial \phi}{\partial x_j} n_i dA = \sum_{neighbour} C_\Gamma \frac{\partial \phi}{\partial x_j} A_{IJ}, \tag{C.9}$$

where C_Γ is the diffusion coefficient at the face centre. Now using a linear approximation of the gradient at the face centre, the expression in eq. (C.9) can be

calculated as [6]:

$$\sum_{neighbour} C_\Gamma \frac{\partial \phi}{\partial x_j} n_i A = \sum_{neighbour} C_\Gamma \frac{\phi_{J'} - \phi_{I'}}{|\underline{I'J'}|} A_{IJ}, \tag{C.10}$$

where $\phi_{I'}$ and $\phi_{J'}$ can be calculated by making use of the gradients at the cell centre as [6]:

$$\phi_{I'} = \phi_I + \frac{\partial \phi}{\partial x_j} |_I \, \underline{I'I}. \tag{C.11}$$

The method for calculating gradients is given in section C.1.7.

C.1.5 Time discretisation

Code_Saturne uses a fractional step scheme (Euler implicit), which is first order accurate. Time scheme is applied to all the terms in a given transport equation after their discretisation in space is completed. The expression in eq. (C.3) is approximated as :

$$\frac{\rho \left(\phi_I V_I\right)^{n+1}}{\Delta t} = \frac{\rho \left(\left(\phi_I V_I\right)^{n+1} - \left(\phi_I V_I\right)^n\right)}{\Delta t} \tag{C.12}$$

C.1.6 Pressure velocity coupling

The time discretisation scheme mentioned in section C.1.5 can be used along with the SIMPLEC [154] method used by *Code_Saturne*. The solution algorithm makes use of a prediction correction method [6]. First the momentum equation is solved by using an explicit pressure gradient from the previous time step. The equation to be solved at the first step of the method is :

$$\frac{M_i^* - M_i^n}{\Delta t} + \frac{\partial}{\partial x_j}\left(u_i^* M_j^n - \mu \frac{\partial u_i^*}{\partial x_j}\right) = -\frac{\partial p^n}{\partial x_i} + S^* \tag{C.13}$$

where $M_i^n = \rho u_i^n$ at time step n, S^*includes the source terms and Δt is the time step. Now a new velocity is obtained from the previous step and is denoted as u^*. In the second step the pressure gradient is obtained to satisfy the continuity

equation. The Poisson equation for the pressure is written as :

$$\frac{\partial}{\partial x_j}\left(\Delta t\frac{(p^{**}-p^{*})}{\partial x_j}\right)=\frac{\partial M_i^{*}}{\partial x_j}. \tag{C.14}$$

After the updated pressure p^{**} has been obtained, the velocity field can be corrected. The corrected velocity is obtained by neglecting convection and diffusion variations:

$$M_i^{**}-M_i^{*}=-\Delta t\frac{\partial}{\partial x_i}\left(p^{**}-p^{*}\right), \tag{C.15}$$

where $p^{**}=p^{n+1}$ and $M^{**}=M^{n+1}$.

C.1.7 Gradient calculation

The cell centre gradient is calculated at the cell faces using the Gauss theorem and then approximated by using the midpoint rule as :

$$\begin{aligned}\frac{\partial\phi}{\partial x_j}\mid_I &= \frac{1}{V_I}\int_A\phi dA \\ &= \frac{1}{V_I}\sum_{neighbour}\phi_{IJ}\underline{n}_{F_{I,J}}A_{IJ}.\end{aligned} \tag{C.16}$$

C.1.8 Boundary conditions

The boundary conditions used in *Code_Saturne* fall into two categories: Dirichlet and Neumann. In Dirichlet boundary conditions the value of a variable at the cell face is specified, whereas in Neumann boundary conditions the gradient of a variable is defined at the cell face. More details on Neumann and Dirichlet boundary conditions can be found in [65, 155].

Bibliography

[1] Abdel-Gayed, R. G. and Bradley, D. (1977). Dependence of turbulent burning velocity on turbulent reynolds number and ratio of flaminar burning velocity to R.M.S. turbulent velocity. In *Symposium (International) on Combustion*, volume 16, pages 1725–1735.

[2] Abdel-Gayed, R. G., Bradley, D., and Lawes, M. (1987). Turbulent burning velocities: a general correlation in terms of straining rates. *Proceedings of the Royal Society A: Mathematical, Physical and Engineering Sciences*, 414(1847):389–413.

[3] Ahmed, I. and Swaminathan, N. (2013). Simulation of spherically expanding turbulent premixed flames. *Combustion Science and Technology*, 185(10):1509–1540.

[4] Anderson, E., Bai, Z., Bischof, C., Blackford, S., Demmel, J., Dongarra, J., Du Croz, J., Greenbaum, A., Hammarling, S., McKenney, A., and Sorensen, D. (1999). *LAPACK Users' Guide*. Society for Industrial and Applied Mathematics, Philadelphia, PA, third edition.

[5] ANSYS Inc (2010). ICEM CFD User manual.

[6] Archambeau, F., Mechitoua, N., and Sakiz, M. (2004). A finite volume method for the computation of turbulent incompressible flows - industrial applications. *Int. J. Finite Volumes*, 1:1–62.

[7] Ashurst, W. T., Kerstein, A. R., Kerr, R. M., and Gibson, C. H. (1987). Alignment of vorticity and scalar gradient with strain rate in simulated Navier Stokes turbulence. *Physics of Fluids*, 30(8):2343.

[8] Batchelor, G. (1952). The effect of homogeneous turbulence on material lines and surfaces. *Proceedings of the Royal Society of London. Series A, Mathematical and Physical Sciences*, 213(1114):349–366.

[9] Bell, J. B., Day, M. S., Shepherd, I. G., Johnson, M. R., Cheng, R. K., Grcar, J. F., Beckner, V. E., and Lijewski, M. J. (2005). Numerical simulation of a laboratory-scale turbulent V-flame. *Proceedings of the National Academy of Sciences of the United States of America*, 102(29):10006–11.

[10] Bilger, R. (2011). The role of combustion technology in the 21st century. In Mastorakos, E.and Echekki, T., editor, *Turbulent Combustion Modeling*, pages 3–18. Springer.

[11] Bilger, R. W. (1976). The structure of diffusion flames. *Combustion Science and Technology*, 13(1-6):155–170.

[12] Bilger, R. W., Pope, S. B., Bray, K. N. C., and Driscoll, J. F. (2005). Paradigms in turbulent combustion research. *Proceedings of the Combustion Institute*, 30(1):21–42.

[13] Blint, R. (1986). The relationship of the laminar flame width to flame speed. *Combustion Science and Technology*, 49(1):79–92.

[14] Bockhorn, H., Habisreuther, P., and Hettel, M. (2009). Numerical modelling of technical combustion. In Hirschel, E. and Krause, E., editors, *100 Volumes of Notes on Numerical Fluid Mechanics*, pages 325–340. Springer Berlin Heidelberg.

[15] Borghi, R. (1985). On the structure and morphology of turbulent premixed flames. In Bruno, C. and Casci, S., editors, *Recent Advances in the Aerospace Sciences*, pages 117–138. Plenum, New York.

[16] Borghi, R. (1988). Turbulent combustion modelling. *Progress in Energy and Combustion Science*, 14(4):245–292.

[17] Borghi, R. (1990). Turbulent premixed combustion: Further discussions on the scales of fluctuations. *Combustion and Flame*, 80(3-4):304–312.

[18] Boussinesq, J. (1877). Theorie de l'ecoulement tourbillant. *Mem. Pres. par div. savant a lacad. sci. Paris*, 23:46.

[19] Bray, K. (1980). Turbulent flows with premixed reactants. In Libby, P. and Williams, F., editors, *Turbulent Reacting Flows*, volume 44 of *Topics in Applied Physics*, pages 115–183. Springer Berlin / Heidelberg.

[20] Bray, K., Libby, P. A., and Moss, J. B. (1982). Turbulent transport in premixed flames. In J.Zierep and H.Oertel, editors, *Convective Transport and Instability Phenomenon*, pages 389–423. G.Braun Karlsruhe.

[21] Bray, K. N. C. (1979). The interaction between turbulence and combustion. *Seventeenth Symposium Symposium (International) on Combustion*, 17(1):223–233.

[22] Bray, K. N. C. (1990). Studies of the turbulent burning velocity. *Proceedings: Mathematical and Physical Sciences*, 431(1882):315–335.

[23] Bray, K. N. C. (1995). Turbulent transport in flames. *Proceedings: Mathematical and Physical Sciences*, 451(1941, Osborne Reynolds Centenary Volume):231–256.

[24] Bray, K. N. C., Libby, P. A., Masuya, G., and Moss, J. B. (1981). Turbulence production in premixed turbulent flames. *Combustion Science and Technology*, 25(3):127–140.

[25] Bray, K. N. C., Libby, P. A., and Moss, J. B. (1984). Flamelet crossing frequencies and mean reaction rates in premixed turbulent combustion. *Combustion Science and Technology*, 41(3):143–172.

[26] Bray, K. N. C., Libby, P. A., and Moss, J. B. (1985). Unified modeling approach for premixed turbulent combustion-Part I: General formulation. *Combustion and Flame*, 61(1):87–102.

[27] Bray, K. N. C. and Moss, J. B. (1977). A unified statistical model of the premixed turbulent flame. *Acta Astronautica*, 4(3-4):291–319.

[28] Bray, K. N. C. and Swaminathan, N. (2006). Scalar dissipation and flame surface density in premixed turbulent combustion. *Comptes Rendus Mécanique*, 334(8-9):466–473.

[29] Brink, A., Mueller, C., Kilpinen, P. I. A., and Hupa, M. (2000). Possibilities and limitations of the eddy break-up model. *Combustion and Flame*, 123:275–279.

[30] Candel, S. and Poinsot, T. (1990). Flame stretch and the balance equation for the flame area. *Combustion Science and Technology*, 70(1):1–15.

[31] Cant, R. (2011). RANS and LES modelling of premixed combustion. In Mastorakos, E.and Echekki, T., editor, *Turbulent Combustion Modeling*, pages 63–90. Springer.

[32] Cant, R. S. (2012). SENGA2 User Guide, CUED/A THERMO/TR67. Technical report, University of Cambridge, Cambridge, United Kingdom.

[33] Cant, R. S. and Bray, K. N. C. (1989a). A theoretical model of premixed turbulent combustion in closed vessels. *Combustion and Flame*, 76(3-4):243–263.

[34] Cant, R. S. and Bray, K. N. C. (1989b). Strained laminar flamelet calculations of premixed turbulent combustion in a closed vessel. *Twenty-second Symposium (International) on Combustion*, 22(1):791–799.

[35] Cant, R. S. and Mastorakos, E. (2008). *An introduction to turbulent reacting flows*. Imperial College Press.

[36] Cant, R. S., Pope, S. B., and Bray, K. N. C. (1991). Modelling of flamelet surface-to-volume ratio in turbulent premixed combustion. *Twenty-third Symposium (International) on Combustion*, 23(1):809–815.

[37] Cant, R. S., Rogg, B., and Bray, K. N. C. (1990). On laminar flamelet modelling of the mean reaction rate in a premixed turbulent flame. *Combustion Science and Technology*, 69(1):53–61.

[38] Çengel, Y. A. and Boles, M. A. (2006). *Thermodynamics: An Engineering Approach*. McGraw-Hill, 5th edition.

[39] Chakraborty, N. and Cant, R. S. (2009). Effects of Lewis number on turbulent scalar transport and its modelling in turbulent premixed flames. *Combustion and Flame*, 156(7):1427–1444.

[40] Chakraborty, N., Champion, M., Mura, A., and Swaminathan, N. (2011). Modelling methods, Scalar dissipation rate approach. In Swaminathan, N. and Bray, K. N. C., editors, *Turbulent Premixed Flames*, pages 74–102. Cambridge University Press.

[41] Chakraborty, N., Katragadda, M., and Cant, R. S. (2010). Statistics and Modelling of Turbulent Kinetic Energy Transport in Different Regimes of Premixed Combustion. *Flow, Turbulence and Combustion*, 87(2-3):205–235.

[42] Chakraborty, N., Klein, M., and Swaminathan, N. (2009). Effects of Lewis number on the reactive scalar gradient alignment with local strain rate in turbulent premixed flames. *Proceedings of the Combustion Institute*, 32(1):1409–1417.

[43] Chakraborty, N., Rogerson, J. W., and Swaminathan, N. (2008). A priori assessment of closures for scalar dissipation rate transport in turbulent premixed flames using direct numerical simulation. *Physics of Fluids*, 20(4):045106.

[44] Chakraborty, N. and Swaminathan, N. (2007a). Influence of the Damköhler number on turbulence-scalar interaction in premixed flames. I. Physical insight. *Physics of Fluids*, 19(4):045103.

[45] Chakraborty, N. and Swaminathan, N. (2007b). Influence of the Damköhler number on turbulence-scalar interaction in premixed flames. II. Model development. *Physics of Fluids*, 19(4):045104.

[46] Chakraborty, N. and Swaminathan, N. (2013). Reynolds number effects on scalar dissipation rate transport and Its modeling in turbulent premixed combustion. *Combustion Science and Technology*, 185(4):676–709.

[47] Chen, Y. and Bilger, R. W. (2002). Experimental investigation of three-dimensional flame-front structure in premixed turbulent combustion: hydrocarbon/air bunsen flames. *Combustion and Flame*, 131(4):400–435.

[48] Chen, Y. and Mansour, M. (1998). Investigation of flame broadening in turbulent premixed flames in the thin-reaction-zones regime. *Twenty-seventh Symposium (International) on Combustion*, 27(1):811–818.

[49] Cheng, R. K. and Shepherd, I. G. (1991). The influence of burner geometry on premixed turbulent flame propagation. *Combustion and Flame*, 85(1-2):7–26.

[50] Cheng, W. and Diringer, J. (1991). Numerical modelling of SI engine combustion with a flame sheet model. In *International Congress & Exposition*, Detroit, MI. SAE International.

[51] Correa, S. M. (1993). A review of NOx formation under gas-turbine combustion conditions. *Combustion Science and Technology*, 87(1-6):329–362.

[52] Correa, S. M. (1998). Power generation and aeropropulsion gas turbines: From combustion science to combustion technology. *Twenty-seventh Symposium (International) on Combustion*, 27(2):1793–1807.

[53] Curtiss, C. F. and Hirschfelder, J. O. (1949). Transport properties of multicomponent gas mixtures. *The Journal of Chemical Physics*, 17(6):550.

[54] Damköhler, G. (1940). Der einfluss der turbulenz auf die flammengeschwindigkeit in gasgemischen. *Zeitschrift für Elektrochemie und angewandte physikalische Chemie*, 46(11):601–626.

[55] Duclos, J., Veynante, D., and Poinsot, T. (1993). A comparison of flamelet models for premixed turbulent combustion. *Combustion and Flame*, 95(1-2):101–117.

[56] Dunstan, T. D. (2008). *Turbulent premixed flame kernel growth during the early stages using Direct Numerical Simulation*. PhD thesis, Cranfield University.

[57] Dunstan, T. D., Minamoto, Y., Chakraborty, N., and Swaminathan, N. (2013). Scalar dissipation rate modelling for Large Eddy Simulation of turbulent premixed flames. *Proceedings of the Combustion Institute*, 34(1):1193–1201.

[58] Dunstan, T. D., Swaminathan, N., and Bray, K. N. C. (2012). Influence of flame geometry on turbulent premixed flame propagation: a DNS investigation. *Journal of Fluid Mechanics*, 709:191–222.

[59] Dunstan, T. D., Swaminathan, N., Bray, K. N. C., and Cant, R. S. (2010a). Erratum to: Geometrical properties and turbulent flame speed measurements in stationary premixed V-flames using Direct Numerical Simulation. *Flow, Turbulence and Combustion*, 87(4):725–728.

[60] Dunstan, T. D., Swaminathan, N., Bray, K. N. C., and Cant, R. S. (2010b). Geometrical properties and turbulent flame speed measurements in stationary premixed V-flames using Direct Numerical Simulation. *Flow, Turbulence and Combustion*, 87(2-3):237–259.

[61] Durbin, P. A. and Pettersson Reif, B. A. (2001). *Statistical Theory and Modeling for Turbulent Flows*. John Wiley and Sons.

[62] Eswaran, V. and Pope, S. B. (1988). An examination of forcing in direct numerical simulations of turbulence. *Computers & Fluids*, 16(3):257–278.

[63] Favre, A. (1965). Equations des gaz turbulents compressibles. *Journal de Mecanique*, 4(3):361–390.

[64] Favre, A. (1969). Statistical equations of turbulent gases. *In Problems of hydrodynamics and continuum mechanics*.

[65] Ferziger, J. H. and Perić, M. (2002). *Computational Methods for Fluid Dynamics*. Springer, 3rd edition.

[66] Frank, J. H., Kalt, P. A., and Bilger, R. W. (1999). Measurements of conditional velocities in turbulent premixed flames by simultaneous OH PLIF and PIV. *Combustion and Flame*, 116(1-2):220–232.

[67] Gu, X., Haq, M., Lawes, M., and Woolley, R. (2000). Laminar burning velocity and Markstein lengths of methane-air mixtures. *Combustion and Flame*, 121(1-2):41–58.

[68] Hanjalić, K. and Launder, B. (2011). *Modelling Turbulence in Engineering and the Environment (Second-Moment Routes to Closure)*. Cambridge University Press.

[69] Hanjalic, K. and Launder, B. E. (1972). A reynold stress model of turbulence and its applications to thin shear flows. *Journal of Fluid Mechanics*, pages 609–638.

[70] Hanjalić, K. and Suas, J. (2004). Second-moment turbulence closure modelling. In Launder, B. and Sandham, N. D., editors, *Closure Strategies for Turbulent and Transitional Flows*, pages 47–101. Cambridge University Press.

[71] Hartung, G., Hult, J., Kaminski, C., Rogerson, J. W., and Swaminathan, N. (2008). Effect of heat release on turbulence and scalar-turbulence interaction in premixed combustion. *Physics of Fluids*, 20(3):035110.

[72] Hewitt, G. F., Vassilicos, J. C., Hunt, J. C. R., Sandham, N. D., Launder, B. E., Monkewitz, P. A., Jones, W. P., Morrison, J. F., Reeks, M. W., and Savill, A. M. (2005). *Prediction of turbulent flows*. Cambridge University Press, 1st edition.

[73] Ihme, M., Poinsot, T., and Vervisch, L. (2012). Combustion - overview. In *Proceedings of Summer Program, Center for Turbulence Research*, pages 385–386. Stanford University, Palo Alto, California.

[74] Intergovernmental Panel on Climate Change (2007). Climate change 2007. Technical report, Intergovernmental Panel on Climate Change, Geneva, Switzerland.

[75] International Energy Agency (2012). World Energy Outlook. Technical report, OECD/IEA, Paris.

[76] Jenkins, K. and Cant, R. (1999). Direct numerical simulation of turbulent flame kernels. In Knight, D. and Sakell, L., editors, *Recent Advances in DNS and LES: Proceedings of the Second AFOSR Conference, Rutgers - The State University of New Jersey, New Brunswick, USA*, pages 191–202. Kluwer, Dordrecht.

[77] Jones, B. (2011a). Application of lean flames in aero gas turbines. In Swaminathan, N. and Bray, K. N. C., editors, *Turbulent Premixed Flames*, pages 309–334. Cambridge University Press.

[78] Jones, B. (2011b). Application of lean flames in stationary gas turbines. In Swaminathan, N. and Bray, K. N. C., editors, *Turbulent Premixed Flames*, pages 335–364. Cambridge University Press.

[79] Jones, W. (1980). Models for turbulent flows with variable density and combustion. In Kollmann, W., editor, *Prediction Methods for Turbulent Flows*, pages 379–421. Hemisphere Publishing Corporation.

[80] Jones, W. (1994). Turbulence modelling and numerical solution methods. In Libby, P. and Williams, F., editors, *Turbulent Reacting Flows*, pages 309–374. Academic Press.

[81] Jones, W. P. and Launder, B. E. (1972). The prediction of laminarization with a two-equation model of turbulence. *International Journal of Heat Mass Transfer*, 15:301–314.

[82] Jones, W. P. and Musonge, P. (1988). Closure of the Reynolds stress and scalar flux equations. *Physics of Fluids*, 31(12):3589–3604.

[83] Kim, S. H. and Pitsch, H. (2007). Scalar gradient and small-scale structure in turbulent premixed combustion. *Physics of Fluids*, 19(11):115104.

[84] King, D., Richards, K., and Tyldesley, S. (2011). International climate change negotiations: Key lessons and next steps. Technical report, Smith School of Enterprise and the Environment, Univeristy of Oxford, Oxford, United Kingdom.

[85] Kolla, H. (2009). *Scalar dissipation rate based flamelet modelling of turbulent premixed flames*. PhD thesis, University of Cambridge.

[86] Kolla, H., Rogerson, J. W., Chakraborty, N., and Swaminathan, N. (2009). Scalar dissipation rate modeling and its validation. *Combustion Science and Technology*, 181(3):518–535.

[87] Kolla, H. and Swaminathan, N. (2009). Modelling of turbulent premixed flames using strained-flamelets. In *Proceedings of the European Combustion Meeting 2009*.

[88] Kolla, H. and Swaminathan, N. (2010a). Strained flamelets for turbulent premixed flames, I: Formulation and planar flame results. *Combustion and Flame*, 157(5):943–954.

[89] Kolla, H. and Swaminathan, N. (2010b). Strained flamelets for turbulent premixed flames II: Laboratory flame results. *Combustion and Flame*, 157(7):1274–1289.

[90] Kolmogorov, A. N. (1941). Local structure of turbulence in incompressible viscous fluid for very large Reynolds number. *Doklady Akademiya Nauk SSSR*, 30:299–303.

[91] Kuo, K. K. (1986). *Principles of Combustion*. John Wiley and Sons.

[92] Launder, B., Reece, G. J., and Rodi, W. (1975a). Progress in the development of a Reynolds-stress turbulence closure. *Journal of Fluid Mechanics*, 68(03):537–566.

[93] Launder, B. and Spalding, D. B. (1974). The numerical computation of turbulent flows. *Computer methods in applied mechanics and engineering*, 3:269–289.

[94] Launder, B. E., Reece, G. J., and Rodi, W. (1975b). Progress in the development of a Reynolds stress turbulence closure. *Journal of Fluid Mechanics*, 68:537–566.

[95] Launder, B. E. and Sharma, B. I. (1974). Application of the energy-dissipation model of turbulence to the calculation of flow near a spinning disc. *Letters in heat and mass transfer*, 1:131–138.

[96] Law., C. K. (2006). *Combustion Physics*. Cambridge University Press.

[97] Libby, P. A. and Bray, K. N. C. (1981). Countergradient diffusion in premixed turbulent flames. *AIAA Journal*, 19(2):205–213.

[98] Libby, P. A. and Williams, F. A. (1976). Turbulent flows involving chemical reactions. *Annual Review of Fluid Mechanics*, 8(1):351–376.

[99] Libby, P. A. and Williams, F. A. (1980). Fundamental aspects. In *Turbulent Reacting Flows*, volume 55, pages 1–43.

[100] Libby, P. A. and Williams, F. A. (1994). *Turbulent Reacting Flows*. Academic Press Limited.

[101] Lindstedt, R. and Vaos, E. (2006). Transported PDF modeling of high-Reynolds-number premixed turbulent flames. *Combustion and Flame*, 145(3):495–511.

[102] Liu, Y., Dowling, A. P., Swaminathan, N., and Dunstan, T. D. (2012). Spatial correlation of heat release rate and sound emission from turbulent premixed flames. *Combustion and Flame*, 159(7):2430–2440.

[103] Magnussen, B. F. and Hjertager, B. r. H. (1977). On mathematical modeling of turbulent combustion with special emphasis on soot formation and combustion. In *Symposium (International) on Combustion*, volume 16, pages 719–729.

[104] Mantel, T. and Bilger, R. W. (1995). Some conditional statistics in a turbulent premixed flame derived from Direct Numerical Simulations. *Combustion Science and Technology*, 110(1):393–417.

[105] Mantel, T. and Borghi, R. (1994). A new model of premixed wrinkled flame propagation based on a scalar dissipation equation. *Combustion and Flame*, 96(4):443–457.

[106] McDonell, V. (2007). Lean combustion in gas turbines. In Dunn-Rankin, D., editor, *Lean Combustion Technology and Control*, pages 121–160. Academic press.

[107] McNaughton, J. (2013). *Turbulence modelling in the near-field of an axial flow tidal turbine using Code_Saturne*. PhD thesis, The University of Manchester.

[108] Metghalchi, M. and Keck, J. (1980). Laminar burning velocity of propane-air mixtures at high temperature and pressure. *Combustion and Flame*, 38:143–154.

[109] Minamoto, Y., Fukushima, N., Tanahashi, M., Miyauchi, T., Dunstan, T. D., and Swaminathan, N. (2011). Effect of flow-geometry on turbulence-scalar interaction in premixed flames. *Physics of Fluids*, 23(12):125107.

[110] Moss, J. B. (1980). Simultaneous measurements of concentration and velocity in an open premixed turbulent flame. *Combustion Science and Technology*, 22(3):119–129.

[111] Mura, A. and Borghi, R. (2003). Towards an extended scalar dissipation equation for turbulent premixed combustion. *Combustion and Flame*, 133(1-2):193–196.

[112] Mura, A., Robin, V., and Champion, M. (2007). Modeling of scalar dissipation in partially premixed turbulent flames. *Combustion and Flame*, 149(1-2):217–224.

[113] Nikolaou, Z. M. and Swaminathan, N. (2013). Direct Numerical Simulation of multi-component fuel mixture combustion with detailed chemistry. In *Proc. European Combustion Meeting ECM2013*, Lund, Sweden.

[114] Nishiki, S., Hasegawa, T., Borghi, R., and Himeno, R. (2002). Modeling of flame-generated turbulence based on direct numerical simulation databases. *Proceedings of the Combustion Institute*, 29(2):2017–2022.

[115] Peters, N. (1986). Laminar flamelet concepts in turbulent combustion. *Twenty-first Symposium (International) on Combustion*, pages 1231–1250.

[116] Peters, N. (1999). The turbulent burning velocity for large-scale and small-scale turbulence. *Journal of Fluid Mechanics*, 384:107–132.

[117] Peters, N. (2000). *Turbulent Combustion*. Cambridge University Press.

[118] Poinsot, T. and Veynante, D. (2005). *Theoretical and numerical combustion*. R.T.Edwards, Inc, 2nd edition.

[119] Pope, S. B. (1985). PDF methods for turbulent reactive flows. *Progress in Energy and Combustion Science*, 11(2):119–192.

[120] Pope, S. B. (1987). Turbulent premixed flames. *Annual Review of Fluid Mechanics*, 19(1):237–270.

[121] Pope, S. B. (1988). The evolution of surfaces in turbulence. *International Journal of Engineering Science*, 26(5):445–469.

[122] Pope, S. B. (1991). Computations of turbulent combustion: Progress and challenges. *Twenty-third Symposium (International) on Combustion*, 23(1):591–612.

[123] Pope, S. B. (2000). *Turbulent Flows*. Cambridge University Press.

[124] Prandtl, L. (1925). Bericht liber untersungen zur ausgebildeten turbulenz. *ZAMM*, 5:136–139.

[125] Prandtl, L. (1945). Uber ein neues formelsystem fur die ausgbildete turbulenz. *Nachr. Akad. Wizz. Gottingen Math-Phys*, 1:6–19.

[126] Prasad, R., Paul, R., Sivathanu, Y., and Gore, J. (1999). An evaluation of combined flame surface density and mixture fraction models for nonisenthalpic premixed turbulent flames. *Combustion and Flame*, 117(3):514–528.

[127] Prosser, R. (2005). Improved boundary conditions for the direct numerical simulation of turbulent subsonic flows. I. Inviscid flows. *Journal of Computational Physics*, 207(2):736–768.

[128] Prosser, R. (2010). Improved boundary conditions for the DNS of reacting subsonic flows. *Flow, Turbulence and Combustion*, 87(2-3):351–376.

[129] Reynolds, O. (1894). On the dynamical theory of incompressible viscous flows and the determination of the criterion. *Phil. Trans. R Soc London*, 56:123–161.

[130] Reynolds, W. C. and Perkins, H. C. (1977). *Engineering Thermodynamics*. McGraw-Hill.

[131] Richardson, L. F. (1922). *Weather Prediction by Numerical Process*. Cambridge University Press.

[132] Robin, V. (2008). *Contribution à la Modélisation des Ecoulements Turbulents Réactifs Partiellement Prémélangés*. PhD thesis, Université de Poitiers.

[133] Robin, V., Mura, A., Champion, M., Degardin, O., Renou, B., and Boukhalfa, M. (2008). Experimental and numerical analysis of stratified turbulent V-shaped flames. *Combustion and Flame*, 153:288–315.

[134] Robin, V., Mura, A., Champion, M., and Plion, P. (2006). A multi-dirac presumed PDF model for turbulent reactive flows with variable equivalence ratio. *Combustion Science and Technology*, 178(10):1843–1870.

[135] Rogerson, J. W. and Swaminathan, N. (2007). Correlation between dilatation and scalar dissipation in turbulent premixed flames. In *Proc. European Combustion Meeting ECM2007*.

[136] Rolls Royce (2005). *The jet engine*. Rolls Royce Technical Publications, 5th edition.

[137] Said, R. and Borghi, R. (1988). A simulation with a "cellular automaton" for turbulent combustion modelling. *Twenty-second Symposium (International) on Combustion*, pages 569–577.

[138] Salehi, M. M. (2012). *Numerical simulation of turbulent premixed flames with conditional source-term estimation*. PhD thesis, The University of British Columbia.

[139] Salehi, M. M. and Bushe, W. K. (2010). Presumed PDF modeling for RANS simulation of turbulent premixed flames. *Combustion Theory and Modelling*, 14(3):381–403.

[140] Sapa, B. (2011). *Contribution á l'extension d'un schéma incompressible pour les flammes á bas nombre de Froude - Pré-requis á la modélisation de l'incendie*. PhD thesis, Université de Poitiers.

[141] Shepherd, I., Hertzberg, J., and Talbot, L. (1992). Flame holding in unconfined turbulent premixed flames. In Hussaini, M., Kumar, A., and Voigt, R., editors, *Major Research Topics in Combustion*, pages 253–270. Springer-Verlag, New York.

[142] Sivasegaram, S. (2007). Stability and Control. In Dunn-Rankin, D., editor, *Lean combustion technology and control*, pages 179–211. Academic Press.

[143] Spalding, D. B. (1971). Mixing and chemical reaction in steady confined turbulent flames. *Proceedings of the Combustion Institute Symposium (International) on Combustion*, 13:649–657.

[144] Spalding, D. B. (1977). Development of the eddy-break-up model for turbulent combustion. *Proceedings of the Combustion Institute*, 16(1):1657–1663.

[145] Speziale, C. G., Sarkar, S., and Gatski, T. B. (1991). Modelling the pressure strain correlation of turbulence: an invariant dynamical systems approach. *Journal of Fluid Mechanics*, 227:245–272.

[146] Steinberg, A. M., Driscoll, J. F., and Swaminathan, N. (2012). Statistics and dynamics of turbulence-flame alignment in premixed combustion. *Combustion and Flame*, 159(8):2576–2588.

[147] Sutherland, J. C. and Kennedy, C. a. (2003). Improved boundary conditions for viscous, reacting, compressible flows. *Journal of Computational Physics*, 191(2):502–524.

[148] Swaminathan, N. and Bilger, R. W. (2001). Scalar dissipation, diffusion and dilatation in turbulent H 2 -air premixed flames with complex chemistry. *Combustion Theory and Modelling*, 5(3):429–446.

[149] Swaminathan, N. and Bray, K. N. C. (2005). Effect of dilatation on scalar dissipation in turbulent premixed flames. *Combustion and Flame*, 143(4):549–565.

[150] Swaminathan, N., Bray, K. N. C., and Jawahar, P. (2005). A revised EBU type model for turbulent premixed flames based on scalar dissipation rate. In *Proc. European Combustion Meeting ECM2005*, Louvain-la-Neuve, Belgium.

[151] Swaminathan, N. and Grout, R. W. (2006). Interaction of turbulence and scalar fields in premixed flames. *Physics of Fluids*, 18(4):045102.

[152] Tennekes, H. and Lumley, J. L. (1972). *A first course in turbulence*. The MIT Press Cambridge, Massachusetts, and London, England.

[153] Trouvé, A. and Poinsot, T. (1994). The evolution equation for the flame surface density in turbulent premixed combustion. *Journal of Fluid Mechanics*, 278:1–131.

[154] Van Doormaal, J. P. and Raithby, G. D. (1984). Enhancements of the SIMPLE method for predicting incompressible fluid flows. *Numerical Heat Transfer, Part B: Fundamentals*, 7(2):147–163.

[155] Versteeg, H. K. and Malalasekera, W. (2007). *An Introduction to Computational Fluid Dynamics The Finite Volume Method*. Pearson Education Limited, 2nd edition.

[156] Vervisch, L., Bidaux, E., Bray, K. N. C., and Kollmann, W. (1995). Surface density function in premixed turbulent combustion modeling, similarities between probability density function and flame surface approaches. *Physics of Fluids*, 7(10):2496.

[157] Vervisch, L., Hauguel, R., Domingo, P., and Rullaud, M. (2004). Three facets of turbulent combustion modelling: DNS of premixed V-flame, LES of lifted nonpremixed flame and RANS of jet-flame. *Journal of Turbulence*, 5:37–41.

[158] Veynante, D., Piana, J., Duclos, J., and Martel, C. (1996). Experimental analysis of flame surface density models for premixed turbulent combustion. *Twenty-sixth Symposium (International) on Combustion*, 26(1):413–420.

[159] Veynante, D. and Poinsot, T. (1997). Effects of pressure gradients on turbulent premixed flames. *Journal of Fluid Mechanics*, 353:83–114.

[160] Veynante, D., Trouvé, A., Bray, K. N. C., and Mantel, T. (1997). Gradient and counter-gradient scalar transport in turbulent premixed flames. *Journal of Fluid Mechanics*, 332:263–293.

[161] Veynante, D. and Vervisch, L. (2002). Turbulent combustion modeling. *Progress in Energy and Combustion Science*, 28(3):193–266.

[162] Westbrook, C. K., Mizobuchi, Y., Poinsot, T. J., Smith, P. J., and Warnatz, J. (2005). Computational combustion. *Proceedings of the Combustion Institute*, 30(1):125–157.

[163] Wilcox, D. C. (2006). *Turbulence Modeling for CFD*. DCW Industries, Inc, 3rd edition.

[164] Williams, F. A. (1985). *Combustion Theory*. Perseus Books, second edition.

[165] Yao, M., Zheng, Z., and Liu, H. (2009). Progress and recent trends in homogeneous charge compression ignition (HCCI) engines. *Progress in Energy and Combustion Science*, 35(5):398–437.

[166] Yoo, C. S. and Im, H. G. (2007). Characteristic boundary conditions for simulations of compressible reacting flows with multi-dimensional, viscous and reaction effects. *Combustion Theory and Modelling*, 11(2):259–286.

[167] Zeman, O. and Lumley, J. L. (1976). Modeling buoyancy driven mixed layers. *Journal of the Atmospheric Sciences*, 33(10):1974–1988.

[168] Zhang, S. and Rutland, C. J. (1995). Premixed flame effects on turbulence and pressure-related terms. *Combustion and Flame*, 102(4):447–461.

[169] Zhao, F., Lai, M.-C., and Harrington, D. (1999). Automotive spark-ignited direct-injection gasoline engines. *Progress in Energy and Combustion Science*, 25(5):437–562.